

ON THE MECHANICS OF CROPPING
SINGLE THIN-WALLED METALLIC TUBES

by

RAVI SANJEEVA RAO
B.E., M.Tech., M.Sc.(Lond), DIC

A thesis submitted for the degree of Doctor of
Philosophy of the University of London

JUNE 1980

Department of Mechanical Engineering
Imperial College of Science and Technology
London, S.W.7.

TO MY PARENTS

SUMMARY

Cropping is generally used to obtain metal billets from solid bar stock and these billets are later formed by means of a wide variety of deformation processes. Tube cropping is used mainly from the point of view of its economic viability and productivity. The major practical application of the present work would be in nuclear fuel re-processing plants. Irradiated stainless steel tubes of the fuel elements of Commercial Fast Reactors have to be cropped to allow the entry of nitric acid for leaching out plutonium oxide. The main object of the present research is to ensure that, under cropping action, the tubes of the fuel elements do not distort to the extent that fuel extraction is impaired. This thesis examines the theoretical and experimental aspects of cropping of thin-walled metallic tubes, both empty and filled.

Incremental cropping, dye-penetrant, high speed cinematography, the conducting paint technique and a technique of using the tube as an electrical conductor have all been employed to illustrate various aspects of the tube cropping process in detail. From incremental cropping tests, empirical formulae ~~have been~~ have been established. Dye-penetrant and conducting paint techniques reveal that the crack opens immediately after the maximum cropping load. The general deformation pattern during the cropping process has been studied by identifying relevant frames from cine films in relation to the loading cycle.

The influence of various process parameters has been studied in detail. From the experimental investigation, it has been established that the billet material, its diameter to thickness ratio and the velocity of the blade are the major parameters that influence the quality of billets and the cropping load. Billet quality has been further improved using pre-load conditions.

Cropping results are correlated with the results obtained from standard tensile tests as it was not possible to conduct meaningful torsion tests on the very small thin-walled tubes used in this investigation due to the buckling problem.

The mechanism of fracture in cropping of these tubes was investigated by making fractographic studies. Tearing and shear patterns were observed which suggests domination of the opening and shear modes of ductile fracture in stainless steels. It has also shown that fracture in brittle materials such as alumina, glass, etc., occurs from mechanical defects such as cracks, pores, inclusions, etc.

Theoretical explanations are given for cropping under pre-load and at low temperature conditions. A simple strain theory approach has been used to estimate the deflection at maximum cropping load. An upper-bound solution has been developed to predict the load-deflection graph up to the point of actual first shearing based on plastic work approach and a comparison is then made with the experimental results. Finally, the thesis ends with general conclusions and suggestions for further work.

ACKNOWLEDGEMENTS

I wish to express my gratitude to Professor J.M. Alexander for his initiation of the project and his encouragement, supervision and guidance throughout the course of this work.

I wish to thank all the visitors from BNFL/UKAEA; especially to Mr. J. Williams and the late Mr. J.H.B. Pearce, who have shown keen interest in this project and made valuable suggestions.

I would like to express my sincere appreciation to Dr. T.Y. Reddy and Mr. Y. El-Sai for helpful discussions.

I would like to thank Mr. C. Reaves for his assistance during the experimental work.

I am grateful to UKAEA, Dounreay, for providing financial assistance. I wish to thank Dr. C.C.B. Besant for providing partial financial support for the thesis work.

Many thanks to Mrs. Robertson for her prompt, efficient typing and to Mr. Bharat Bhushan for careful reading of this thesis.

Finally, my special thanks go to my brother-in-law, Dr. Chand and sister, Dr. Leela, for their unending moral support throughout the entire duration of the project.

CONTENTS

	<u>Page</u>
SUMMARY	(i)
ACKNOWLEDGEMENTS	(iii)
CONTENTS	(iv)
SYMBOLS	(viii)
<u>CHAPTER 1</u> <u>GENERAL INTRODUCTION</u>	
1.1 Introduction	1
1.2 Different techniques of billet production	3
1.3 The cropping process	6
1.4 Cropping techniques	7
1.5 Cropping parameters and their effects	10
1.6 Origin of the present work	12
1.7 Approach to the problem	14
1.8 Aims of the research project	18
<u>CHAPTER 2</u> <u>EXPERIMENTAL INVESTIGATION OF TUBE CROPPING PROCESS AND ITS PARAMETERS</u>	
2.1 Introduction	20
2.2 Experimental equipment for cropping	21
2.2.1 The cropping rig	21
2.2.2 The press	24
2.2.3 Instrumentation	27
2.3 Single tube cropping	33
2.3.1 Empty tubes	33
2.3.2 Filled tubes	34
2.4 Tube cropping under pre-load	52
2.4.1 Tensile pre-load	52
2.4.2 Compressive pre-load	53

	<u>Page</u>
2.5 Single tube cropping at low temperature	53
2.6 Bar cropping	53
2.7 Different techniques used to explain tube cropping process	64
2.7.1 Incremental cropping	64
2.7.2 Dye penetrant	64
2.7.3 Conducting paint technique	67
2.7.4 Tube as electrical conductor	70
2.7.5 High speed cinematography	71
2.8 Discussion of experimental results	86
2.8.1 A typical tube cropping cycle	86
2.8.2 Bar cropping	91
2.8.3 The effect of independent variables	93
 <u>CHAPTER 3 MECHANICAL PROPERTIES OF MATERIALS</u>	
3.1 Introduction	102
3.2 Theory	102
3.3 Instrumentation	106
3.4 Experiments	107
3.5 Results and discussions	119
 <u>CHAPTER 4 FRACTOGRAPHIC STUDY OF THE MECHANISMS OF FRACTURE IN CROPPING</u>	
4.1 Introduction	123
4.2 Equipment and specimen preparation	124
4.3 Mechanisms of fracture	126
4.4 Conclusions	145

	<u>Page</u>
<u>CHAPTER 5</u> <u>THEORETICAL WORK</u>	
5.1 Introduction	147
5.2 Theoretical explanations for cropping under pre-load	148
5.3 Theoretical explanations for cropping at low temperatures	149
5.4 Prediction of cropping load based on shear yield stress	150
5.5 Prediction of deflection at maximum cropping load	152
5.6 Upper-bound solution for tube cropping	154
5.7 Comparison of experimental and theoretical results	167
<u>CHAPTER 6</u> <u>GENERAL DISCUSSION</u>	
6.1 Introduction	189
6.2 The behaviour of materials when subjected to shearing load	189
6.3 The tube cropping process	194
<u>CHAPTER 7</u> <u>GENERAL CONCLUSIONS</u>	
7.1 Introduction	199
7.2 Tube cropping process	199
7.3 Effect of the process parameters	200
7.4 Mechanism of fracture	202
7.5 Theoretical aspects	203
<u>CHAPTER 8</u> <u>SUGGESTIONS FOR FURTHER WORK</u>	
8.1 Development of the cropping rig	204
8.2 Investigation of the fracture mechanism	204
8.3 Development of the theoretical analysis	205

	<u>Page</u>
<u>APPENDIX I DESIGN OF LOAD CELLS</u>	206
<u>APPENDIX II COMPUTER PROGRAMME</u>	208
<u>REFERENCES</u>	211

SYMBOLS

A	Mean radius of the tube
A_c	Current area of cross-section
A_f	Final area of cross-section
A_0	Initial area of cross-section
B	Plastic modulus
D	Deflection of blade
D_{max}	Deflection at maximum load
D_i	Inside diameter of tube
D_m	Mean diameter of tube
D_o	Outside diameter of tube
E	Young's modulus
G	Shear modulus
H	Length of flat
L	Decay length
L_c	Decay length on constrained tube
L_f	Decay length on billet
L_1	Length of the longitudinal hinge (billet side)
L_2	Length of the longitudinal hinge (constrained part)
M_0	Limiting moment without shear
M_p	Plastic moment per unit length of tube wall
P	Load
P_{max}	Maximum load
Q_0	Limiting shear without moment
R	Instantaneous radius of the tube
R_i	Inside radius of tube
S_1	Height of the deformed triangular shape (billet end)
S_2	Height of the deformed triangular shape (constrained part)

T	Thickness of the tube wall
T_q	Torque
T_1	Tension on the tight side
T_2	Tension on the slack side
UTS	Ultimate Tensile Strength
W	Total plastic work
W_A	Work done in flattening the top surface of billet
W_B	Work done in deforming the top surface of tube
W_C	Work done in changing the curvature from $1/A$ to $1/R$
W_D	Work done in stretching
W_1	Work done in the longitudinal hinges of billet
W_2	Work done in the longitudinal hinges of tube
W_3	Energy dissipated by mismatching
W_4	Work done in the curved hinge across the tube
W_5	Work done in the transverse hinge
Y	Yield stress in simple tension
a,b,c,n	constants
d	Mean value of the indentation diagonal
d_{\min}	Minimum diameter of the distorted billet
d_{\max}	Maximum diameter of the distorted billet
e	Engineering strain
k	Shear yield stress
ℓ_c	Current length
ℓ_0	Gauge length
p	Measuring force
x	Chosen length for strain analysis
μ	Coefficient of friction
Ω	Maximum angle of rotation of plastic hinge
Ω_1	Change in the angle due to change in radius from A to R

θ	Angle of contact
ϕ	Angle of twist
ρ	Change of curvature
$\bar{\epsilon}$	Equivalent strain
$\epsilon_1, \epsilon_2, \epsilon_3$	Principal strains
$\bar{\epsilon}_c$	Effective strain at maximum cropping load
$\epsilon_x, \epsilon_\theta, \epsilon_t$	Longitudinal, hoop and 'through thickness' strains respectively
γ	Shear strain
$\bar{\sigma}$	Equivalent stress
σ_f	Stress at fracture
σ_0	Flow stress
$\sigma_1, \sigma_2, \sigma_3$	Principal stresses
τ	Shear stress

CHAPTER 1

GENERAL INTRODUCTION

1.1 INTRODUCTION

Manufacturing as an activity can be defined as "the making of goods and articles by hand or, especially, by machinery, often on a large scale and with division of labour" [1]. It has been practiced for several thousand years, beginning with the production of stone, ceramic, and metallic articles. Since the advent of the industrial revolution at the end of the 18th century, development has been marked by the rapid succession of milestones in various fields such as casting, machining, deformation. Even today, in a developing country like India, these ancient crafts are practiced, although on a small scale, by the village blacksmiths and goldsmiths for making agricultural tools and jewellery.

One of the shortest routes from raw material to finished product or the first phase in the manufacture of any component is that of melting the metal and pouring it into a shape that approaches that of the finished component or ingot. An ingot of metal has very little use until it is formed into a shape. An ingot can then be heated to above the critical temperature, so that the metal is reasonably soft and easy to work. The metal is then hot-worked by a process such as rolling, extrusion, or forging. These processes produce material in the form of sheet, strips, or bars. Because of scaling and other disadvantages of working steel at elevated temperatures, most ferrous metals are cold-worked or cold-finished after hot-working to obtain good surface finish, high dimensional accuracy, and improved mechanical properties. The small-scale processes which are used in the cold-working

of metal are wire-drawing, tube-drawing, deep drawing, sheet bending, roll forming, pressing, stretch forming, tube and section bending, 'impact' extrusion, 'impact' forging and coining [2].

Thus, most metallic materials are subjected at one or other stage of processing, to plastic deformation. This means that the shape of the work piece is changed without its volume being changed (unlike machining) and without it being brought into the liquid state (unlike casting). These processes are of great interest to the production engineer, since they are flexible, can be combined in different ways, and studied to improve the overall economics of production. Over recent decades techniques of metal forming by plastic deformation have been developed and are increasingly being used for the following two reasons: conservation of material is achieved by the manipulation of the metal into the desired shape rather than by the wasteful machining or cutting away of surplus material, and improvement in the physical properties of materials such as surface hardness and overall strength [3].

In general the material used in the manufacture of engineering components is purchased in bar form, commonly in the rolled, drawn or extruded condition as explained above. Many sectors of the hot and cold metal forming industry have a demand for a wide range of materials in discrete lengths known as billets or crops. These billets, which are needed in large quantities, can either be produced by machining or by a chipless forming process such as cropping or shearing.

Since the end of the Second World War, increasing attention has been directed at widening the scope of chipless metal forming methods [4]. Chipless billet production methods meet the criteria of minimum intrinsic cost and highest productivity, and are exemplified in such specific processes as cropping, billet breaking and "planar cold-flow shearing" [5]. While a logical production sequence would therefore seem to be

chipless billet separation followed by chipless forming, certain factors offset the advantages which chipless separation would appear to hold over the chip-producing counterparts. Since the cost of the formed article reflects the total cost of producing the billet, it follows that the cheapest and most productive method is the most attractive [6].

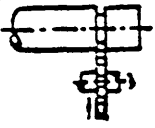

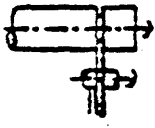

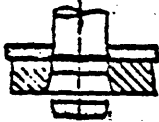


It is well known that cropping is by far the cheapest method of billet production because of the material saving and the process is readily adopted for automation leading to high productivity. However, cropped billets suffer from both geometrical distortions and metallurgical defects. Over the last decade a great deal of effort has been devoted to the design and development of cropping tools and techniques which yield improved billets and these have shown some measure of success. In this country, the mechanics of the process have been investigated in detail, particularly at the Department of Mechanical Engineering, University of Birmingham. So far most of the research in this area has been done on solid bars. Very little information is available on the cropping of tube and sections and hence it has been decided to investigate the behaviour of thin-walled metallic tubes subjected to shearing loads.

1.2 DIFFERENT TECHNIQUES OF BILLET PRODUCTION

As explained earlier, a billet or slug is a piece which has been produced from bar stock by chip producing processes such as sawing, parting off, abrasive cutting or by chipless separation processes such as cropping, blanking, cross-rolling, guillotining. The advantages and limitations of these processes are summarized by Ahmed as shown in Table 1.1 [7].

A narrow slitting cutter becomes a cold saw. When the teeth are laid out into a straight line, one obtains a hacksaw or, if the saw blade

TABLE 1.1: TECHNIQUES OF BILLET PRODUCTION [Ahmed (7)]

	ADVANTAGES	PROCESS	LIMITATIONS
CHIP PRODUCTION TECHNIQUES	Minimum distortion. No limit for billet shape. Suitable for large sizes. No work-hardening. Relatively inexpensive equipment.	<u>Sawing:-</u> 	Burrs at edges. Material losses in the form of chips (high for short billets). Relatively slow.
	Minimum distortion. Accurate lengths for short billets. No work-hardening. Relatively faster.	<u>Parting-off:</u> 	Projections at billet centre. Material losses. Suitable for circular billets only.
	The fastest metal cutting technique. No geometrical distortion. Suitable for high strength materials.	<u>Abrasive cutting:</u> 	Hardening of the sheared surfaces. Burnt edges due to heat generation. Material losses. Relatively expensive.
CHIPLESS TECHNIQUES	No material losses. High productivity. Cheapest as-cropped billets.	<u>Cropping:</u> 	Severe distortions and work-hardening. Not suitable for large sizes. Often needs annealing and sizing.
	High productivity. Wider choice of billet profiles. Piercing can be combined.	<u>Blanking:</u> 	High material waste. Limited plate thickness. Burrs at edges.
	No material losses. Minimum metallurgical defects. High productivity.	<u>Cross-rolling:</u> 	Limited to circular bars only. Semispherical ends. Very small diameters.
	No material losses. High productivity.	<u>Guillotining:</u> 	Severe distortions. Suitable for plates only.

is flexible and made into an infinite loop, a band saw. A plane perpendicular to the lathe axis is produced by moving the single point tool in the carriage so that the feed motion is toward the centre of the lathe. Parting off accomplishes the same task but two surfaces are simultaneously generated (see Table 1.1). An abrasive wheel can cut ferrous and non-ferrous bars. Cutting action depends upon the abrasive grains in the wheel. Thus all materials can be converted into billets by any of the above chip producing processes [8-10]. They are generally slow, expensive, and result in considerable waste of material, but the form and surface conditions are good. Six different chip producing processes are compared with shearing by Widmont [11]. His investigation shows shearing to be clearly the cheapest method and abrasive cut-off the most expensive.

The Russians have developed a cross rolling process for the continuous production of steel balls, and other components of small length to diameter ratio [12]. For the manufacture of rolls on one side may be plain, and the other side may have a helical rib of a pitch corresponding to the length of the rollers required, the arrangement being shown in Table 1.1. As the bar is carried through the pitch zone, the rollers are progressively severed as the height of the rib increases. Similarly rings for ball and roller bearings have been produced with some modifications. Guillotining is almost similar to shearing and is suitable for plates. Guillotine shears can also be equipped with simple straight blades or with two or more short blades having specific shapes [13]. Blanking from strip or plate, and cropping from bar are shear or fracture processes. In blanking, the product is a shaped piece of metal punched from a strip [14]. Stainless steel razor-blades, for example, are produced by blanking. Cropping involves the shearing of a long bar into short pieces, and is normally used for preparing billets

for hot and cold forming processes. Unlike chip producing processes, each one of the chipless forming processes has a special purpose and hence confusion exists as to the best method and type of process to use for the most economical production of billets.

Each method has its particular advantages and disadvantages and the ultimate choice is usually a compromise between the often conflicting claims of cost, convenience, accuracy, and quality required of the billets [15]. The distinction between billets produced by the different chipless processes lies principally in the appearance and properties of the fracture surface and the amount of work hardening in the immediate vicinity of that surface. On the whole, cropping is faster, cheaper, and more economical but can lead to loss of form and introduce defects. Perhaps these are the main reasons why cropping is the most widely used process at the present time.

1.3 THE CROPPING PROCESS

Cropping is essentially a shearing process. For example, simple shear occurs in cutting a paper by ordinary hand scissors. Shearing action can also be observed in the action of a chisel or in the action of two counteracting shearing knives. Shearing is commonly applied to large sheets of metal and strip stock, because it is the only logical method of cutting off. Shearing of sheets and plates is broadly classified by the type of blade used, namely, straight or rotary. Straight blade shearing is used for squaring and cutting flat stock to the required shape and size. It is most often used for square and rectangular shapes, although triangular and other straight-sided shapes are also sheared with straight blades. Rotary shearing is used for producing circular or other contoured shapes from sheet or plate. In all cases, the final

effect of shearing on the material ought to be the same, namely, the separating of two adjacent sections of the material by means of a reciprocal translation.

The terms "cropping" and "shearing" have long been used synonymously in this country. However, cropping is an established name for shearing bars and sections. Organ and Mellor have suggested that shearing should be applied to the process in which the stock is severed progressively from one side to the other by an angled blade and cropping only to processes involving fracture of the bar when failure is induced simultaneously across the entire cross section [16]. Thus the cropping blade contacts the whole of the top surface of the bar and a suitable unidirectional crack is initiated and propagated between the blade cutting edges with the minimum of prior permanent plastic distortion, that is, fracturing is completed with the minimum penetration of the blade. In conventional cropping, bars are cropped between upper and lower blades in which only the upper blade is movable. As the upper blade is forced down parallel to the stationary lower blade in a plane perpendicular to the axis, the bar is caused to fracture and final separation occurs between billet and bar, as shown in fig. 1.1.

1.4 CROPPING TECHNIQUES

In conventional cropping, the billet is subjected to an instantaneous impulse from the moving blade. The blade and billet then move together and remain in contact until final separation occurs between the billet and the remaining bar. This occurs after a finite penetration of the moving blade. In the absence of any constraint, the bar would rotate under the action of the forces of the blades and would also elongate owing to the compressive stress developed under the moving blade. This

would cause the stationary blade to move away from the face of the moving blade. As shown in fig. 1.2, the bar is constrained in a work holder. In this open-tool cropping, the axial movement of the bar is restricted. However, this would create the bending of the off-cut, as this is the most serious factor affecting billet quality. Bending of the billet induces a non-uniform stress field across the cross-section of the bar, which interferes with the linear propagation of the crack. Consequently, over a period of time various techniques have been developed, aiming at reducing or eliminating the asymmetry of forces during cropping. In the single crop tool, bending can be minimized if the underside of the billet is supported during cropping or the billet is contained wholly within the closed moving blade [17]. A direct way of supporting the billet during cropping is by employing 'closed' type blades which encircle the bar profile, as shown in fig. 1.3. It is a good technique but it limits the size of bar. This can have a significant effect on the cost of billets of small length to diameter ratio, which are so often required for cold-forging operations. A similar technique, which avoids this feeding problem, uses 'split' type blades with counter pressure on the opposing halves of the tool, as shown in fig. 1.4.

The Hungarians have developed a technique to improve the quality of billets. It is known as "Planar Cold-Flow Shearing". As shown in fig. 1.5, the bar stock is fed through a closely fixed blade, into a similarly closely fitting moving blade and against an abutment. Before and during blade penetration, an axial load introduces a high value of compressive stress in the region of deformation, and the object is to suppress all tendency for a crack to occur. This leads to a mirror-like finish as the fracture is suppressed and controlled. The process is successful for small size bars of relatively soft materials. A new

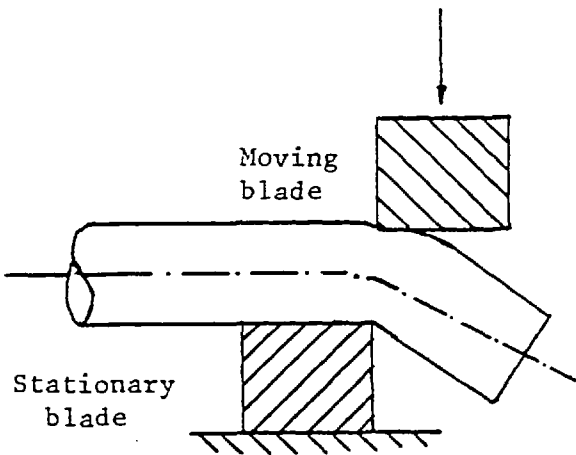


FIG. 1.1. CONVENTIONAL CROPPING

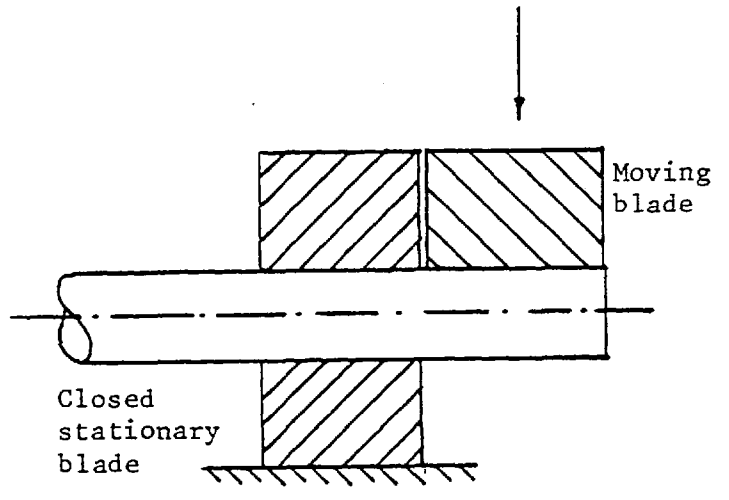


FIG. 1.2. OPEN-TOOL CROPPING

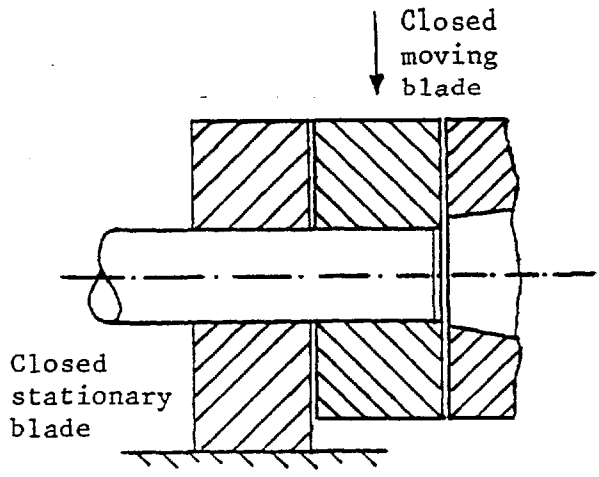


FIG. 1.3. CLOSED-TOOL CROPPING

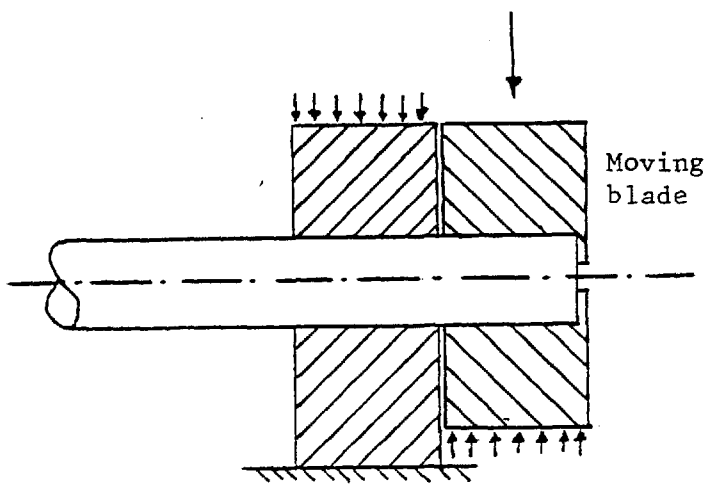


FIG. 1.4. COUNTER-PRESSURE CROPPING

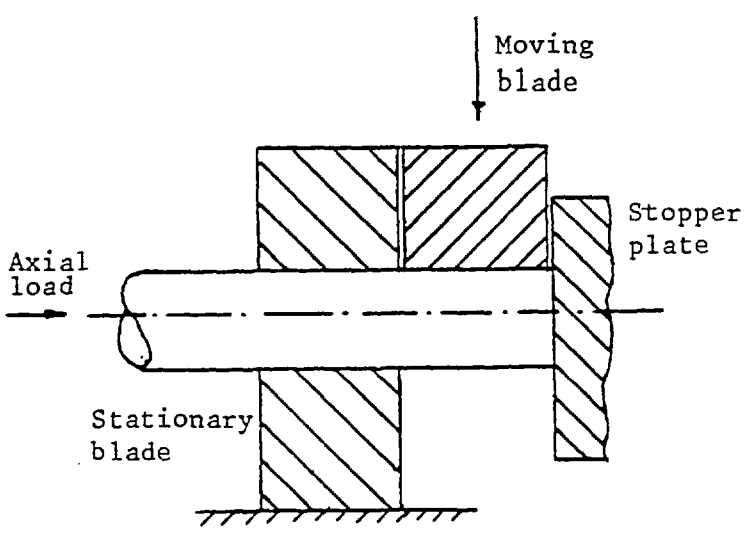


FIG. 1.5. COLD-FLOW SHEARING

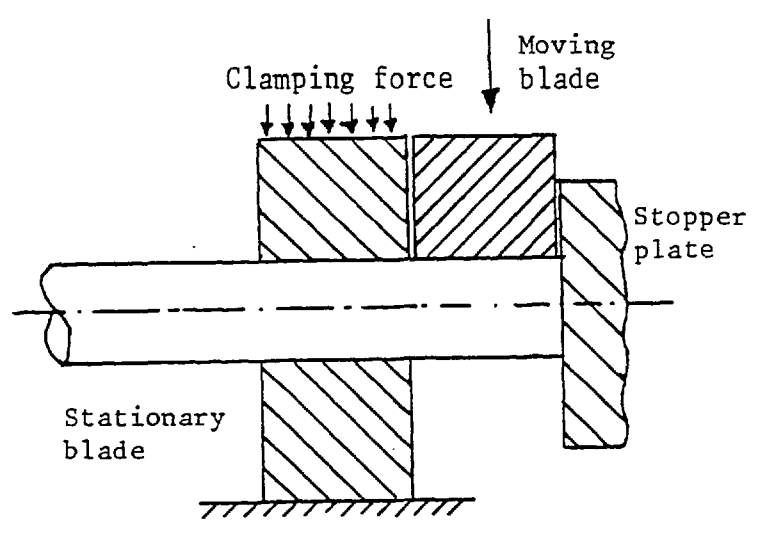


FIG. 1.6. CLAMPED SHEARING

cropping method 'clamp shearing' has been developed by Nakagawa, which makes it possible to obtain a sheared billet with a smooth sheared surface and high dimensional accuracy [18]. It is derived from cold-flow shearing. As shown in fig. 1.6, the bar on the feed side is held and clamped vertically by a clamping plate and the end surface of the bar on the cutting-off side is in contact with the stopper plate and is also restricted to move axially. Due to this restriction, an axial pressure is generated, leading to improvement through reduced bending and partial suppression of fracture.

Double and multiple cropping techniques have also been developed [19]. "Petro-crop" machines have been developed especially for high speed cropping by Das and Tobias [21-22]. They have concluded that high cropping speeds lead to substantial improvements of billet quality.

1.5 CROPPING PARAMETERS AND THEIR EFFECTS

General cropping parameters are cropping configuration, blade clearance, blade geometry, blade velocity, cross-sectional shape of the work piece, length to diameter ratio of billet, material and temperature. These parameters influence the quality of billet, the forces required for cropping and the stresses developed in the cropping blades. Investigation of the cropping process has generally involved an experimental approach in which the process parameters are altered one at a time and the effect on plastic deformation of the bar and billet observed, the crack initiation and propagation in the work material, and the forces involved. However, many of the process parameters interact and their individual effects cannot be effectively isolated.

Several investigators have concluded that unsupported cropping should be avoided in designing cropping tools to minimize the bending

effect. The choice of blade clearance depends on the material to be cropped, its metallurgical condition, the bar geometry and the conditions of bar and billet constraint. Literature in this context reveals that too great a clearance produces rough cropped faces with multidirectional fracture surfaces in the centre of the billet, or a scar at the perimeter of the billet or if the clearance is further increased, the crack initiated at one blade runs beyond the second blade before a crack can be initiated at that blade. On the other hand, if the clearance is too small, transverse fracture surfaces are formed which tend to form a narrow transition zone between the central area of fracture surface and the peripheral region in which tongues of material are formed. In cropping ground bars across the diagonal, using semi-circular blades, Zapf found that often no satisfactory fracture surface is obtained if the blade clearance remains constant throughout the cropping operation [22].

Herbst found that the cropping surface of blades had a minor effect on the geometry of the cropped billet [23]. However, the quality of billet can be expected to deteriorate with increasing blade wear [24]. The quality of billet is normally influenced by blade velocity. Organ found that high cropping speeds result in a dramatic improvement in billet quality of a wide range of materials [25]. However, velocity has little influence on high strength steels.

In general, the quality of cropped solid billets is influenced by billet length only in the cropping of billets having length/diameter ratios less than unity. Distortion of the peripheral surface increases with decreasing length/diameter ratios below unity and this limits the minimum length of billet that can be successfully cropped [23].

Ductility of bar material is an important parameter to be studied in cropping. There is an optimum ductility in metals for cropping, and departures from this optimum can lead to either increased distortion

or uncontrolled cracking arising from the non-uniform stress field across the section caused by the uneven loading on the section [26]. This stress field results in surface irregularities and defects and distortions of the original cross-section.

The ratio of the cropping load at the test temperature to that at room temperature decrease with increasing temperature [27]. Distortion is also dependent on billet temperature. It has also been stated that loss of parallelism is least for cropping material at 350 °C, but diametral distortion is least when billets are cropped at -196 °C.

1.6 ORIGIN OF THE PRESENT WORK

The majority of scientists believe that the best way of bridging the energy gap, when oil runs out towards the end of the present century, is nuclear energy. It is the most concentrated form of energy, made accessible by nuclear reactors. The energy contained in one kilogram of uranium, if it were all to be released in a nuclear reactor, would be equivalent to that produced by burning some 3000 tonnes of coal [28]. It is not, of course, quite that simple for several reasons. If suitable reactors and other facilities are provided, it becomes possible to exploit uranium. The most recent development in this field is the fast breeder reactor which breeds a new fuel in quantities as large or even larger than it consumes. Several fast breeder reactors have been built and tested in advanced countries of the Western world like the U.S.A. and the U.K. and the feasibility of achieving a breeding ratio that is greater than one has been established [29]. In this country, an Experimental Fast Reactor has been in operation since 1959 at Dounreay. The next step is the demonstration that a practical large-scale fast breeder reactor can be built.

Consequently, a prototype Fast Reactor has been built with the ultimate requirements of a large commercial plant in mind, resulting in features being incorporated directly applicable to larger power plants. The major contribution made by the PFR is the confidence generated in the U.K. that, provided the size of components is not extrapolated too far, an early commercial plant of 1300 MW electrical output is entirely feasible. The proposed commercial station will use fuel sub-assemblies and a core support arrangement almost identical to the PFR system. The fuel is in the form of cylindrical pellets, initially as a mixture of oxide UO_2 and PuO_2 , inserted into stainless steel tubes. The outside diameter of the tubes is approximately 0.230" and the thickness is 0.015". This small diameter is dictated by the high peak rating. The active length is 36" and there is an axial breeder of natural uranium 8.97" long above and below the core region. The fuel rods are made up into hexagonal subassemblies each containing 325 fuel rods. The core contains 78 subassemblies, and there are a further 42 subassemblies of natural uranium rods in the radial breeder.

One feature distinguishes nuclear power technology from all others: the waste material. Unlike the ash, say, from a coal fired power station, the used fuel from a nuclear power station contains both very valuable material and uniquely troublesome radioactive waste. Hence, fissile uranium and plutonium have to be recovered from the spent fuel. It is not that they are too valuable to throw away, but recovering them is necessary to avoid the problem of disposal. Plutonium is far too dangerous to be released into the environment. Accordingly, the irradiated fuel from a reactor is usually 're-processed'.

For the purpose of the re-cycling of commercial fast-reactor fuel, spent fuel elements must be broken down in such a way that the fuel can be extracted from the stainless steel tubes. The irradiated fuel

rod bundles have to be cropped into short lengths of approximately one inch, followed by leaching out of the burnt fuel from the resulting chopped pieces by nitric acid. An experimental investigation of tube cropping has been proposed to characterise the process and to ensure that under the cropping action, the tubes do not distort to the extent that fuel extraction is impaired. The present work focusses on single tube cropping, both empty and filled, and it is expected to guide the later programme, the cropping of the tube bundles. This project is of great practical interest to the United Kingdom Atomic Energy Authority, Dounreay. *In this context, the quality of the tube essentially refers to the distortion of the billet and the tube which should be a minimum.*

1.7 APPROACH TO THE PROBLEM

Different cropping techniques, general defects in cropped billets, and their effects have been discussed above. These discussions were based on solid bar cropping because of the lack of literature on tube cropping. Since this investigation of the cropping of single thin-walled tubes is *one of the very few* of its kind, it was decided to investigate the tube cropping process in detail, starting from conventional methods. However, literature on bar cropping is expected to guide the present work.

The parameters in single tube cropping can be divided into two groups, namely (1) Dependent variables and (2) Independent variables. The dependent variables are (a) cropping load variation with time throughout the cropping action and (b) tube cross-sectional distortion after cropping. An example of the measure of distortion is shown in fig. 1.7. It is the ratio of minimum diameter to the maximum diameter of the cropped end of tube (which tends to unity for no distortion). The major independent variables are (i) Tube dimensions - diameter and thickness, (ii) Tube material properties, (iii) Cropping blade velocity

and (iv) Cropping blade geometry. A number of parameters obtainable from the stress-strain curve may be used to characterise the properties of the material under cropping conditions. Ductility is particularly important in the present study because of the low values shown by irradiated metal and because of its anticipated significance in relation to distortion. An approximate measure of material strength is suggested by the literature to be the true tensile stress at instability. However, the ultimate tensile strength may prove to be a more readily attainable value which is equally significant. The independent variables are considered to be of prime importance and the experimental programme has concentrated on fully investigating their effect on the two dependent parameters, distortion and cropping load. A brief description of the experimental programme is given below.

The material properties have been determined for each tube size and material included in the investigation, by evaluating the stress-strain curve to fracture in simple tension and torsion tests. Axial load is increased incrementally to failure and the extension of a gauge length measured so that a tensile stress-strain curve up to the point of failure can be produced. From this curve various measures of tensile strength can be determined, for example, yield stress and ultimate tensile stress. As a measure of material ductility, reduction of cross-sectional area at fracture is the most relevant parameter and this has been determined for each test. Alternatively, when this proves too difficult, the percentage elongation at fracture of a specified gauge length, constant for all specimens, can be more easily measured.

Since tube cropping is largely a shearing action, it was proposed that a shear stress-shear strain curve could also be established for each tube size and material. This may be achieved by a torsion test in which one end of the cylindrical specimen is gripped and an incrementally

increasing torque applied to the other end. By measuring the angle of twist of the tube for each increment up to failure a torque against angle of twist per unit length curve can be established and from this a shear stress-shear strain curve evaluated. Care was taken in these tests to ensure that the specimen did not fail by buckling rather than torsion. Hardness tests were conducted to determine the degree of relative hardness of the tubes. The results of tests described in this section provided a comprehensive coverage of materials property data for correlation with results from cropping experiments.

For all single tube cropping experiments the tube was supported all round its circumference and a straight-edge blade used for cropping, as shown in fig. 1.8. It consisted mainly of a work holder and a moving flat blade. As the blade makes contact with the tube material, the pressure builds up rapidly, producing a stress field in the material and causing distortion at the cutting edge. After a certain amount of penetration a crack was initiated and propagated at the cutting edge and eventually tube separation takes place. To preserve a measure of consistency throughout the cropping experiments the clearance between blade and work piece support was maintained constant at the minimum value which can reasonably be achieved. The sharpness of the blade was checked at frequent intervals. A constant blade speed of about 0.4 in/sec and a cropped tube length of 1" was proposed for those experiments. It was also proposed that investigations be carried out over a range of material properties and tube dimensions such that the expected parameter values appropriate to commercial fast reactor fuel tubes were adequately covered. The parameters to be measured for each test were as follows:

(a) Variation of cropping load with time throughout the shear action. The load applied was the minimum for cropping.

(b) Dimensions d_{\min} and d_{\max} of the tube cross-section after cropping were as shown in fig. 1.7.

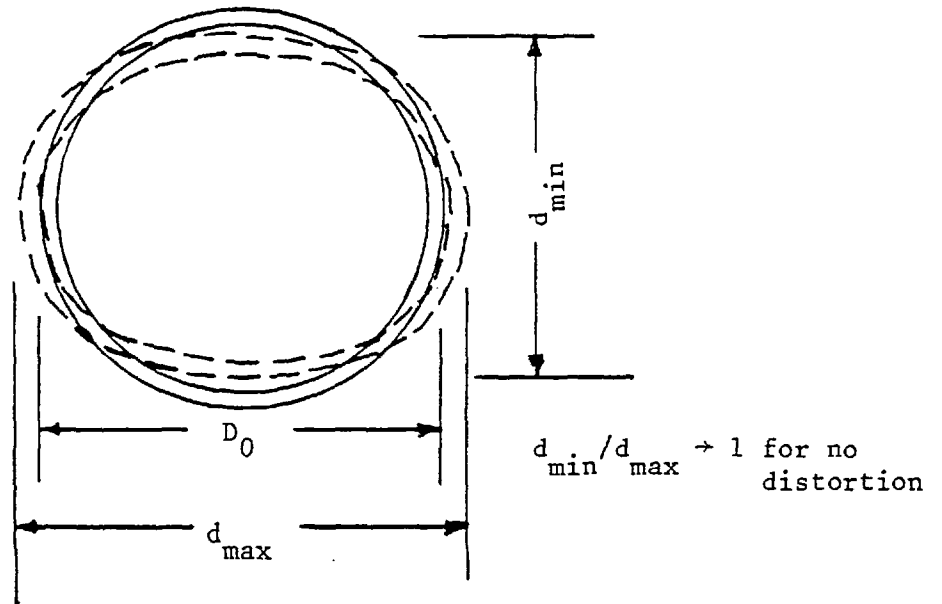


FIG. 1.7. CROSS-SECTIONAL DISTORTION OF BILLET

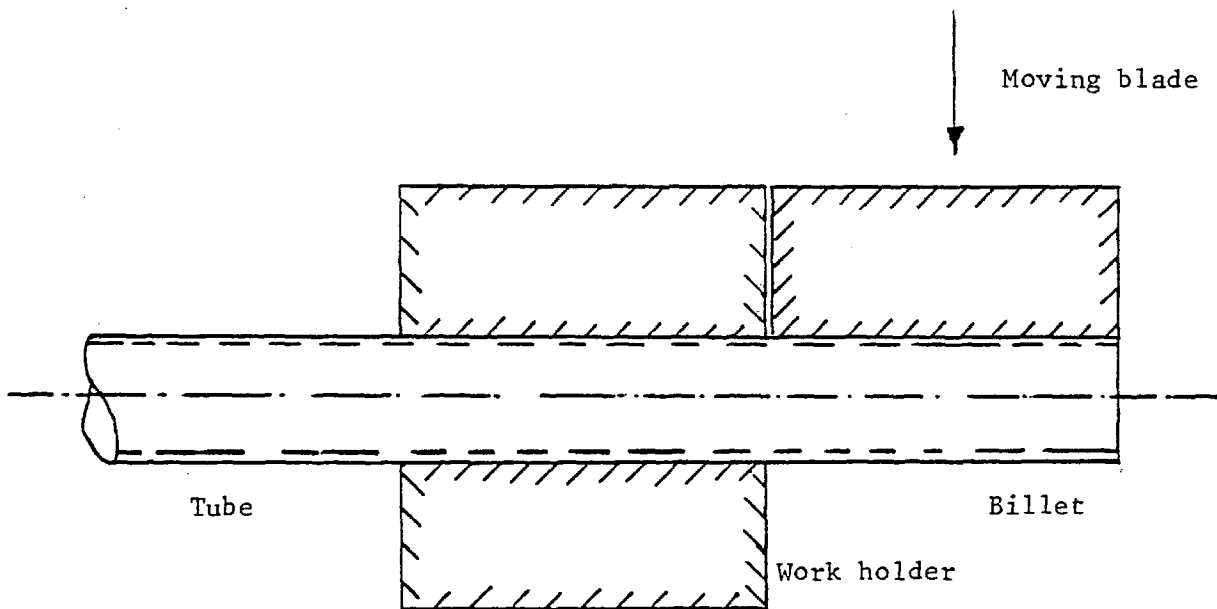


FIG. 1.8. SIMPLE TUBE CROPPING PROCESS

It was also proposed that an attempt be made to obtain high speed cine film of the cropping action to provide some information on the mechanism taking place. In addition to the tests described above, incremental cropping tests were conducted for a number of different materials with various ductilities to explain the cropping cycle in detail. The second stage of the investigation of single tube cropping introduced tube fillings with differing material properties as another variable. Choice of a suitable parameter to characterise the filling material in this instance was more difficult as irradiated fuel is of a brittle ceramic nature. Perhaps ordinary glass and alumina are the nearest equivalent materials to the irradiated fuel. All the above tests were to be repeated for filled tubes. Fractographic analysis was applied in a microscopic investigation to detect the modes of fracture involved in the cropping process. It was proposed that attempts be made to predict the load-deflection diagram up to the maximum load, theoretically.

1.8 AIMS OF THE RESEARCH PROJECT

As explained above, the present problem is purely of a mechanical nature which affects the fuel reprocessing process. A nuclear fuel reprocessing plant is a chemical plant - but it is no ordinary chemical plant. Because its raw material, irradiated fuel, is intensely radioactive, all the operations must be carried out by remote control, behind heavy shielding. The process equipment must be highly reliable, and require a minimum of maintenance. Once in operation it is contaminated by the radioactivity, and any malfunction necessitates months, indeed years, of decontamination before it can be put right. Accordingly, the process line uses as few mechanical parts as possible, and depends instead on gravity flow and simple valves. For these reasons, a thorough

investigation of the tube cropping process must be made and the above proposed programme was expected to fulfil the following objectives:

- (1) A detailed explanation of the tube cropping process at each and every stage of penetration of the cropping tool was required. Different techniques like incremental crop experiments, high speed cinematography, microscopic examination of the cropped surfaces were to be used to explain the cropping cycle in detail.
- (2) A prime requisite of this experimental investigation was to obtain a qualitative knowledge of the effect of independent parameters on the two dependent parameters, distortion and cropping load. This should give some kind of statistical data regarding the cropping parameters. From the data, optimum conditions should be established for any given material to minimize the end distortion of ^{the} cropped billet. The ductility of irradiated fuel and canning depends on the temperature at which the fuel rods are taken from the reactor. Hence ductility is particularly important in the present study.
- (3) An empirical formula was to be established on the basis of the experimental results. These results should be correlated with the material properties.
- (4) A theoretical solution must be developed to predict the load-deflection curve at least up to the point of first shearing. The object of this theory would be to predict the maximum cropping load for any given material and size of a thin-walled metallic tube.

CHAPTER 2

EXPERIMENTAL INVESTIGATION OF TUBE CROPPING PROCESS

AND ITS PARAMETERS

2.1 INTRODUCTION

The experimental work involved in this study can be divided into three parts, namely, an experimental investigation of tube cropping, determination of the mechanical properties of the materials used, and fractography. Details of the cropping rig, its instrumentation, the various techniques used to explain the tube cropping cycle and the effect of cropping parameters are described in this chapter.

Incremental cropping, dye penetrant, high speed cinematography, the conducting paint technique and a technique of using the tube as an electrical conductor have all been employed in this work to study the tube cropping process in detail. Suitable instrumentation has been provided for the continuous monitoring of load variation and deflection of the tool throughout the cropping cycle. For each experiment, the cross-sectional distortion of the cropped billet has been measured using an optical projector. The object of the experimental work was to study the tube cropping process in detail and to investigate the effect of the main cropping parameters for both empty and filled tubes.

2.2 EXPERIMENTAL EQUIPMENT FOR CROPPING

2.2.1 The cropping rig: A rectangular die set with four pillars forms the main part of the cropping rig. Design details are shown in figs 2.1(a) and 2.1(b) and a description of them is as follows.

The four pillar rectangular die set was supplied by Desoutter Brothers Limited of Middlesex, England. Standard die sets are manufactured by them to very close limits. A high quality material, Meehanite grade G.E., is used for the die bolster because it is consistent in quality, close grained, free machining and free from blow-holes. Pillars and bushes are made from good quality steels, case hardened to a depth of 0.0512" with a hardness figure in excess of Rockwell 60c, ground to very close tolerances and with a surface finish of 0.2 μ CLA. This accuracy is preserved by the fitting of oil reservoirs which supply continuous lubrication.

'Daylight' is the term used to refer to the distance between inner faces of the punch holder and die bolster, with the press at the bottom of its stroke. If 'shut height' is specified, this will be interpreted as 'Daylight' plus the thickness of the punch holder and die bolster with the press at the bottom of its stroke. Pillars and bushes are of a length that will ensure that the pillars are approximately 0.197" below the top of the bolster at the bottom of the stroke, thus allowing for successive tool regrinds. Where the daylight dimension permits, the length of bushes fitted will ensure that they are in engagement with the pillars at the top of the stroke.

The main cropping tools were manufactured in the workshop of the Department of Mechanical Engineering, Imperial College of Science and Technology. It consists of a moving blade and a fixed work holder. The material of the blade is high speed tool steel and its hardness is Rockwell 65, c-scale. The dimensions of the blade are 1" x 3/4" x 1/4".

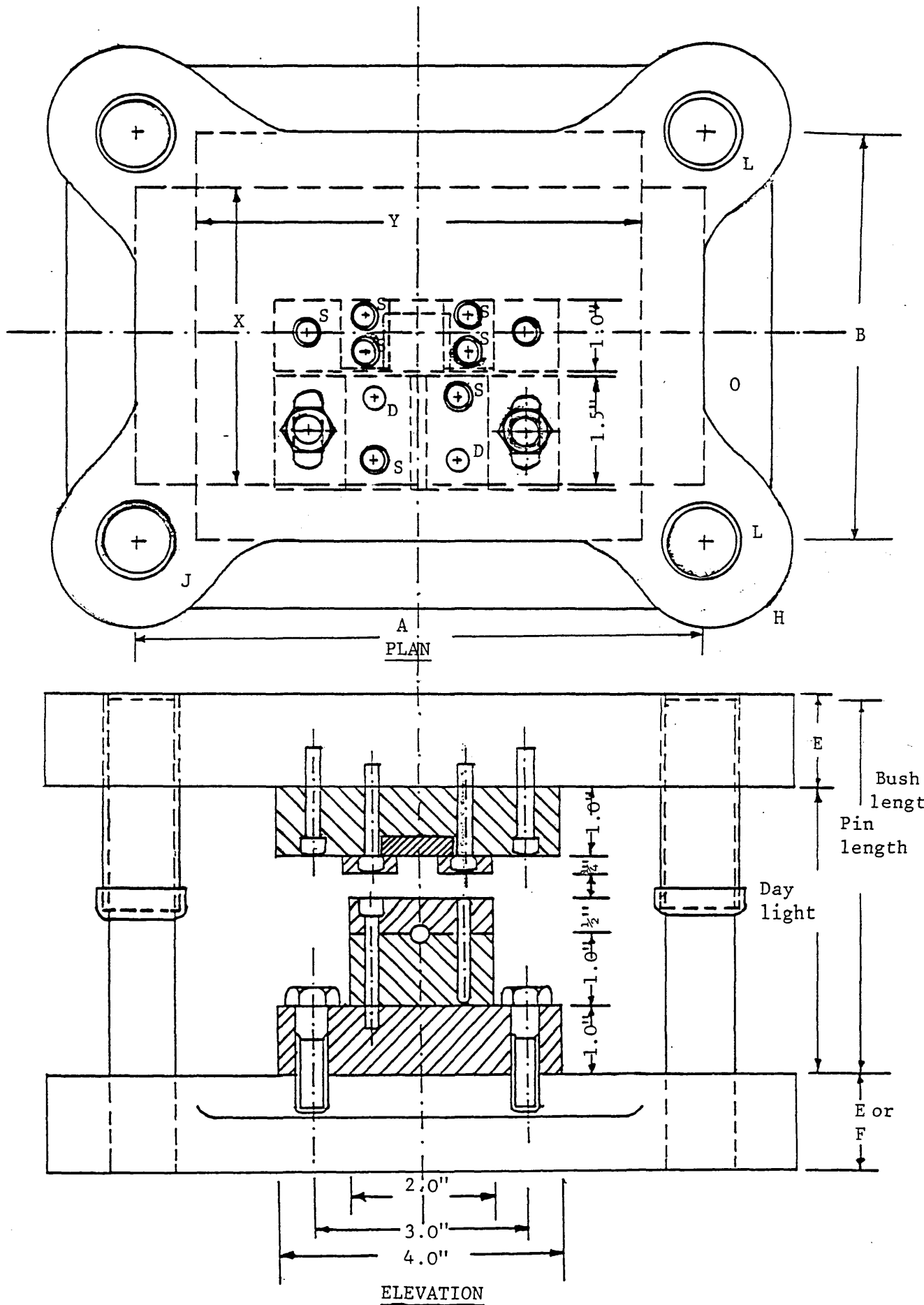
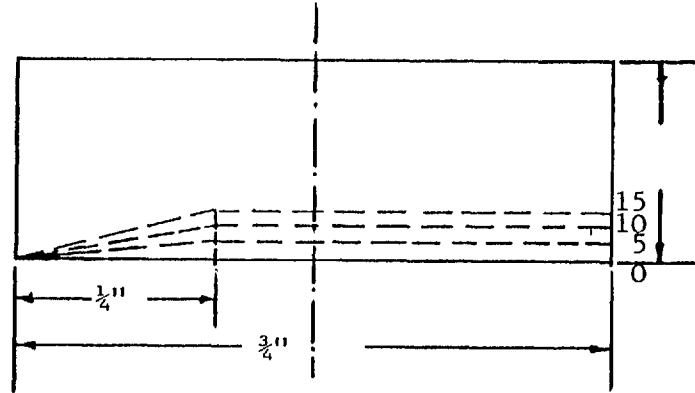


FIG. 2.1(a). FOUR PILLAR RECTANGULAR DIE SET



END VIEW OF TOOL STEEL BLADE
(4 TIMES FULL SIZE)

BLADE DIMENSIONS: $1'' \times \frac{3}{4}'' \times \frac{1}{2}''$

D - DRILL HOLE TO SUIT $\frac{1}{4}''$ DOWEL PIN

S - DRILL HOLE TO SUIT $\frac{1}{4}''$ C/B CAP SCREW

DIMENSIONS IN MILLIMETRES UNLESS OTHERWISE STATED

Scale: Half size

CAT. NO.	DIE SPACE		A	B	E AND F		H	J	L	N	O	BUSH LENGTH RANGE	PIN LENGTH RANGE	APPROX. WEIGHT Kg
	A×X	B×Y			LIGHT TOP & BASE	HEAVY ONLY								
FPR 8	200×100 8"×4"	145×160 5½"×6½"	203.20	146.05	35	45	32	24	25	19	25	50-130	65-200	28

FIG. 2.1(b) FOUR PILLAR RECTANGULAR DIE SET

It is held in position in a mild steel block of 4" x 1" x 1" with two identical supporting pieces. The whole arrangement is screwed to the punch holder of the die-set. There are four blades of the same dimensions with different angles: 0° , 5° , 10° and 15° defining the orientation of the cutting edge of the blade respectively, as shown in fig. 2.1(b).

The material of the work holder is mild steel. It comprises three blocks; the bottom block having a slot and bolt arrangement to enable the clearance between the blade and the holder to be adjusted. During an experiment, this clearance should be a minimum. The sub-assembly is attached to the bolster of the die by means of screws. One half of the tube fits into the top block, the other half into the middle block. The two blocks are positioned by means of dowels and screwed with counter bore screws. Twelve sets of blocks have been made to accommodate tubes of outside diameters ranging from 0.121" to 0.5". A photograph of the experimental equipment is shown in fig. 2.3.

2.2.2 The press: A press for fatigue testing had been designed and built previously under the supervision of Dr. B. Lengyel of the Department of Mechanical Engineering, for the fatigue testing of high pressure cylinders, by Dr. D.C. Harvey [30], as part of his Ph.D. research. Dr. Harvey used the press for the application of combined repeated internal pressure and static or dynamic fluid support pressure to cylindrical specimens of En 25 steel. To carry out the above tests, he needed a machine that would operate at a low cycling rate with a typical container life of 10^5 cycles. The press was designed for a maximum load of 20 tons.

A photograph of the overall layout of the press is shown in fig. 2.2. The press frame and the hydraulic cylinder, the hydraulic valve gear and

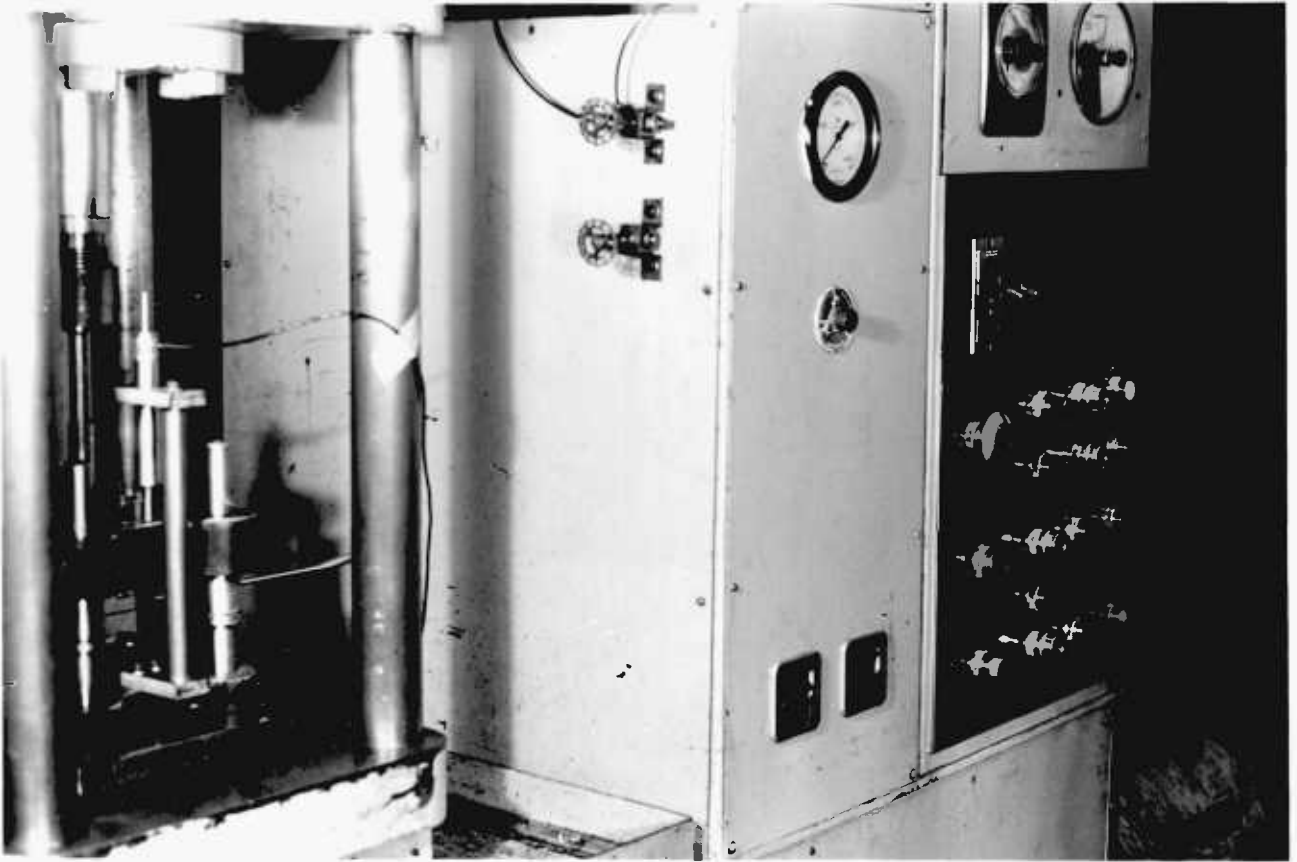


FIG. 2.2. OVERALL LAY OUT OF THE PRESS

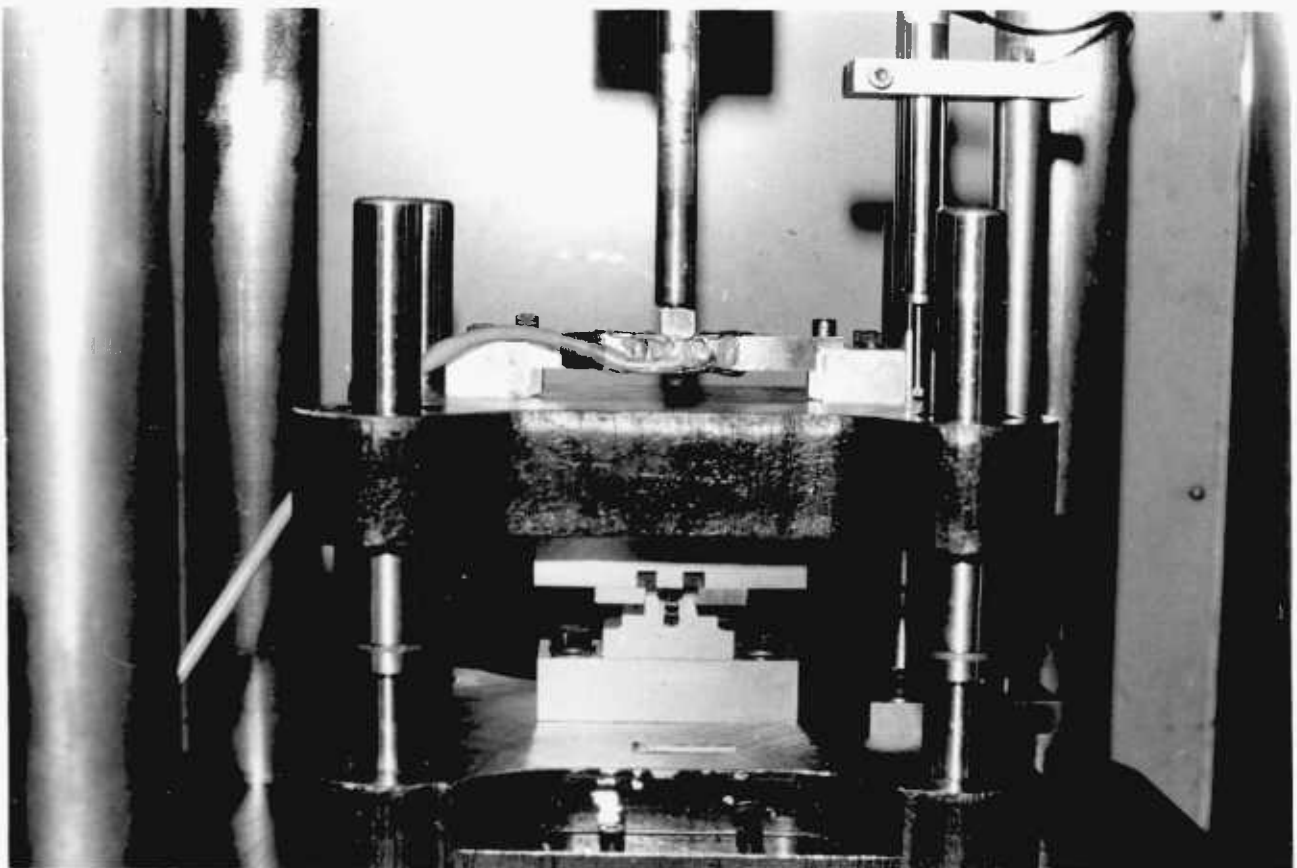


FIG. 2.3. EXPERIMENTAL SET-UP

a separate electrical control cabinet are mounted on a 1/2" thick mild steel table. The table is supported by a welded angle frame which contains an 80 gallon oil tank and hydraulic pump gear. An electric motor is flange mounted to the pumps and extends from the back of the unit. A separate pump and motor unit for supplying and replenishing high pressure fluid to the test rig is mounted above the hydraulic valve gear in the top compartment of the press.

The press frame, which houses the rig under test, consists basically of 19" square, 2 7/8" thick top and bottom plates held in position by four 2½ diameter columns. The spacing between the columns is 12½" which limits the width of test rig which can be accommodated. The test rig rests on the bottom plate and is fixed by placing a 1" thick plate in between the test rig and bottom plate of the press, all being secured with counterbore screws.

Oil is supplied to the system by a pump at a rate variable between 0 and 60 in³/sec and up to a maximum system pressure of 3,500 lbf/in². The flow rate is adjusted by a hand-wheel at the side of the press. By changing the flow rate, the speed of the ram, which presses the top block of the test rig through a load cell, can be varied. The load can also be calculated approximately, knowing the pressure and the diameter of the hydraulic cylinder.

To operate the controls the main switch is first switched on. The motor can be started by pressing the "PUMP ON" button and the pumps will then deliver oil which is directed by the main control valve back to the oil tank. The main selector switch may be turned either to 'HAND' or 'AUTO' and the corresponding indicator lights are then illuminated. It is possible to move the ram by pressing the 'UP' or 'DOWN' button which then energises the appropriate solenoid. When the button is released, the control valve will return to neutral and the ram is held in position.

2.2.3 Instrumentation

The cropping load, the deflection of blade and time throughout the cropping cycle have to be recorded for each experiment to study the velocity of the blade and the load variation with time. The deflection and load measurements are described below.

(a) Deflection measurements: A displacement transducer was supplied by R.D.P. Electronics Ltd., Wolverhampton, having a range of ± 0.5 " which is sufficient to accommodate all the tubes of outside diameter, ranging from 0.121" to 0.500". The type, length and diameter of the transducer are D2-LVDT, 4.75" and 13/16" respectively.

Basically the linear variable transformer type transducer consists of a multi-layer primary winding and two equally disposed secondary windings, all wound on to a suitable former. The coil assembly is mounted inside a steel case which helps to distribute the magnetic flux along the length of the coils. The two secondary coils are connected together in such a manner that the output represents the difference between the voltages induced in them, and in an ideal case this would be equal to zero if no armature is present in the centre of the transducer. This assembly forms one part of the LVDT and the armature and push rod form the other. The armature is a suitable length of high permeability magnetic material mounted into a brass push rod assembly, and it is the displacement of this from the mean position which causes the differential output from the transducer. It does this by increasing the magnetic flux passing through one secondary coil and at the same time reducing the flux in the other. This is the basic principle employed in all LVDT transducers.

This range of transducer is primarily designed to provide a compact and inexpensive, yet reliable, means of measuring or controlling

displacement. The unit is completely sealed and will operate under difficult environmental conditions.

<u>Specification</u>	<u>D2-DC-LVDT</u>
Supply	6 volts D.C. at 50 mA approx.
Linearity	Better than 1% of full scale deflection
Typical sensitivity	3.0 volts D.C. per inch
Temp. coeff. of sensitivity	Less than 0.1% per °C
Recommended load	10 K Ω for low impedance output greater than 1 M Ω for filtered output
Operating temp. range	From -10 °C to +50 °C

The transducer was calibrated in conjunction with a UV recorder. The position of the transducer and its clamping arrangement is shown in fig. 2.3, and the calibration curve obtained from it is shown in fig. 2.4. A resistor in series with the supply enabled the scale to be set to any convenient value for the cropping experiment being carried out, as shown in fig. 2.5.

(b) Load measurement

A load cell was designed for a maximum load of one ton and was cycled for 1000 times at a load of 20% above this in order to relieve any residual stresses which might have been introduced during manufacture. The final material chosen for the load cell was a high strength steel to specification En 24. After machining it was carefully heat treated at 850 °C for an hour and oil quenched at the same temperature. Then it was tempered at 650 °C to obtain a yield strength of between 45 and 50 tons per square inch.

Four 120 Ω electrical resistance strain gauges were secured to the load cell using adhesive designated methyl-2-cyanoacrylate (M-Bond 200 adhesive).

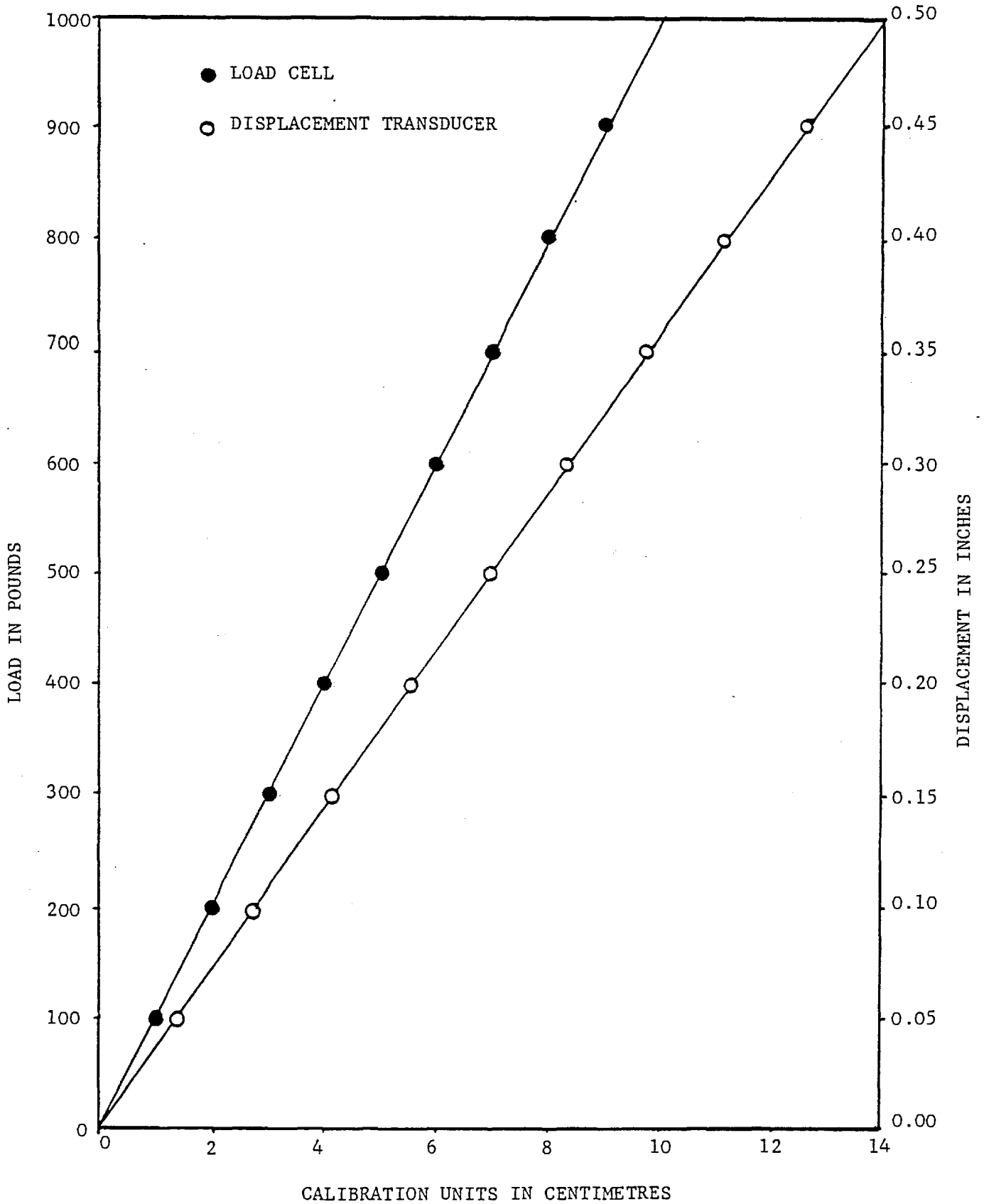


FIG. 2.4. CALIBRATION CURVES

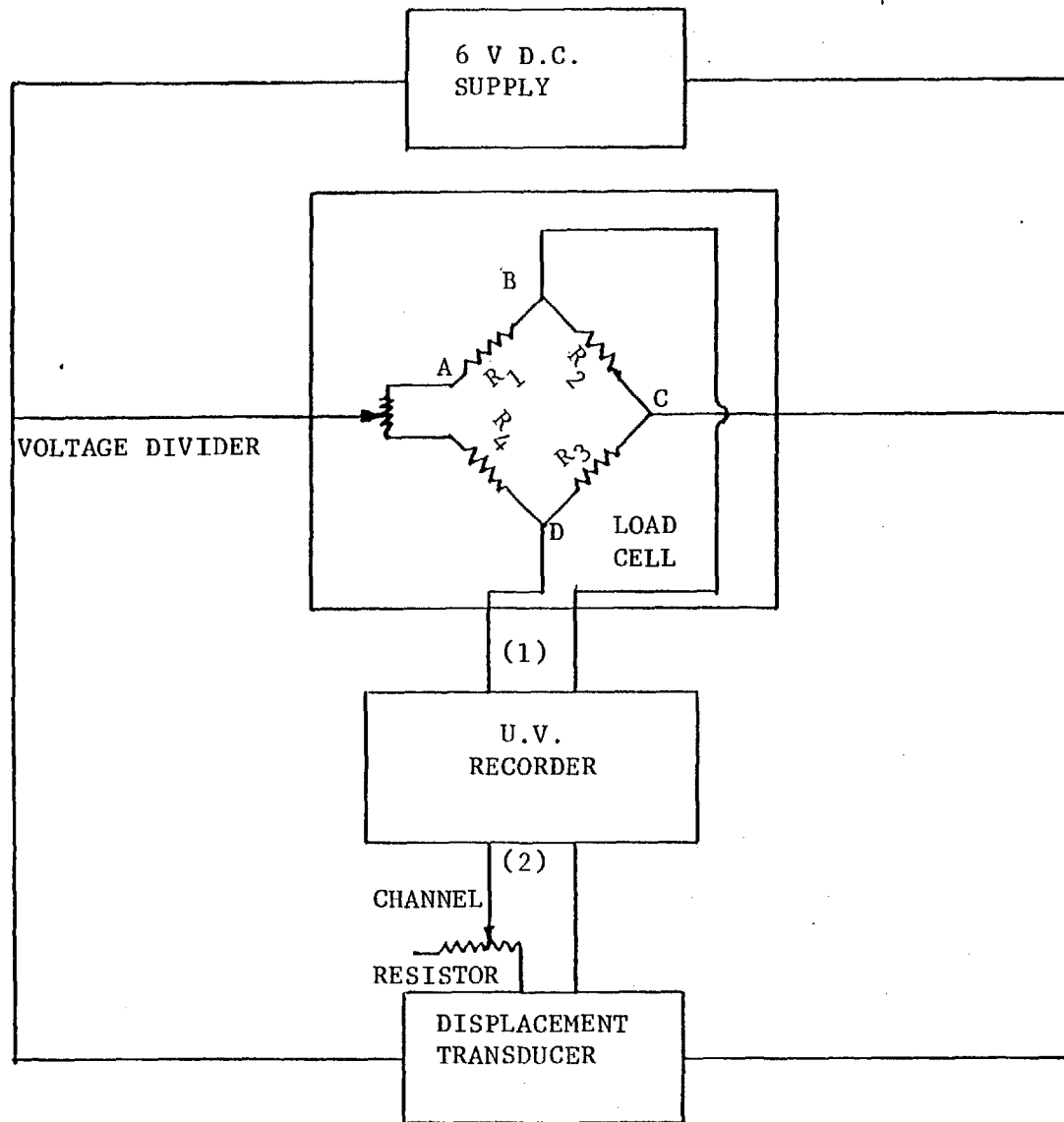


FIG. 2.5. SCHEMATIC DIAGRAM OF THE INSTRUMENTATION

The four gauges form a Wheatstone bridge and by virtue of their position they are self-compensating for changes of temperature. Proper installation procedure was followed in securing the gauges to the load cell. M-Bond 200 was used as the adhesive because of its fast room temperature cure and ease of application. The normal operating temperature for this adhesive is -5°C to $+65^{\circ}\text{C}$ and is compatible with all micro-measurement strain gauges and all common structural materials.

The electrical connections are shown in fig. 2.5. The load cell was calibrated in a Tinius-Olsen Testing Machine which itself is capable of holding and recording load to better than 1%, the accuracy claimed for the galvanometer of the recorder. The calibration curve for the load cell is shown in fig. 2.4.

Later on it was found that one ton load was insufficient for the filled tubes. A conventional compressive load cell was therefore designed for a maximum load of 5 tons. Design details of the load cells are given in Appendix I.

(c) The recording instrument

Continuous monitoring of load and deflection of blade with time was effected by feeding the outputs to an ultra violet recorder, S.E. Laboratories, type 3006, as shown in fig. 2.6.

The galvanometer is the heart of the recorder and can be changed to vary the instrument's sensitivity and frequency response. The instrument houses a series of moving-coil light beam galvanometers mounted in magnetic blocks. The galvanometer drives a mirror which reflects light through a lens system on to light-sensitive paper. The deflection of the galvanometer is amplified optically and provides a displacement on the record proportional to the strain magnitude. The paper speed is controlled by the motor and gear train driving the paper-feed mechanism; it can be adjusted to give various time scales on the abscissa of the record.



1.U.V.Recorder 2.Power pack 3.Junction box

FIG. 2.6. INSTRUMENTS USED IN CROPPING TESTS

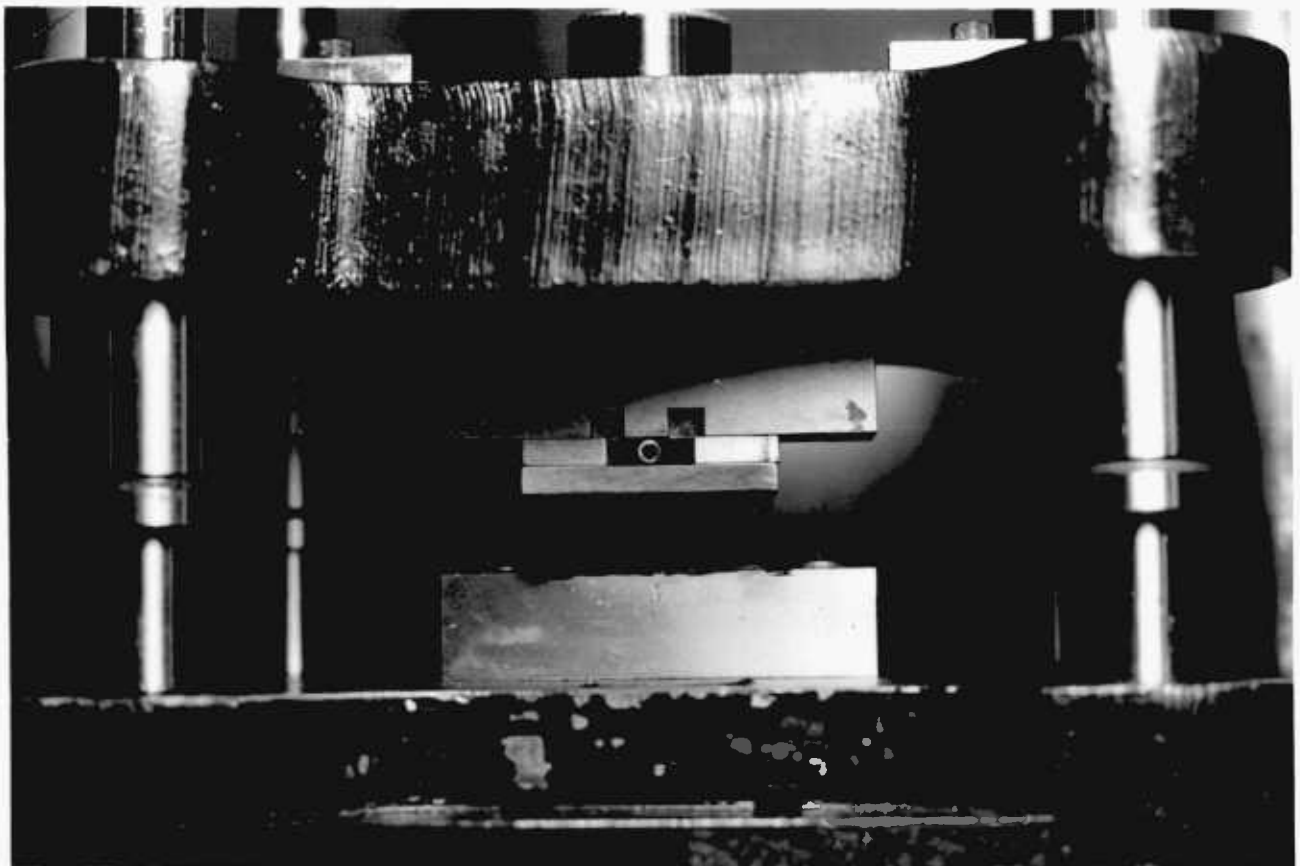


FIG. 2.7. MODIFIED TEST RIG WITH A SUPPORT UNDER BILLET

2.3 SINGLE TUBE CROPPING

2.3.1 Empty tubes

The experiments may be divided into two groups, namely, 1) initial cropping experiments with different velocities of blade and geometry; 2) cropping experiments on all fourteen different tubes at a particular cropping speed for comparison. Two materials, M316 and PE16, of the same size as used in the fast breeder reactor were chosen for the initial experiments.

Six experimental results with different velocities of the blade are shown for the ductile M316 and the relatively less ductile nimonic-PE16. The profiles of the cropped billets and tubes were traced using a "Hilger Universal Measuring Projector". The results are presented in Table 2.1. Experiments were carried out on M316 and PE16 tubes for the different blade angles already mentioned, 0° , 5° , 10° and 15° . Also, experiments were conducted with a support under the billet as shown in fig. 2.7. In all the above experiments the general pattern of load and deflection variation with time are the same except for slight changes in magnitude as shown in Table 2.2.

Experiments were carried out on fourteen different tubes using a flat blade and maintaining a minimum clearance between blade and work holder. The main variables in these experiments were tube size and material. The velocity of the blade was maintained constant at 0.4 inches per second throughout the experiment and three experiments were conducted on each tube. The average values of the load and deflection variation with time of three experiments for each condition were taken and they are shown in figs 2.8 to 2.21. The magnified profiles of three different materials are shown in figs 2.32 to 2.34. The details of tube, velocity of blade, maximum cropping load, deflection of the blade at maximum load, wear of the blade, cross-sectional distortions

of billet and tube with respect to inside and outside diameters are shown in Table 2.3.

2.3.2 Filled tubes

(a) Tubes filled with alumina

The type M446 stainless steel was heat treated at 1050 °C for one hour in air followed by a precipitation treatment for 100 hours at 475 °C. The results obtained from cropping embrittled M446 stainless steel tubes filled with one inch pieces of alumina are shown in fig. 2.22 and the profiles are shown in fig. 2.34. Load and deflection variation with time for the M316 and PE16 tubes filled with one inch pieces of alumina are also shown in fig. 2.23 and the results are presented in Table 2.5.

(b) Tubes filled with glass

The glass rods supplied by 'The Jencons (Scientific) Ltd., Herts, are of high borosilicate heat resistant (pyrex type) glass processed to 0.0005" tolerance. All the tubes were filled with the appropriate glass rods, maintaining a constant clearance of about 0.002" between tube and filling. Experiments were carried out on all fifteen filled tubes, maintaining a constant blade velocity of 1.0" per second, and the load deflection variations with time are shown in figs 2.8 to 2.21. The maximum cropping load, deflection at maximum load and cross-sectional distortions are shown in table 2.4. Some of the profiles are shown in figs 2.32 to 2.34.

The effect of clearance between tube and filling was studied by varying the clearances, namely 0.0025", 0.0015" and 0.001". For this purpose, M316 reference tube was chosen and the results are presented in Table 2.5 and load, deflection variations with time are shown in Figure 2.24.

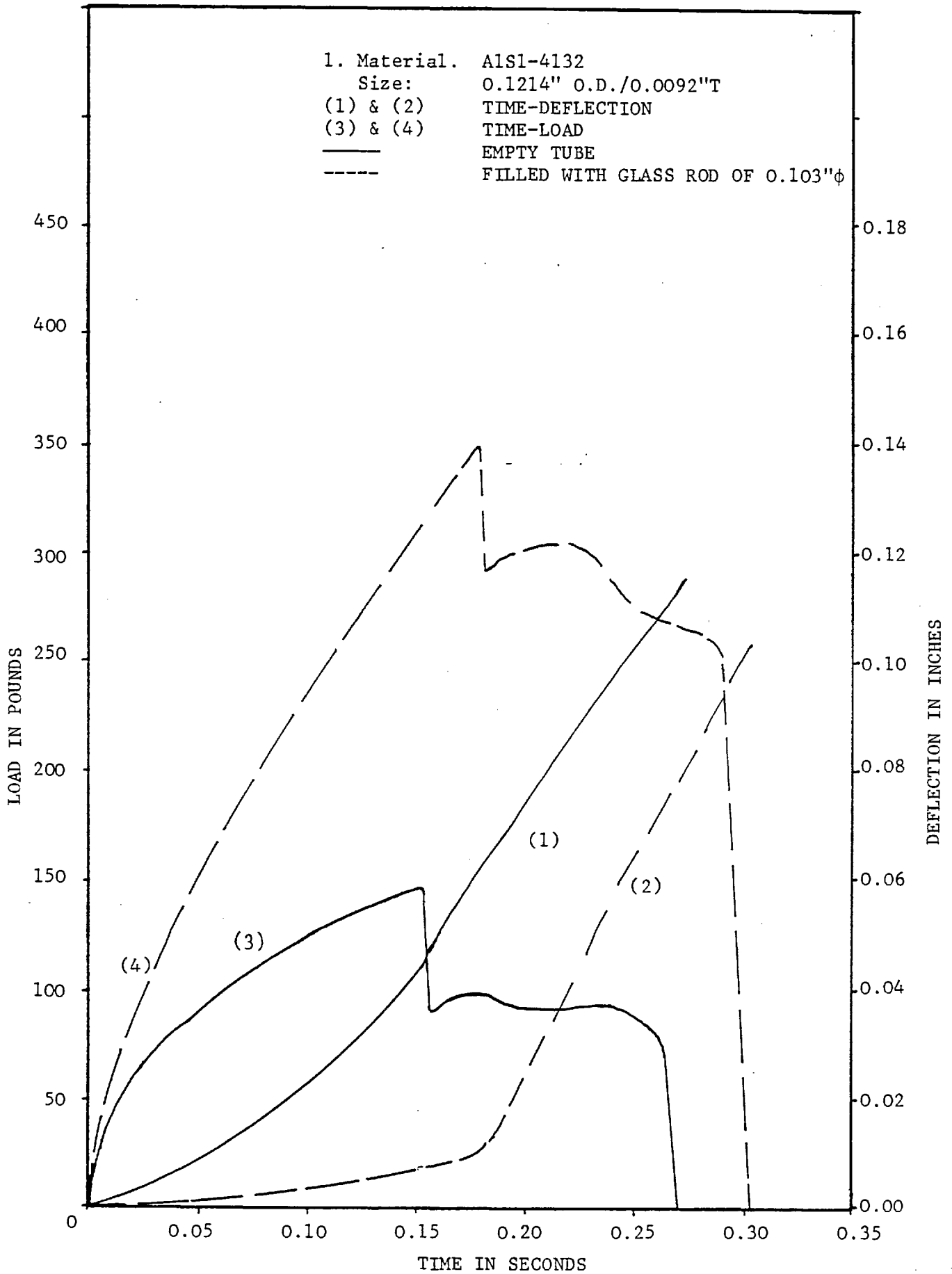


FIG. 2.8

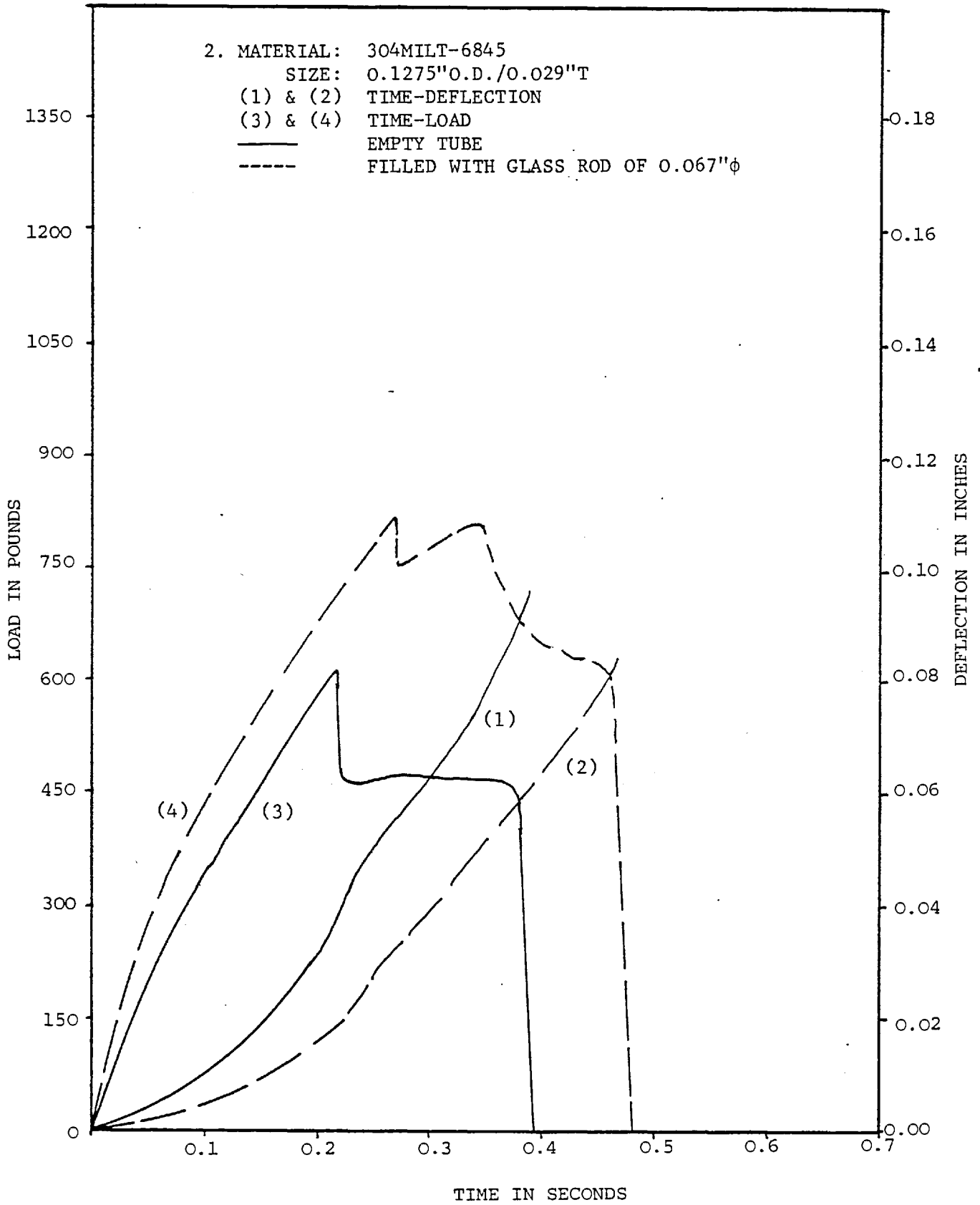


FIG. 2.9

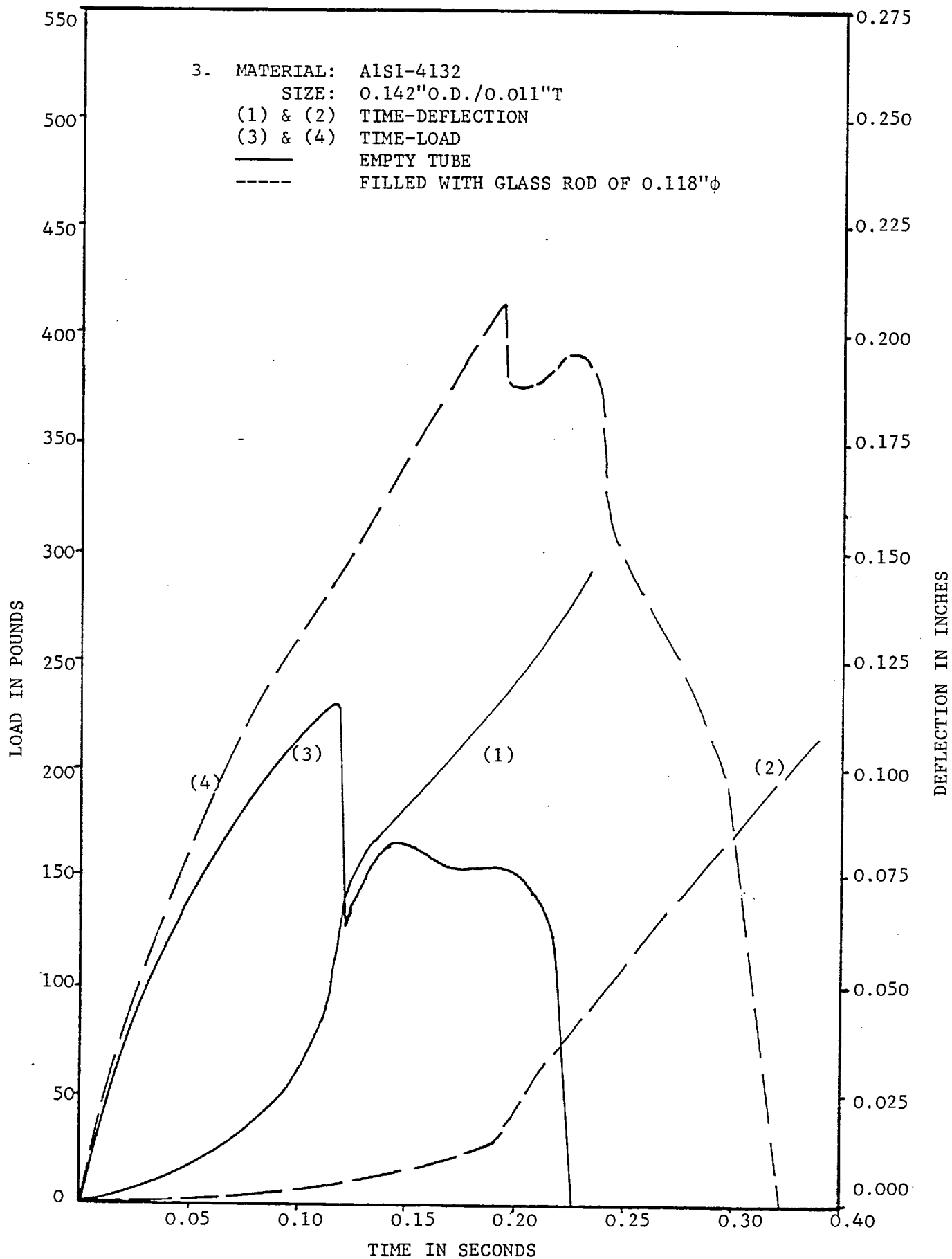


FIG. 2.10

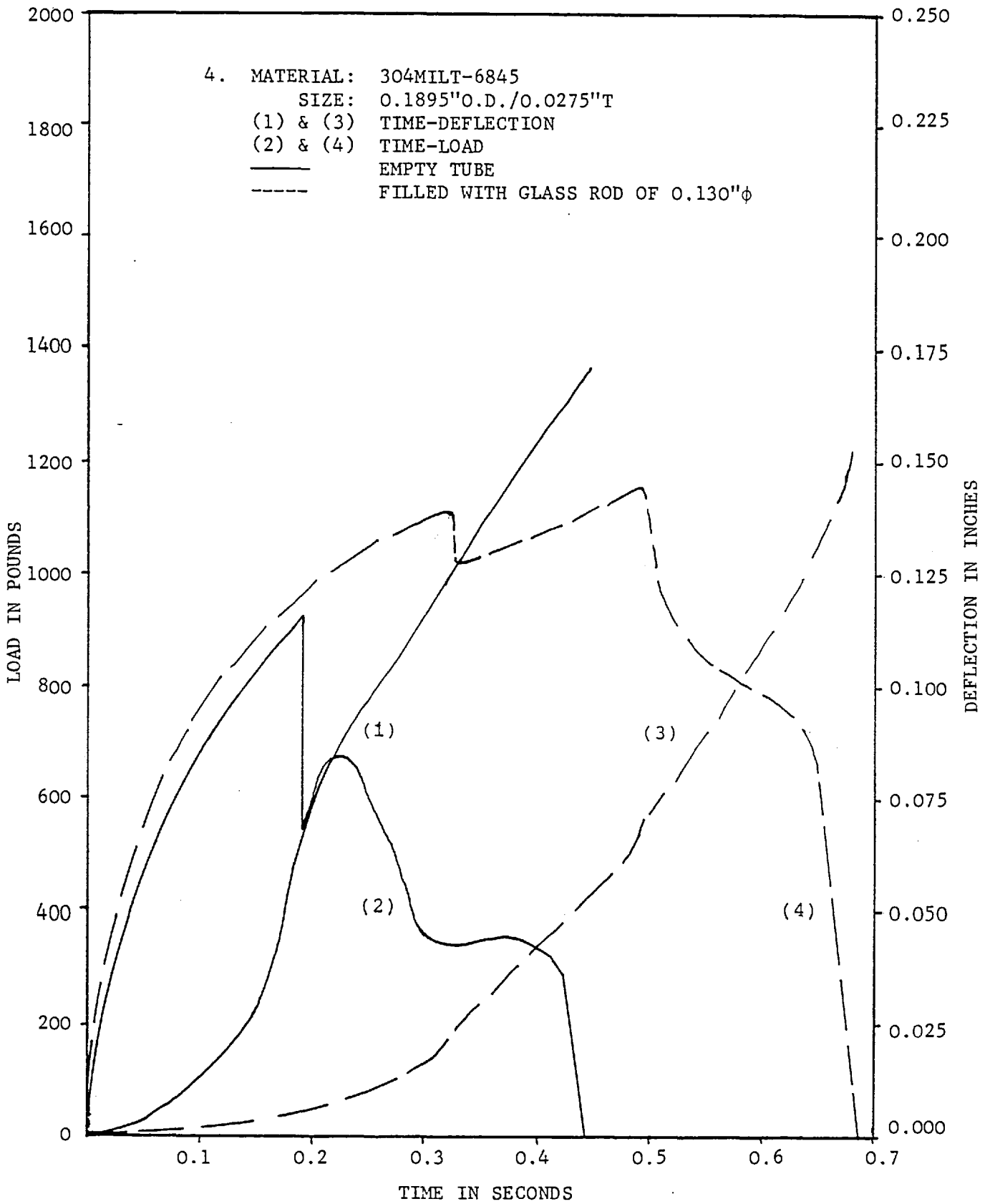


FIG. 2.11

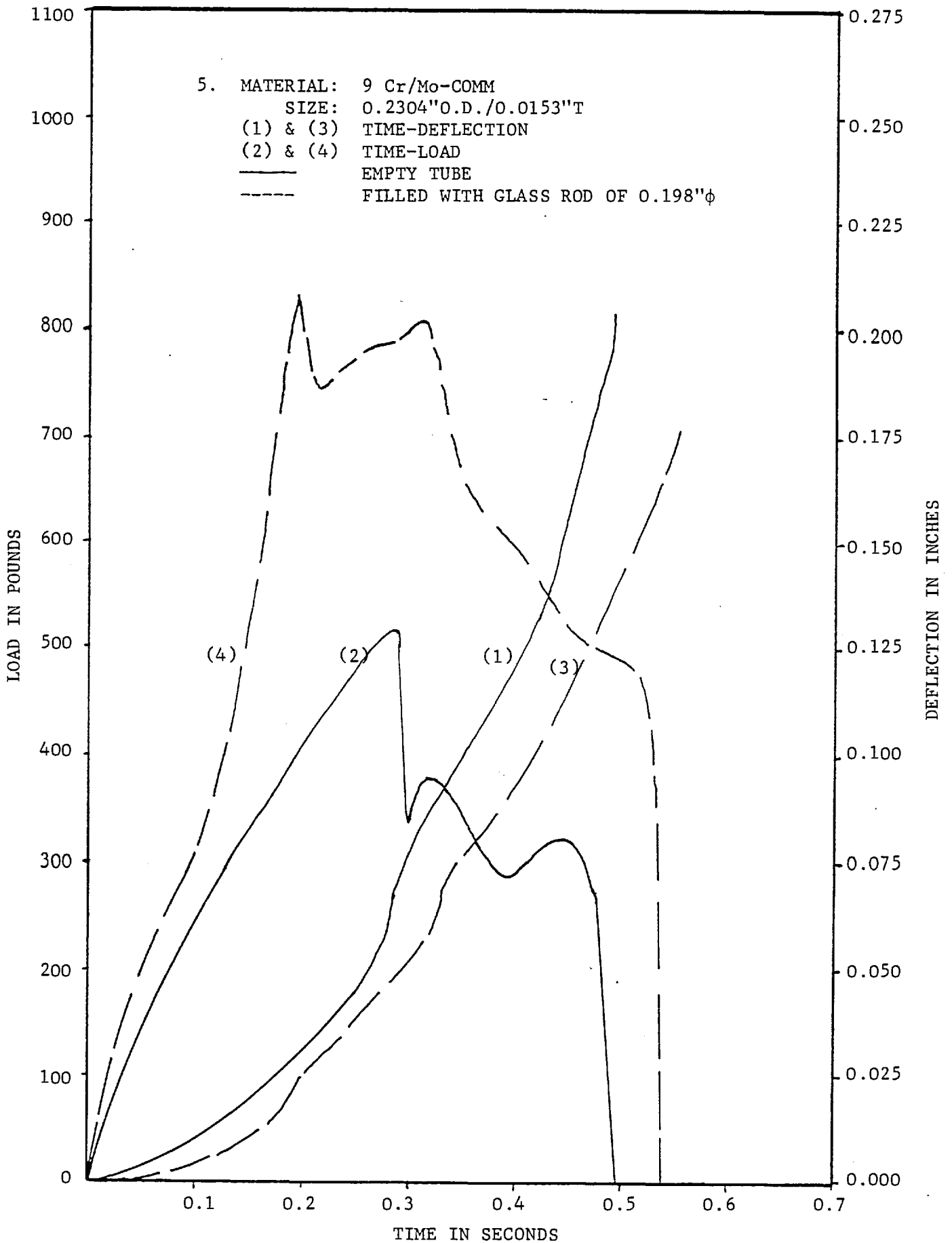


FIG. 2.12

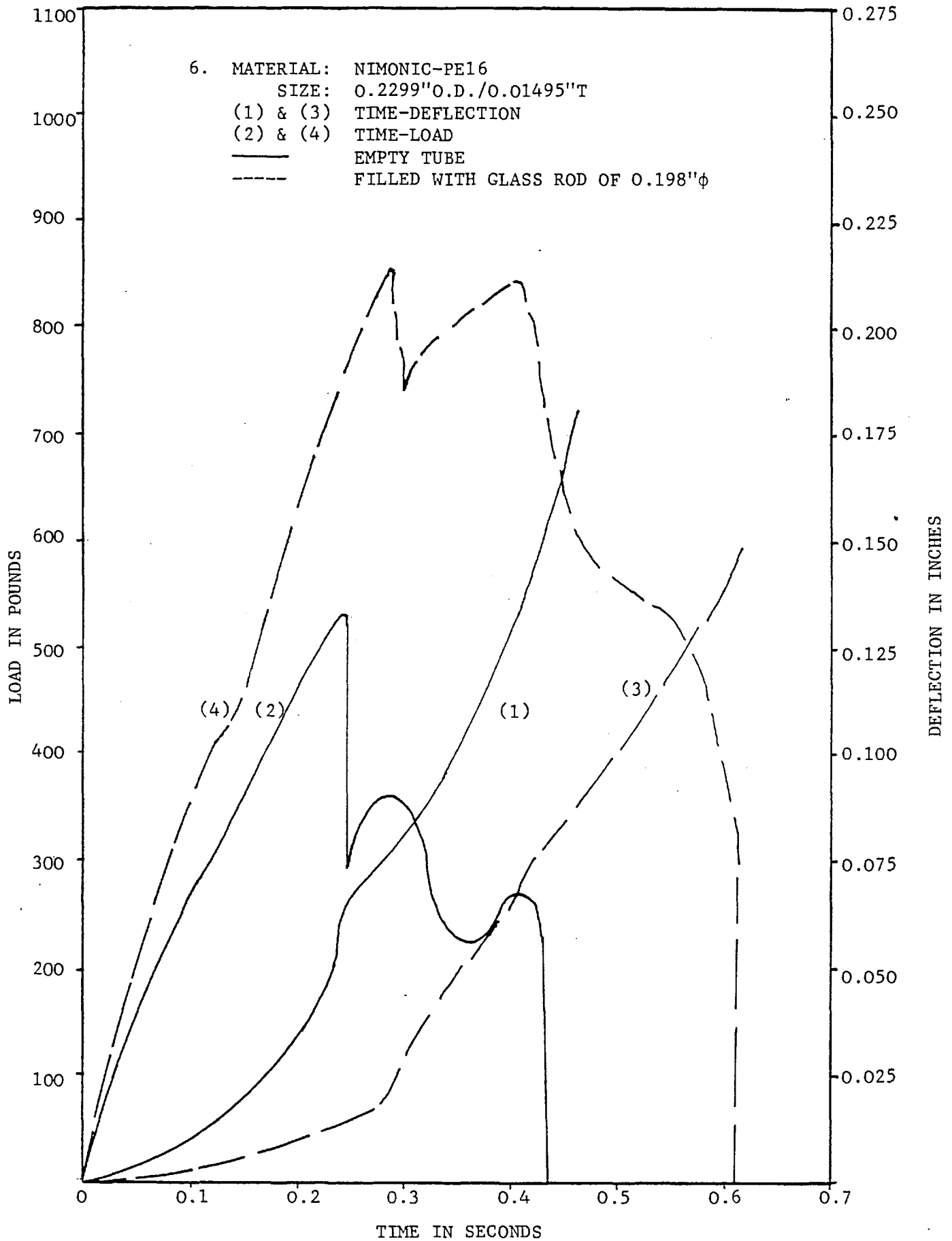


FIG. 2.13

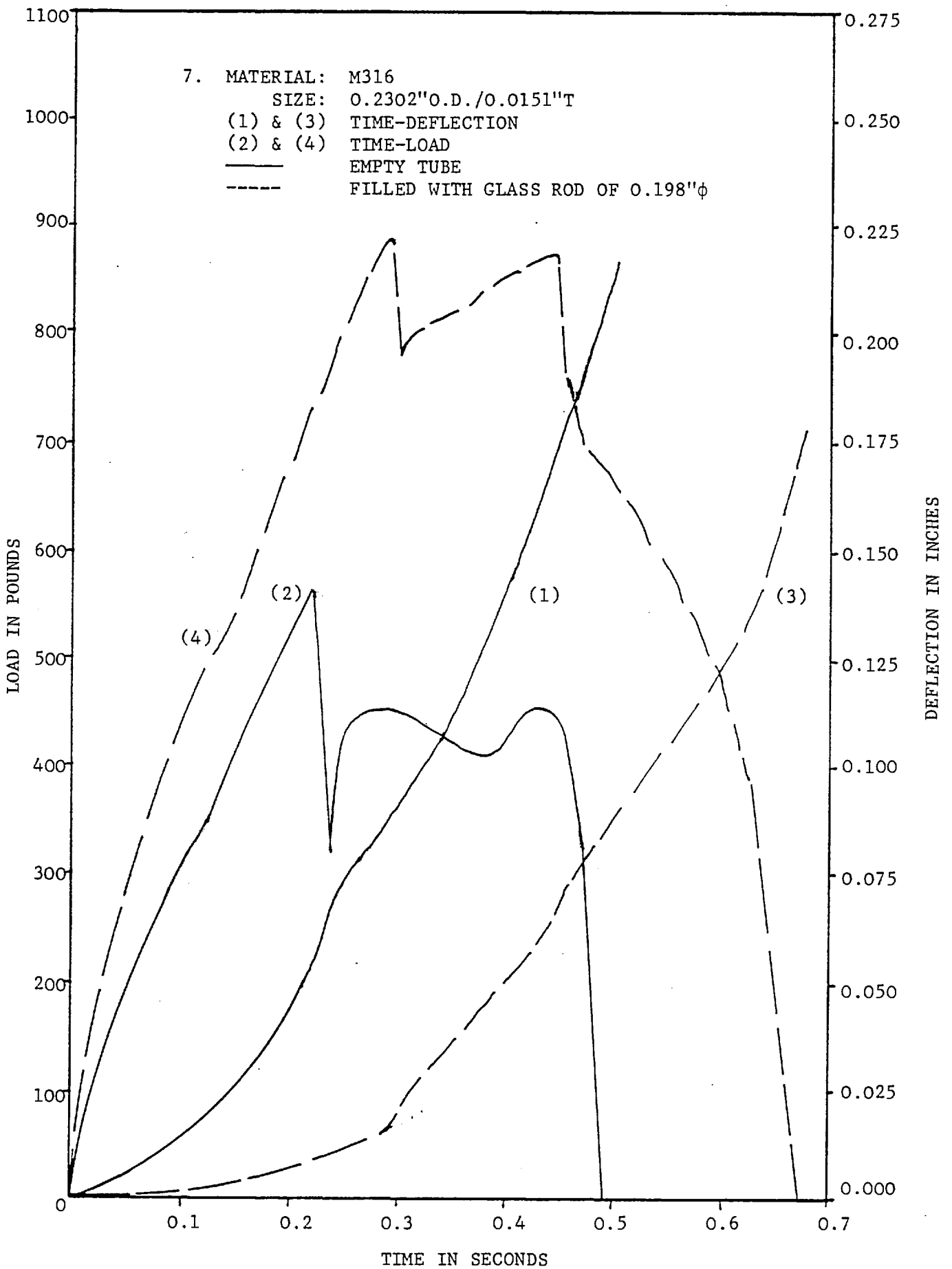


FIG. 2.14

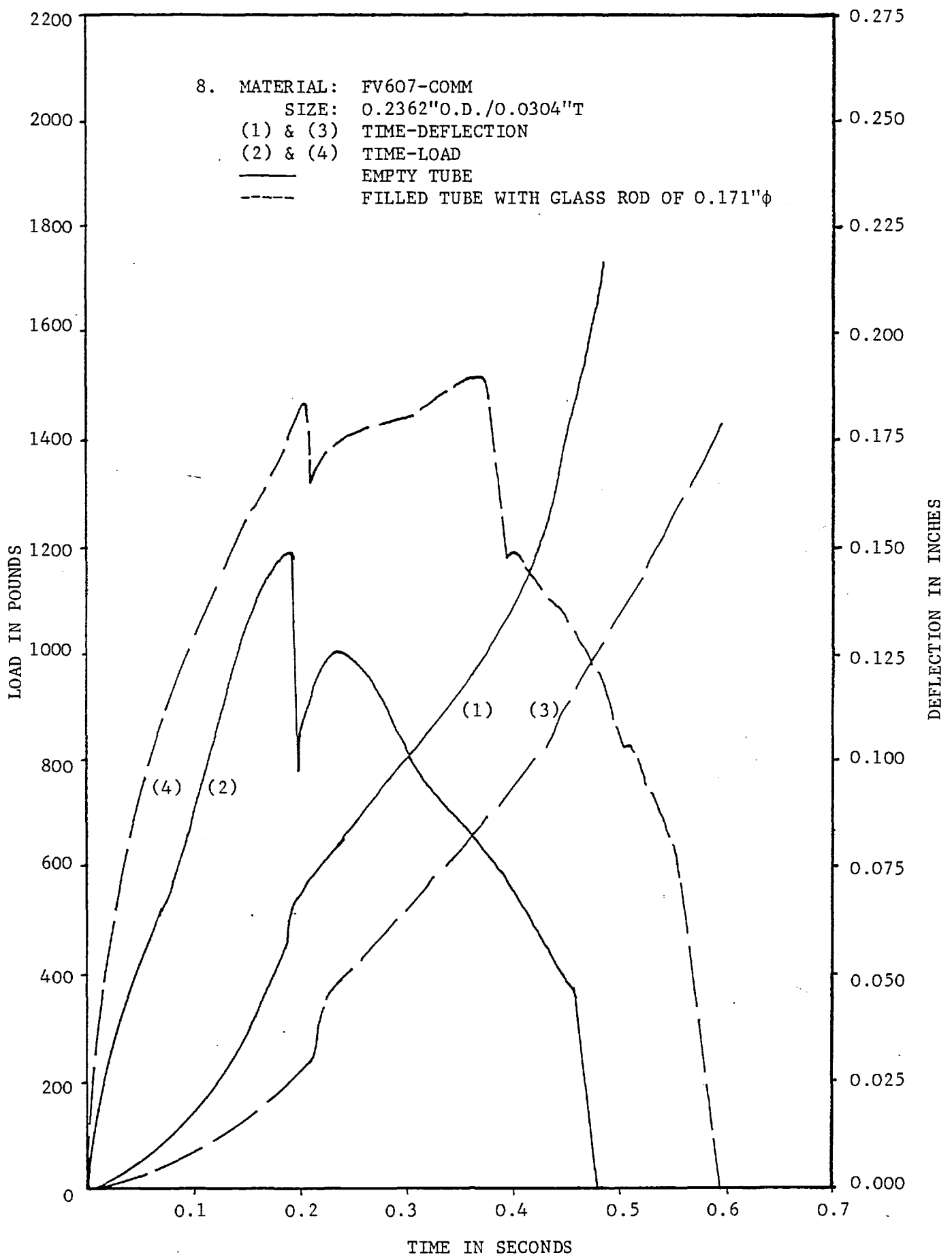


FIG. 2.15

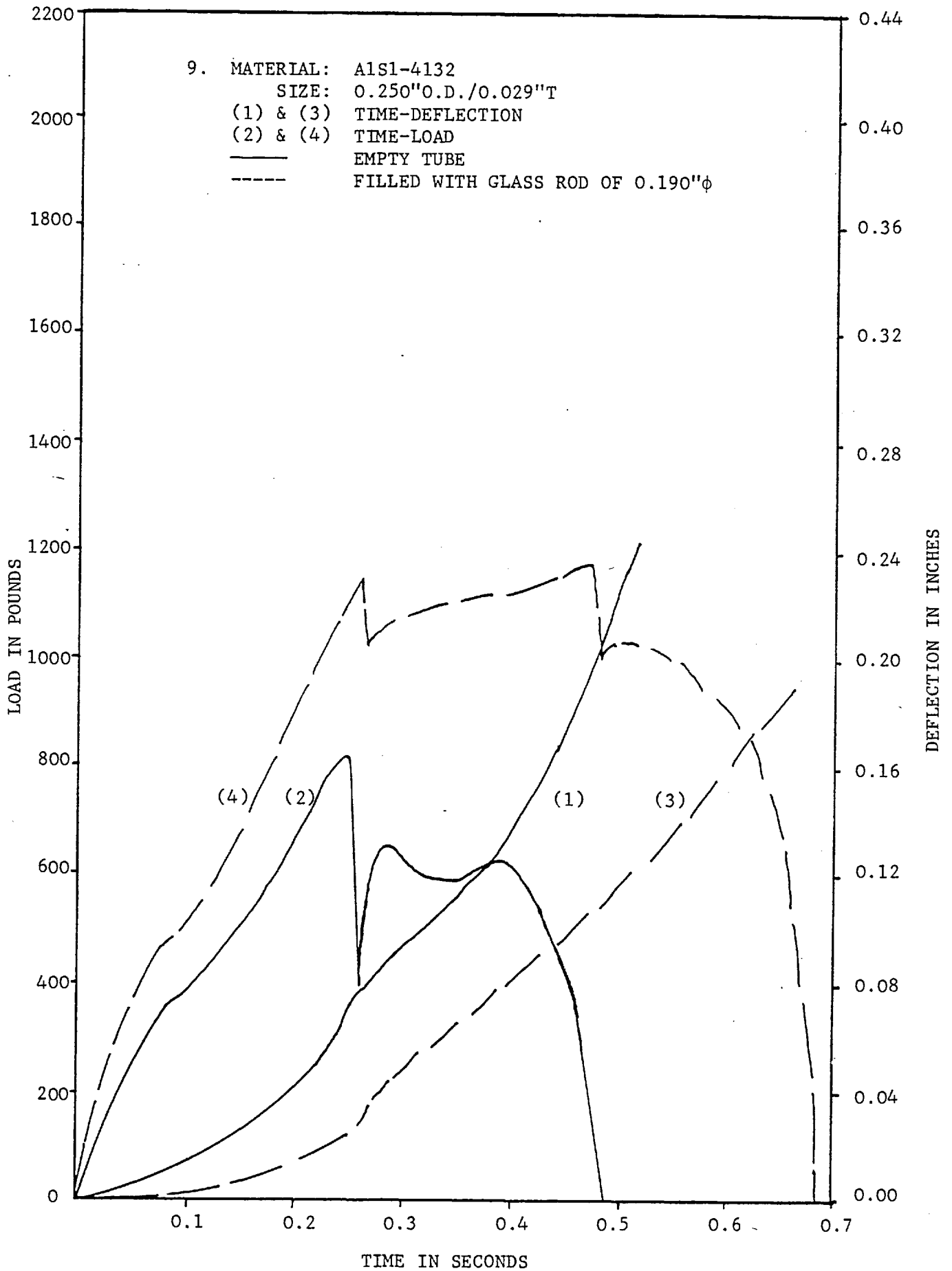


FIG. 2.16

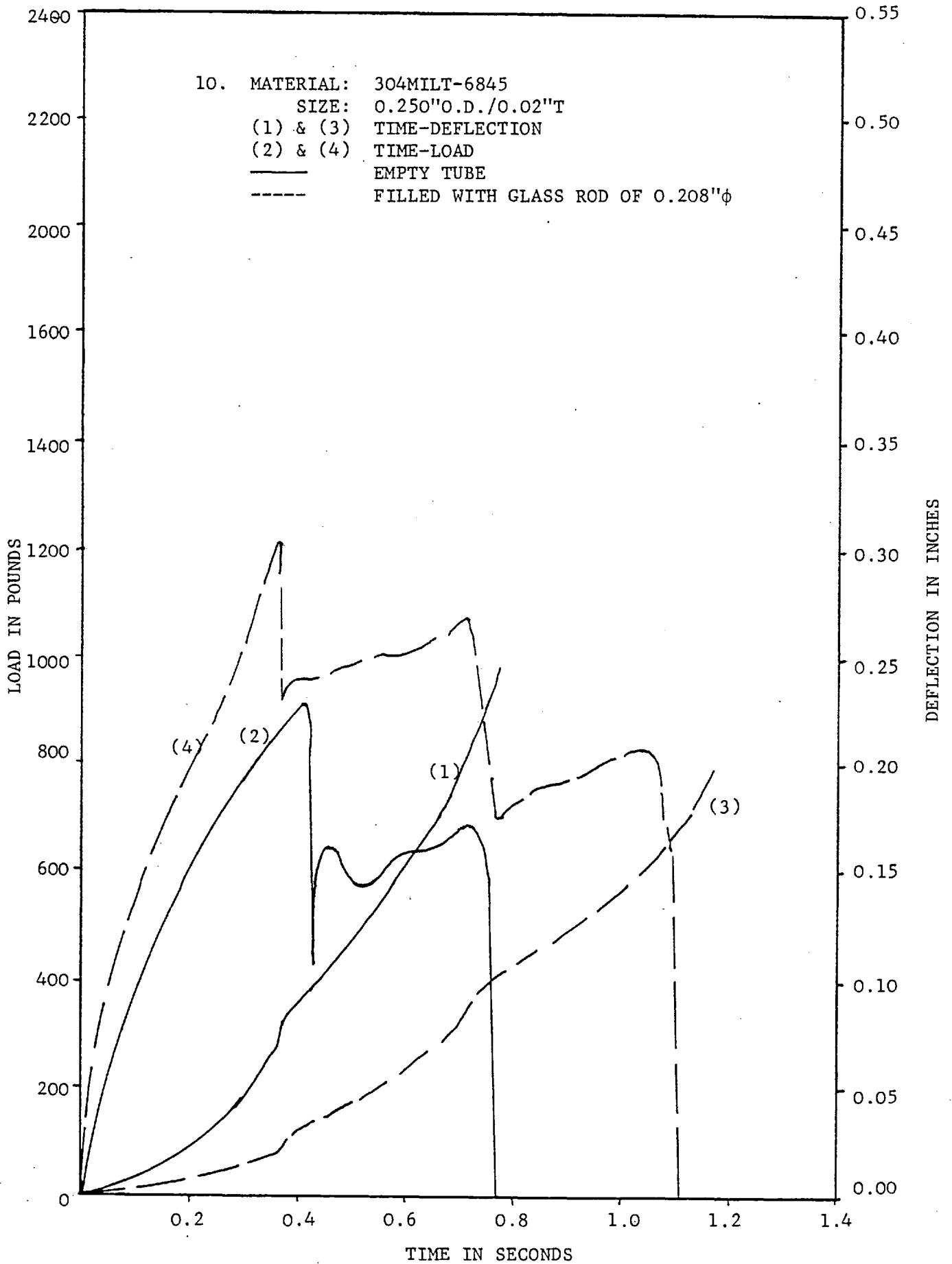


FIG. 2.17

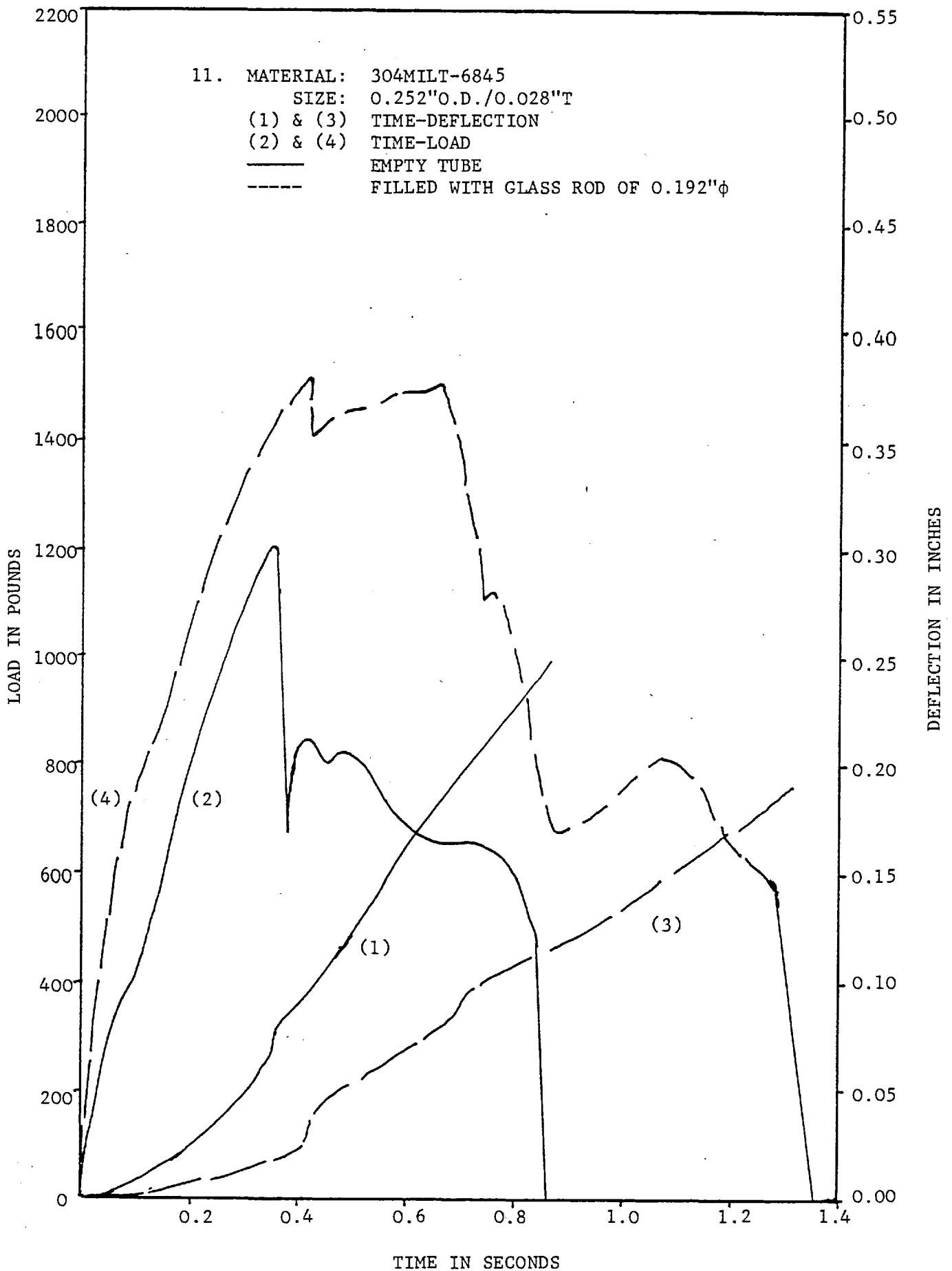


FIG. 2.18

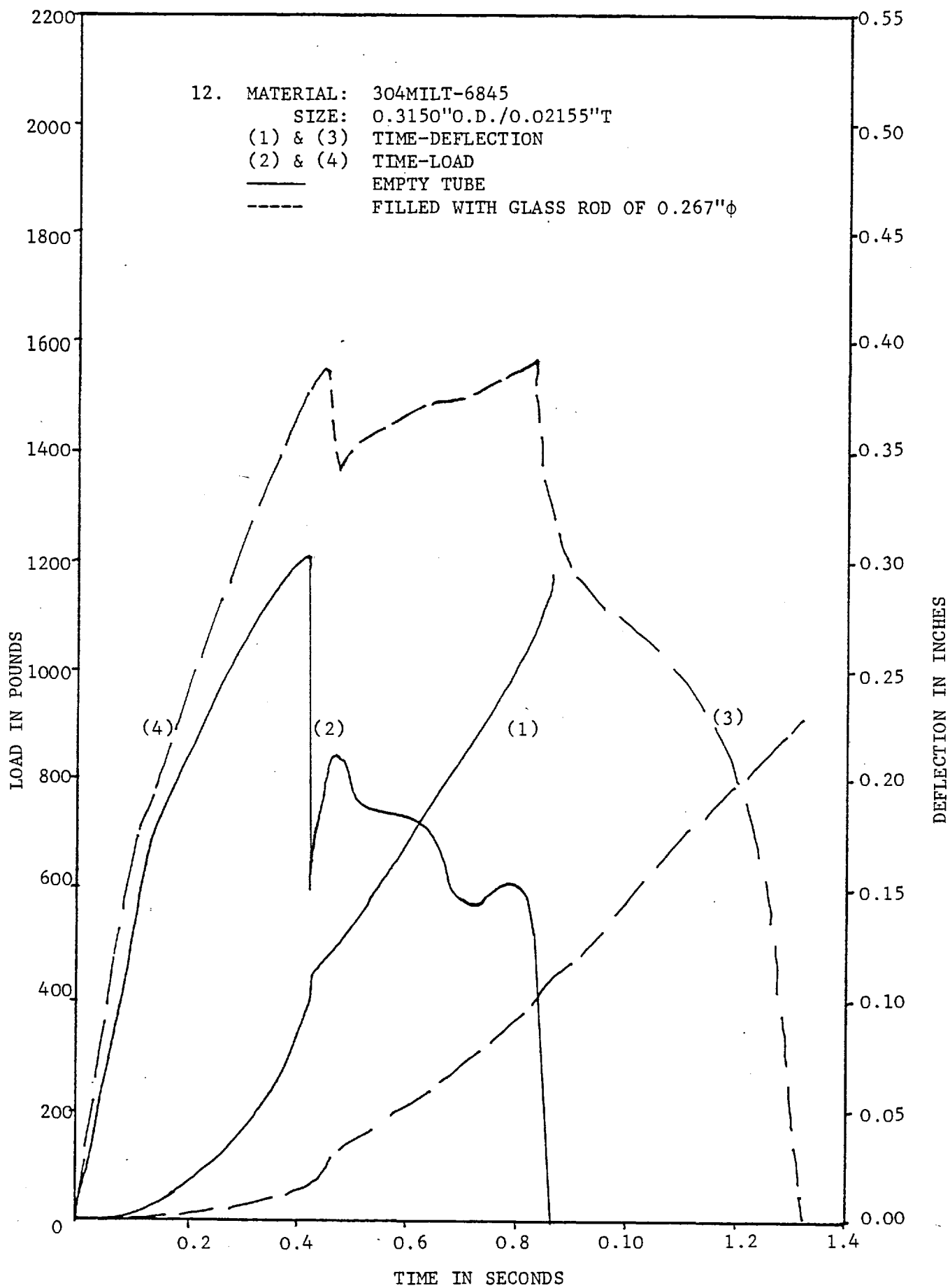


FIG. 2.19

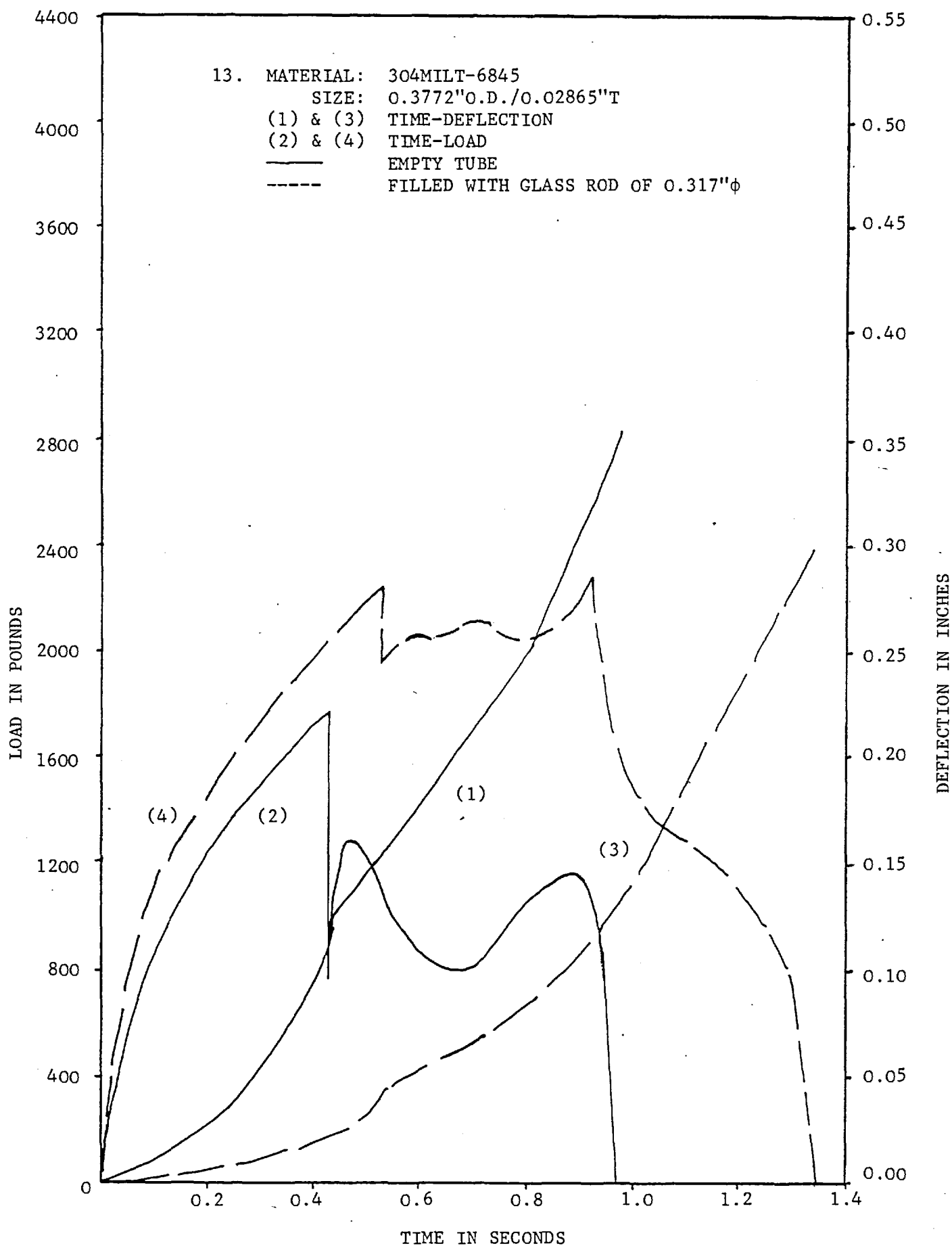


FIG. 2.20

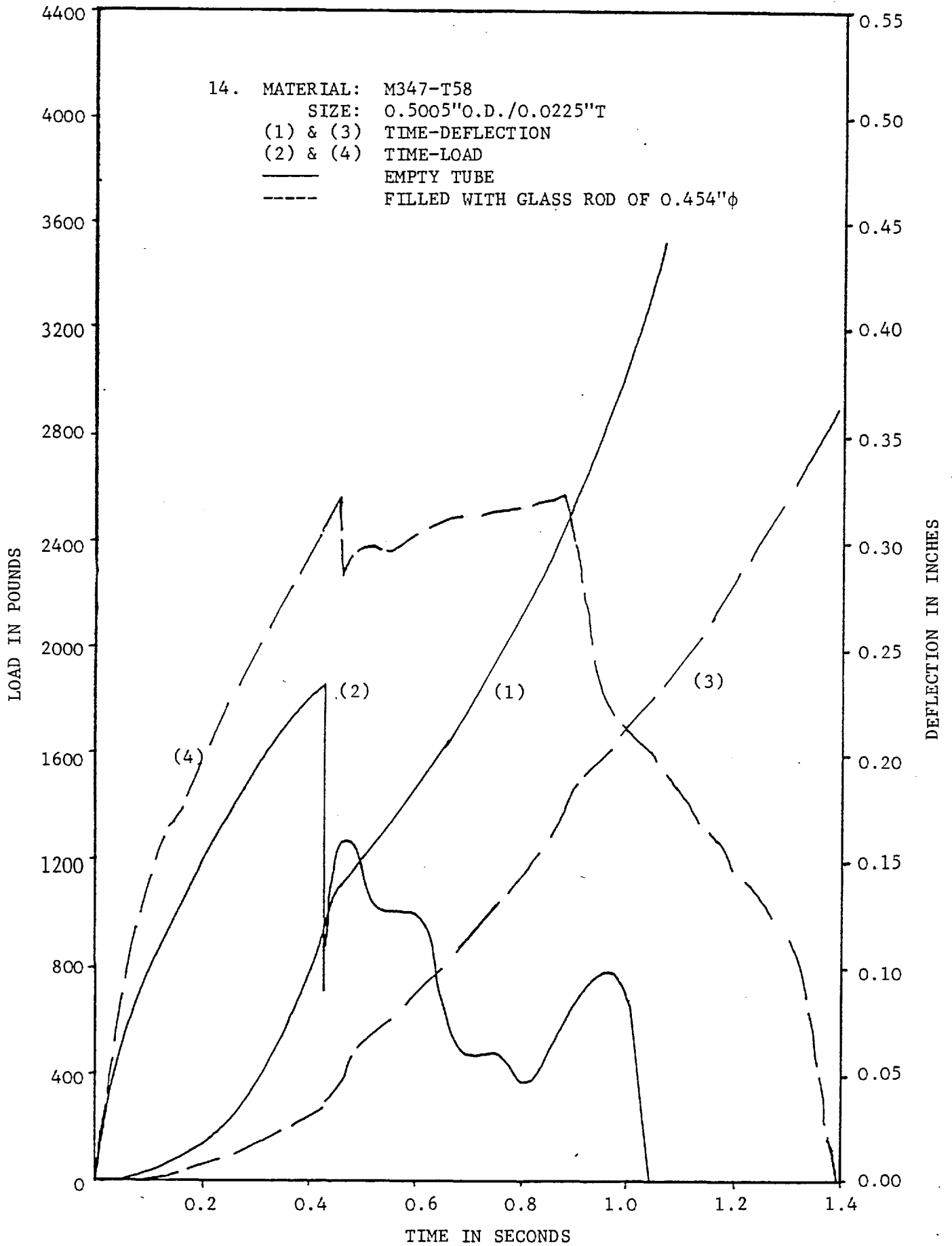


FIG. 2.21

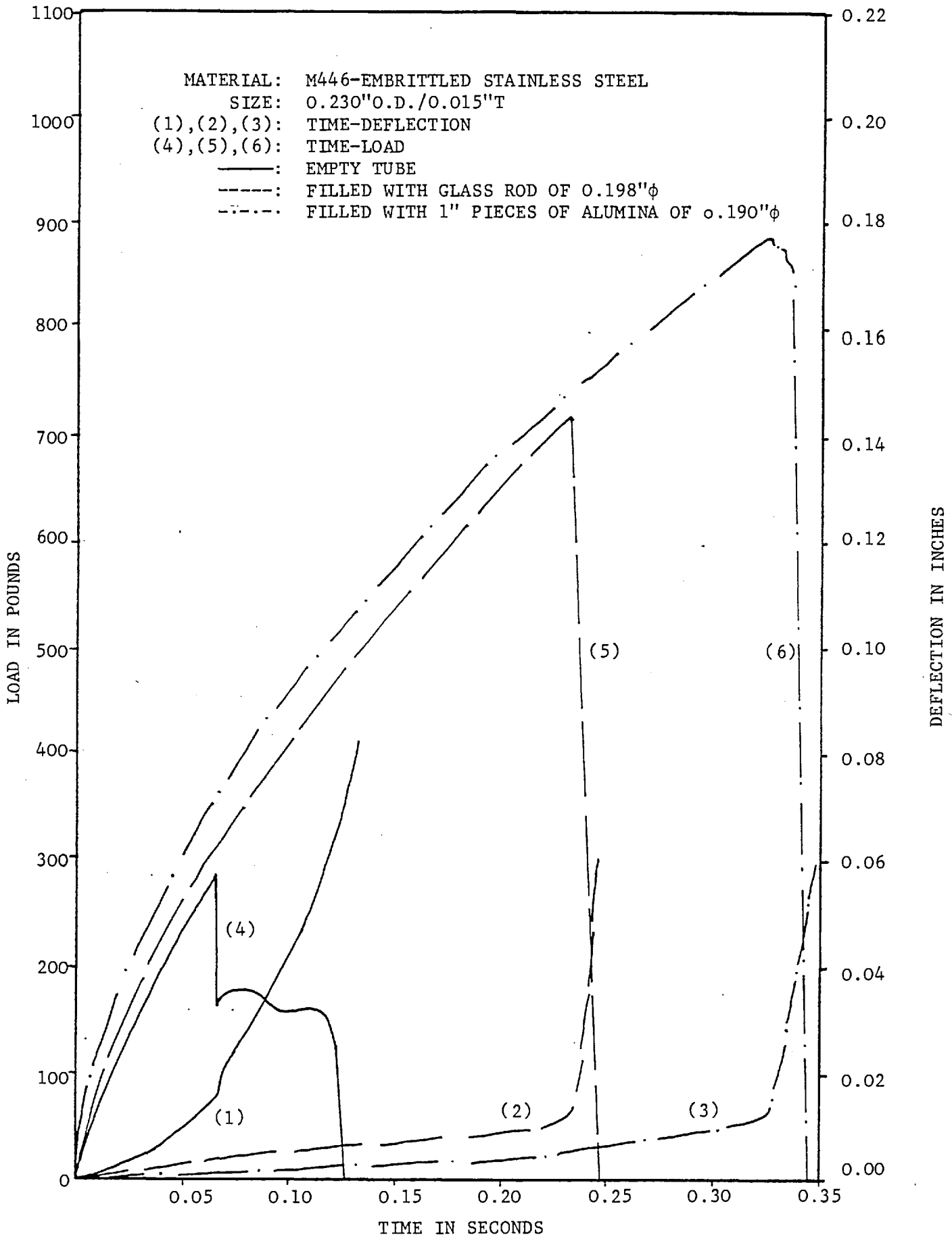


FIG. 2.22

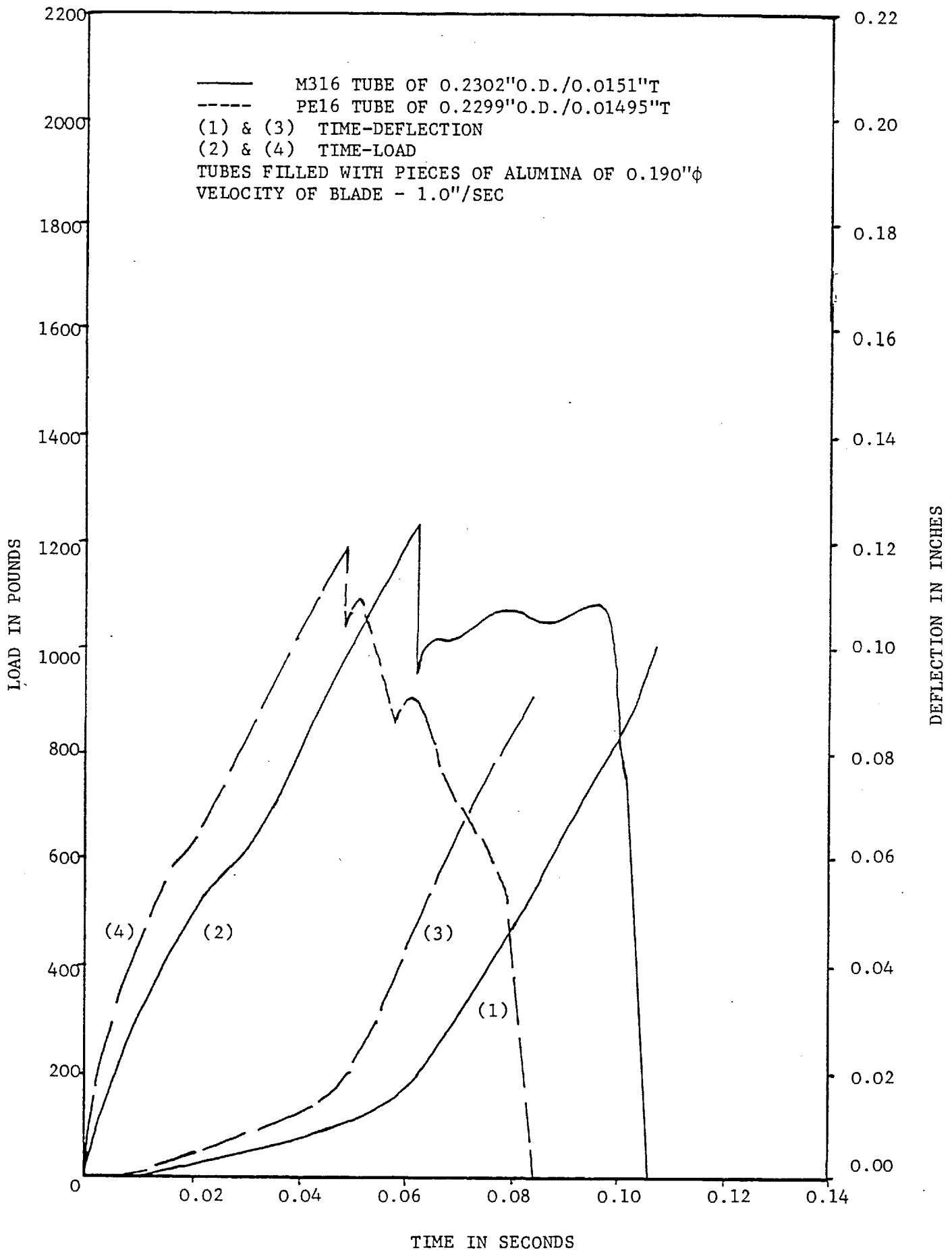


FIG. 2.23

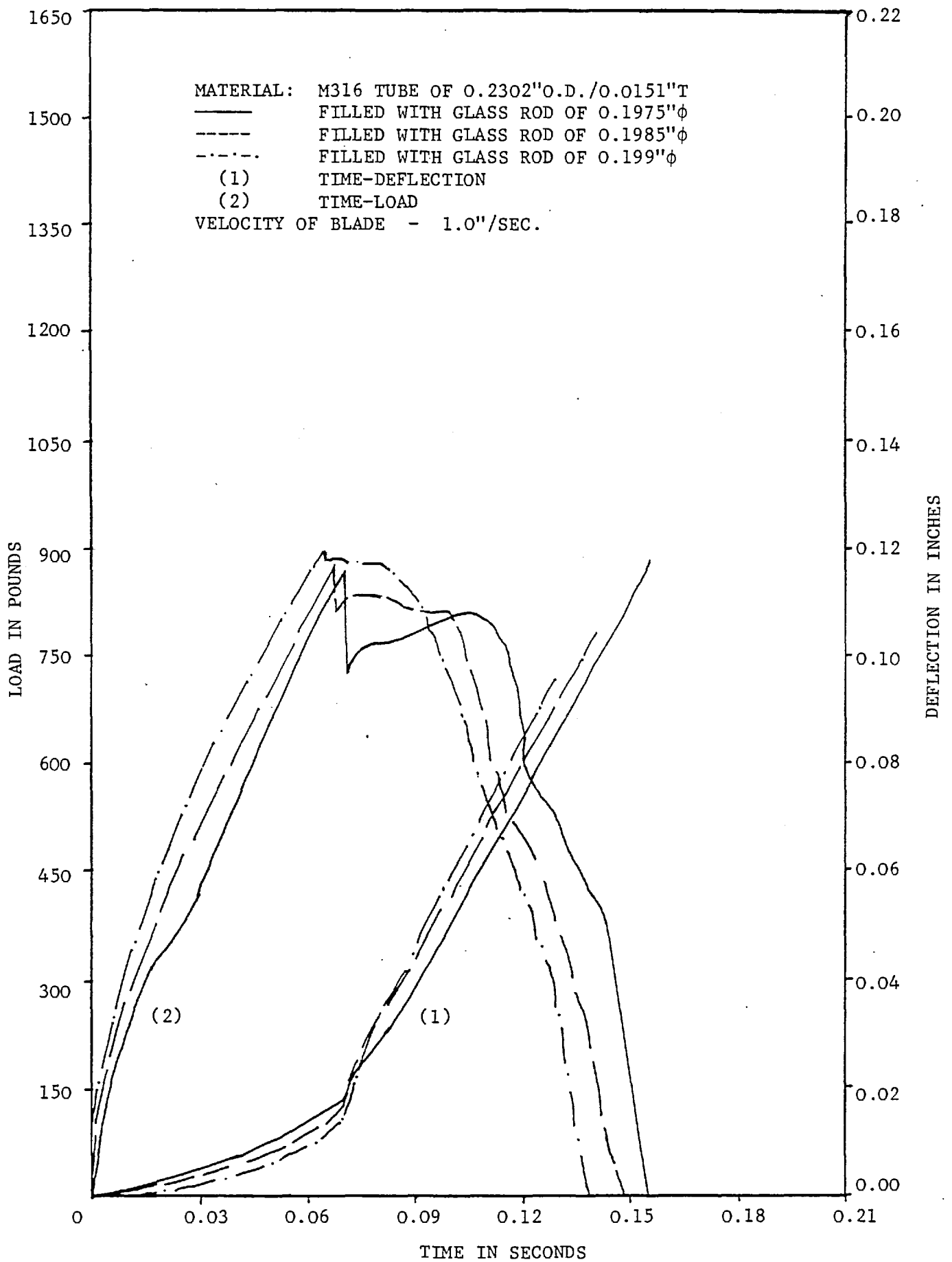


FIG. 2.24

2.4 TUBE CROPPING UNDER PRE-LOAD

2.4.1 Tensile pre-load

A suitable length of the cropped end of the tube was filled with silver steel and fitted into a grip. A nylon rope was passed over a pulley of 4½" diameter and one end tied to the grip. Suitable weights of about 300 pounds were attached to one end of the rope to achieve 200 pounds tensile load on the slack side. The design details were as follows.

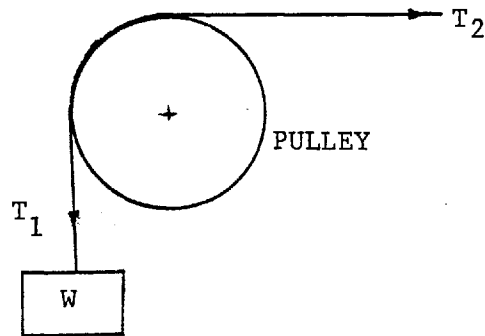


Figure 2.25

For nylon rope, $\mu = 0.25$

$$T_1 = 300 \text{ pounds, } \theta_1 = \frac{\pi}{2}$$

$$\frac{T_1}{T_2} = e^{\mu\theta_1} \tag{2.1}$$

Substituting the above values in eqn (2.1),

$$T_2 \approx 200 \text{ pounds}$$

A photograph of the equipment for providing the tensile pre-load is shown in fig. 2.35. Load and deflection variation with time diagrams for M316 and PE16 tubes are shown in figs 2.26 and 2.27. The results are presented in Table 2.6.

2.4.2 Compressive pre-load

The arrangement for providing a compressive pre-load was the same as that for the tensile pre-load except for the provision of an additional lever arm to reverse the load as shown in fig. 2.36. The results are shown in Table 2.6 and the load-deflection graphs are shown in figs 2.28 and 2.29.

2.5 SINGLE TUBE CROPPING AT LOW TEMPERATURE

A metal box was made to enclose the work holder and secured to the die bolster. Liquid nitrogen was poured continuously into the box before and during the cropping process to submerge the whole of the tube and work holder. The metal box was covered with a packing material to maintain the liquid nitrogen temperature as near as possible to -196°C . Experiments were carried out on M316, PE16 and embrittled M446 steel using both empty and filled tubes. The results are shown in Table 2.6.

2.6 BAR CROPPING

Experiments were carried out on M316 and PE16 rods of 1/4" diameter for comparison with tube cropping. M316 stainless steel tube was tightly filled with a mild steel rod of 0.1995" ϕ and the cropping experiment carried out. The load-deflection diagrams for the above three experiments are shown in fig. 2.30 and the results are presented in Table 2.6. Load, deflection variations with time for glass rod and tube are shown in fig. 2.31.

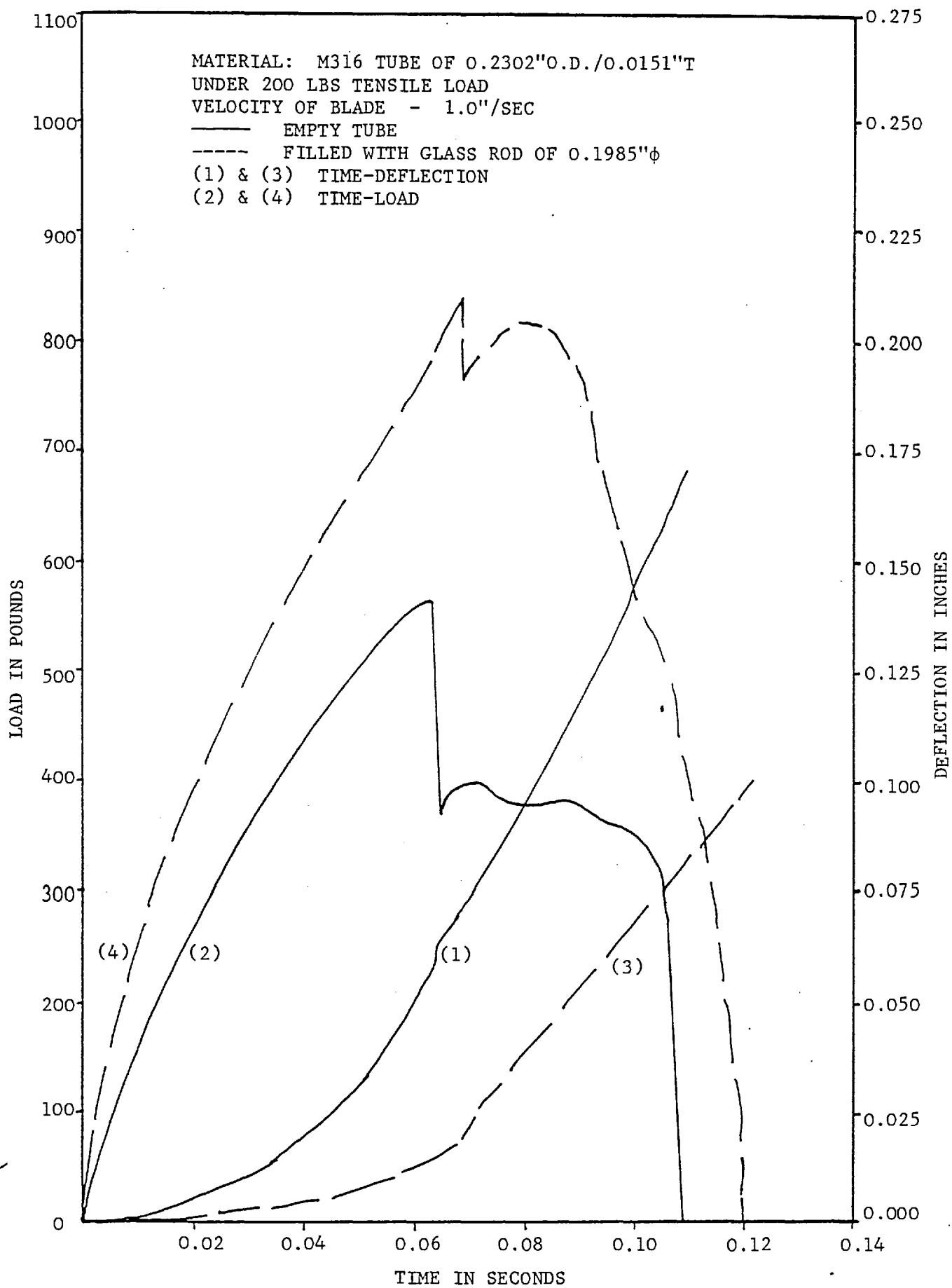


FIG. 2.26

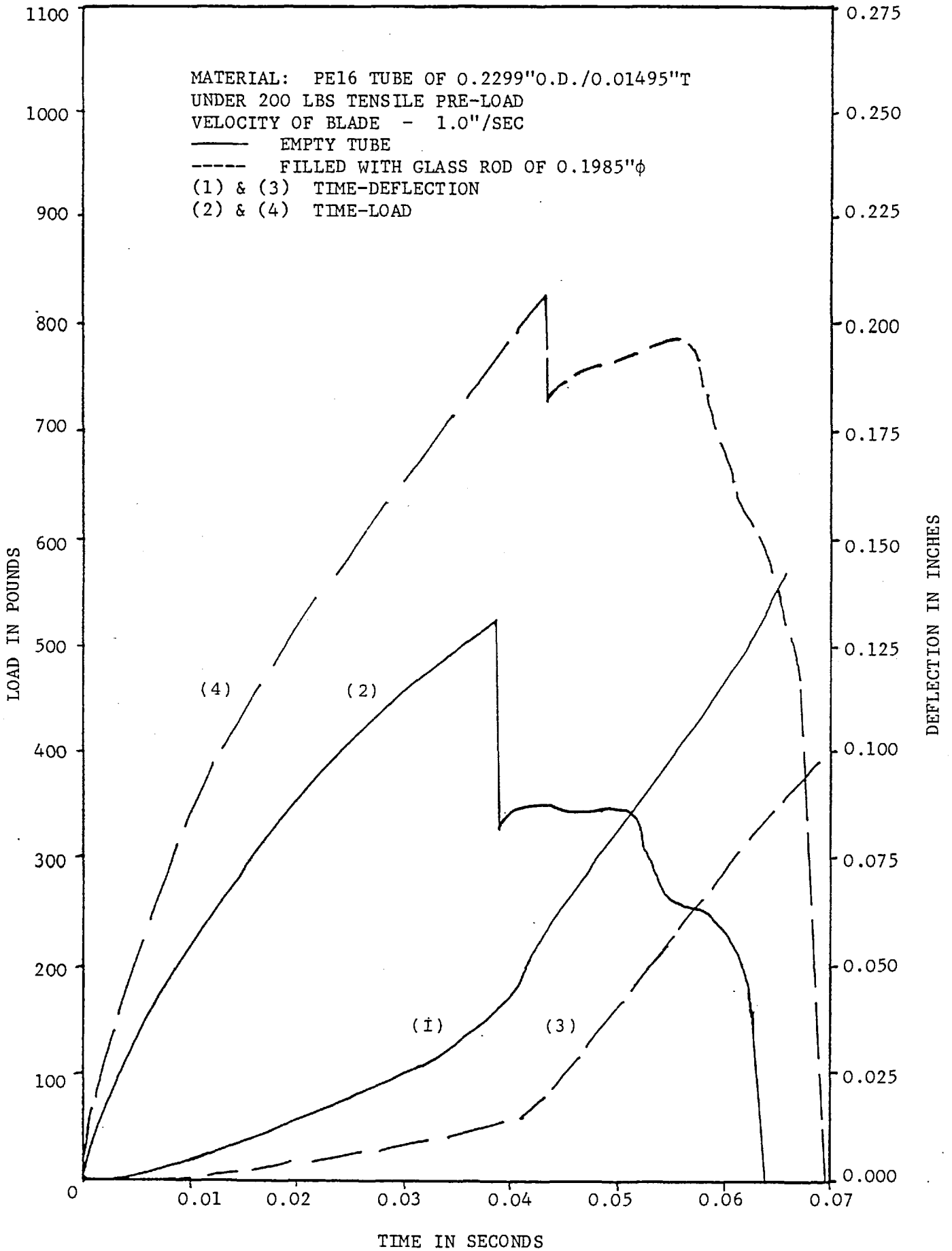


FIG. 2.27

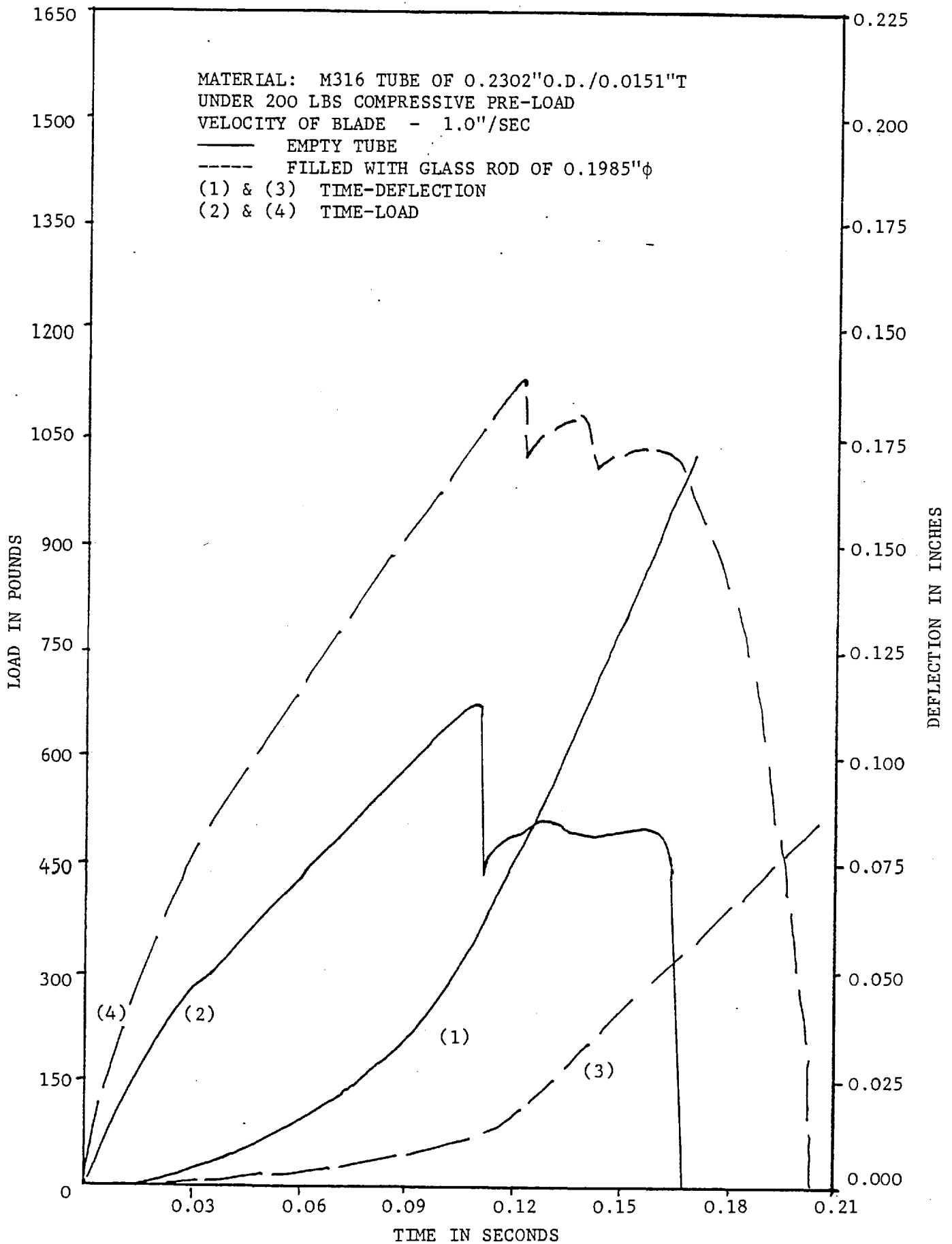


FIG. 2.28

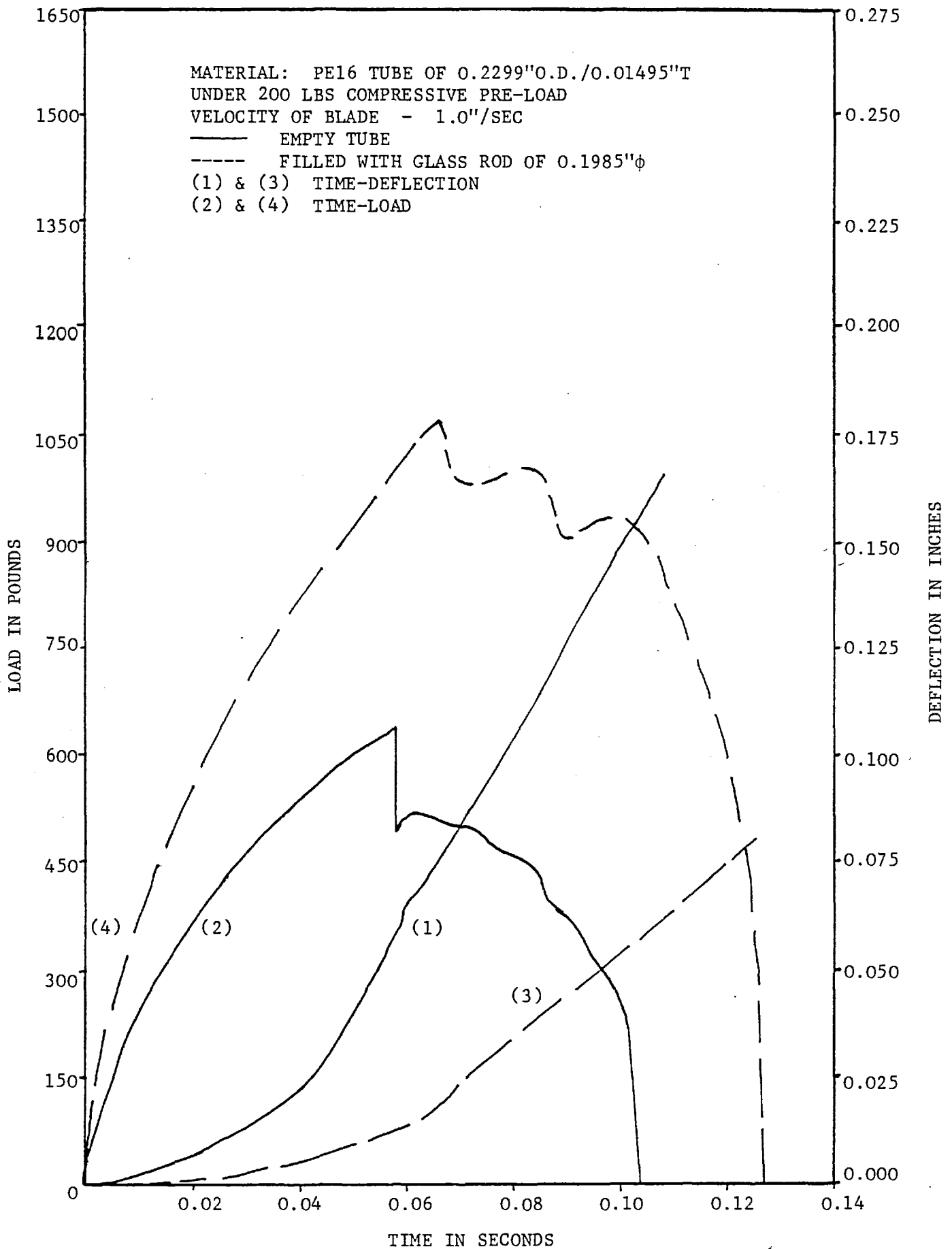


FIG. 2.29

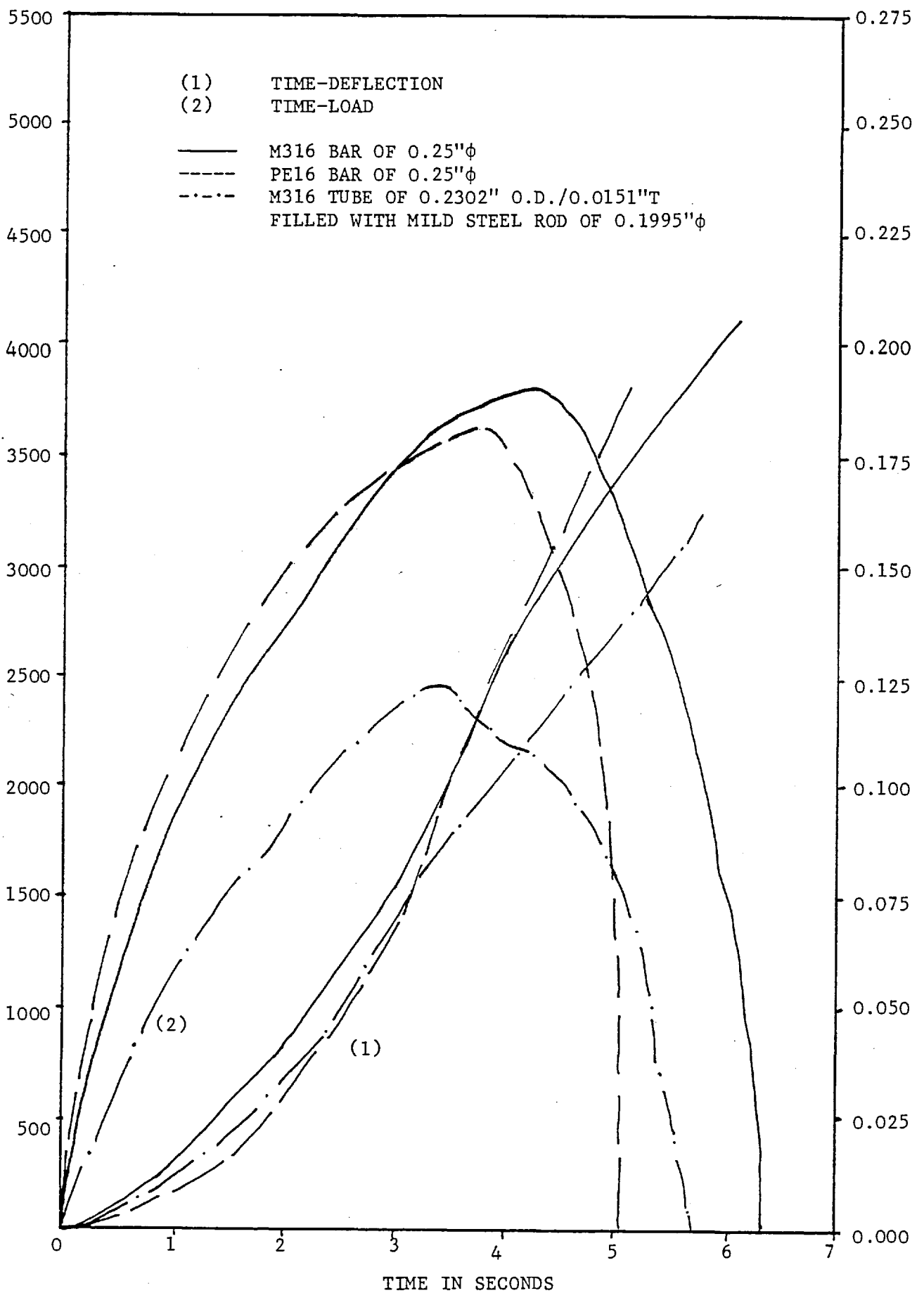


FIG. 2.30

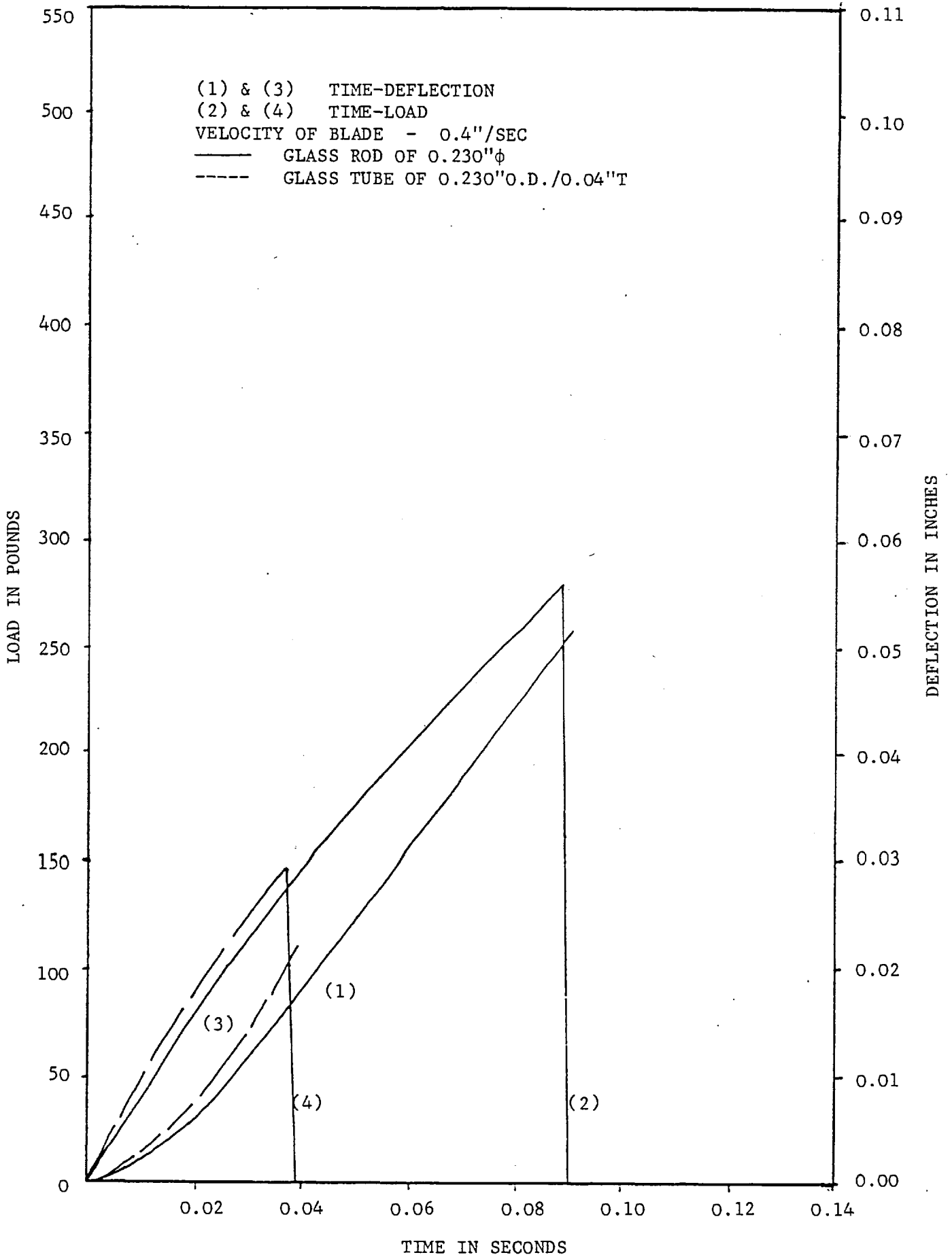
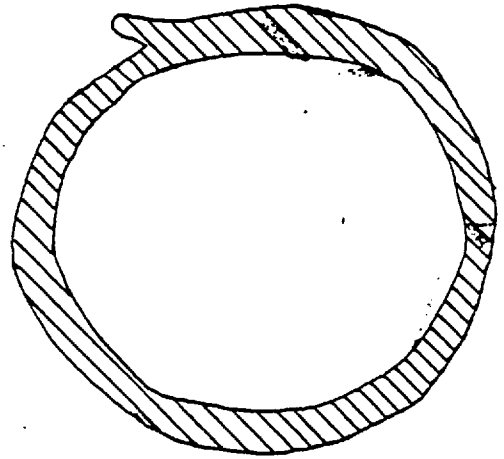
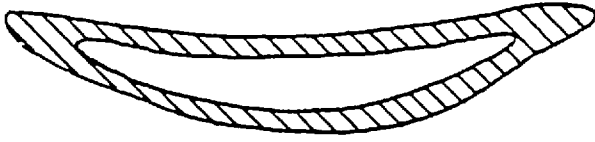
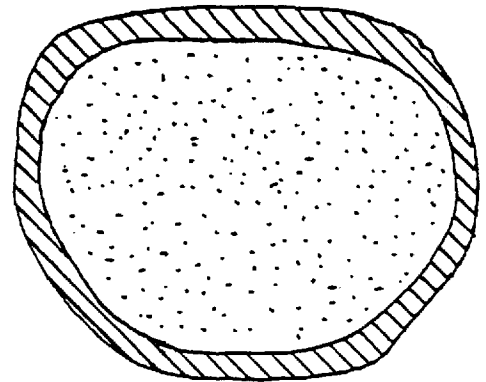
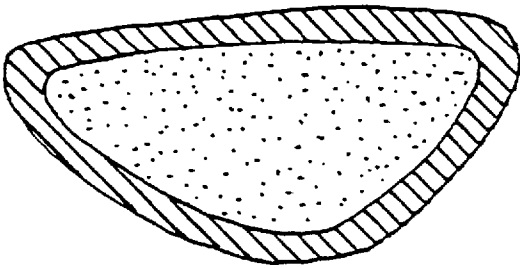


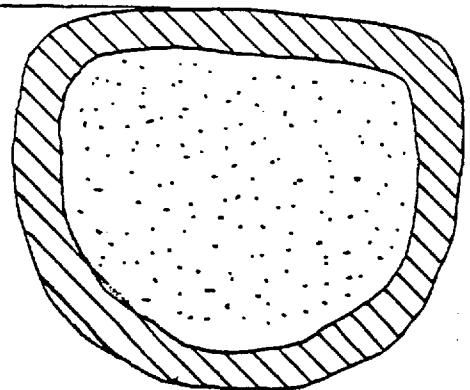
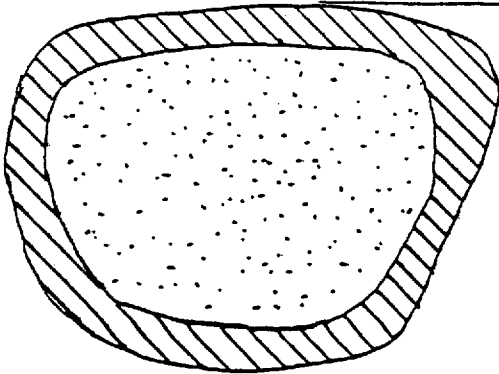
FIG. 2.31



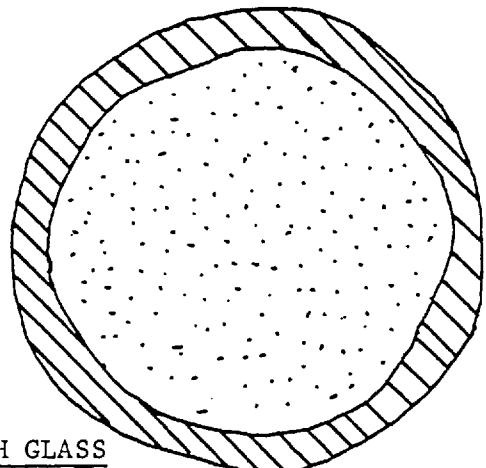
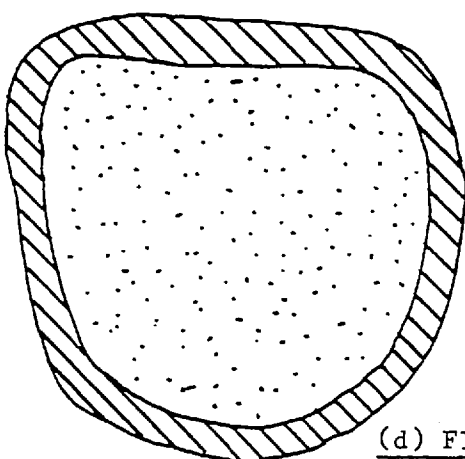
(a) EMPTY TUBE



(b) FILLED WITH GLASS ROD
(VELOCITY OF BLADE - 0.4"/SEC)

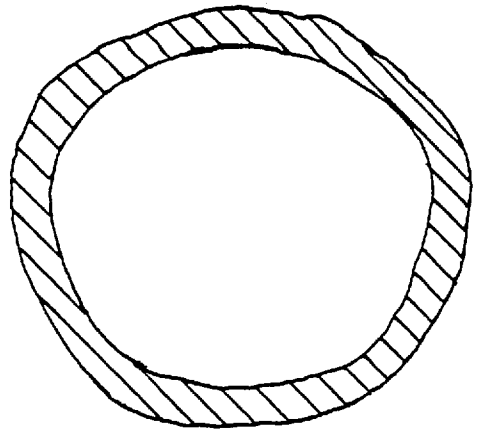
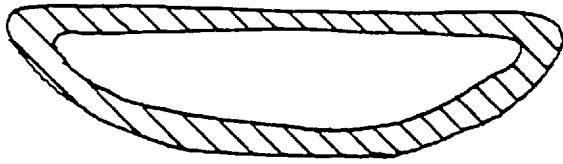
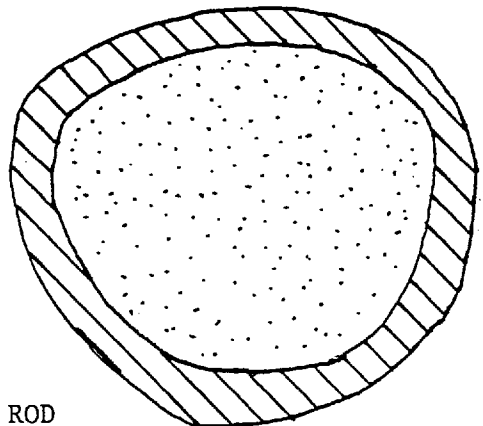
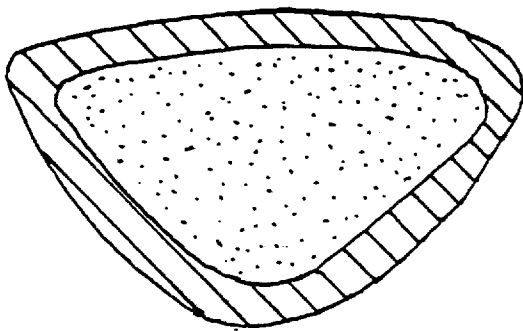
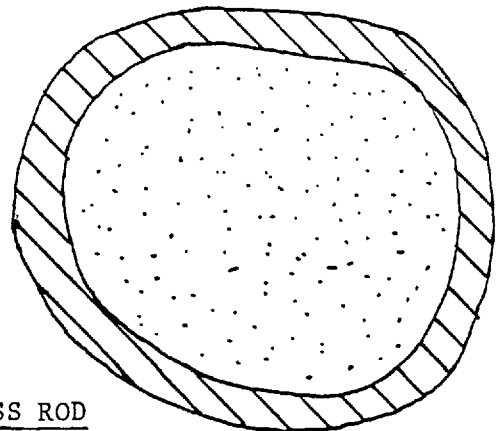
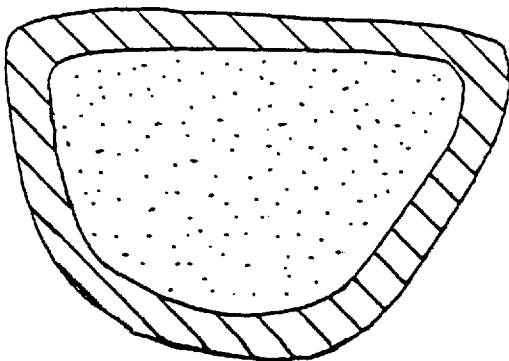
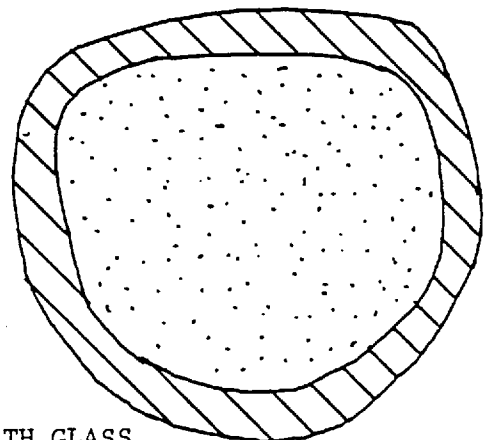
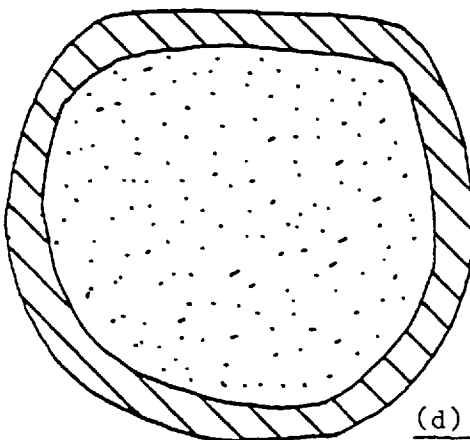


(c) FILLED WITH GLASS ROD
(VELOCITY OF BLADE 1.0"/SEC)



(d) FILLED WITH GLASS
ROD (UNDER PRE-LOAD)

FIG. 2.32. MAGNIFIED PROFILES OF CROPPED M316 TUBE (x10)

CROPPED END OF TUBECROPPED END OF BILLET(a) EMPTY TUBE(b) FILLED WITH GLASS ROD
(VELOCITY OF BLADE - 0.4"/SEC)(c) FILLED WITH GLASS ROD
(VELOCITY OF BLADE - 1.0"/SEC)(d) FILLED WITH GLASS
ROD (UNDER PRE-LOAD)FIG. 2.33. MAGNIFIED PROFILES OF CROPPED PE16 TUBE (×10)

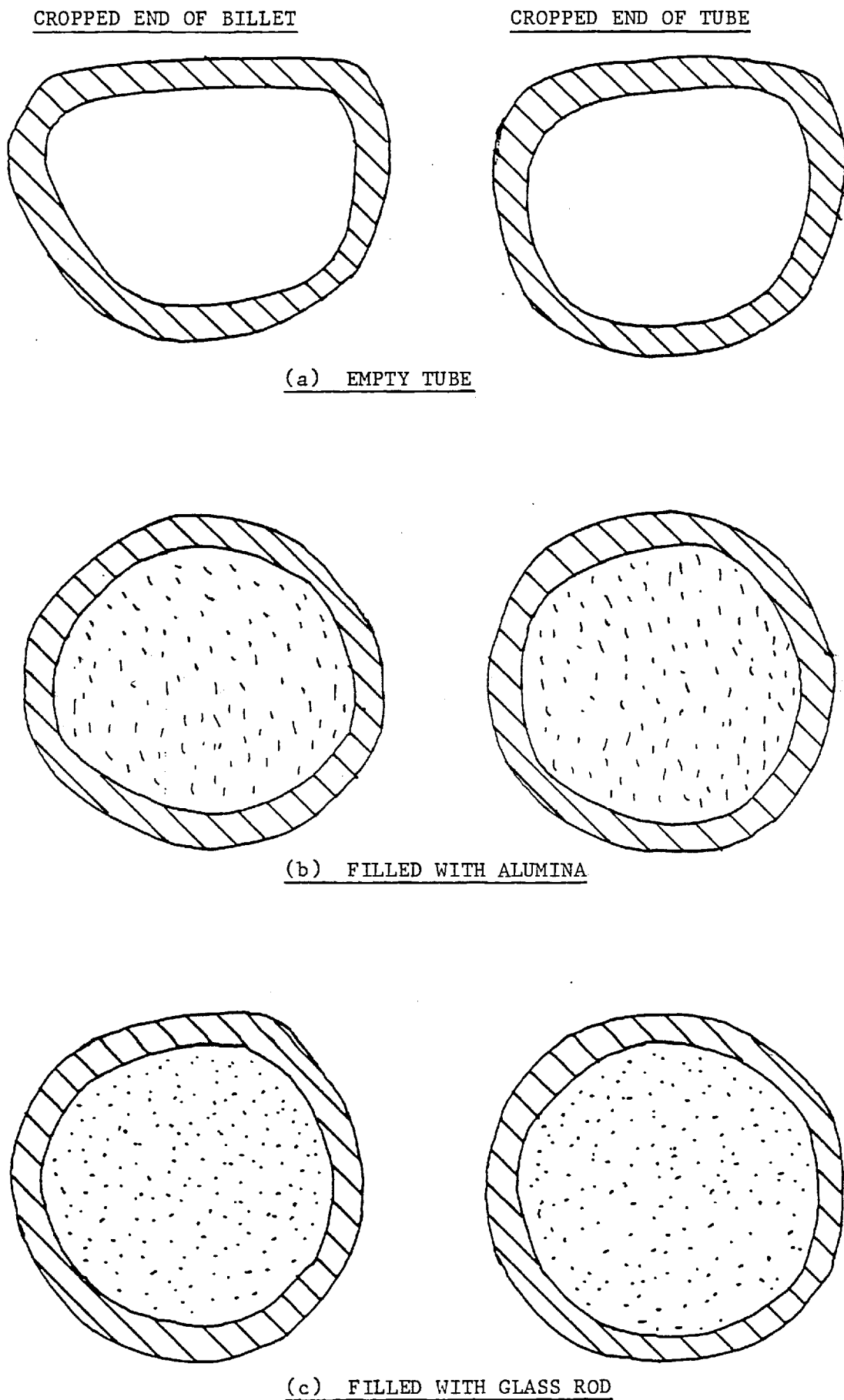


FIG. 2.34. MAGNIFIED PROFILES OF CROPPED M446-EMBRITLED TUBE ($\times 10$)

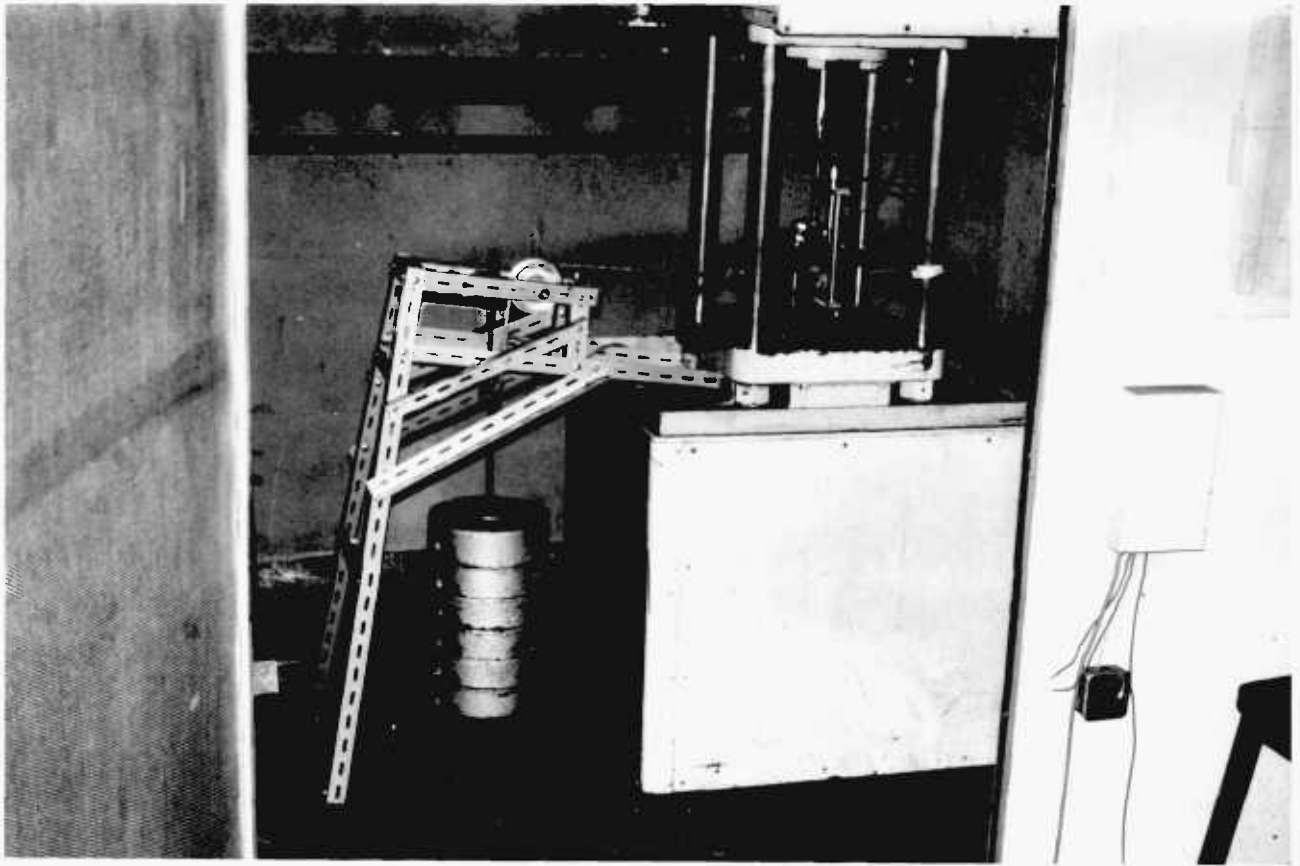


FIG. 2.35. EQUIPMENT FOR PROVIDING TENSILE PRE-LOAD

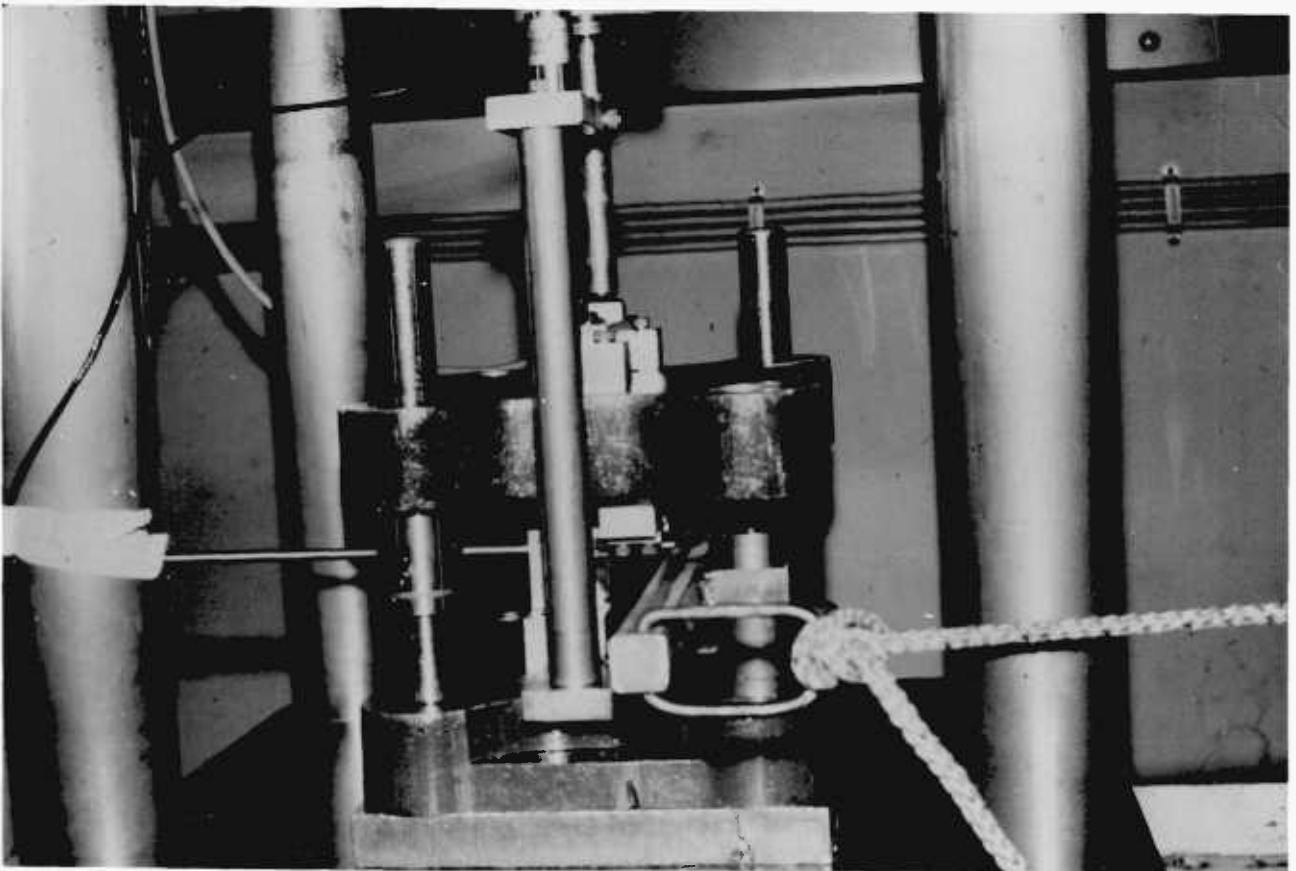


FIG. 2.36. EQUIPMENT FOR PROVIDING COMPRESSIVE AXIAL LOAD

2.7 DIFFERENT TECHNIQUES USED TO EXPLAIN TUBE CROPPING PROCESS

2.7.1 Incremental cropping

Incremental cropping experiments were carried out on M316 and PE16 tubes respectively and the load and corresponding deflection for each increment are shown in Table 2.7. Photographs of the two tests, viewed in two different positions at each increment, are shown in figs 2.37 and 2.38. These tests were extended to the rest of the tubes and empirical formulae for decay lengths on billet and tube were established as shown in Table 2.8.

2.7.2 Dye penetrant

The dye penetrant technique was used to check the deformed tube at the maximum cropping load for any cracks. Inspection with dye penetrant is probably the oldest of the major non-destructive testing techniques in use today. Firstly, the surface of the deformed tube was cleaned with 'Spotcheck' cleaner. A coloured penetrating liquid, trade name 'Spotcheck Formula A', was applied to the surface of the specimen by spraying. About 30 minutes was allowed for the liquid on the surface to seep into any openings or discontinuities. Then the liquid remaining on the surface was removed by wiping the surface with a clean cloth, without removing any appreciable amount of the liquid from the surface openings. The developer, SKD-NF, was applied by spraying on to the surface.

The developer aids in drawing the penetrant liquid out of any surface openings to the surface and spreading it into the developer coating over an area much wider than the opening itself. After allowing 10 to 15 minutes, the defects which were revealed were inspected for red lines which denote cracks and red dots which denote pores.

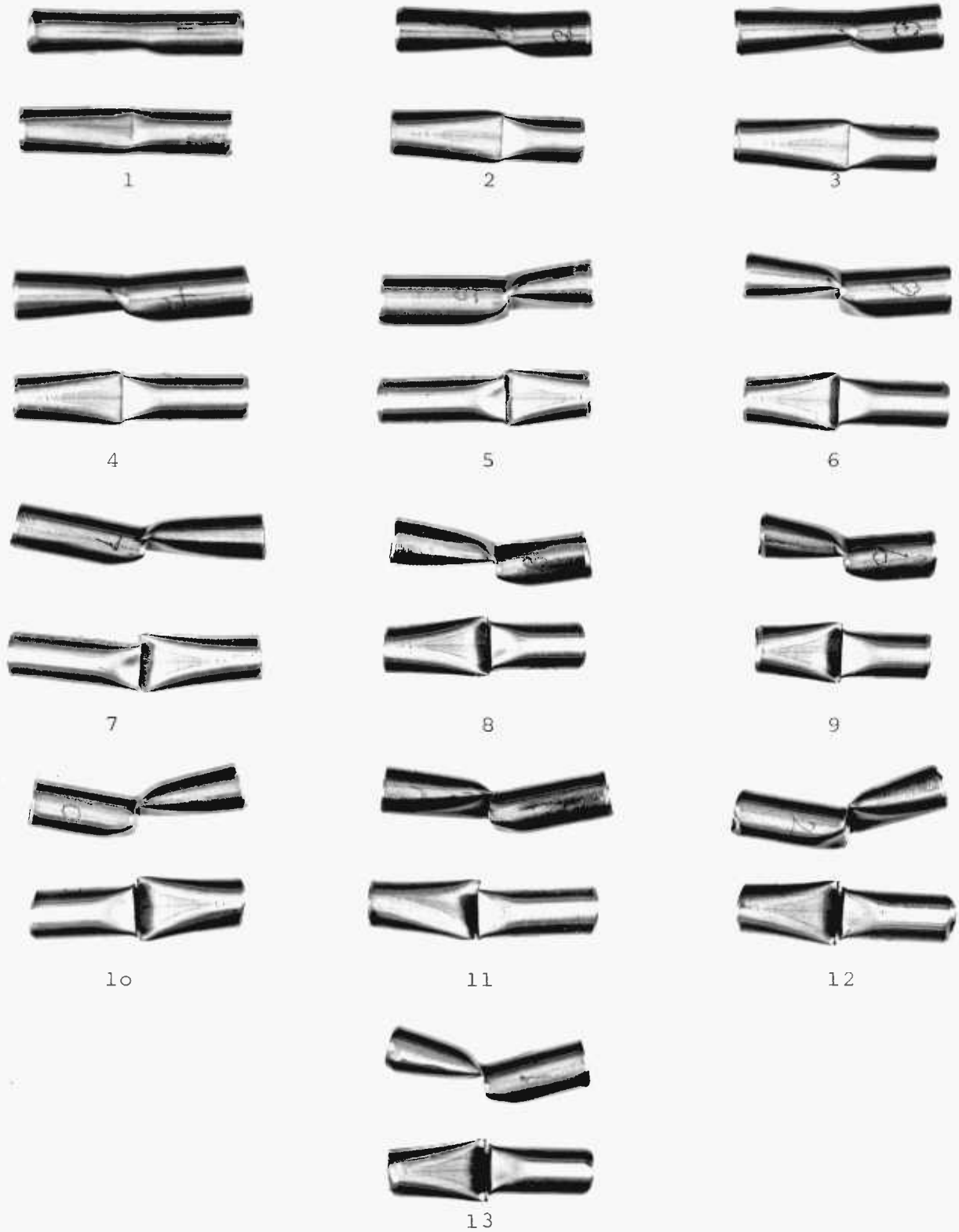


FIG. 2.37. INCREMENTAL CROPPING OF M316 TUBE (SEE TABLE 2.7)

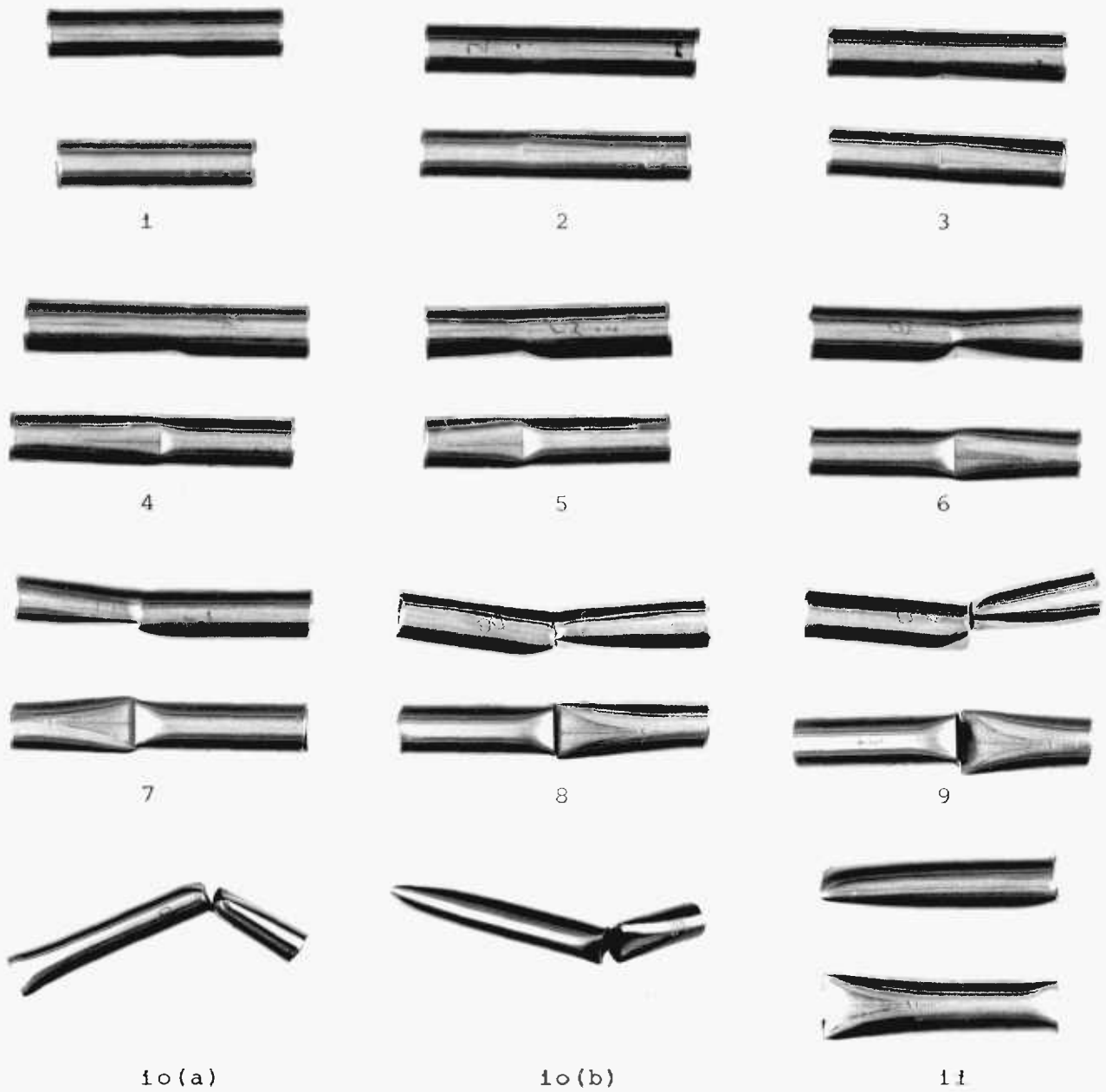


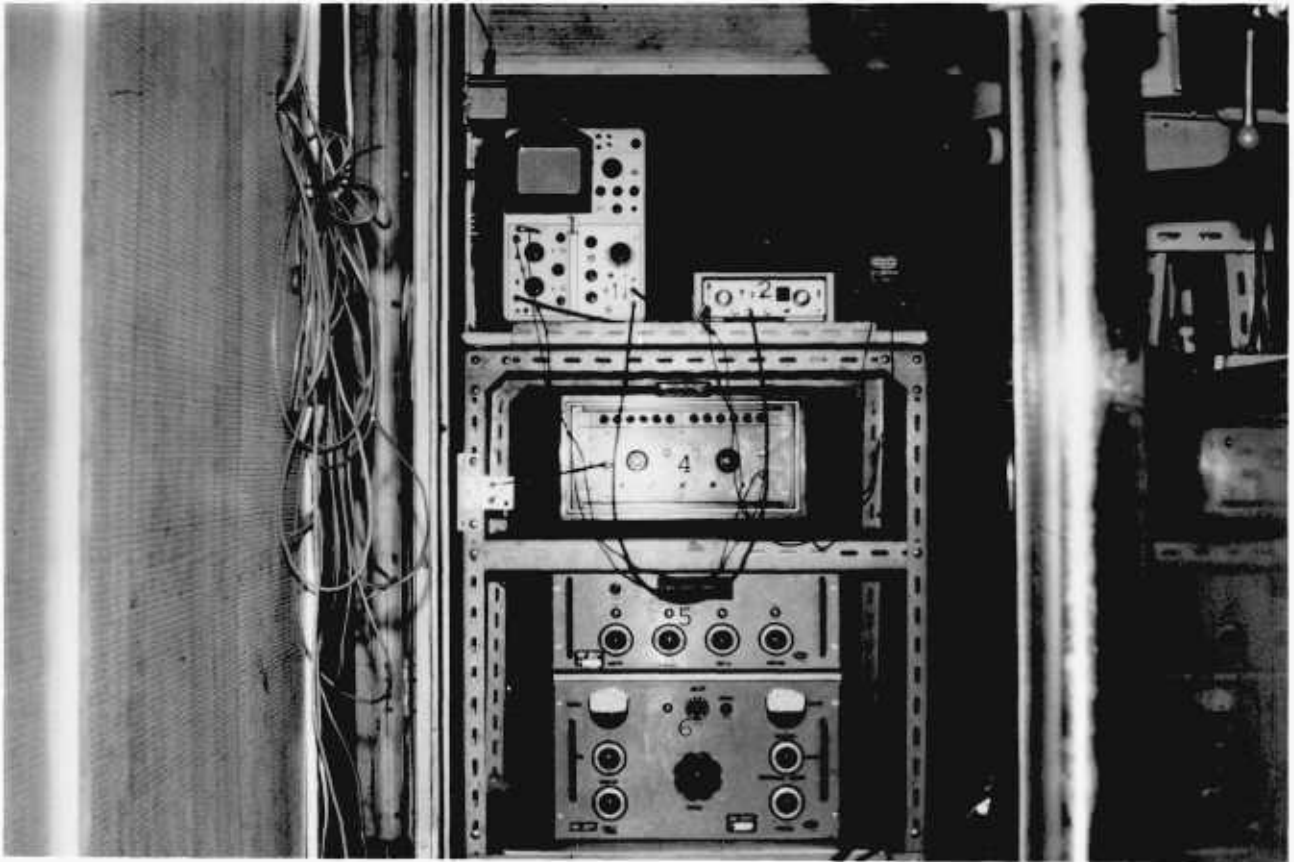
FIG. 2.38. INCREMENTAL CROPPING OF PE16 TUBE (SEE TABLE 2.7)

2.7.3 Conducting paint technique

The paint trace was connected in parallel with a by-pass resistance. A Transient Recorder, DL901, was used in conjunction with an oscilloscope, as shown in fig. 2.39.

The DL901 Transient Recorder is a digital instrument designed to capture single shot or low repetition events and present them for continuous display on an oscilloscope which is then read out to a Y/t plotter. One of the main applications of the DL901 is to record unique signals. Once the wave form has been digitised and stored in the memory using the single shot mode, it will remain there permanently unless the operator instructs the unit to take a fresh record, or power is removed from the instrument. The DL901 is ideal for continuous monitoring of low repetition rate signals whether they be fast or slow. A signal of a few milliseconds duration repeating 4 or 5 times a second is extremely difficult to view on an ordinary oscilloscope. By connecting the DL901 to the oscilloscope and using the continuously triggered mode, each signal is displayed on the screen until a new record replaces it.

The cathode-ray oscilloscope is a voltmeter which can be employed to measure transient voltage signals. The cathode-ray tube is a highly evacuated tube where electrons are produced by heating a cathode. The electrons are then collected, accelerated and focussed on to a fluorescent screen on the face of the tube. The impinging stream of electrons form a bright point of light on the fluorescent screen. Voltages applied to the horizontal and vertical deflection plates located in the cathode-ray tube will deflect the stream of electrons and move the bright spot of light over the face of the tube. It is this ability to deflect the stream of electrons which permits the cathode-ray tube to be employed as a dynamic voltmeter having an inertialess indicating system.



1.Oscilloscope 2.Transient recorder 3.Power pack 4.Amplifier 5.Control unit WG25
6.Power unit WG15

FIG.2.39.INSTRUMENTS USED IN CONDUCTING PAINT TECHNIQUE AND HIGH SPEED PHOTOGRAPHY

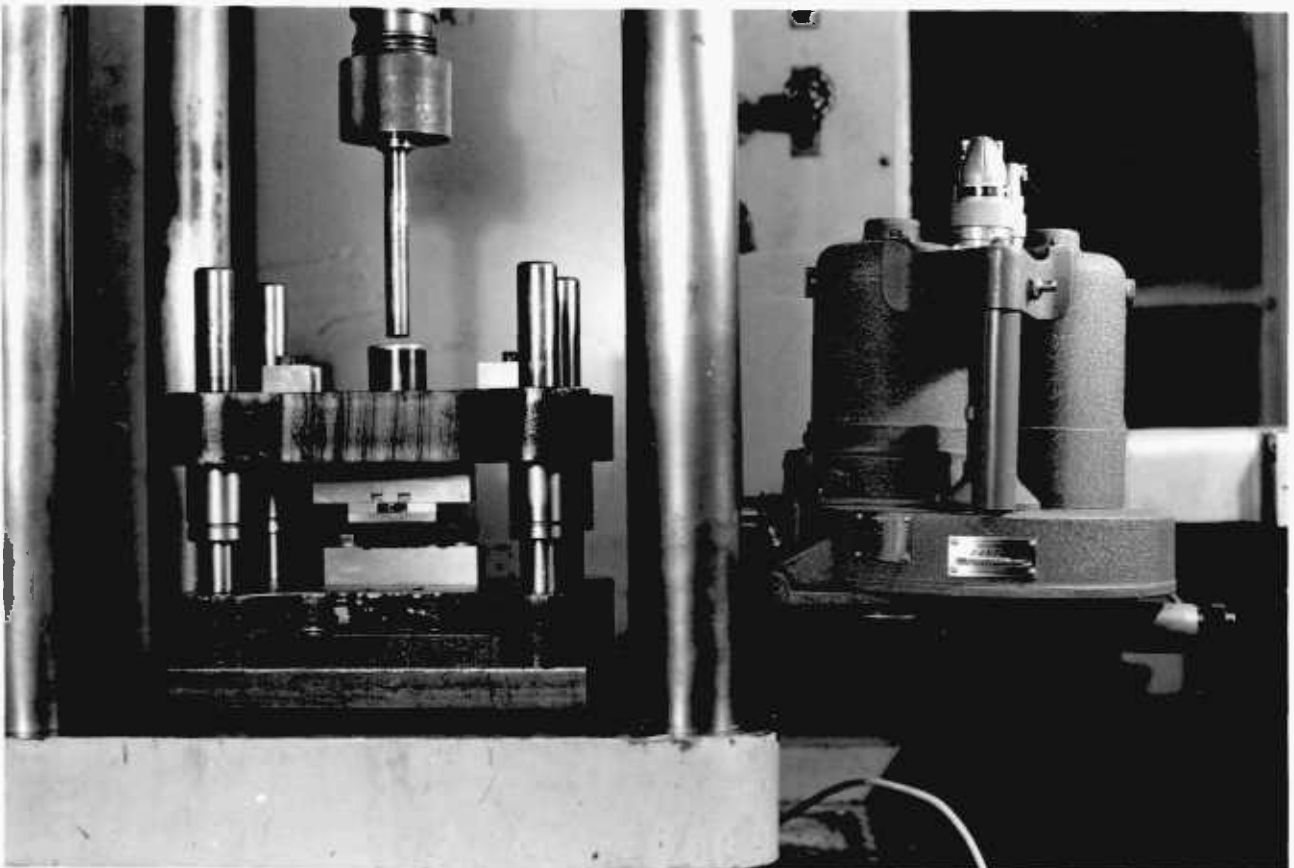


FIG.2.40.POSITION OF FASTAX CAMERA

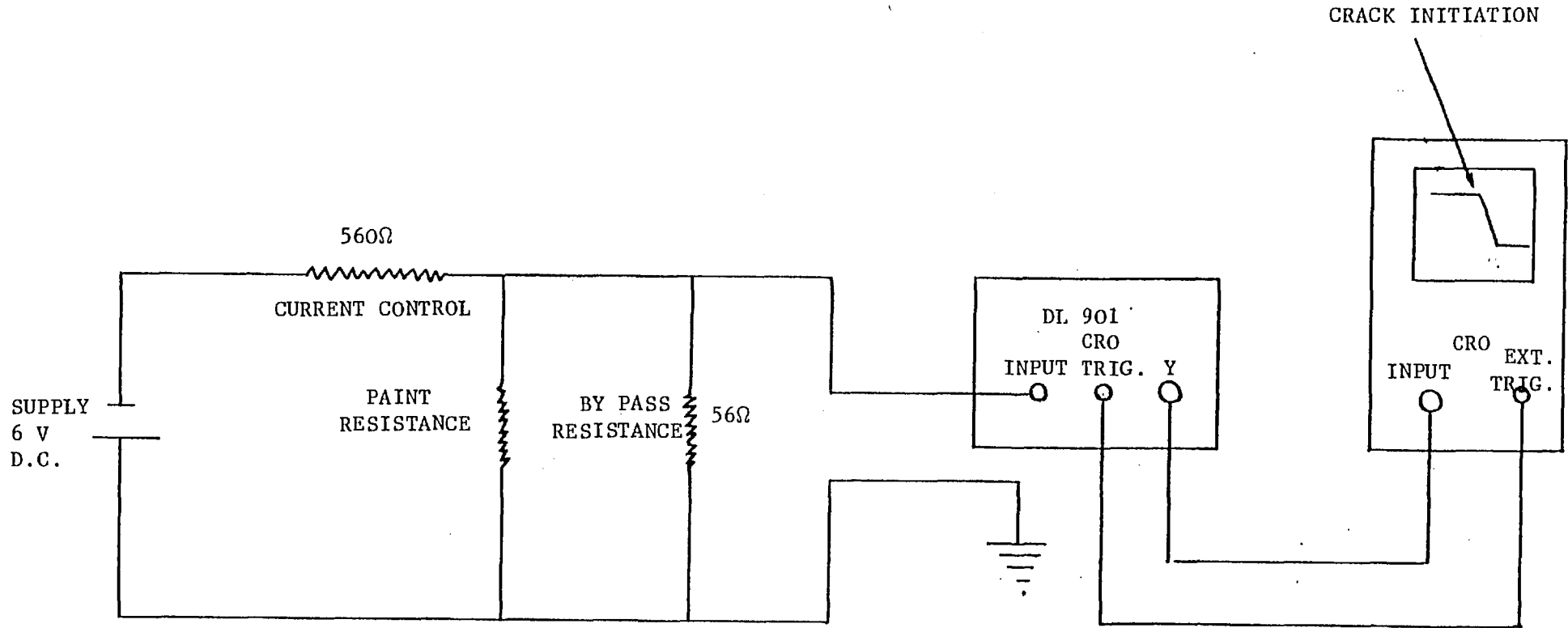


FIG. 2.41. CIRCUIT DIAGRAM OF SILVER PAINT TECHNIQUE

A dispersion of silver (DAG 915) will produce a thin, smooth, adherent, flexible silver coating of high electrical conductivity on a wide variety of materials, including plastics. DAG 915 consists of silver, methyl isobutyl ketone and n-butyl acetate [63].

Equal parts of epoxy encapsulant compound resin and hardener were mixed and stirred thoroughly. After two hours, the mixture was applied to the surface of the tube and the specimen was clamped to squeeze out the excess resin and to obtain a thin uniform layer. The paint was thoroughly shaken before use to ensure homogeneity. A thin layer of paint was applied with a fine brush to the stainless steel tube. The resistance of the paint trace was checked and it was then connected in parallel with the by-pass resistance. The D.C. input, current control resistance, the paint resistance, by-pass resistance, the DL 901 Transient Recorder and oscilloscope were connected as per the circuit diagram shown in fig. 2.41.

The time to fracture as observed fracturing of the paint trace was of the order of 10 μ -seconds; it was recorded on the oscilloscope incorporated in the circuit as shown in fig. 2.41. The crack initiation point was identified and related to the cropping load trace which was recorded simultaneously on the second channel of the oscilloscope.

2.7.4 Tube as electrical conductor

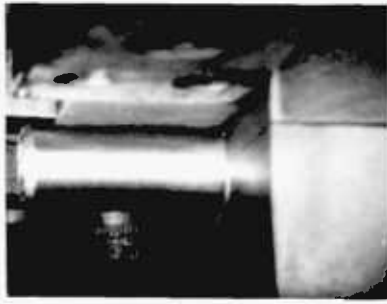
This technique is virtually the same as the conducting paint technique except that the paint trace is replaced by the tube itself. The crack initiation point in relation to the cropping load trace is the same as before. However, the technique was not as successful as the previous one because of the very low resistance of the tube material.

2.7.5 High speed cinematography

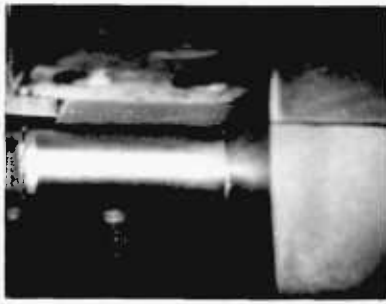
Wollensak Fastax cameras are designed for speeds of 150 to 18,000 pictures per second. Two motors, which can be operated from an A.C. to D.C. source, are used to drive and take up the film. A cut-off switch automatically interrupts power to the motors when the film is exhausted. A time-marking device is provided in the camera, in order that data recorded on the film can be accurately timed. The device normally consists of the inert gas lamps in close proximity to the film, and fired by a suitable power supply. One thousand cycles per second is recommended for speeds of 1000 frames and higher. The second timing light may be used to indicate event time, that is, to provide a time datum starting at a specific point in the sequence under study. The position of the camera is shown in fig. 2.40.

The Weinberger power and programming control units were used in conjunction with the Fastax camera to provide precise operational control, as shown in fig. 2.39. They provide accurate synchronisation of camera run with lighting and the event to be photographed so that consistently satisfactory film records are obtained even at the highest speed. Power unit WG-15 supplies the current for all 16 mm and 8 mm cameras of up to 120 metres capacity. Control unit WG-25 ensures timing control and synchronization. The short exposures at high camera speeds of very fast events require precise timing of the course of the event and running of the camera.

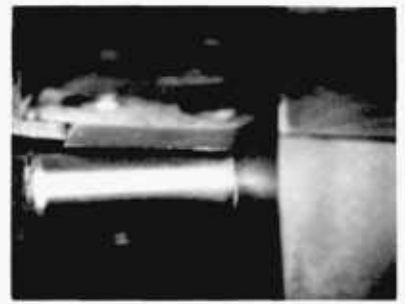
High speed cine films have been taken of cropping M316 and embrittled M446 steel tubes, both empty and filled. Some important pictures are shown in figs 2.42 and 2.43 for M316 and in figs 2.45 and 2.46 for M446. These pictures are identified in relation to the load-deflection diagrams as shown in figs 2.44 and 2.47 respectively.



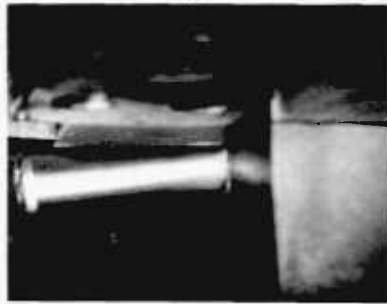
1



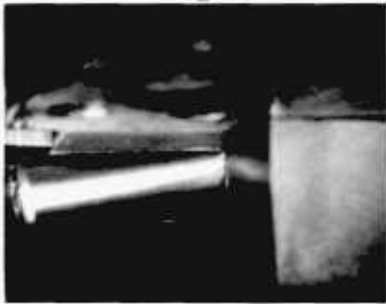
2



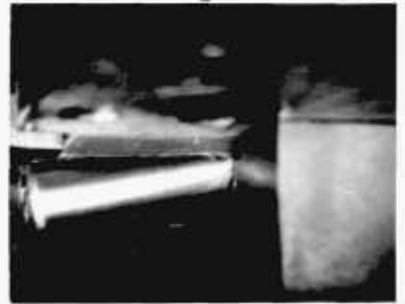
3



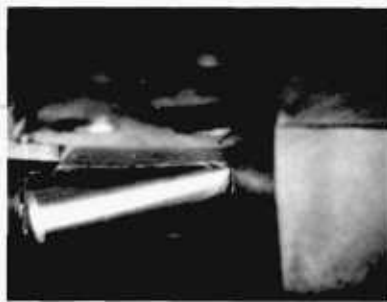
4



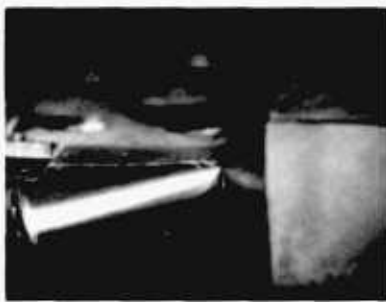
5



6



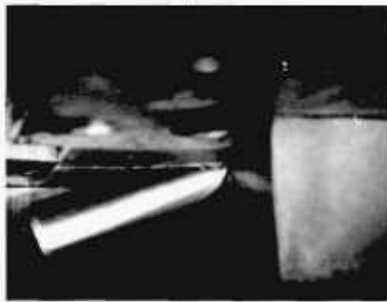
7



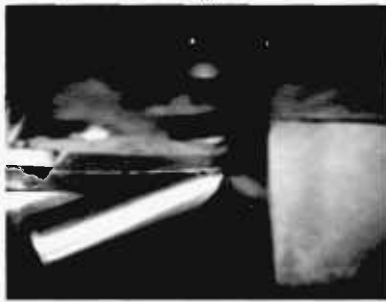
8



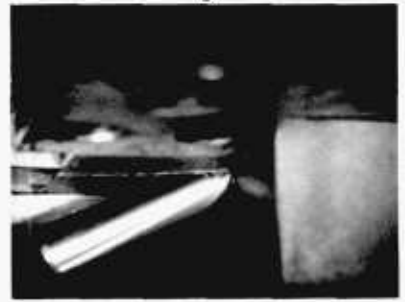
9



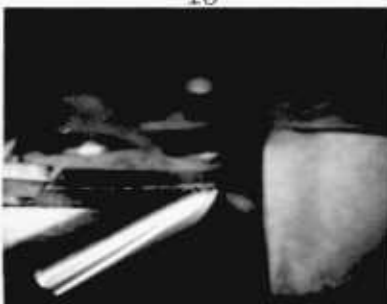
10



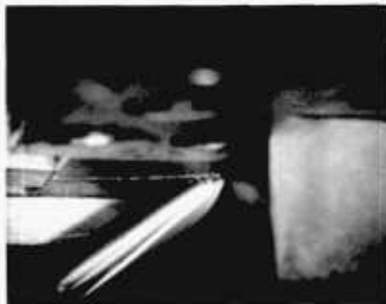
11



12



13



14



15

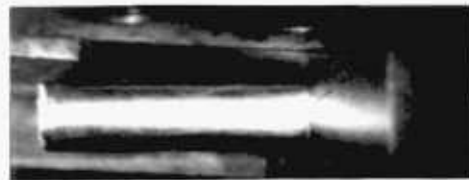
FIG. 2.42. SOME IMPORTANT FRAMES TAKEN FROM A HIGH SPEED FILM OF M316-EMPTY TUBE



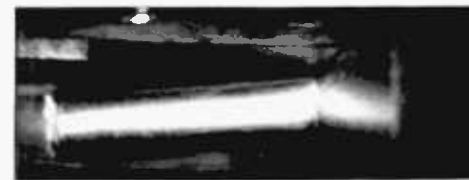
1



2



3



4



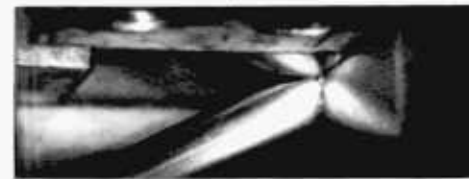
5



6



7



8



9



10



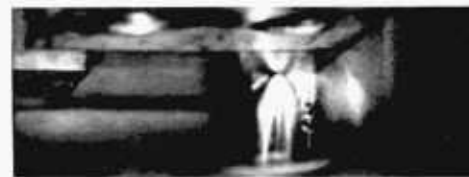
11



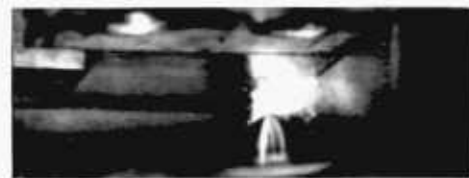
12



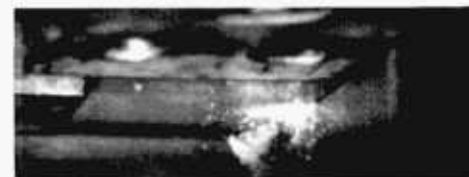
13



14



15



16

FIG. 2.43. SOME IMPORTANT FRAMES TAKEN FROM A HIGH SPEED CINE FILM OF M3i6-FILLED WITH GLASS

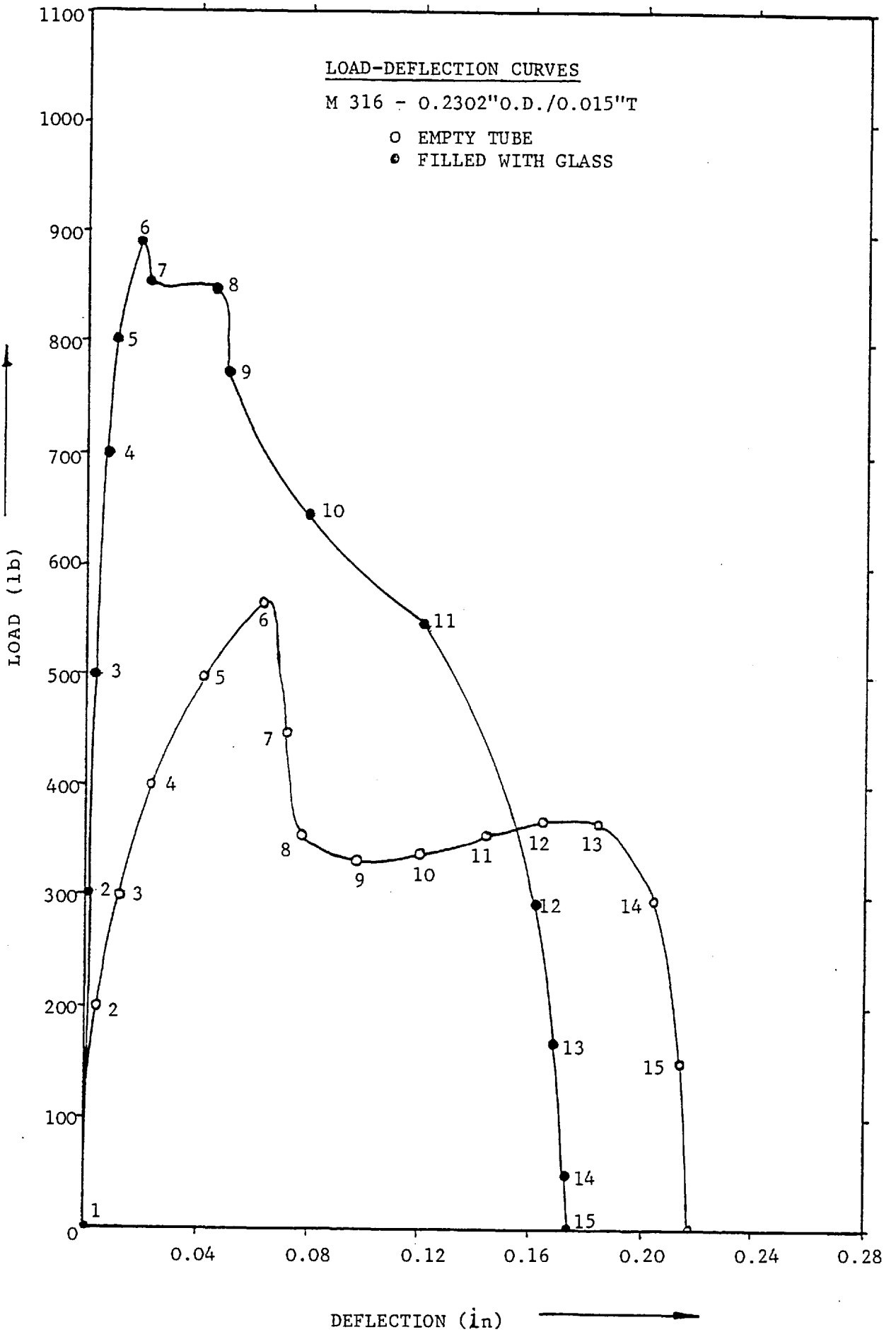
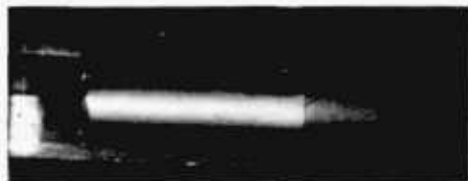


FIG. 2.44 (See Figs 2.42 and 2.43)



1



2



3



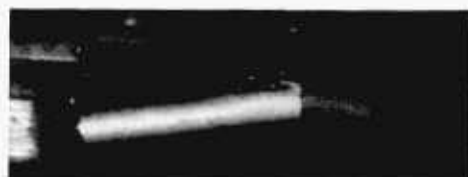
4



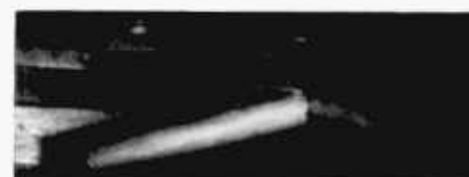
5



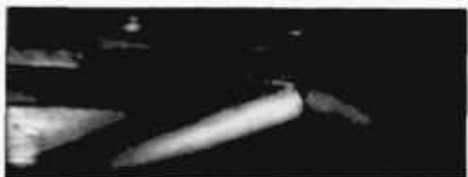
6



7



8



9



10



11



12



13



14

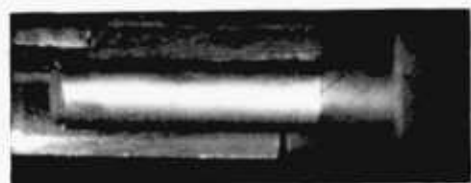


15

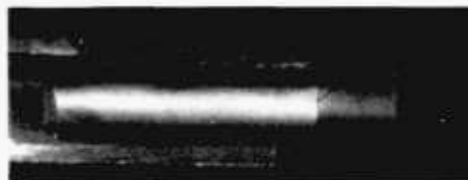


16

FIG. 2.45. SOME IMPORTANT FRAMES TAKEN FROM A HIGH SPEED FILM OF EMBRITTLED M446-EMPTY TUBE



1



2



3



4



5



6



7



8



9



10



11



12



13



14



15



16

FIG.2.46. SOME IMPORTANT FRAMES TAKEN FROM A HIGH SPEED FILM OF EMBRITTLED M446 TUBE-FILLED WITH ALUMINA

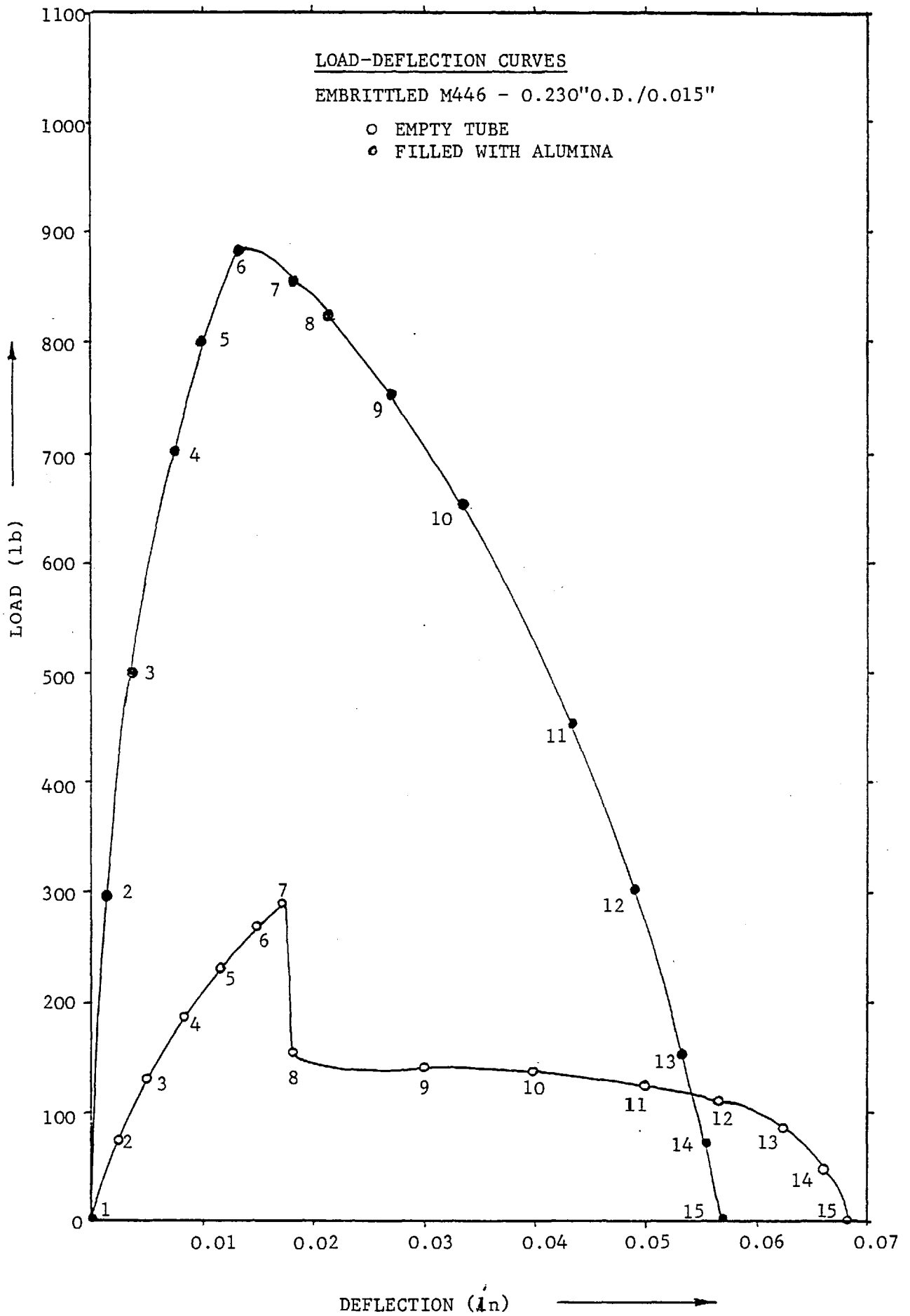


FIG. 2.47 (See Figs 2.45 and 2.46)

TABLE 2.1

S1. No.	Details of the tube O.D/T in inches	Maximum cropping load in pounds	Velocity of the blade at the max. load in inches per second	Distortion of the billet w.r.t. its outside dia. (d_{\min}/d_{\max})	Distortion of the billet w.r.t. its inside dia. (d_{\min}/d_{\max})	Distortion of the tube w.r.t. its outside dia. (d_{\min}/d_{\max})	Distortion of the tube w.r.t. its inside dia. (d_{\min}/d_{\max})
1	M316-55 0.2302/0.0151	570	0.050	0.186	0.088	0.913	0.942
2	"	565	0.066	0.200	0.100	0.926	0.932
3	"	563	0.833	0.090	0.048	0.910	0.960
4	"	560	1.087	0.098	0.048	0.960	0.915
5	"	560	1.160	0.122	0.041	0.936	0.905
6	"	555	1.930	0.100	0.077	0.980	0.925
7	PE16-Nimonic 0.2299/0.01495	537	0.050	0.392	0.348	0.940	0.918
8	"	537	0.200	0.387	0.343	0.952	0.920
9	"	535	0.605	0.400	0.340	0.950	0.929
10	"	534	0.980	0.405	0.349	0.955	0.930
11	"	531	1.320	0.409	0.355	0.952	0.939
12	"	530	2.100	0.410	0.360	0.960	0.948

TABLE 2.2

Sl. No.	Details of the tube O.D/T in inches	Angle of blades in degrees	Maximum cropping load in pounds	Velocity of the blade in inches per second	Distortion of the billet w.r.t. its outside dia. (d_{\min}/d_{\max})	Distortion of the billet w.r.t. its inside dia. (d_{\min}/d_{\max})	Distortion of the tube w.r.t. its outside dia. (d_{\min}/d_{\max})	Distortion of the tube w.r.t. its inside dia. (d_{\min}/d_{\max})
1	M316-SS 0.2302/0.0151	0	570	0.4	0.203	0.154	0.990	0.902
2	"	5	568	"	0.170	0.126	0.987	0.980
3	"	10	568	"	0.182	0.124	0.990	0.970
4	"	15	565	"	0.169	0.130	0.986	0.990
5	PE16-Nimonic 0.2299/0.01495	0	538	"	0.347	0.324	0.942	0.898
6	"	5	537	"	0.340	0.310	0.944	0.900
7	"	10	537	"	0.330	0.312	0.942	0.890
8	"	15	535	"	0.334	0.309	0.927	0.877
9	M316-SS 0.2302/0.0151 (with a support under billet)	0	575	"	0.194	0.138	0.980	0.940
10	PE16-Nimonic 0.2299/0.01495 (with a support under billet)	"	540	"	0.357	0.344	0.986	0.920

TABLE 2.3

Sl. No.	Details of tube O.D/T in inches	Maximum cropping load in pounds	Velocity of the blade in inches per second	Deflection of the blade at max. load inches	Wear of the blade in microns	Distortion of the billet w.r.t. its outside dia.		Distortion of the billet w.r.t. its inside dia.		Distortion of the tube w.r.t. its outside dia.		Distortion of the tube w.r.t. its inside dia.	
						(d_{min}/d_{max})	(d_{min}/d_{max})	(d_{min}/d_{max})	(d_{min}/d_{max})	(d_{min}/d_{max})	(d_{min}/d_{max})		
1	AISI-4132 0.1214/0.0092 (1Cr, 0.2Mo, 0.3C, 0.5Mn, 98.0)	148	0.4	0.060	0	0.144	0.079	0.592	0.491				
2	304MILT-6845 0.1275/0.029 (18.0Cr, 10.0Ni, 0.06C, 1.5Mn, 70.44Fe)	610	"	0.040	0	0.370	0.160	0.960	0.870				
3	AISI-4132 0.142/0.011 (1.0Cr, 0.2Mo, 0.3C, 0.5Mn, 98.0Fe)	230	"	0.055	0	0.190	0.130	0.675	0.600				
4	304MILT-6845 0.1895/0.0275 (18.0Cr, 10.0Ni, 0.06C, 1.5Mn, 70.44Fe)	930	"	0.060	0	0.550	0.460	0.925	0.680				
5	9Cr/Mo-COMM 0.2304/0.0153 (9.0Cr, 0.2Mo, 0.3C, 0.5Mn, 90.0Fe)	522	"	0.060	0	0.185	0.130	0.950	0.945				
6	PE16-UCAR 0.2299/0.01495 (16.5Cr, 0.05C, 3.5Mo, 1.2Ti, 44.0Ni, 34.8Fe)	535	"	0.052	5	0.394	0.342	0.950	0.935				
7	M316-SS 0.2302/0.0151 (16.7Cr, 13.4Ni, 0.04C, 2.4Mo, 1.8Mn, 0.42Si, 65.0Fe)	567	"	0.065	5	0.122	0.048	0.945	0.920				
8	FV607-COMM 0.2362/0.0304 (11.0Cr, 0.6Ni, 0.15C, 0.8Mo, 0.25V, 87.2Fe)	1196	"	0.060	8	0.475	0.325	0.870	0.760				
9	AISI-4132 0.2514/0.0281 (1.0Cr, 0.2Mo, 0.3C, 0.5Mn, 98.0Fe)	825	"	0.070	10	0.143	0.120	0.769	0.680				
10	304MILT-6845 0.251/0.0208 (18.0Cr, 10.0Ni, 0.06C, 1.5Mn, 70.44Fe)	907	"	0.075	10	0.118	0.070	0.670	0.584				
11	304MILT-6845 0.2520/0.028 (18.0Cr, 10.0Ni, 0.06C, 1.5Mn, 70.44Fe)	1208	"	0.070	10	0.185	0.098	0.751	0.640				
12	304MILT-6845 0.3150/0.02155 (18.0Cr, 10.0Ni, 0.06C, 1.5Mn, 70.44Fe)	1216	"	0.100	10	0.130	0.082	0.927	0.960				
13	304MILT-6845 0.3772/0.02865 (18.44Cr, 10.0Ni, 0.06C, 1.5Mn, 70.44Fe)	1780	"	0.1125	10	0.128	0.098	0.975	0.892				
14	M347-T-58 0.5005/0.0225 (18.0Cr, 11.0Ni, 0.06C, 0.7Nb, 1.5Mn, 68.74Fe)	1874	"	0.125	10	0.375	0.300	0.954	0.923				

TABLE 2.4

Sl. No.	Details of O.D/T in inches (filled with glass)	Maximum cropping load in pounds	Velocity of the blade in inches per second	Deflection of the blade at max. load inches	Wear of the blade in microns	Distortion of the billet w.r.t. its outside dia. (d _{min} / d _{max})		Distortion of the billet w.r.t. its inside dia. (d _{min} / d _{max})		Distortion of the tube w.r.t. its outside dia. (d _{min} / d _{max})		Distortion of the tube w.r.t. its inside dia. (d _{min} / d _{max})	
1	AISI-4132	350	0.4	0.012	10	0.375	0.360	0.820	0.790				
	0.1214/0.0092	355	1.0	0.011	10	0.390	0.365	0.830	0.810				
2	304MILT-6845	820	0.4	0.030	10	0.500	0.300	0.885	0.650				
	0.1275/0.029	828	1.0	0.029	10	0.540	0.360	0.960	0.920				
3	AISI-4132	414	0.4	0.015	10	0.580	0.510	0.930	0.970				
	0.142/0.011	426	1.0	0.013	10	0.810	0.740	0.980	0.980				
4	304MILT-6845	1160	0.4	0.032	10	0.400	0.300	0.775	0.660				
	0.1895/0.0275	1174	1.0	0.030	10	0.520	0.450	0.805	0.750				
5	9Cr/Mo-COMM	828	0.4	0.019	10	0.570	0.465	0.730	0.630				
	0.2304/0.0153	847	1.0	0.017	10	0.610	0.605	0.760	0.640				
6	PE16-UCAR	860	0.4	0.018	11	0.615	0.545	0.916	0.850				
	0.2299/0.01495	870	1.0	0.017	11	0.720	0.674	0.970	0.830				
7	M316-SS	890	0.4	0.019	11	0.500	0.488	0.870	0.780				
	0.2302/0.0151	910	1.0	0.018	11	0.750	0.710	0.960	0.850				
8	FV607-COMM	1592	0.4	0.035	11	0.560	0.385	0.920	0.833				
	0.2362/0.0304	1610	1.0	0.033	11	0.580	0.405	0.850	0.800				
9	AISI-4132	1095	0.4	0.034	11	0.418	0.333	0.860	0.780				
	0.2514/0.0281	1098	1.0	0.032	11	0.490	0.360	0.750	0.707				
10	304MILT-6845	1208	0.4	0.022	11	0.343	0.260	0.777	0.660				
	0.2510/0.0208	1212	1.0	0.021	12	0.360	0.320	0.650	0.580				
11	304MILT-6845	1510	0.4	0.029	12	0.370	0.275	0.810	0.690				
	0.2520/0.028	1526	1.0	0.029	12	0.390	0.285	0.805	0.700				
12	304MILT-6845	1570	0.4	0.025	12	0.360	0.281	0.590	0.484				
	0.3150/0.02155	1570	1.0	0.023	12	0.530	0.451	0.906	0.901				
13	304MILT-6845	2278	0.4	0.049	12	0.385	0.310	0.810	0.780				
	0.3772/0.02865	2280	1.0	0.037	12	0.510	0.490	0.820	0.790				
14	M347-T-58	2590	0.4	0.052	12	0.495	0.480	0.962	0.925				
	0.5005/0.0225	2602	1.0	0.039	12	0.589	0.525	0.960	0.930				

TABLE 2.5

Sl. No.	Details of the tube O.D./T in inches	Filling material & size in inches	Velocity of blade in inches per second	Maximum load in pounds	Deflection of blade at max. load in inches	Distortion of billet w.r.t. its outside dia. (d_{\min}/d_{\max})	Distortion of billet w.r.t. its inside dia. (d_{\min}/d_{\max})	Distortion of tube w.r.t. its outside dia. (d_{\min}/d_{\max})	Distortion of tube w.r.t. its inside dia. (d_{\min}/d_{\max})
1	0.230/0.04 Glass tube	On its own	0.4	148	0.002	0.990	0.982	0.996	0.994
2	0.230 ϕ Glass rod	"	"	285	0.005	0.988	0.986	0.996	0.992
3	0.230/0.015 Embrittled M446	Empty	0.4	290	0.017	0.720	0.707	0.847	0.842
4	"	"	1.0	290	0.013	0.735	0.705	0.900	0.885
5	"	0.190 ϕ Alumina	0.4	885	0.013	0.945	0.930	0.970	0.965
6	"	"	1.0	865	0.012	0.950	0.923	0.978	0.976
7	"	0.1975 ϕ Glass rod	0.4	720	0.012	0.980	0.974	0.998	0.996
8	"	"	1.0	702	0.010	0.985	0.982	0.998	0.995
9	0.2299/0.01495 PE16-UCAR	0.190 ϕ Alumina	1.0	1190	0.018	0.760	0.725	0.913	0.897
10	M316-SS 0.2302/0.0151	0.190 ϕ Alumina	1.0	1235	0.019	0.795	0.651	0.920	0.982
11	"	0.1975 ϕ Glass rod	"	870	0.020	0.642	0.630	0.968	0.945
12	"	0.1985 ϕ Glass rod	"	890	0.018	0.756	0.720	0.940	0.928
13	"	0.199 ϕ Glass rod	"	895	0.016	0.785	0.792	0.985	0.964

TABLE 2.6

Sl. No.	Details of the specimen OD./T in inches	Filling material & size in inches	Cropping & conditions	Velocity of blade at max. load in in./sec.	Maximum cropping load in pounds	Deflection at max. load in inches	Distortion of billet w.r.t. its outside dia.		Distortion of tube w.r.t. its outside dia.	
							(d_{min}/d_{max})	(d_{min}/d_{max})	(d_{min}/d_{max})	(d_{min}/d_{max})
1	PE16-UCAR 0.2299/0.01495	Empty	Under 200 lbs tensile pre-load	1.0	526	0.050	0.376	0.343	0.743	0.717
2	"	0.1985 ϕ Glass rod	"	"	827	0.017	0.880	0.875	0.905	0.884
3	M316-SS 0.2302/0.0151	Empty	"	"	570	0.055	0.251	0.223	0.644	0.620
4	"	0.1985 ϕ Glass rod	"	"	840	0.018	0.910	0.902	0.980	0.972
5	PE16-UCAR 0.2299/0.01495	Empty	Under 200 lbs compressive load	"	645	0.062	0.400	0.376	0.845	0.798
6	"	0.1985 ϕ Glass rod	"	"	1069	0.017	0.884	0.870	0.984	0.974
7	M316-SS 0.2302/0.0151	Empty	"	"	680	0.062	0.296	0.274	0.940	0.894
8	"	0.1985 ϕ Glass rod	"	"	1135	0.017	0.897	0.890	0.980	0.978
9	PE16-UCAR 0.2299/0.01495	Empty	-196°C	"	690	0.055	0.405	0.376	0.953	0.926
10	"	0.1985 ϕ Glass rod	"	"	1220	0.016	0.730	0.695	0.954	0.935
11	M316-SS 0.2302/0.0151	Empty	"	"	745	0.065	0.101	0.088	0.942	0.915
12	"	0.1985 ϕ Glass rod	"	"	1270	0.018	0.548	0.522	0.910	0.896
13	M446-Embrittled SS 0.230/0.015	Empty	"	"	210	0.006	0.930	0.928	0.994	0.990
14	"	0.190 ϕ Alumina	"	"	640	0.007	0.974	0.964	0.988	0.982
15	M316-SS 0.2302/0.0151	0.1995 ϕ Mld. stl rd	Conventional	0.1	2450	0.090	0.688	0.625	0.895	0.865
16	M316-SS 0.250	-	"	"	3830	0.140	0.715	0.705	0.890	0.882
17	PE16-UCAR 0.250									

TABLE 2.7

No. of the increment	M316-SS of 0.2302"/0.0151"		PE16-Nimonic of 0.2299"/0.01495"	
	Load in pounds	Deflection in inches	Load in pounds	Deflection in inches
1	374	0.029	122	0.000
2	495	0.040	224	0.006
3	540	0.055	316	0.012
4	572	0.068	352	0.016
5	352	0.120	409	0.025
6	350	0.135	457	0.036
7	380	0.147	547	0.052
8	340	0.158	410	0.086
9	320	0.164	350	0.124
10	406	0.178	330	0.168
11	374	0.187	0	0.200
12	380	0.189	-	-
13	358	0.192	-	-
14	0	0.215	-	-

TABLE 2.8

Sl. No.	Decay length (billet end) (in)		Decay length (constrained end) (in)	
	Experimental (measured length)	Empirical $L_f = D_m \sqrt{R_i/T}$	Experimental (measured length)	Empirical $L_c = A \ln(R_i/T)$
1	0.26	0.26	0.12	0.10
2	0.13	0.15	0.03	0.04
3	0.27	0.29	0.12	0.10
4	0.23	0.25	0.07	0.07
5	0.52	0.55	0.19	0.20
6	0.47	0.55	0.18	0.20
7	0.50	0.55	0.19	0.20
8	0.30	0.35	0.12	0.11
9	0.38	0.41	0.15	0.14
10	0.50	0.52	0.18	0.18
11	0.39	0.42	0.13	0.14
12	0.70	0.74	0.25	0.27
13	0.78	0.82	0.30	0.30
14	1.35	1.52	0.45	0.55

2.8 DISCUSSION OF EXPERIMENTAL RESULTS

2.8.1 A typical tube cropping cycle

(a) Empty tubes: A typical cropping cycle may be explained by splitting the load variation with time and deflection with time diagrams into three zones, namely A, B and C respectively as shown in fig. 2.49.

Zone A

This zone is identified as first shearing. At the beginning of the process the whole surface of the tube makes contact with the blade. If there is no support under the free end of the tube, it suffers a rotation. This rotation causes the contact length to change and the loads to become concentrated near the cutting edge (see figs 2.37 and 2.38). With a further downward motion of the moving blade, the concentrated load near the cutting edge deforms the tube and becomes distributed over a small length. The load generated during this motion of the blade causes the tube to bend, which introduces a tendency for outward flow of the material in the axial direction. Such a tendency would generate frictional forces on the blade contact surface. With progressive increase of the cropping load at some part near the cutting edge, the generated stresses on the tube will cause the material to change from the elastic state to the plastic state permitting penetration of the blade. At the maximum load, the contact between the material and the blade is only at the edges and is shown diagrammatically in the figure below.

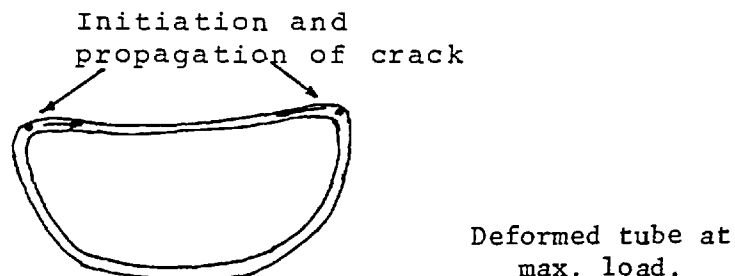


Figure 2.48

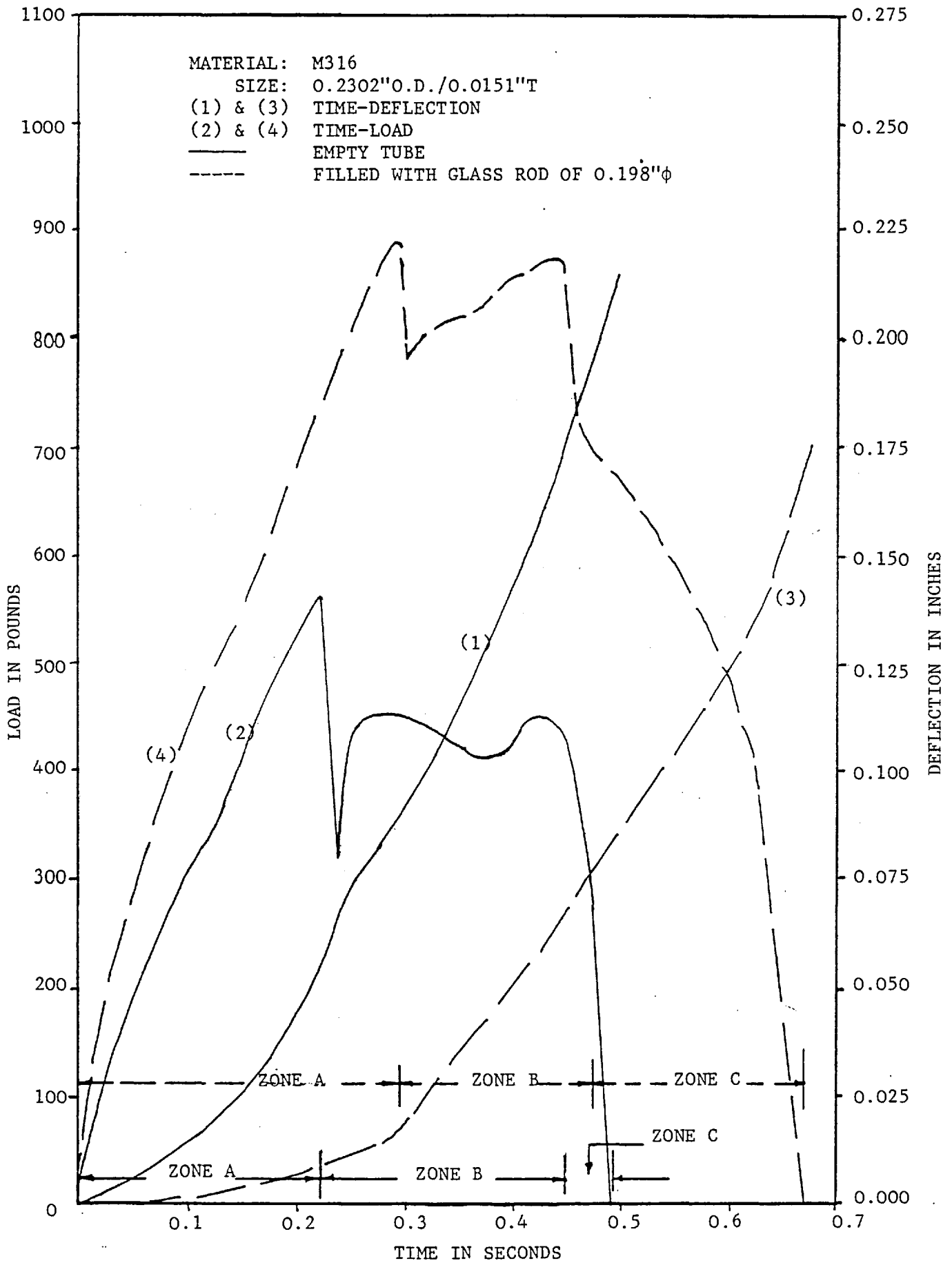


FIG. 2.49

After a certain depth of penetration of the blade, the cracks *apparently* initiated at both edges simultaneously and propagates towards the centre as shown in the above diagram and separation of the material occurs on the flattened part of the tube. Examination of the incrementally cropped tubes just before and just after the maximum cropping load (see figs. 2.37 and 2.38) clearly shows that initiation of the crack starts immediately after the maximum load. These specimens have also been examined by ordinary microscope and dye penetrant techniques. No crack was observed on the specimen before maximum cropping load.

A sudden change in the velocity of the blade at maximum load shows an indication of the initiation of the crack just after maximum load. A sudden jump of the blade at maximum load has also been observed on the high speed film. The crack initiation point recorded using the conducting point technique coincides with the cropping load trace at maximum cropping load. Once the crack is opened, the load drops off quickly, to a certain extent.

Zone B

This zone is identified as a sliding and tearing zone. After initiation, the crack must proceed within the tube in a path determined by the characteristics of the stress-field. If the strain energy stored by the body is sufficiently large then only such crack propagation can take place. An attempt was also made to study the crack propagation rate using the conducting paint technique but it was not successful because of large deformation of the tubes during the cropping process. Once crack initiation starts, contact between blade and material at the cutting edge ceases. The time taken to break the silver paint on the tube is about 10 μ -seconds, as recorded on the oscilloscope. Only the top flattened part of the tube is being sheared in the first instance whereas the rest of the tube acts as a rigid support. The blade, which

is out of contact for a fraction of a second, comes into contact with the material again and increases the load slightly. The final load at the end of this zone depends on the area of cross-section of the unsheared tube. It is also the load required to tear the tube through to its bottom surface. More extensive deformation of the tube occurs in this zone because the tube is being compressed by the moving blade and tearing takes place simultaneously. The velocity of the blade in this zone is greater than in the cutting zone. This is a typical zone and only occurs in the cropping of thin-walled tubes - it is not observed in bar cropping. For a glass tube, the load drops off quickly to zero after maximum load, which indicates that whole cycle is completed within zone A.

Zone C

This zone may be identified as the second shearing zone. The load slightly increases at the end of the tearing zone for ductile materials such as stainless steel and decreases for relatively less ductile materials such as nimonic-PE16. The blade shears the flattened bottom part of the tube and once again the crack initiates and propagates till complete separation of the tube occurs. The load drops off quickly to zero and the cropping cycle is therefore completed. The load required to shear the bottom part of the tube is higher when compared to the bottom sheared area. This is due to the cumulative effect of the load required to deform the whole billet and to shear the bottom part of the tube. The deformation across the entire cross-section of the tube at different loads can be observed from photographs of the incremental crops as shown in figs. 2.37 and 2.38.

(b) Filled tubes

A typical cropping cycle may be explained for filled tubes in the same way as for empty tube cropping (see fig. 2.49).

Zone A

This zone may be identified as first shearing. During the cropping operation, the load on the blade increases with penetration of the blade into the material. When the cropping load approaches the shearing strength of glass, a scratch is being made on the surface of the glass rod inside the tube due to the pressure exerted by the blade. Glass rod then breaks in the cutting zone only if a suitable flaw exists in this zone. If no such flaw exists, then fracture will commence at a flaw in a zone of smaller pressure close to the cutting edge. It has been proved that the glass rod definitely breaks somewhere between zero and first peak load, most probably just above the shearing load of the glass. This is actually observed by carrying out incremental tests and then carefully observing the glass pieces by dissolving the stainless steel material in *acqua regia* (1:3 ratio of nitric acid to hydrochloric acid), leaving the glass.

Once the load reaches a maximum, localized yielding occurs near the cutting edge of the blade. With this yielding, the blade penetrates into the material which suffers crack initiation. Unlike empty tube cropping, the blade shears a small portion of the tube in the first instance, resulting in a small sudden drop in the load as shown in fig. 2.49.

Zone B

This zone is identified as second shearing. As the blade advances further by flattening the tube, the load slightly increases till the second peak; this load is less than the first in most cases and vice versa in a few cases depending on the influence of the frictional forces developed between tube and tool. Then the blade shears the flattened part of the tube, resulting in a further drop in load immediately after

the second peak, simultaneously causing extensive deformation. The glass rod, which has already broken right across its cross-section, starts breaking further into small pieces then into powder in the cutting zone due to the pressure exerted by the blade. The load drops continuously, to a certain extent.

Zone C

This zone is similar to the last part of the bar cropping diagram. There is sufficient strain energy stored in the body and therefore fracture propagates around the circumference of the unsheared tube. In this situation the inside glass rod induces failure across the entire cross-section of the unsheared tube. Then the load drops off quickly to zero and hence the cycle is completed.

2.8.2 Bar cropping

(a) Metallic bars: The behaviour of M316 and PE16 rods subjected to shearing load exhibits no sign of a sudden load drop during the cycle, as shown in fig. 2.30. Even when the M316 stainless steel tube is filled with a mild steel rod without any clearance and is subjected to a shearing load, it behaves like a solid rod without any sudden drop of load during the cycle.

During bar cropping the load increases with blade penetration. Under the influence of the load the material becomes highly stressed, localized yielding occurring near the cutting edge of the blade. With this yielding the cutting edge penetrates which leads to crack initiation. There are passive forces such as those due to friction and inertia and their influences on the stress situation are also important. The actual mode of failure of the bar section will be governed by the resulting stress field and its influence on the properties of the bar material. The material of the bar, M316 stainless steel, is highly ductile and

permits large penetration of the blade before initiation of the crack. On the other hand, less ductile materials like PE16 are crack sensitive and hence permit smaller penetration of the blade. After a certain depth of penetration, fracture propagates and the cropping load decreases. This decrease is rapid in less ductile materials such as PE16 and occurs slowly in ductile materials such as M316. Cropping of solid rods involves fracture when failure is induced simultaneously across the entire cross-section of the bar whereas tube cropping involves fracture in two stages as explained earlier. There is no discontinuity in the loading cycle for bar cropping.

(b) Non-metallic bars

It is not possible to fill the tubes with spent fuel because of its radioactivity, but it is possible to simulate spent fuel by using ceramic or glass-like materials. Hence it is necessary to know the behaviour of glass, subjected to shearing load during the cropping process. As shown in fig. 2.31, the load increases to a maximum and then drops rapidly to zero. Penetration of the tool into glass is very much less than it would be into any metal and another interesting observation is that the load increases with increasing velocity of the blade. Examination of the cropped billets of glass and alumina shows that they shatter in a random manner. The observed irregularities in fracture increase with increasing velocity of the blade, particularly for glass rods. There is no sudden load drop during the cropping cycle as for metallic tubes.

Perhaps the most distinctive property of glass is its brittleness, a property easy to recognize, but not so simple to define in a quantitative manner. It is generally found that a brittle substance possesses relatively high elasticity, fair tensile strength, and shows no signs of plastic flow before fracture [31]. Once the tool makes contact with the glass rod, the

pressure between the tool and the material builds up quickly in the transverse direction at the cutting edge of the tool. The fissure commences from the surface for some distance at least and proceeds in a direction perpendicular to the surface. Once the crack has started, the distribution of stresses in glass changes, so that after a time the direction of maximum tension at the head of the crack may no longer be parallel to the glass surface. It is assumed that the glass surface breaks only from flaws; the blade, which produces a greater area of highly stressed surface, has a greater chance of finding a flaw within the highly stressed zone and therefore the breaking strength is relatively low. It has been known for more than fifty years that the time of loading has an effect on the breaking strength of glass, the strength declining with increase in the duration of load [32], presumably because glass is a super-cooled liquid. It is obviously important that the rate of loading should be standardized in experiments designed to investigate the effect of sample dimension on the strength.

2.8.3. The effect of independent variables

The general shapes of the graphs are similar for all the fifteen different empty tubes including embrittled M446 tube, as shown in figs 2.8 to 2.22. However, changes in the shape of the curve after reaching maximum load can be observed. After reaching the maximum cropping load, the crack is opened and the load drops off quickly by about 60% and then rises quickly by about 30%. It is steady for some time and then falls to zero. In all the experiments the penetration of the blade is nearly 100% from the top to the bottom surface of the tube before the billet is separated from the tube and this leads to distortion. Though the speed of the ram is held constant, approximately at 0.6" per second, the velocity of the blade varies from 0.4" per second to 0.6" per

second depending on the material and size. By slightly varying the speed of the ram, a number of experiments can be conducted. From these experiments the particular one having the velocity of the blade approximately 0.4" per second has been chosen. This has been done to compare the billets of different materials at a particular velocity of the blade as shown in Table 2.3. In general, distortion of the billet is very much greater than the cropped end of the tube in the work holder.

The general loading pattern is similar for all the filled tubes. It can be seen that there are two distinct peaks on the load-time curves. The cropping cycle has been explained in detail above. About 15% of the glass falls as 'fines' at the end of each experiment. The cropping load for a filled tube is about 2 to 10% higher than the sum of the shearing loads when they are cropped separately. These values are very close for smaller tubes. As far as the quality of the billet is concerned, of course there is quite a lot of improvement from an empty tube to a filled tube. This is because the tube is being supported by the glass rod. Discussion of several of the important parameters follows:

1. Clearance between the tool and the work holder

Experience in single cropping shows that optimum clearance is an inverse function of the material strength, i.e., with higher strength material, smaller clearance should be maintained [33]. In the present work it has been observed that a minimum clearance is better for stainless steel tube. In practice it is not possible to maintain zero clearance between the tool and work holder. Hence the minimum possible clearance has been maintained throughout the experimental work for both empty and filled tubes.

2. Blade geometry

As shown in Table 2.2, blade geometry has considerably less influence on the dependent variables (cropping load and cross-sectional distortion of the billet). It has been observed that cropping load decreases slightly with sharpness of the cutting edge of the blade. However, the blade geometry has virtually no influence on the quality of the billet for both empty and filled tubes. Hence a flat blade was used for both empty and filled tubes to study the influence of the other cropping parameters.

3. Cutting edge of the blade

It is important to check the blade wear because it affects the clearance between blade and work holder. The quality of the cropped billet can be expected to deteriorate with increasing blade wear [34]. With this idea in mind, the wear of the blade has been checked after each experiment. It is found that wear of the blade increases with number of crops. However the maximum wear after 1000 crops is only about 15 microns which can be neglected. It is so small because the tool is made of high quality steel.

4. Support under the billet

In conventional cropping, the moving blade exerts a moment about the stationary blade, which causes the billet to bend, producing a flat on the top surface of the billet, which is in direct contact with the blade. This is due to the asymmetry of forces acting upon the bar material during the cropping operation. The cropping region of the billet is severely distorted partly owing to the bending effect. The influence of the bending effect on the cropping load and cross-sectional distortion has been studied for the two materials M316 and PE16, by providing a support under the billet. As shown in Table 2.2, the bending

effect has little influence on cropping load. However, there is a slight improvement in the quality of billets.

5. Size of the billet

As shown in Table 2.3, the quality of the billet is better for lower diameter to thickness ratios. From the literature on bar cropping, it is known that the quality of the billet is influenced by billet length only in the cropping of billets having length to diameter ratios less than unity. In the present work it is intended to crop one inch length billets and, since the diameter of the biggest tube is half an inch, the length to diameter ratio is greater than unity.

From Table 2.3, it is observed that the deflection of the blade at maximum cropping load increases as the size of the tube increases.

6. Blade velocity

From Table 2.1 it is evident that cropping load decreases slightly with increasing velocity. However, it has no influence on the quality of billets for empty tubes. Perhaps a slight improvement in the quality of billets can be observed for relatively less ductile materials such as PE16.

It has been observed that the load increases with increasing velocity for tubes filled with glass. As discussed earlier, this is justified in the sense that the time of loading has an effect on the breaking strength of glass, the strength declining with increase in the duration of load. It was found from the experiments that a velocity of one inch per second is the optimum value for tubes filled with glass. Velocities higher than this would not improve the quality of billets but might produce defects. A visual comparison of the tubes produced at low speed, (0.4 inch per second) and at high speed (1.0 inch per second) shows that the distortion is lower at higher velocity. It is interesting to recall that this is

exactly the trend reported by Organ and Mellor [16] for high speed bar cropping.

There is a distinct improvement in the quality of billets for filled tubes as against empty tubes. It is observed that some materials such as PE16, FV607 exhibit a sensitivity to the speed of working. This means that these metals which suffer considerable distortion as a result of their ductility at low speeds tend to exhibit less distortion when cropped at high speeds.

7. Billet material

Although the general shape of the curves is the same, there are slight changes in the load trace after maximum cropping load, depending on the material. For example, the load is steady for some time for ductile materials such as M316 but decreases steadily for less ductile material such as PE16 before it drops off quickly to zero. The time taken to complete the cropping process and the deflection of the blade at maximum load are less for PE16, FV607 and M347 materials than for other stainless steel materials, for both empty and filled tubes. Cropping load mainly depends on the material and size of the tube. Comparing the same size tubes, the cropping load for M316 is higher than PE16.

There is no significant change in the values of distortion for the three crops for each condition. From Table 2.3, it is evident that the cross-sectional distortions of the materials, PE16, FV607, 9Cr/Mo, M347 are less compared to the other steels M316, M309, A S 4132, for both empty and filled tubes. Unlike the other tubes, the fracture mode is different for these four tubes in that the plane of the fracture surface is not perpendicular to the axis of the tube. A characteristic feature of the cropped PE16 tube is that a small piece of material is separated from the bottom surface of the billet.

The quality of an empty embrittled M446 steel billet has been improved to a greater extent than the cold-worked steel billets. However, the loading pattern is the same as for the other tubes. There is virtually no distortion for embrittled M446 steel filled with glass or alumina. However, the material shatters in a random manner due to its high brittleness, which gives a tendency to cause uncontrolled cracking. The loading diagram is different from other filled tubes, for filled embrittled M446 steel, in that the load increases to its maximum and drops to zero quickly.

8. Filling materials

Some tubes have been filled with glass and alumina respectively to study the influence of different filling materials. The cross-sectional distortion of the billets and the loading pattern are the same for tubes filled with glass and alumina. Cropping loads are higher for tubes filled with alumina, however.

9. Clearance between tube and filling

As shown in fig. 2.24, the loading pattern varies with clearance between tube and filling. As clearance decreases, maximum cropping load increases and the sudden load drop decreases. From fig. 2.24, it can be predicted that the filled tube with zero clearance would behave like a solid rod, as far as the loading cycle is concerned. The cross-sectional distortion is less for a tightly filled tube.

10. Tube cropping under tensile pre-load

M316 and PE16 materials have been chosen for these tests. Single tube cropping experiments under 200 pounds tensile pre-load show that there is improvement in the quality of billets by about 12% for PE16 and 10% for M316 empty tubes. There is a reduction in the maximum load and cycle time for both the tubes. The quality of billets is improved

by about 16% for both PE16 and M316 filled tubes and there is 7% reduction in the load for PE16 and 4% for M316.

Before and during the process, tensile pre-load induces a high value of tensile stress in the region of deformation. The object of pre-load in cropping is to cause the initiation of a crack in the tube at the earliest opportunity and therefore as a result of the least possible plastic deformation.

11. Tube cropping under compressive axial load

Cross-sectional distortion is less for tubes cropped under 200 pounds compressive axial load and the quality of billets is improved by about 6% for empty tubes and 15% for filled tubes. Cropping loads have increased by about 14% for empty tubes and 23% for filled tubes. Load, deflection variations with time are similar to those obtained from cropping under tensile pre-loads.

This technique depends upon greatly increasing the compressive stress in the shear zone to a degree at which crack initiation is inhibited and a clean, burnished surface is created on the billet by plastic shearing. The axial load required to produce a high quality billet depends upon the material. In the light of a patented Hungarian billet preparation process [5] known as "planar cold-flow shearing", it is desirable to adopt a more limiting definition of cropping. In cold-flow shearing, the bar stock is fed through a closely fitting fixed blade, into a similarly closely fitting moving blade and against an abutment. Before and during blade penetration, an axial load produces a high value of compressive stress in the shear zone with the objective of suppressing all tendency for crack initiation. The billet is then removed from the bar by a mechanism more closely akin to continuous machining than to a fracture process. In cropping, on the other hand, (without applied compressive stress) the aim is different. It is to

induce the formation of a crack which ultimately extends from the cutting edge of the blade. With this in mind, it is possible to state the fundamental objective of tube cropping development in general. That is to initiate a suitable, unidirectional crack at the cutting edge of the blade with the absolute minimum of prior permanent plastic distortion, and is synonymous with saying that cracking should be completed with the minimum possible blade penetration.

12. Cropping at low temperature

From the results obtained, it is evident that the cropping load increases at low temperature, -196°C , for both M316 and PE16 tubes. However, there is no change either in the shape of the load-deflection diagrams or in the cross-sectional distortion of the billets.

In considering the mechanical properties of metals at quite low temperatures, one of the shortcomings is the brittle behaviour of ordinary carbon steel. Some metals, however, such as aluminium, copper, nickel and most of their alloys as well as such alloys as the 'series 300' austenitic stainless steels and many others, do not exhibit the phenomenon of low temperature brittleness. It was discovered quite early that there is a good correlation between the type of crystal lattice and the brittle or non-brittle behaviour of the metal at low temperatures [35]. Face-centered cubic metals and alloys do not become brittle whereas body-centered cubic metals do.

Austenitic chromium-nickel steels such as M316 are, of course, one of the most interesting classes of ferrous alloys. Originally it was their unique combination of great ductility with immunity from atmospheric and many other forms of corrosion which made them particularly attractive. One of the remarkable features of these most interesting materials is the magnitude of the increase in yield and ultimate stress combined with a relatively small change in ductility which takes place with decrease in

temperature. It is evident from these experiments that low temperatures do not influence the quality of the stainless steel billets.

CHAPTER 3

MECHANICAL PROPERTIES OF MATERIALS

3.1 INTRODUCTION

One of the main purposes of mechanical testing is to provide data for design. The designer can thereby formulate a fairly precise estimate of the loads that a structure or machine will be required to withstand. Having devised methods of dealing with these loads, it is possible to define the nature of the stresses that will be imposed on the various components. Determination of the shapes and sizes of these components requires knowledge of permissible stresses in materials considered for use, and this knowledge is derived from mechanical testing. Usually, tests are undertaken by well-established methods at the manufacturing stage, with the object of ensuring that certain properties of the material are satisfactory for the proposed application, by matching the observed properties against some specification.

In this chapter, tension, torsion and hardness tests are described to give a comprehensive coverage of mechanical properties of all the materials. As explained in the first chapter, the main object of these tests is to correlate cropping results with mechanical properties data.

3.2 THEORY

(a) Tension test: If a material is subjected to a complex state of stress, the criterion of Maxwell (von Mises) postulates that yielding will occur when the second invariant of the deviatoric stresses reaches a critical value, i.e., when the function

$$[(\sigma_1 - \sigma_2)^2 + (\sigma_2 - \sigma_3)^2 + (\sigma_3 - \sigma_1)^2] \quad (3.1)$$

reaches a critical value. This may be expressed in terms of the flow stress in simple tension which leads to the definition of "equivalent stress".

$$\bar{\sigma} = \frac{1}{\sqrt{2}} [(\sigma_1 - \sigma_2)^2 + (\sigma_2 - \sigma_3)^2 + (\sigma_3 - \sigma_1)^2]^{1/2} \quad (3.2)$$

If no work hardening occurs $\bar{\sigma}$ is constant but in general $\bar{\sigma}$ increases with strain and this change may be expressed by plotting $\bar{\sigma}$ against a similar function of the logarithmic strain, again defined by the "effective strain" in simple tension as

$$\bar{\epsilon} = \frac{\sqrt{2}}{3} [(\epsilon_1 - \epsilon_2)^2 + (\epsilon_2 - \epsilon_3)^2 + (\epsilon_3 - \epsilon_1)^2]^{1/2} \quad (3.3)$$

Thus, if we plot $\bar{\sigma}$ versus $\bar{\epsilon}$ for different states of stress, we should produce a single curve. In the case of simple tension, the constants $\frac{1}{\sqrt{2}}$ and $\frac{\sqrt{2}}{3}$ in equations (3.2) and (3.3) have been chosen to give

$$\begin{aligned} \bar{\sigma} &= \sigma \\ \bar{\epsilon} &= \epsilon \end{aligned} \quad (3.4)$$

Hence plotting σ against ϵ gives the basic curve of $\bar{\sigma}$ versus $\bar{\epsilon}$. Simple tension, however, is limited by the onset of necking which takes place when the force-extension curve reaches a maximum. If the current area of the specimen is ' A_c ' and load ' P ', then

$$P = \sigma A_c \quad (3.5)$$

$$\therefore \frac{dP}{P} = \frac{d\sigma}{\sigma} + \frac{dA_c}{A_c} = 0 \quad \text{for necking} \quad (3.6)$$

If ' l_c ' is the current gauge length, for constant volume

$$A_c l_c = \text{constant} \quad (3.7)$$

$$\therefore \frac{dA_c}{A_c} = -\frac{dl_c}{l_c} = -d\epsilon \quad (3.8)$$

Hence from equations (3.6) and (3.8)

$$\frac{d\sigma}{d\varepsilon} = \sigma \quad (3.9)$$

Equation (3.9) is the condition of instability at necking

or
$$\frac{d\bar{\sigma}}{d\bar{\varepsilon}} = \bar{\sigma} \quad (3.10)$$

$$A_c \ell_c = A_0 \ell_0 \quad (3.11)$$

where A_0 = Initial area of cross-section

and ℓ_0 = gauge length.

For a tube

$$A_0 = \frac{\pi}{4} (D_0^2 - D_i^2)_0 \quad (3.12)$$

$$A_c = \frac{\pi}{4} (D_0^2 - D_i^2)_c \quad (3.13)$$

From equations (3.11), (3.12) and (3.13)

$$\frac{\ell_c}{\ell_0} = \frac{(D_0^2 - D_i^2)_0}{(D_0^2 - D_i^2)_c} \quad (3.14)$$

$$\therefore \varepsilon = \ln(\ell_c/\ell_0) = \ln \left[\frac{(D_0^2 - D_i^2)_0}{(D_0^2 - D_i^2)_c} \right] \quad (3.15)$$

$$\text{Ultimate Tensile Stress (UTS)} = \frac{P_{\max}}{A_0} \quad (3.16)$$

$$\text{Per cent Elongation} = \frac{\ell_c - \ell_0}{\ell_0} \times 100 \quad (3.17)$$

$$\text{Per cent Reduction of Area} = \frac{A_0 - A_f}{A_0} \times 100 \quad (3.18)$$

where A_f = Final area of cross-section.

(b) Torsion Test

For a tube, the torque ' T_q ' is given by

$$T_q = 2\pi A^2 \tau T \quad (3.19)$$

where τ = shear stress

T = Thickness of the tube

A = Mean radius.

For substitution in the general equation for $\bar{\sigma}$, the principal stresses are required, namely

$$\begin{aligned} \sigma_1 &= \tau \\ \sigma_2 &= -\tau \\ \sigma_3 &= 0 \end{aligned} \quad (3.20)$$

Substituting the above values in equation (3.2)

$$\bar{\sigma} = \sqrt{3} \tau. \quad (3.21)$$

The engineering strain in torsion may be taken as $\gamma = \tan \phi$ where ' ϕ ' is the angle of twist on the gauge length ' l_c '

$$\gamma = \tan \phi = \frac{\theta^c a}{l_c} \quad (3.22)$$

where θ^c = The angle of twist in radians.

Also

$$\begin{aligned} \epsilon_1 &= \frac{\gamma}{2} \\ \epsilon_2 &= -\frac{\gamma}{2} \\ \epsilon_3 &= 0 \end{aligned} \quad (3.23)$$

Substituting the above values in equation (3.3)

$$\epsilon = \frac{\gamma}{\sqrt{3}} \quad (3.24)$$

Hence $\bar{\sigma}$ and $\bar{\epsilon}$ may be determined. Tension and torsion tests should be coincident at least within reasonable limits.

(c) Hardness Test

The Vickers hardness is determined by producing an indentation with a pyramid-shaped diamond, and optically measuring this indentation. The Vickers pyramid has a square base. The included angle between opposed pyramid faces is 136° , and the depth of penetration measures about one seventh of the length of the diagonal of the indentation.

The Vickers hardness is found by using the formula,

$$HV \text{ (kp/mm}^2\text{)} = \frac{1.8544p}{d^2} \quad (3.25)$$

where p = Measuring force in kp

and d = Mean value of the indentation diagonal in mm.

3.3 INSTRUMENTATION

(a) Tension Test

Tensile tests have been performed using an Instron Testing Machine at the low speed of 0.02 in/min. This testing machine incorporates a highly sensitive electronic weighing system employing bonded-wire strain gauges for detecting and recording the tensile load applied to the sample under test. The moving cross-head, to which the pulling jaw is attached, is operated by two vertical drive screws from a unique positional-servo drive that provides a considerable flexibility of control

over the motion of this jaw. The chart of the recorder is driven synchronously at a wide variety of speed ratios with respect to the cross-head, thus enabling measurements of sample extension to be made with a large choice of magnification factors.

The accuracy of the load detecting system is independent of the range in use, and is better than $\pm 0.5\%$. The Instron 'X-Y Chart-Drive System' has been made use of to record extension versus load graphs for all the tensile tests.

(b) Torsion Test

Torsion testing of M316 stainless steel has been carried out using an Avery Torsion Machine.

(c) Hardness Test

A mini-load hardness tester has been used for non-destructive hardness tests with small measuring forces (0.005 to 2 kg). It is of particular value for thin materials where a spot hardness is required.

3.4 EXPERIMENTS

(a) Tension Test

Two specimens have been prepared from each size of the fourteen tubes. A standard gauge length of three inches was maintained for all specimens. A suitable length of both ends of each specimen was filled with a close fitting silver steel rod in order to prevent the specimen from collapsing in the grips.

Tensile tests were carried out on an Instron Testing Machine at the low speed of 0.02 in/min. The average values of yield strength, 0.2% proof stress, ultimate tensile strength, true fracture stress, per cent elongation and per cent reduction of area are shown in Table 3.1. True

stress-strain curves of all fifteen tube materials and PE16 and M316 bar materials are shown in figs 3.1 to 3.9.

(b) Torsion Test

Suitable grips were made for the stainless steel tube, of outside diameter 0.230" and thickness 0.015". Torsion tests were made on an Avery Torsion Machine. A nominal torque was applied to secure the specimen in the jaws. The torque at convenient values together with corresponding displacement was recorded. This was continued until the specimen failed. The true stress-strain curve was derived from the torsion test and is shown in fig. 3.4.

(c) Hardness Test

Specimens of length about half an inch were cut from bars by sawing and mounted in plastic. The basic method of mounting is to place the specimen face down in the die and then pour the plastic material into the die. The mount is conveniently an inch diameter and half an inch high. It is essential to verify that the structure of the metal is not affected by any heat and pressure applied in forming the mount.

Silicon carbide cloths were used to polish the specimens. Then mechanical polishing was done in two stages with coarse and fine abrasive respectively. After polishing, the specimens were thoroughly washed and dried.

Micro-hardness tests were conducted using a mini-load hardness tester. The average value of six readings on each specimen is shown in Table 3.1.

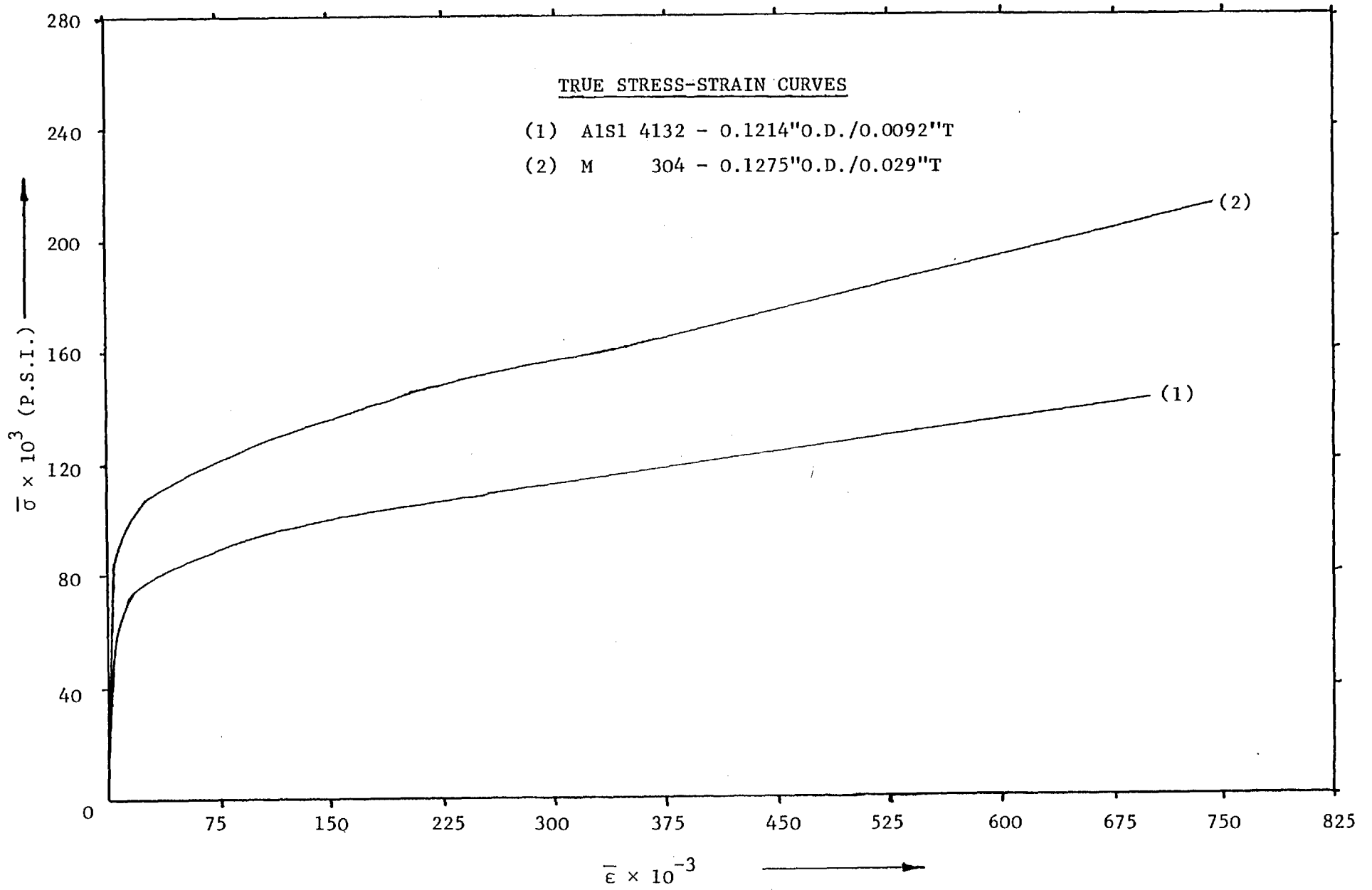


FIG. 3.1

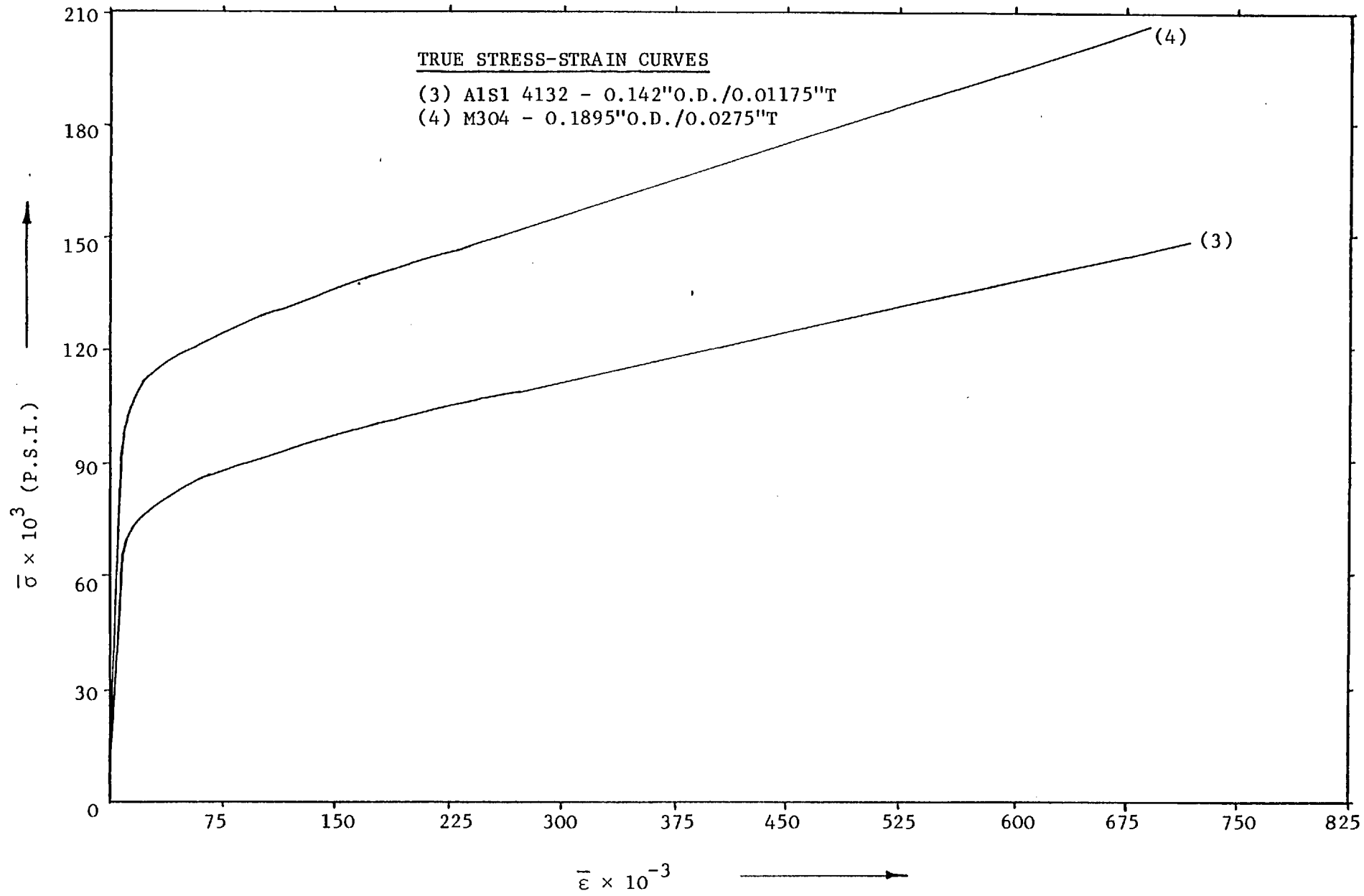


FIG. 3.2

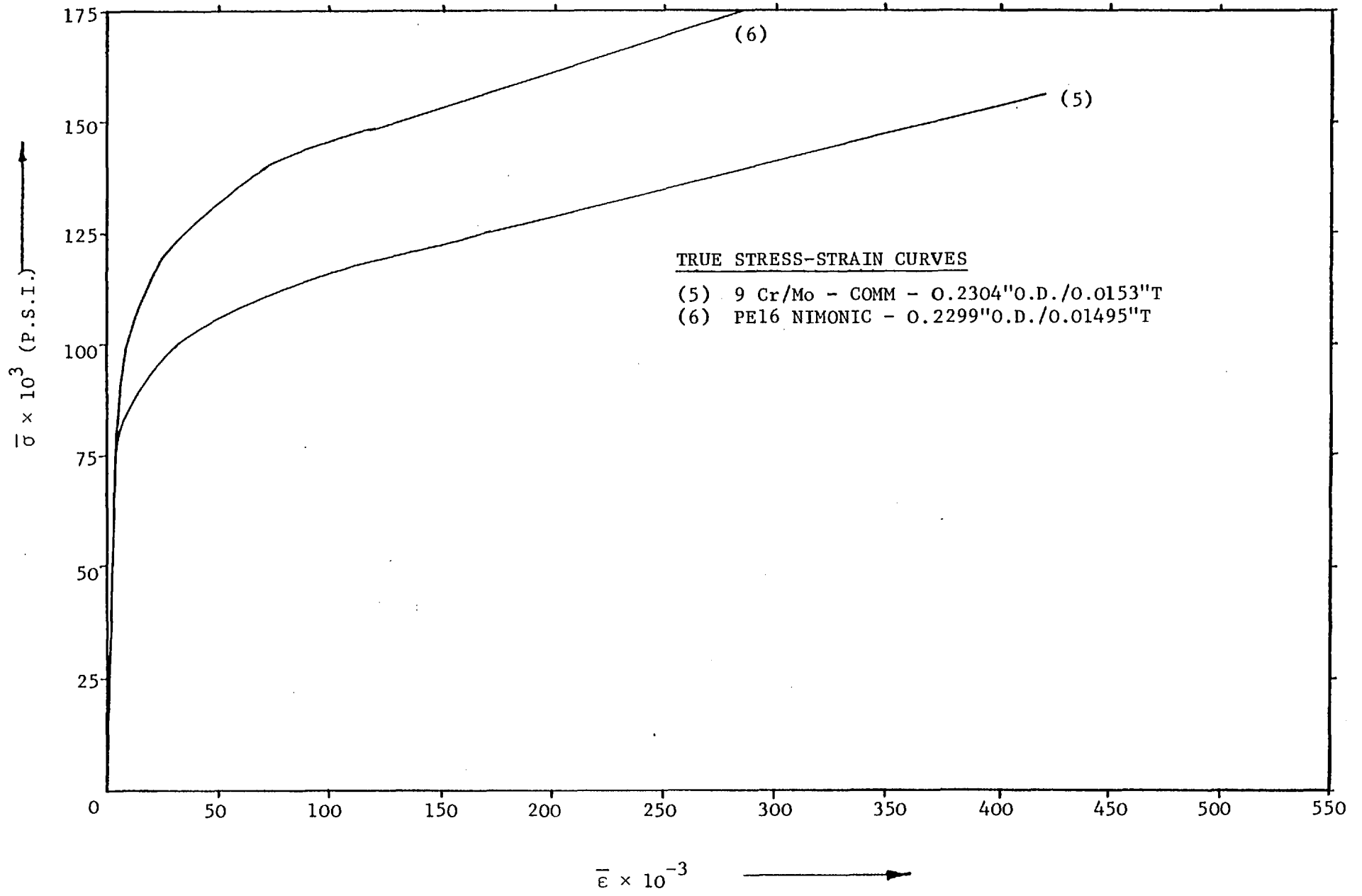


FIG. 3.3

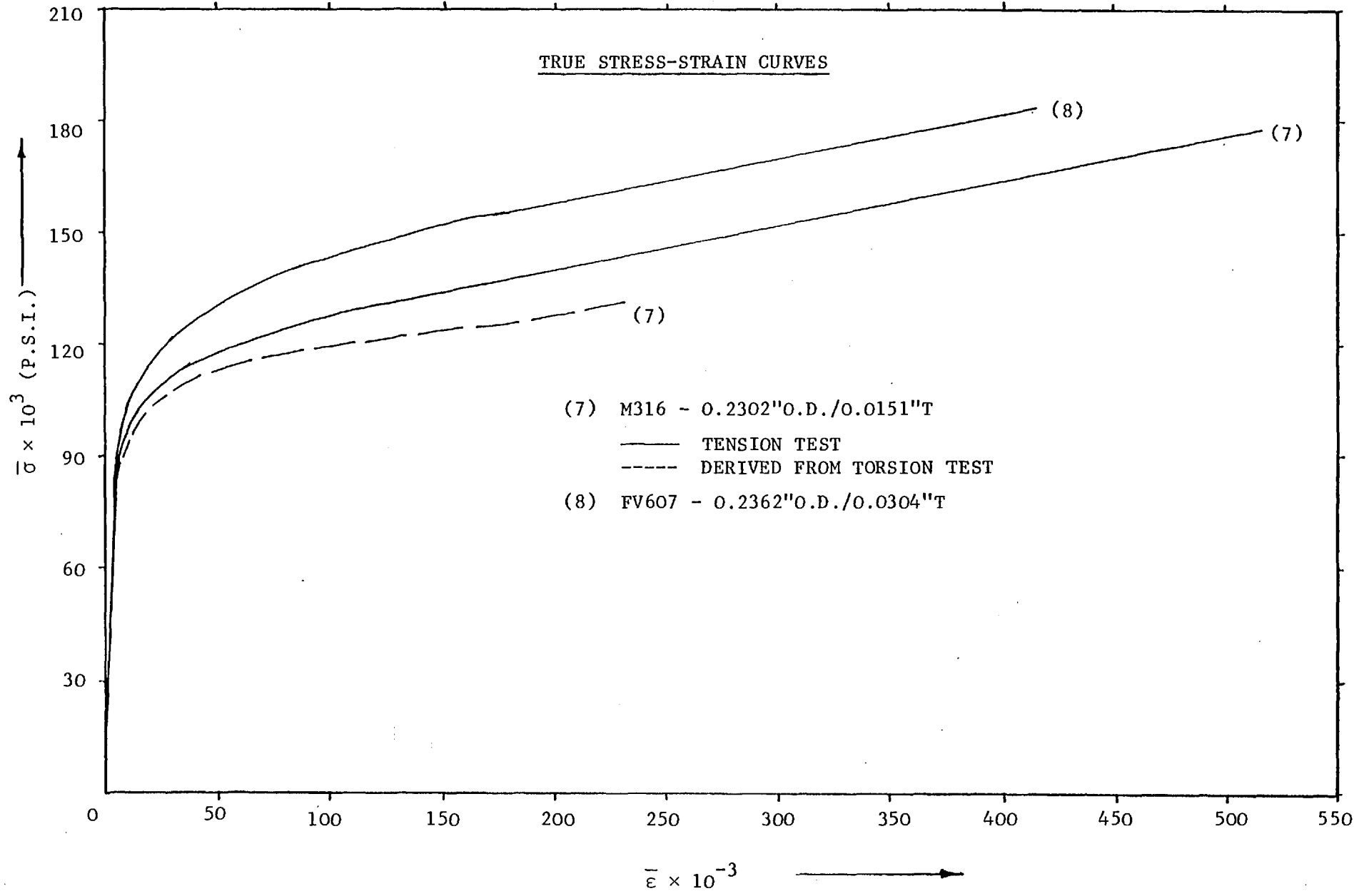


FIG. 3.4

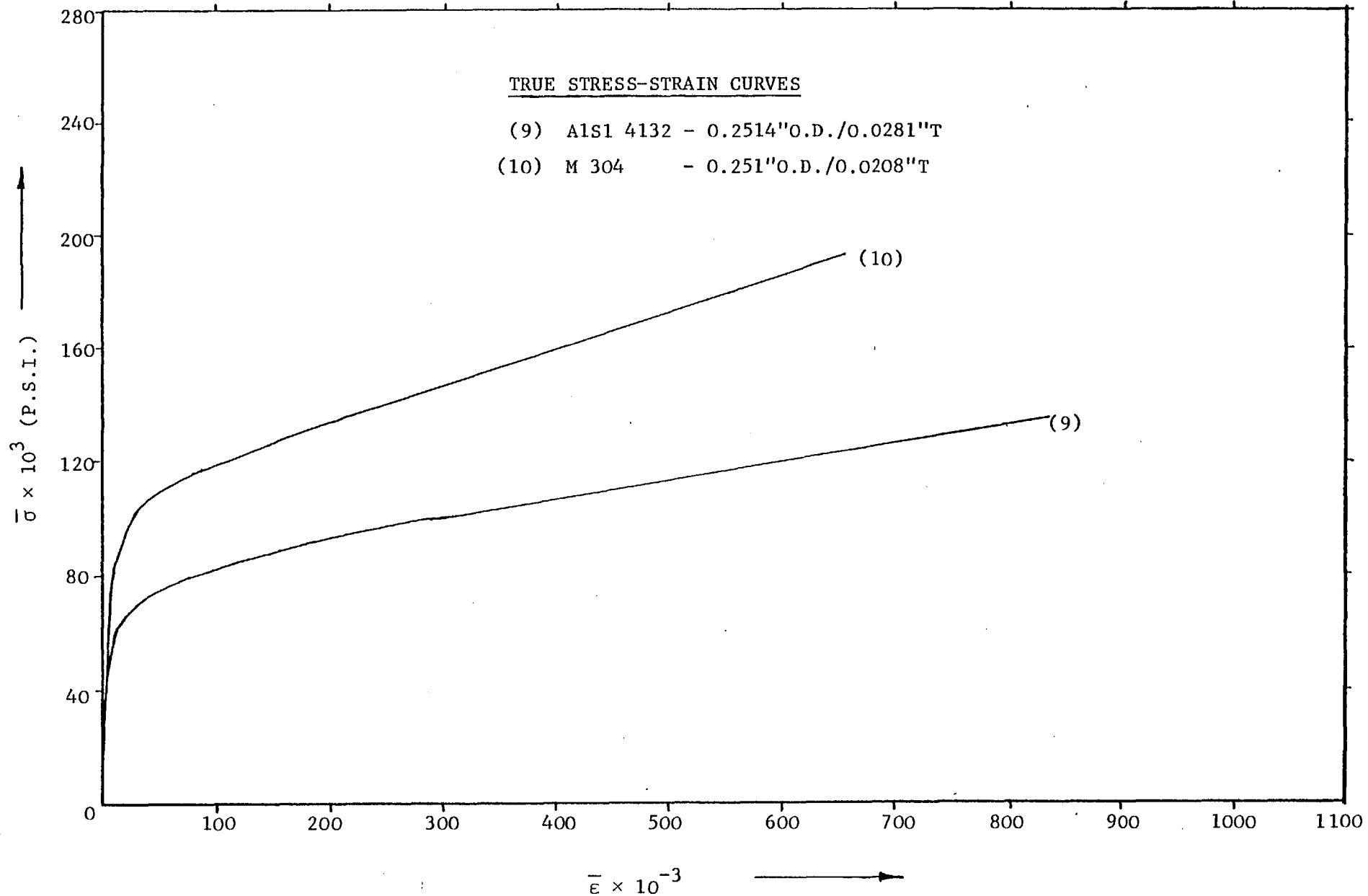


FIG. 3.5

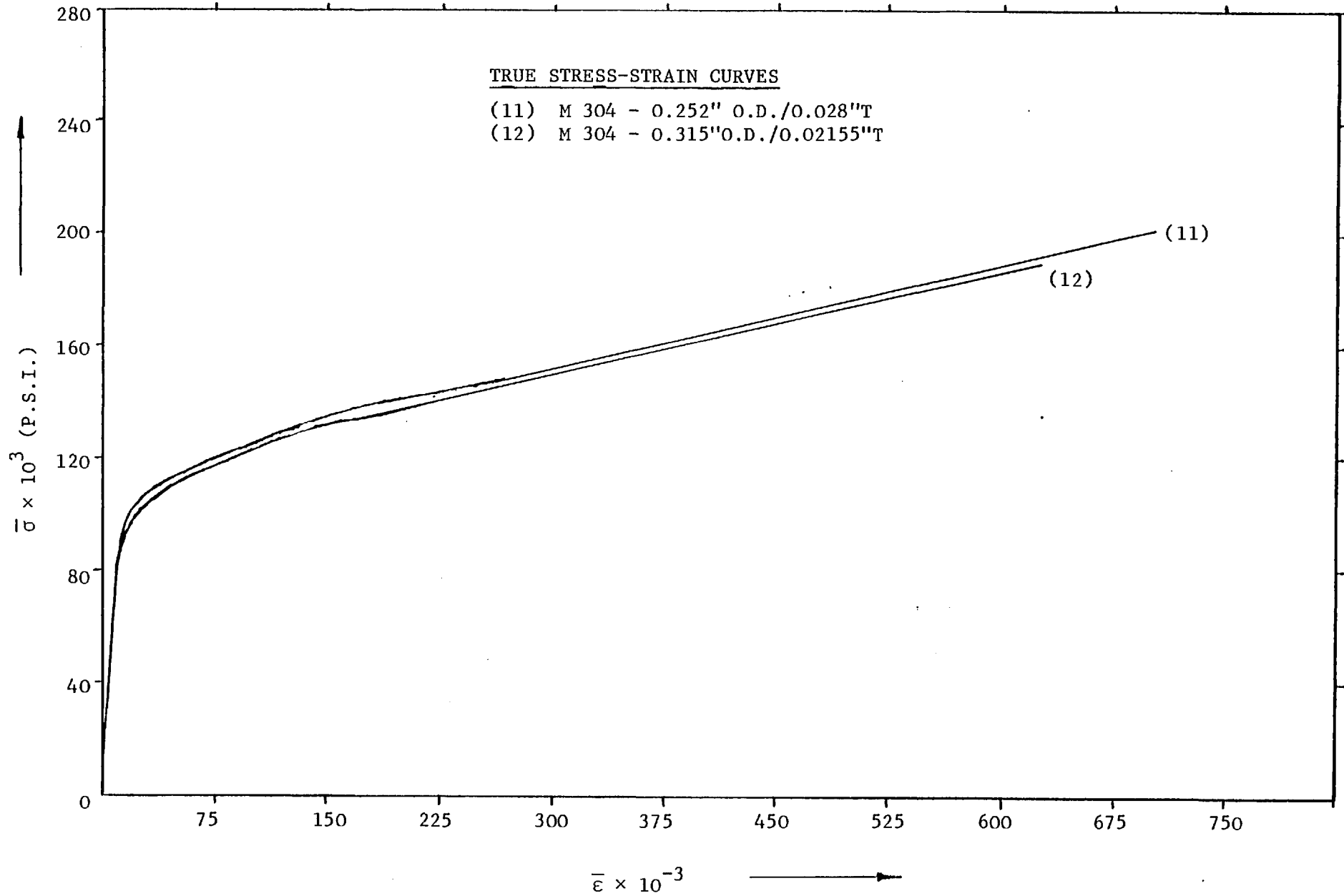


FIG. 3.6

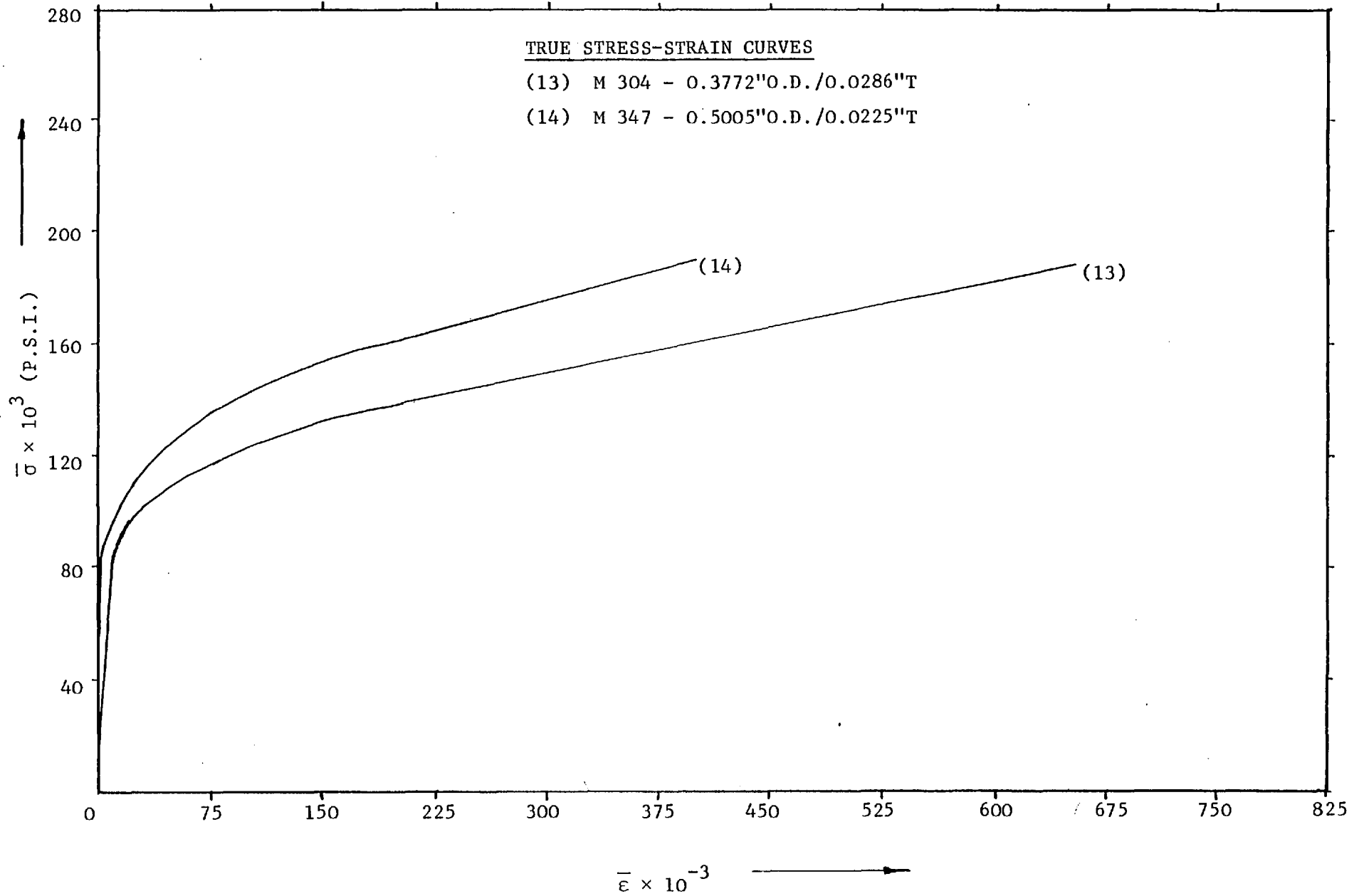


FIG. 3.7

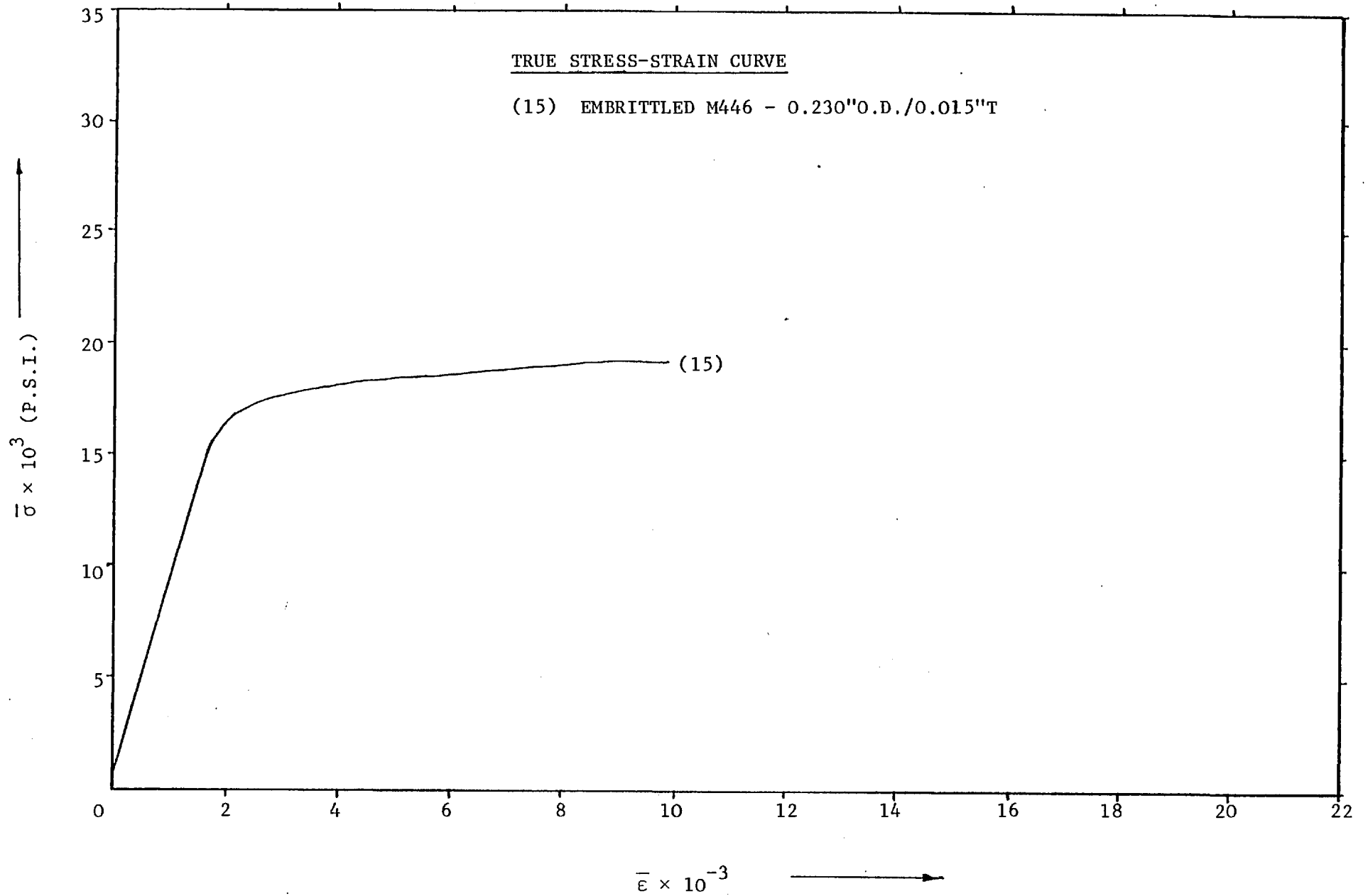


FIG. 3.8

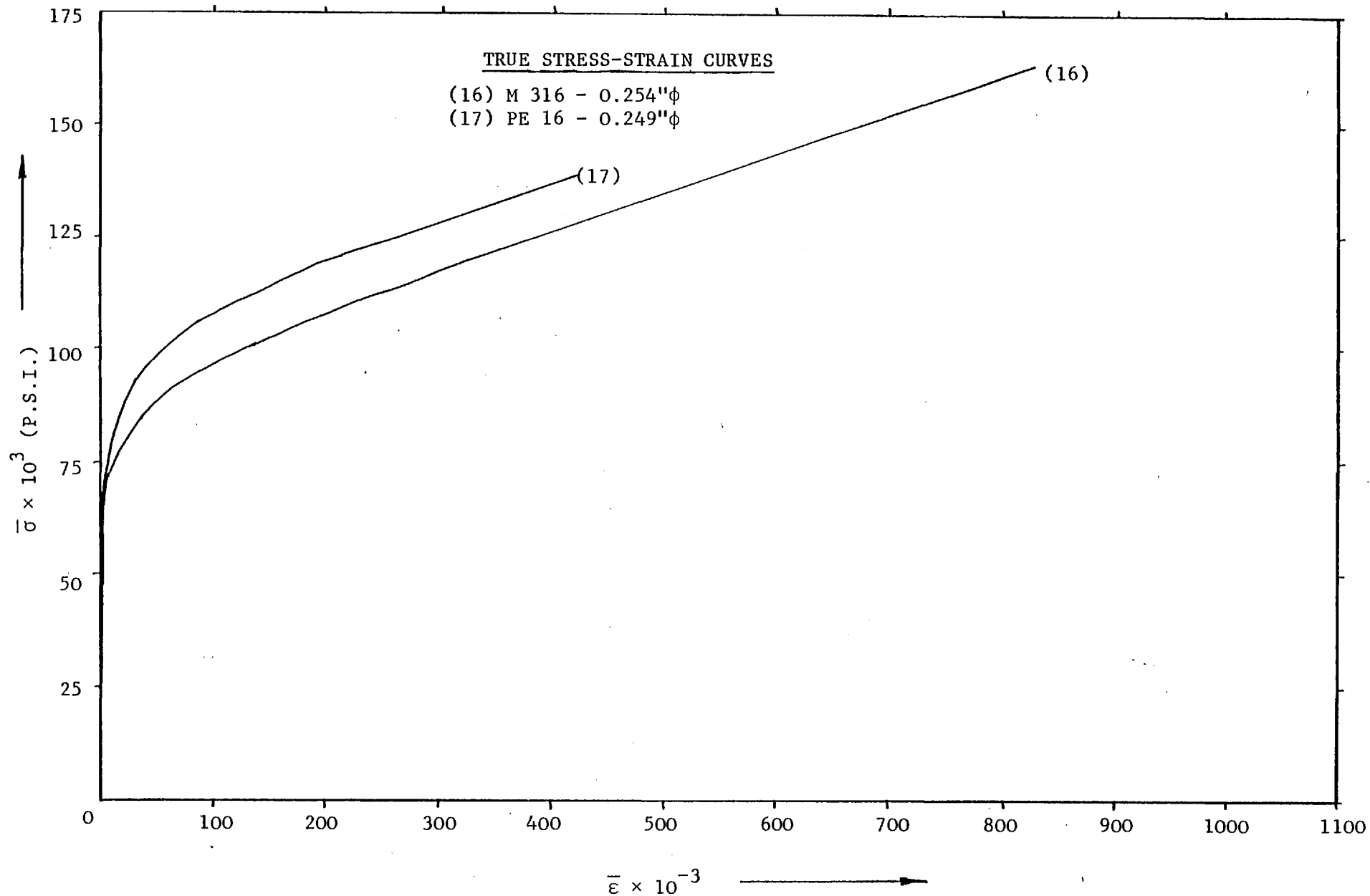


FIG. 3.9

TABLE 3.1

Sl. No.	Details of tube/rod (in) (O.D./T)/ ϕ		0.2% proof stress (tons/sq.in)	U.T.S. (tons/sq.in)	Fracture stress of true (tons/sq.in)	% Elongation	% Reduction of area	HV
	Material	Size Original after fracture						
1	AlSi-4132	0.1214/0.0092 0.080/0.007	24.6	38.06	63.96	23.2	50.5	273
2	M304-MILT	0.1275/0.029 0.089/0.0195	30.4	49.52	95.17	38.0	52.6	299
3	AlSi-4132	0.142/0.01175 0.097/0.0085	23.0	37.65	66.12	18.1	50.8	272
4	M304-MILT	0.1875/0.0275 0.139/0.0185	29.6	51.03	92.43	31.9	50.7	307
5	9 Cr/Mo-COMM	0.2304/0.0153 0.192/0.012	31.5	51.54	69.74	9.6	34.4	292
6	PE16-nimonic	0.2299/0.01495 0.213/0.012	37.2	61.42	78.36	9.0	24.9	333
7	M316	0.2302/0.0151 0.187/0.011	38.4	50.44	79.27	22.5	40.4	290
8	FV607	0.2362/0.0304 0.193/0.0245	31.9	60.14	82.27	12.7	34.0	337
9	AlSi-4132	0.2514/0.0281 0.173/0.0175	22.4	36.25	60.05	26.4	56.6	274
10	M304-MILT	0.2510/0.0208 0.186/0.0145	32.6	47.58	85.14	36.7	48.0	300
11	M304-MILT	0.2520/0.0280 0.182/0.019	31.2	49.75	89.93	32.7	50.6	305
12	M304-MILT	0.3150/0.0215 0.234/0.0155	32.5	49.52	83.92	34.0	46.4	303
13	M304-MILT	0.3772/0.0286 0.280/0.020	30.2	48.72	84.72	39.3	47.8	297
14	M347-T-58	0.5005/0.0225 0.409/0.0185	34.8	62.19	84.80	24.1	32.8	307
15	M446-Embrittled	0.230/0.015 0.228/0.014	8.0	8.3	8.5	0.9	1.0	390
16	M 316 bar	0.254 ϕ 0.172 ϕ	34.5	40.6	73.0	26.2	54.2	298
17	PE16-nimonic bar	0.249 ϕ 0.210 ϕ	35.9	47.5	62.0	12.5	28.8	309

3.5 RESULTS AND DISCUSSIONS

The tensile test is a standardised test for determining the mechanical properties of materials and the quantities derived from a tensile test are best considered by reference to the deformation behaviour of a test piece when subjected to a continuously increasing tension load until it breaks. When the maximum load is reached, necking occurs. The true stress after necking requires a correction, since a triaxial state of stress is induced. After necking has been initiated, deformation continues only in the necked portion of the specimen, whereas the remaining specimen ceases to deform further. Hence strains beyond necking can be calculated only from deformation in the necked region. Necking in tension is a condition of strain in which uniform deformation ceases and local plastic deformation ensues. It is the point on a tensile stress-strain curve at which the maximum load is reached and at which necking begins. It is thus a condition of instability, at which the rate of load change with respect to the area change of the tube becomes zero. If necking is once initiated, plastic straining continues only in the necked portion of the specimen and consequently no further straining will take place in the remainder. It is thus a limiting condition of straining and generally reduces the permissible deformation achievable in the deformation processes in which tensile loading occurs. It is therefore a forming limit.

It is not possible to measure the instantaneous area of cross-section of a tube during the tension test. Hence the true stress-strain curve is drawn up to the maximum load based on extension. The final true stress is calculated by taking the ratio of load to the cross-sectional area of the tube at fracture. Hence the curve has been approximated by joining the point before necking to the final true stress at fracture. From the curves, it is evident that the stress increases

continuously with increasing strain. Each point on the curve represents a definite state of tensile deformation.

Materials such as cold-worked steels exhibit the 'yield-point' phenomenon. Hence, the yield condition for these materials must be defined in a different manner. In these cases, yielding is defined in an arbitrary way; the 'yield strength' is generally determined by drawing a line parallel to the elastic limit line but intersecting the abscissa at a value of, say, 0.002 strain. The stress corresponding to the intersection of this line with the stress-strain curve is called the 0.2% proof stress. Higher values of off-set, e.g., 0.005 strain, often have to be chosen for this determination, in order to avoid the initial non-uniform yielding of some steels. The Bridgman correction factor [36] was taken into account in calculating stresses for solid rods. All the results are presented in Table 3.1.

Another important parameter is the ductility of the material. Elongation to fracture in a tensile test is dependent on specimen length, and is partly controlled by the shape of the stress-strain curve, which fixes the point at which necking begins. Elongation values cannot be regarded as measurements of basic ductility and their use is restricted to comparative testing. Values of reduction of area at fracture are much more directly related to basic ductility, but a disturbing factor still occurs with very ductile materials which form a deep neck before fracture. As explained earlier, the stress system in such a deep neck departs considerably from simple uniaxial tension: effectively a superimposed triaxial tensile stress is introduced and this has the effect of reducing the ductility of the material. A torsion test can be conducted to check the results obtained from the tension test.

One advantage of a torsion test over a tension test is that, providing local buckling of a tubular specimen does not occur, there is no significant change in the dimensions of the test specimen either for small elastic strains or for very large plastic strains. As a consequence there is no need to measure the change in diameter of the specimen or radius of the neck. As shown in fig. 3.4, the true stress-strain curves produced from the tension and torsion for M316 material are coincident within limits. However, the results obtained from torsion test cannot be accepted because the specimen in fact failed by buckling rather than by shear. Therefore it was decided not to carry out any more torsion tests.

Hardness is measured in various ways and indicates different properties depending upon the way in which it is measured. It represents the ability of a material to resist scratching, abrasion, cutting or penetration. The type of hardness to be tested in a material depends upon its service requirements. The indentation hardness test is the most common, and a variety of instruments are used to measure this type of hardness. The indenter, which is either a ball, cone, or pyramid, is usually made of hard steel or diamond and is most commonly used under static loads. Either the load to produce a given depth of indentation or the size of indentation produced by a given load is used to denote the hardness.

Unlike the tension test, the hardness test is a comparative test because the state of stress produced in the material by the test is complex, and it is therefore very difficult to link the behaviour of the material in the test with its behaviour in the tensile test. However, hardness values for most materials are approximately in proportion to the values of ultimate tensile strength as shown in Table 3.1.

Although the materials are the same, the tension results obtained from solid rods of M316 and PE16 are different from those for cold-worked steels. Comparing the results obtained from tubular and solid specimens, as shown in Table 3.1, the material strength for cold-worked steel tubes is very much higher than for solid rods. The reasons for this will be discussed in detail later in chapter 6.

CHAPTER 4FRACTOGRAPHIC STUDY OF THE MECHANISMS OF FRACTUREIN CROPPING4.1 INTRODUCTION

The large depth of field and high useful magnification available in the electron microscope make this instrument an admirable tool in the study of fracture-surface topographies. An increasing number of investigators are using electron fractography in their studies of the micromechanisms of fracturing processes, and it may well be that understanding these processes will lead to information which will aid in the design of suitable alloys.

Since the main object of all cropping techniques is to improve the billet quality, it is necessary to examine the quality of billets obtained in cropping and the influence of various factors such as geometrical, metallurgical etc. The geometrical aspects of billets have been described in previous reports. As fracture is the dominant mode of separation in cropping for most engineering materials, it has been found necessary to study that aspect in detail in order to describe the nature of the mechanism of fracture involved in the process. In the present work the primary goal is to investigate the mechanisms of fracture in cropping thin-walled metallic tubes filled with ceramic and glass-like materials.

4.2 EQUIPMENT AND SPECIMEN PREPARATION

(a) The Scanning Electron Microscope

The Stereoscan 600 displays information derived from the action of an electron probe scanning the surface of a specimen; the displayed image has a three-dimensional appearance. The microtopography of solid bulk specimens can be examined as can surfaces whose roughness or other characteristics render their observation extremely difficult or impossible by means of a conventional transmission electron microscope, using either direct or extraction replica methods. The specimen detail resolution is always better than 25 nm under satisfactory conditions, with a depth of focus that is at least 300 times greater than that of a light microscope at the limit of resolution, when both types of microscope are adjusted for optimum performance. The Stereoscan has a switched magnification range between $\times 20$ and $\times 50,000$, which represents a second area on the specimen from $6 \text{ mm} \times 5 \text{ mm}$ to $2.4 \text{ }\mu\text{m} \times 2 \text{ }\mu\text{m}$ at $10 \text{ }\mu\text{m}$ working distance. The true magnification at all working distances is indicated by a μ -mark on the display.

The electron gun produces a beam of electrons with an effective source of about 50 microns. The condenser lenses produce successive stages of demagnification and the final lens focuses the demagnified image of the source on to the specimen. The electron beam (or probe) is scanned across the specimen in a raster, similar to the way in which a television picture is scanned using the flying spot technique.

Low energy secondary electrons (generated in the specimen by the probe) and high energy primary electrons (reflected from the specimen surface) travel towards a collector system. The collector has a grid, which can be biased either positively so that both low and high energy electrons are detected, or negatively such that only high energy electrons are able to pass. Behind the grid is a positively-biased

scintillator, optically coupled to a photomultiplier. When electrons impinge on the scintillator, photons are emitted which travel along a light guide to the photocathode of the photomultiplier.

Signals from the photomultiplier are passed through a head amplifier and then to the display unit, where the amplified signals modulate the brightness of the cathode ray tube. The tube is scanned in synchronism with the scanning of the specimen by the electron probe. The resultant image has a marked three-dimensional appearance because contrast is produced by the variation in the number of electrons emitted or reflected from different parts of the specimen, which is a function of the inclination of the source to the incident electron beam. A camera is mounted over the display tube to record the image. A series of specimen mounting pallets is available providing X and Y (lateral), Z (vertical, rotation and tilt) movements of the specimen. The maximum specimen size will depend on the pallet in use and can be as large as 50×50×25 mm.

(b) Specimen preparation

It is necessary to remove the portion containing a fracture from the total part, because the total part is to be repaired or to reduce the size of the specimen to be examined to a size that is convenient to handle. Small pieces have been cut from the billets in such a way that fracture faces and areas adjacent to them are not damaged or altered in any way. Then the specimens have to be cleaned for the purpose of removing protective coatings, corrosion products, and loose deposits such as dust, which may obscure part of the fracture or make interpretation difficult. The specimens are attached to the stub by using adhesive. Care must be taken to ensure that the specimen is not electrically insulated from the stub. Colloidal silver is used for making electrical

contact between the edge of the specimen and the stub. Since the ceramic and glass specimens are electrically non-conducting, they are coated with a thin conducting layer of gold.

4.3 MECHANISMS OF FRACTURE

(i) Mechanisms of fracture in general

Fracture is defined as an inhomogeneous process of deformation that causes regions of the material to separate into two or more parts under the action of stresses. The fracture process includes two distinct stages, namely crack initiation and crack propagation. The first clear understanding of fracture mechanisms was due to Griffith, who recognised that the strength of real solids is 100-1000 times less than would be expected from the strength of atomic bonds. He introduced the idea of the presence in brittle solids of small cracks that act as stress concentrators and so span the difference between the low applied stress and the high atomic bond strength. Pulling atoms apart is drastic and requires a direct stress of about $E/5$, where Young's modulus E is a measure of resistance to extension.

Shearing atoms over one another is less drastic and even without the involvement of dislocations, requires a shear stress of only about $G/10$, where the shear modulus G is a measure of the resistance to shear. It is known that plastic deformation occurs in fcc metals before there is any possibility of the tensile breaking of atomic bonds. Bcc metals can be ductile and they can also be brittle when fracture occurs along cleavage planes, but even then there is a clear involvement of prior plastic deformation. Even alumina, which appears quite brittle, shows a marked temperature-dependence of strength that is inconsistent with true brittleness and suggests control by a mechanism of plastic deformation.

Thus, the normal situation is that fracture occurs as a consequence of a plastic shearing process.

(a) Ductile fracture

Normally, metals fracture by a ductile mechanism. Inclusion-free metals may fracture simply by plastic deformation, giving up to 100% reduction of area. However, in real situations, second-phase particles are important. Cavities are formed at these either by breaking of the particles themselves under the influence of the plastic deformation of the matrix or by separation of the matrix from the particles. When further deformation of the matrix becomes unstable, these cavities grow together by a process of internal necking and so produce a ductile fracture crack. It follows directly from this mechanism that the form and number of second-phase particles is very important in ductile fracture. Another important factor is the rate of work hardening, $d\sigma/d\varepsilon$, since plastic instability, which determines the onset of cavity coalescence, occurs at a stress $\sigma = d\sigma/d\varepsilon$. Thus, a low work hardening rate favours the early onset of cavity coalescence. Also, once a ductile crack has been established, the localised deformation required for its propagation will be more confined if the work-hardening rate is low.

If the plastic zone at the crack is small compared to the through-thickness of the metal, the crack propagates as a flat, plane strain fracture. With a larger plastic zone it propagates as an inclined "shear" fracture. The main form of shear fracture is shear rupture which normally occurs on planes inclined ^{at} 45° to the tensile axis in the well known "cup-and-cone" fracture of the tensile test.

(b) Cleavage fracture

Cleavage fracture is common in bcc and cph metals, occurring at lower plastic strains than ductile fracture. Cleavage fractures are characterised by a rapid rate of crack propagation with no gross deformation or energy consumption. First, there is the production of a crack nucleus, for example by the coalescence or reaction of dislocations, the blockage of twins or by the fracture of a brittle second-phase as a result of plastic deformation of the matrix. Second, this nucleus must be able to propagate. Thus, a propagation condition is central to theories of ductile-cleavage transition. Factors that raise the stress available for propagation of the nucleus favour cleavage. Consequently, the triaxial tension system generated by plastic deformation at a notch, low temperatures, solution or precipitation hardening, irradiation hardening and other factors that raise the yield stress will favour cleavage. Fine grain size also raises the yield stress, but a more important point is that it reduces the size of the initial nucleus and so fine grains are important inhibitors of cleavage.

(ii) Mechanisms of fracture in cropping

The main part of each of the fractographs shown in figs 4.3 to 4.8, demonstrates the burnished area of penetration resulting from pure plastic deformation by shear. It indicates ductile rupture. In the broad sense, ductile rupture implies the noncleavage separation of a crystal. In the restricted sense currently used by electron fractographers it refers to the growth and coalescence of voids during the plastic deformation of metal and, in particular, during the failure of the metal piece. Differentiation between cleavage and ductile rupture mechanisms is quite readily made when the fracture surface is observed in the electron

microscope, but it is not always apparent to the unaided eye. The one outstanding characteristic of most ductile-rupture surfaces is the presence of numerous smooth, rounded, concave depressions on both surfaces. These depressions have been called "cupules" and "dimples" by various investigators. These dimples are formed from voids that grow under plastic strain conditions within the metal piece until they unite with one another. Thus one portion of each void becomes a dimple on one rupture surface and the remaining portion a dimple on the other surface. This type of fracture occurs as a result of void sheet formation. The presence of a central crack which acts as an internal notch tends to concentrate the deformation at its tips in narrow bands of intense shear strain. Under the combined action of the tensile stress and the resulting shear strain, sheets of voids are formed in these bands. These sheets deform continually until void coalescence occurs, producing local fracture of the "void sheet". Some interesting aspects of void-sheet formation have been observed by Cox and Low [37]. In their study it was noted that the fracture surface of a 4340 steel was covered by two distinct populations of dimples, one large and the other smaller *by an* order of magnitude. They found that the large voids were nucleated at manganese sulfide inclusions and the smaller ones at carbide particles. The first voids formed at manganese sulfide inclusions and grew with little interaction between them. Then, at strains within a few percentage points of the total fracture strain, extensive coalescence occurred between the large voids by the propagation of crack-like features at an orientation of approximately 45° with the tensile axis, which link adjacent large voids. After this point final fracture occurred catastrophically. A schematic drawing of the coalescence mechanism by Cox and Low is given in fig. 4.1. They explained that during void

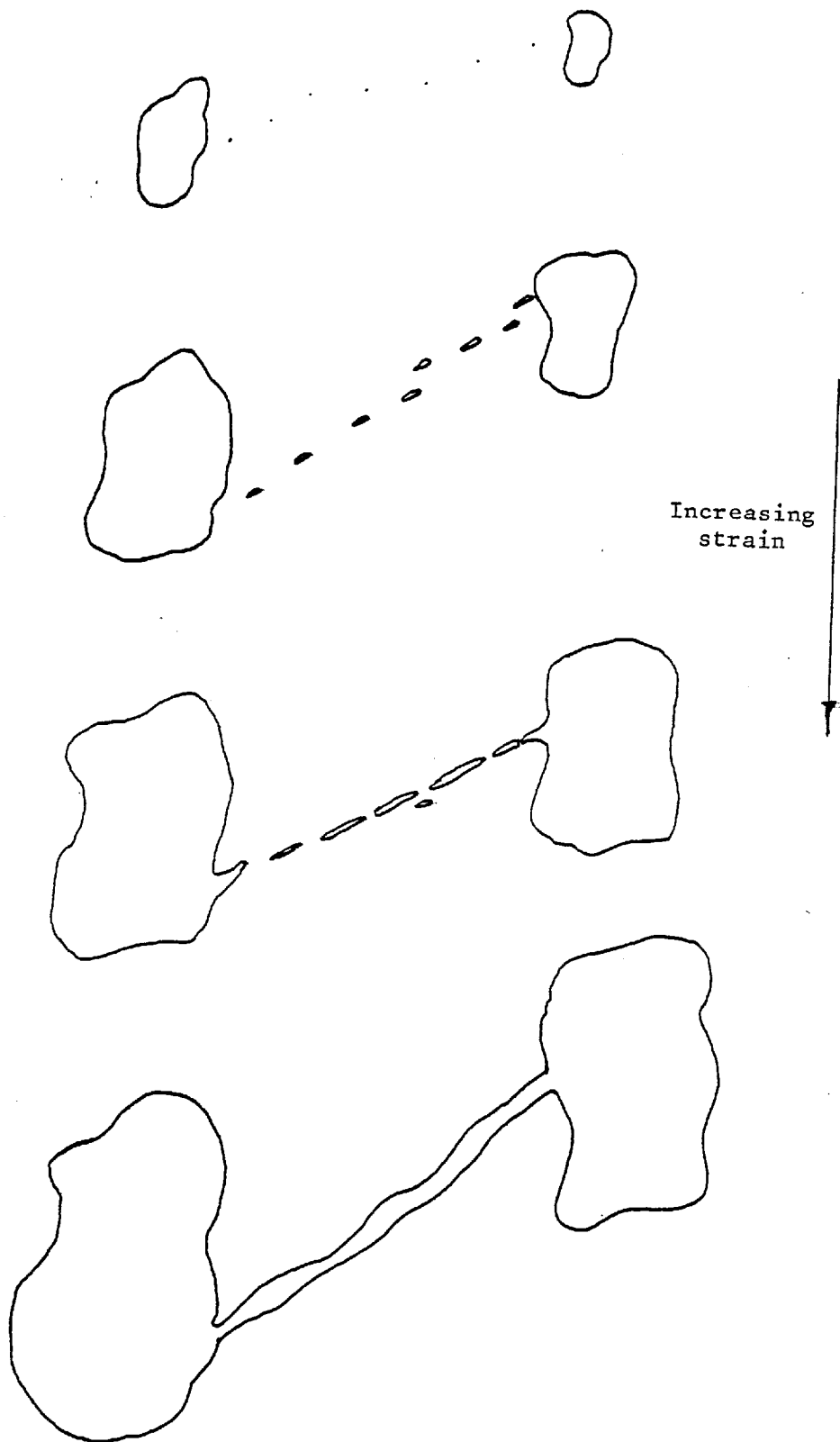


FIG. 4.1 SCHEMATIC DIAGRAM OF VOID COALESCENCE [AFTER COX AND LOW (37)]

growth deformation was concentrated between large voids along the maximum shear stress line which caused void formation at smaller particles, resulting in coalescence along the maximum shear stress direction. The above analysis can be applied to the present fractographic study of fracture mechanisms in cropping (figs 4.3 to 4.8).

Since several of the key observations (M316, M304 stainless steels etc.) involved dimple shapes, a brief description of the origin of these shapes is in order. There are three basic types of dimples as shown in fig. 4.2. (1) equiaxed dimples, which form when the surfaces pull directly away from one another in a direction perpendicular to the plane of the local crack, creating rounded dimples of the same shape on both fracture surfaces, fig. 4.2(a): (2) shear dimples, which form when the two surfaces are being displaced in opposing directions parallel to the plane of shear as well as being separated in directions perpendicular to the plane, fig. 4.2(b): and (3) tear dimples, which form when a strain gradient exists at the crack tip which causes the voids to be opened up first on the sides nearest the crack tip, fig. 4.2(c). Both shear dimples and tear dimples are open ended, resembling parabolæ; but are readily distinguishable because the parabolic dimples on matching surfaces point in opposite directions for shear dimples, but in the same direction - toward the crack origin - for tear dimples. The shapes of dimples often indicate the local crack propagation direction.

According to the subdivisions of ductile fracture as stated before, and as presented in the "Atlas of Fractographs" [39], the dimples shown in fig. 4.3 can be recognised as "equiaxed type". This type of dimple resembles "tensile-shearing" conditions due to the prevailing tensile components of stresses. This fractograph (fig. 4.3) has been taken at the origin of the crack (at the corner of the deformed M316 tube). The fractograph shows ^{the} equiaxed dimples of rather uniform size that are

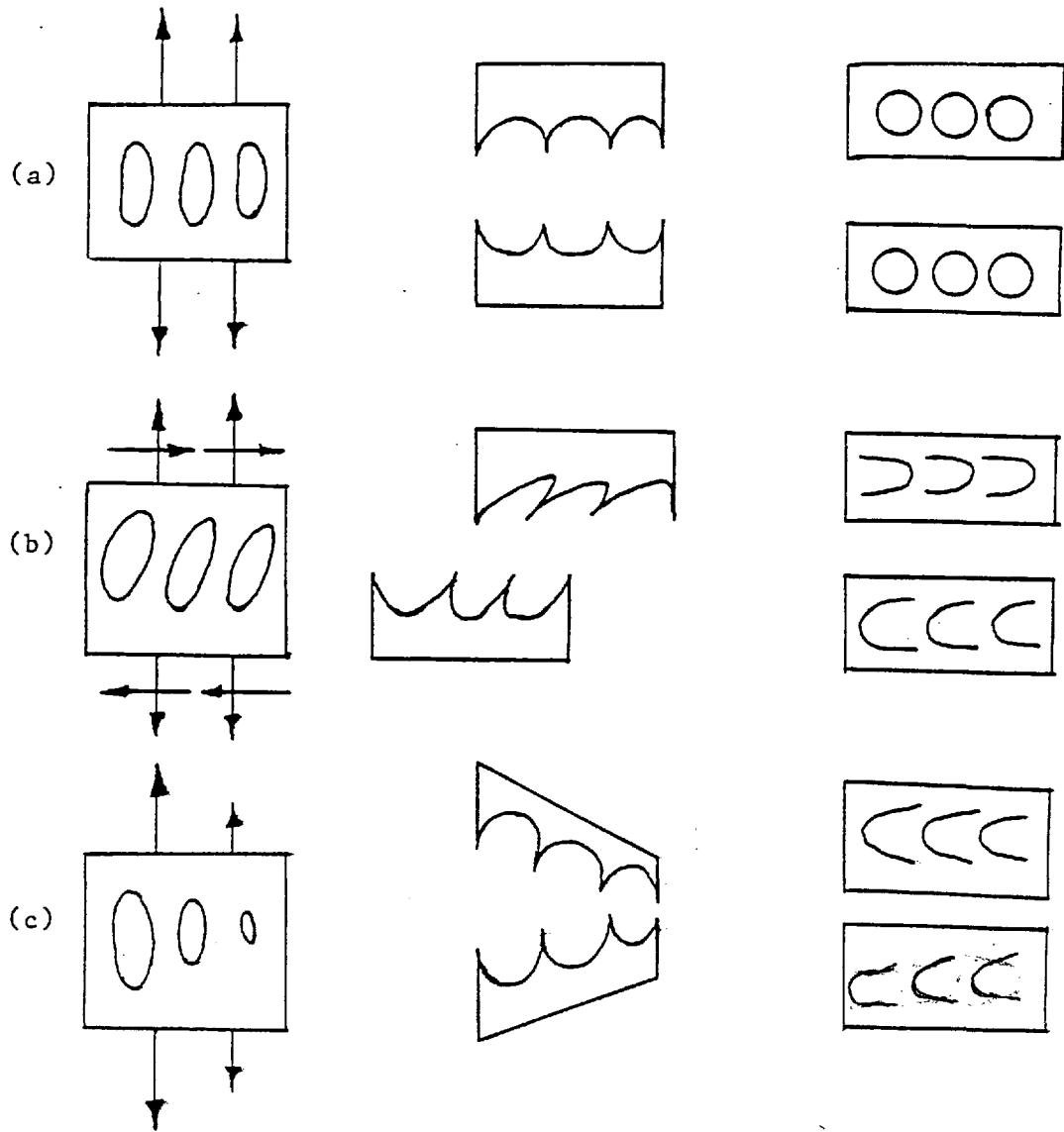


FIG. 4.2. Three basic types of dimples. For each mode, the sketches show from left to right: material stressed almost to the point of local rupture; local rupture and the directional sense of the dimples on the fracture surfaces. The arrows indicate the direction and character of plastic strains. Equiaxed dimples are formed in (a), shear dimples in (b), and tear dimples in (c).

(From ref. 38.)

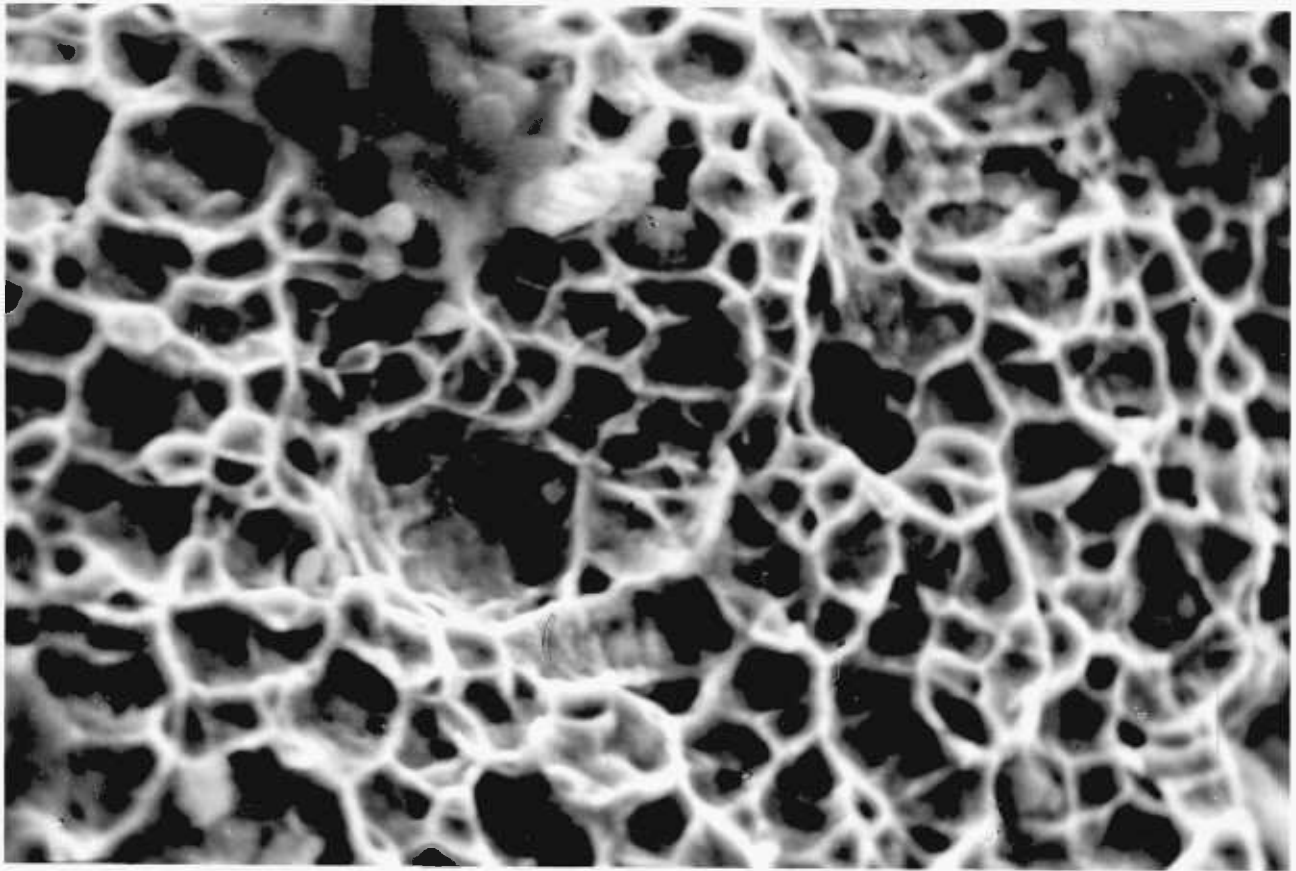
10 μ

FIG. 4.3. M316- EQUIAXED DIMPLES

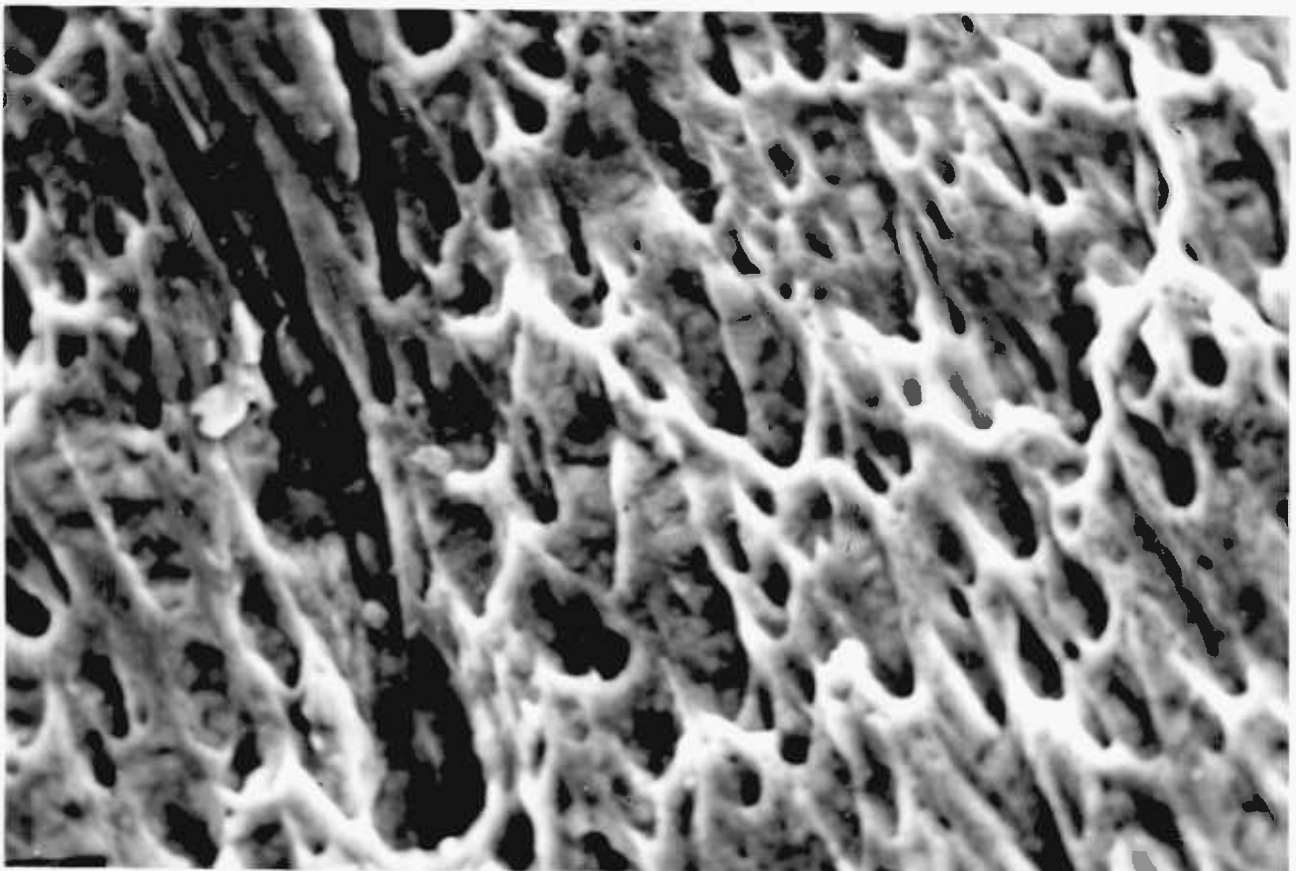
10 μ

FIG. 4.4. M316- SHEAR AND TEAR DIMPLES

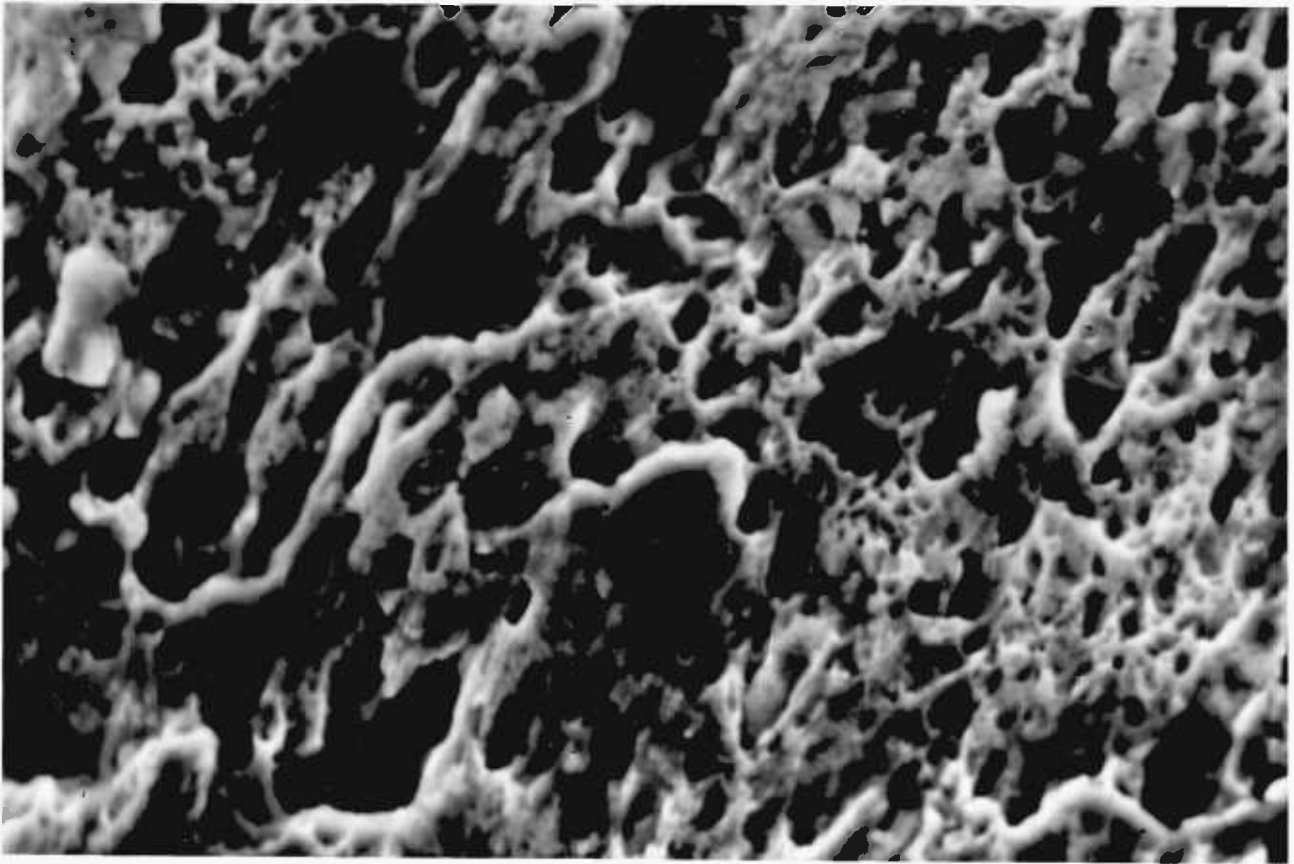
10 μ

FIG.4.5. M347-SHEAR AND TEAR DIMPLES

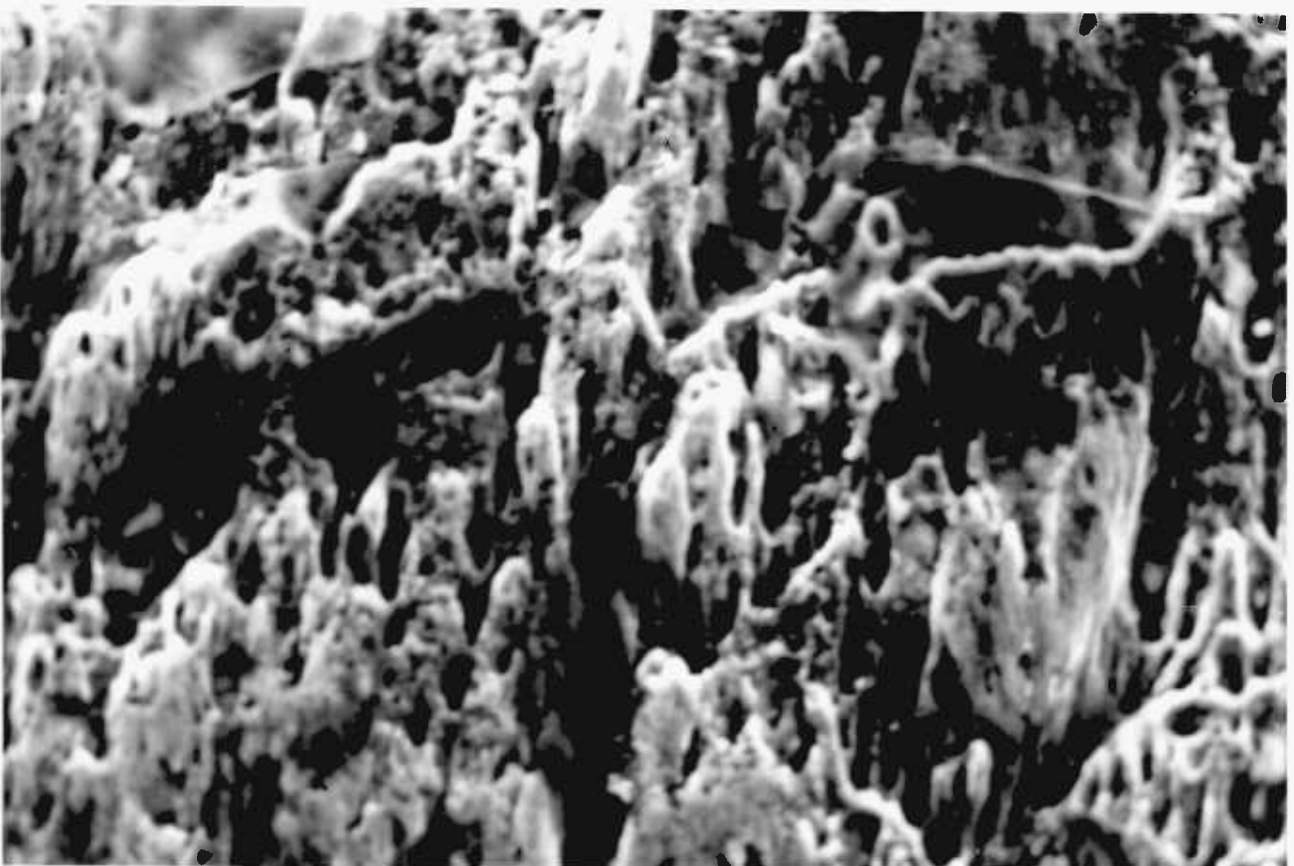
10 μ

FIG. 4.6. M304- DIMPLED FRACTURE THAT RUPTURED IN SHEAR MODE

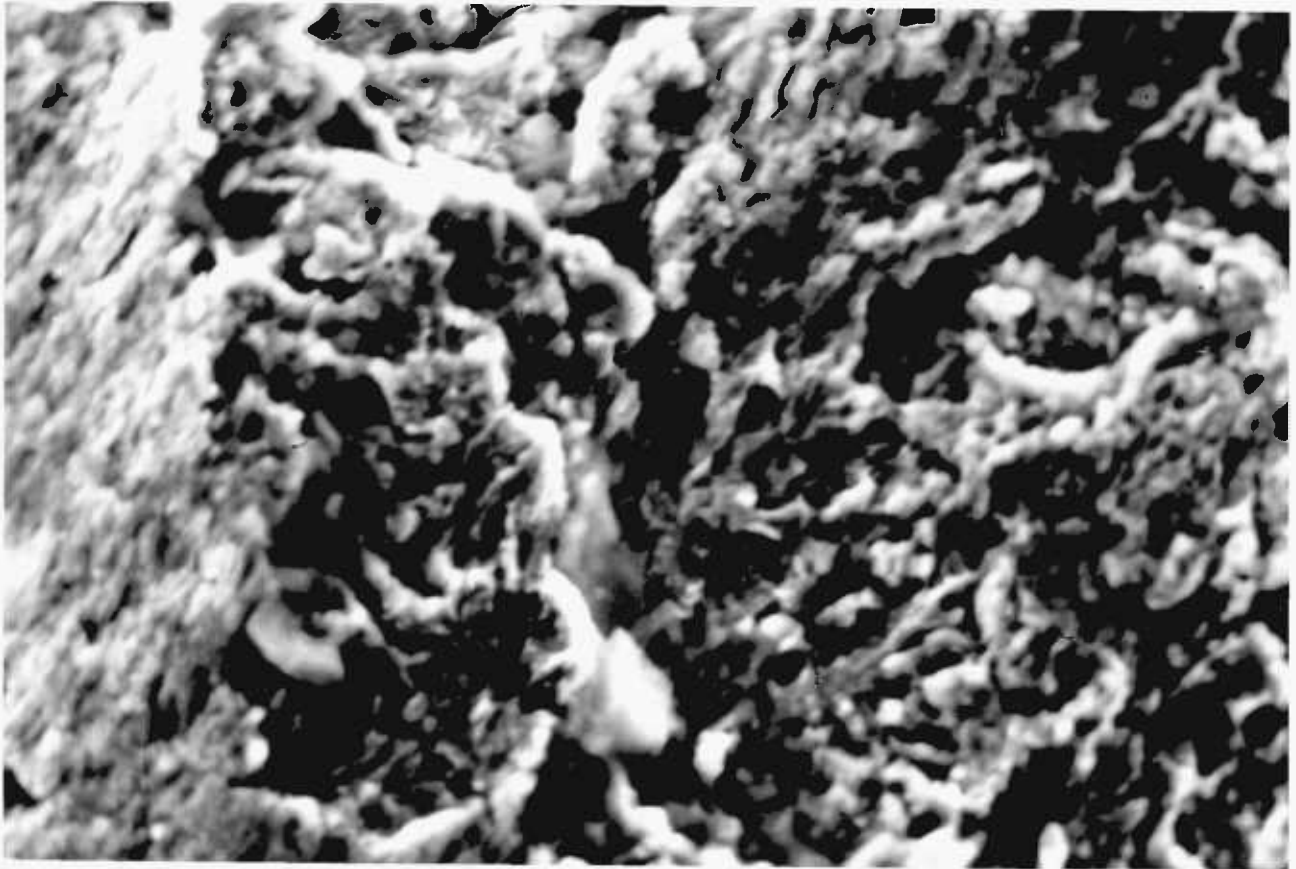
10 μ

FIG.4.7. FV607- DUCTILE FRACTURE AND FEW CLEAVAGE STEPS

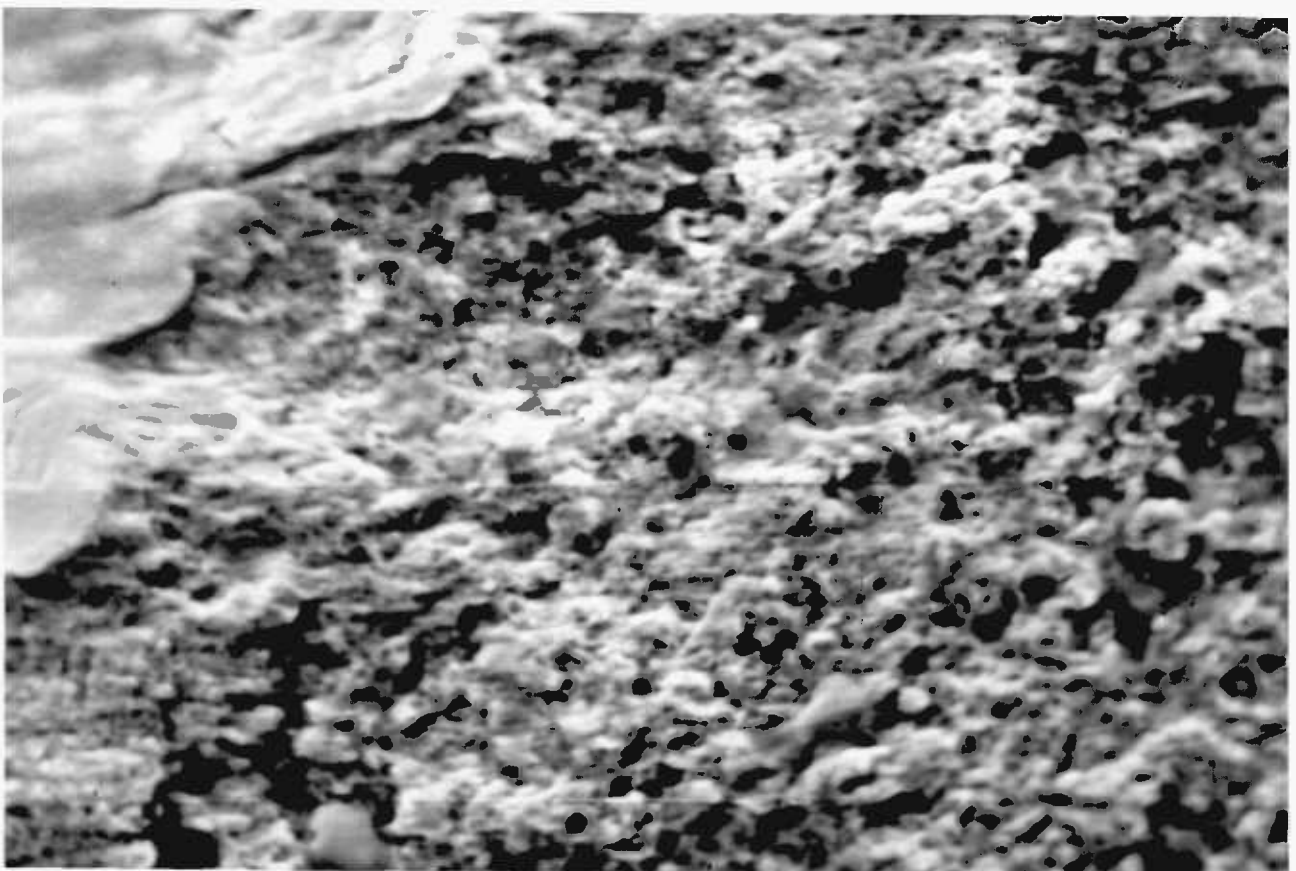
10 μ

FIG.4.8. AISI4132- A FINELY DIMPLED STRUCTURE

expected in this type of fracture. The fractograph shown in fig. 4.4 indicate that the fracture events occurred in a mixed mode involving both shear and tear. Microvoid coalescence here has produced shear dimples with characteristic elongated shape (see fig. 4.4). The coalescence of voids under combined normal and shear strains is called "shear rupture". Shear rupture surfaces may be identified by the fact that the dimples point in the direction of shear on both fracture surfaces. Since the relative shear directions are opposite for the two halves, the dimples point in opposite directions on the matching surfaces. The shape of the shear rupture dimples depends upon the ratio of normal strain to shear strain during the growth and coalescence of the voids, with a high-ratio giving short, almost rounded dimples and a low ratio giving long dimples. When a ductile metal fails under non-uniform normal stress as in fig. 4.2(c), the voids do not coalesce with one another, but are individually intersected by, and coalesce with, the tip of a growing crack. This rupture process is called "tearing". Tearing produces dimples with the same quasi-parabolic shape as those that are formed during shear rupture but with one important distinguishing characteristic - on both rupture surfaces they point in the opposite direction from the direction of crack growth. The right hand side of fig. 4.4 shows tearing under conditions in which the plastic strain in the direction of the applied load is almost the same at the tip of the crack as it is in the bulk of the material, producing short dimples. The left hand side of fig. 4.4 shows tearing under conditions in which the plastic strain in the direction of the applied load is much greater at the tip of the crack than in the bulk of the material ahead of the crack, producing long dimples. The shape of dimples produced by tearing depends largely upon the ratio of plastic strain at the tip of the crack

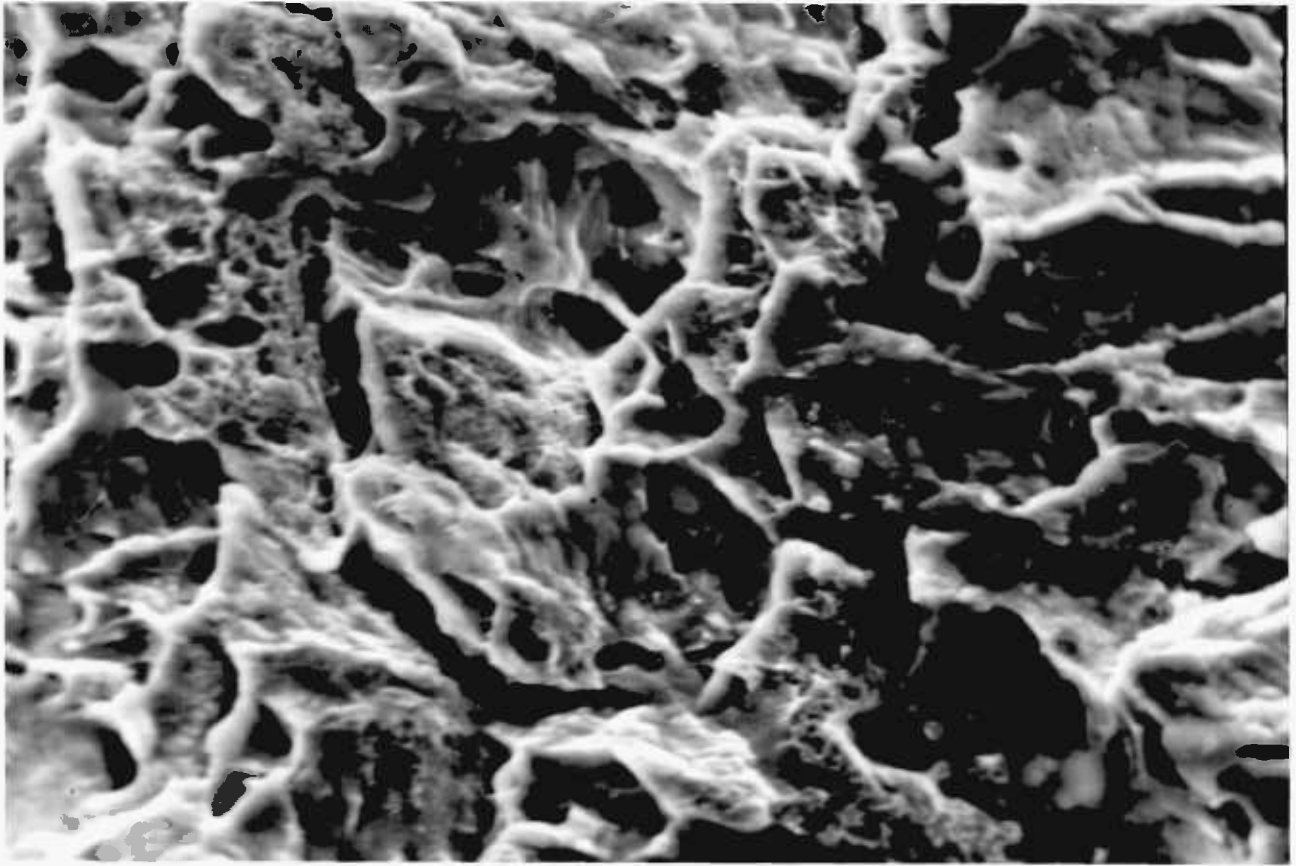
10 μ

FIG.4.9. PE16- QUASI - CLEAVAGE FRACTURE

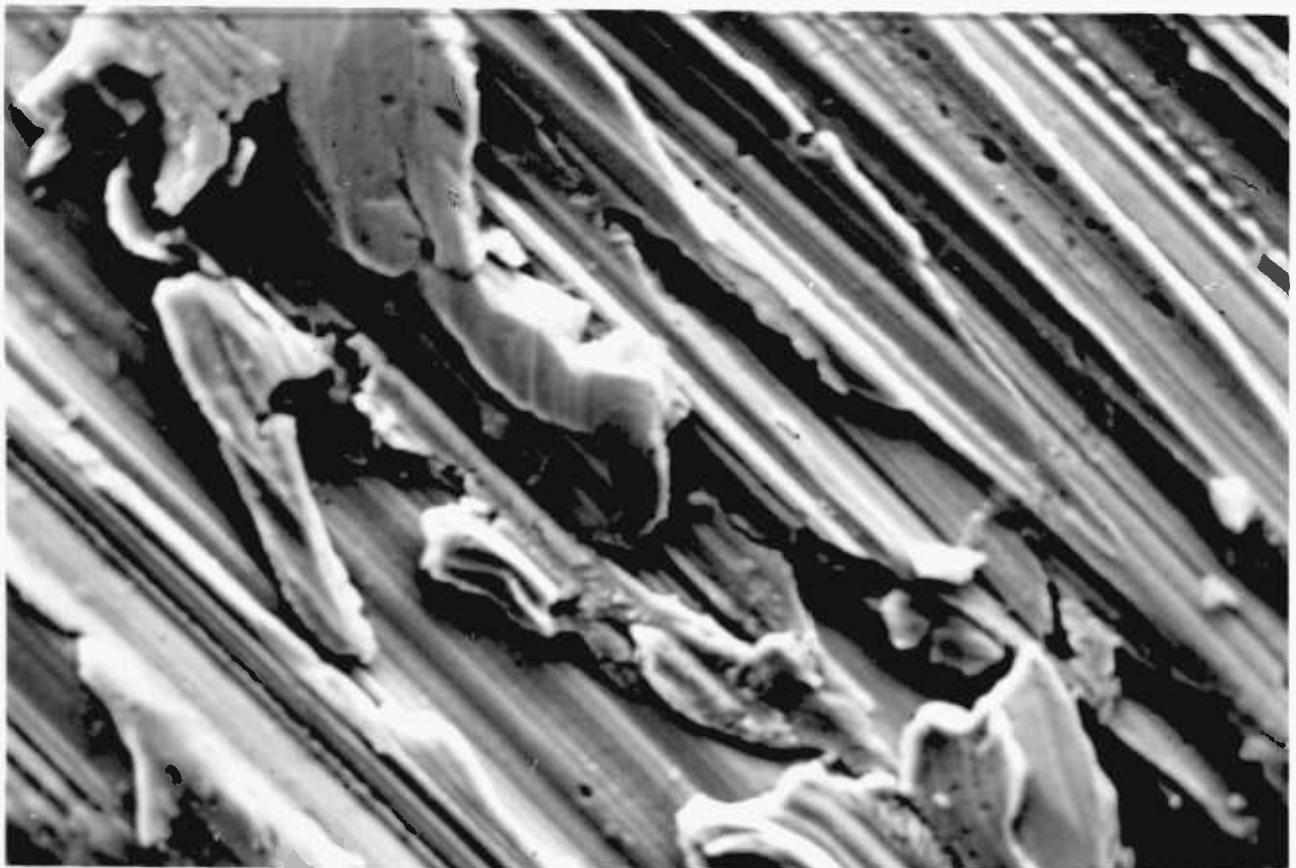
10 μ

FIG.4.10. PE16- FAST FRACTURE AND BLACK LINES SUGGEST CLEAVAGE STEPS

to the plastic strain in the material ahead of the crack. As the crack grows, the material at its tip becomes more restricted by increasing triaxial stress, and the ratio of plastic strain at the tip of the crack to that ahead of the crack decreases. Therefore, dimples are elongated in the early stages of crack growth and become equiaxed just before the remainder of the tube fails by shear fracture (stainless steel tubes, figs 4.3 to 4.8) or quasi-cleavage (nimonic-PE16, figs 4.9 and 4.10). Thus the usual ductile-rupture surfaces (figs 4.3 to 4.8) consist of mixtures of the three types of dimples described above.

As shown in figs 4.9 and 4.10, nimonic PE16 shows quasi-cleavage. Troughs form in fracture surface by nucleation, growth and coalescence of linear microvoids during fast fracture. Fractures resulting from microvoid coalescence and from cleavage are relatively easy to identify, and the mechanisms of separation are reasonably well understood. Quasi-cleavage is a mixed mechanism involving both microvoid coalescence and cleavage. These fractures are not to be confused with those in which cleavage appears in brittle second phases with characteristic dimples of microvoid coalescence appearing in the more ductile matrix. In quasi-cleavage, there is no apparent boundary between a cleavage facet and a dimpled area bordering on the cleavage facet. In fig. 4.10 the black lines suggest cleavage steps which might be caused due to rubbing between tool and material during the shearing action.

The fracture mechanism in embrittled stainless steel M446 is cleavage (see figs 4.11 and 4.12). On a macroscopic and microscopic basis it is difficult to distinguish between transgranular and intergranular cleavage. Fortunately the electron microscope is able to distinguish between the two modes of cleavage. The intergranular cleavage fracture surfaces are smooth and they do not contain any river

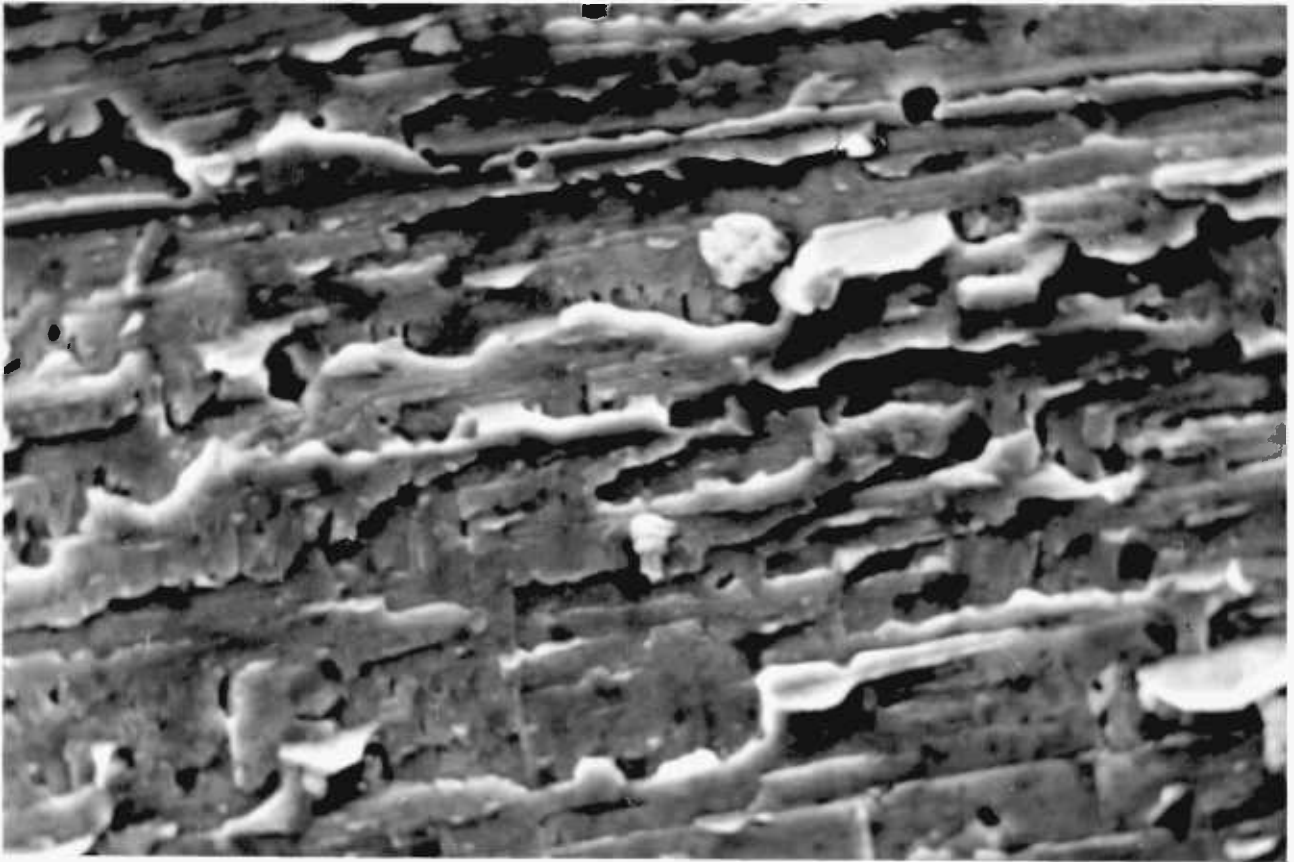
10 μ

FIG. 4.11. EMBRITTLED M446-TRANSGRANULAR CLEAVAGE

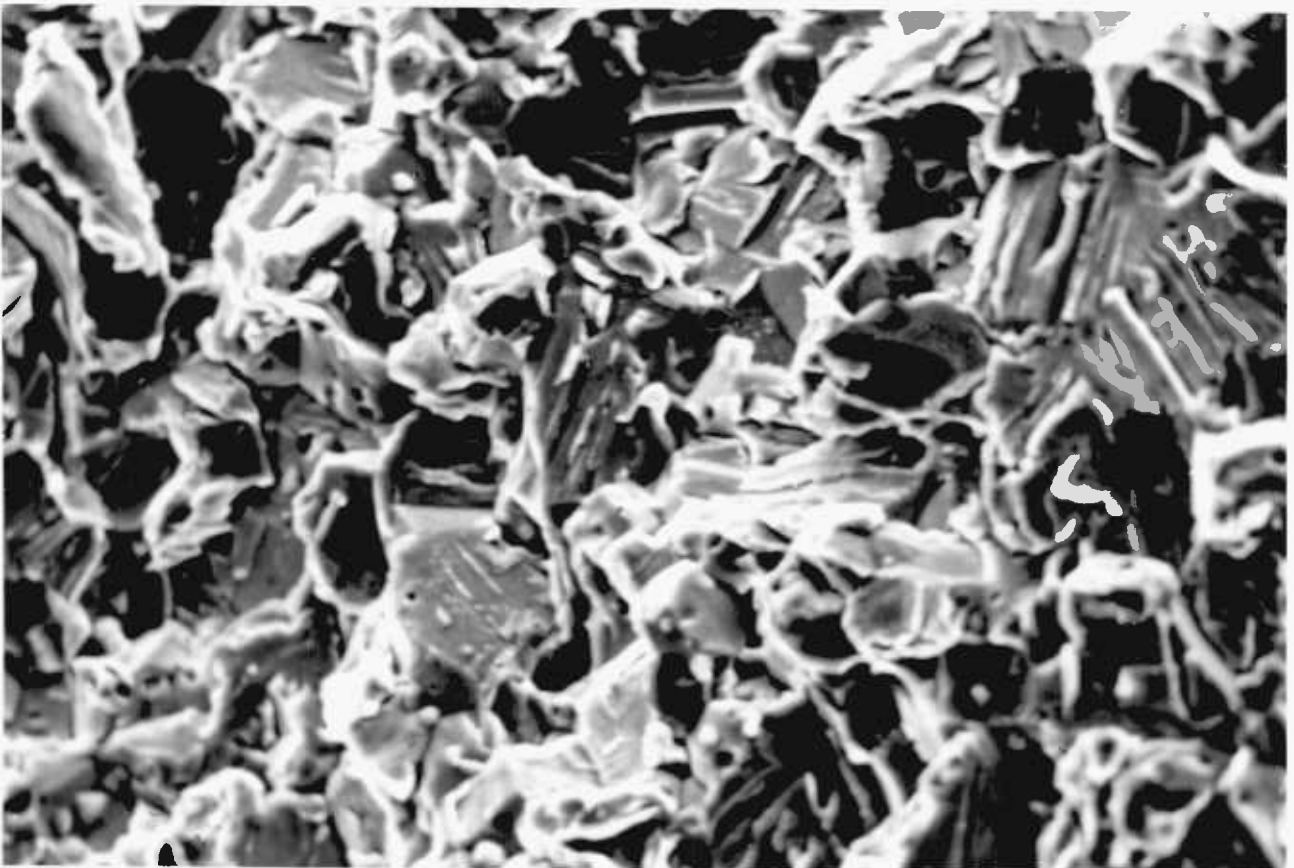
20 μ

FIG. 4.12. EMBRITTLED M446--MIXED INTER-TRANSGRANULAR CLEAVAGE

markings. This is so because these fractures closely follow the plane of a grain boundary which has been embrittled by second-phase particles or traces of impurity. If fracture occurs through the grains, it is called transgranular fracture. Figs 4.11 and 4.12 show mixed versions of intergranular and transgranular cleavage fracture. Crack propagation is by transgranular cleavage through alpha and beta phases as shown in fig. 4.11. Each striation is formed by a cleavage mechanism of fracture and shows the direction of crack propagation.

The brittle behaviour of glass is evident from figs 4.13 and 4.14. In contrast with many crystalline materials, the fracture behaviour of glass is relatively straightforward: glasses are always extremely brittle below their softening points; there are no complications arising from anisotropy or intercrystalline boundaries, neither does dissolved 'impurity' produce any pronounced changes in behaviour. Brittle fracture occurs by the formation and propagation of a crack, but only recently have the phenomena associated with propagation rather than initiation of cracks become apparent, particularly in glasses [40]. It is assumed that the glass surface breaks only from flaws. Examination of fracture surfaces (figs 4.13 and 4.14), reveals a variety of markings. Ripples indicate the actual profile of the crack. Striations are steps in the fracture surface parallel to the local direction of crack propagation and they occur when adjacent sections of a crack front follow paths at slightly different levels. Since there are no regular planes of atoms in glass, there are no preferred planes of fracture within the material itself and a crack propagates along a surface perpendicular to the instantaneous local maximum stress at its tip. The initial plane of propagation is therefore perpendicular to the maximum applied load. As the crack expands under high stress, the energy release rate increases and rougher fracture surfaces are produced.

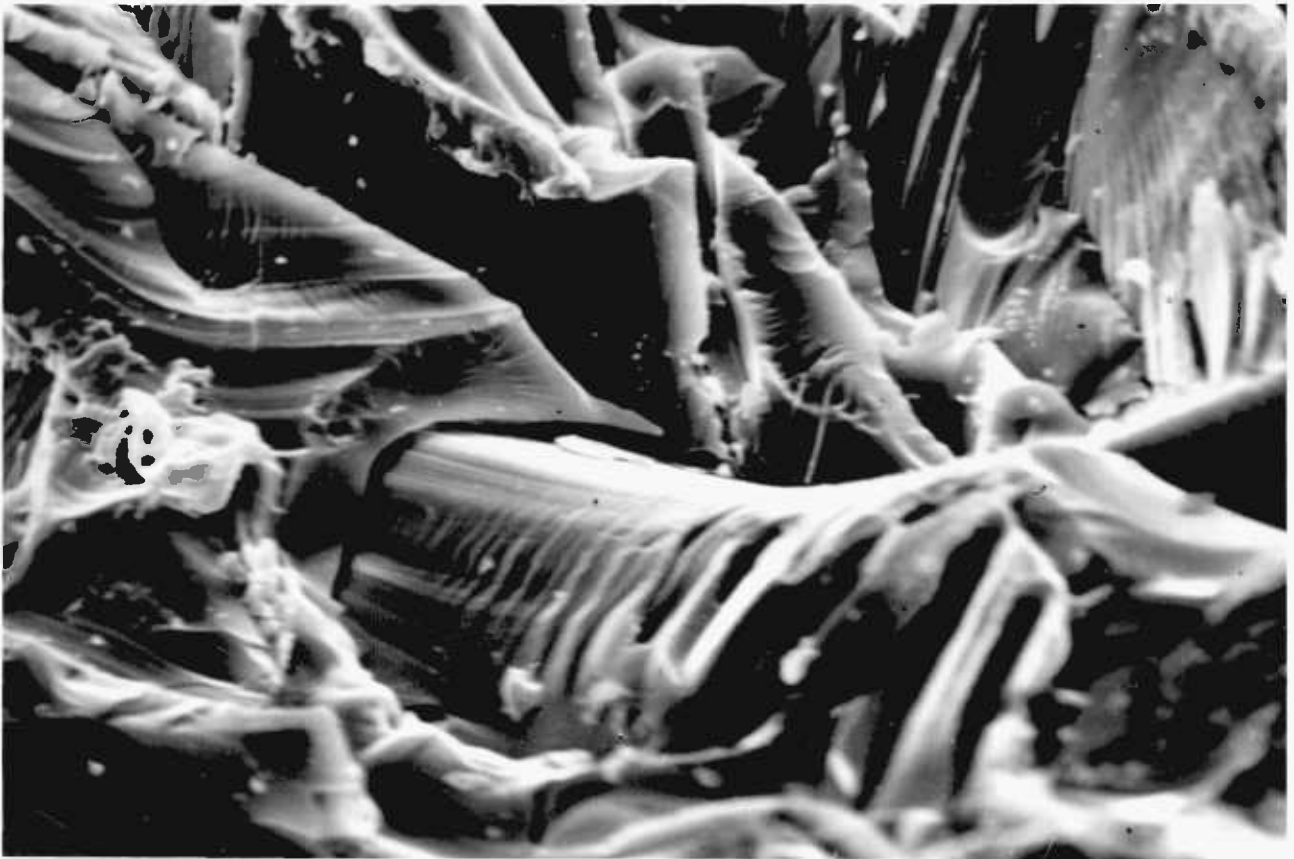
20 μ

FIG.4.13.GLASS-CLEAVAGE FRACTURE

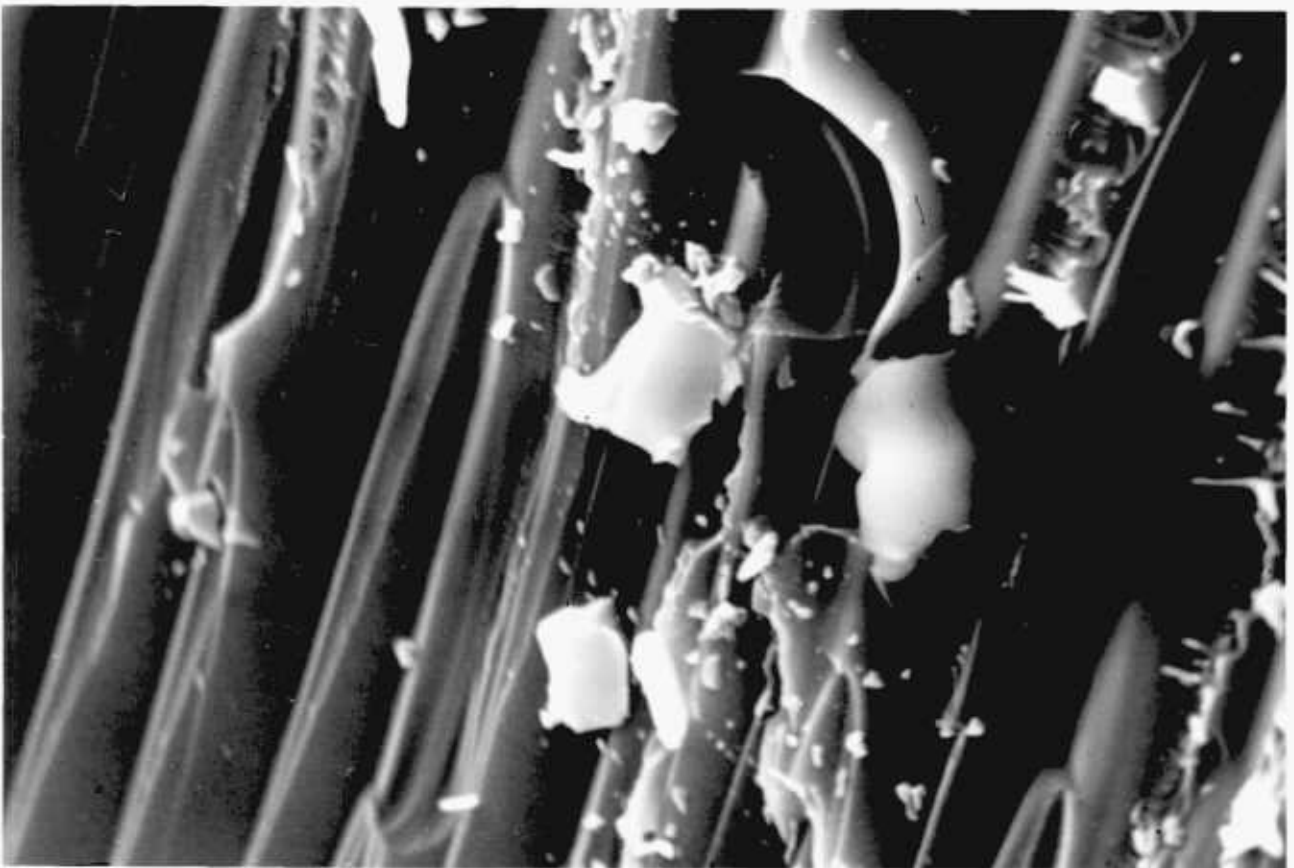
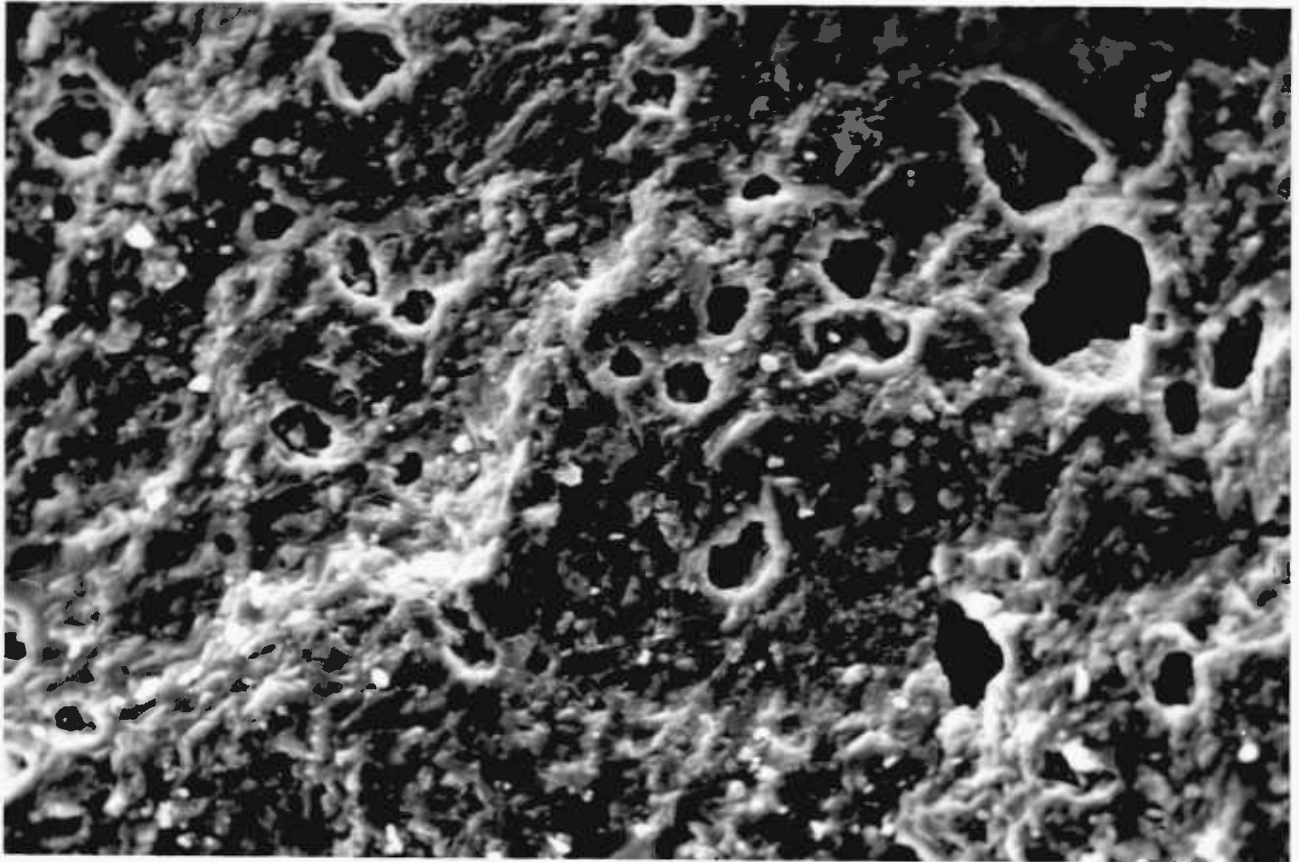
10 μ

FIG.4.14.GLASS-STRIATIONS SHOW THE DIRECTION OF CRACK PROPAGATION

The fracture surfaces in alumina shown in figs 4.15 and 4.16, reveal that fracture took place through the grains. This is called transgranular cleavage fracture. The dark round areas of fig. 4.15 are pores. It is also noted that the pores present in these samples vary in size from very small to very large. These holes must originate during sintering of the alumina body. These pores can also arise due to diffusion at high temperatures which can lead to clustering and collapse of vacancies at grain boundaries. Grain pull-out on fracture faces will also appear as sharp-edged pores, but in many cases it is possible to distinguish when the porosity is in the body of the alumina or when it arises from grain pull-out. The sliding of the grain in the hole and cracks along the grain boundaries (see right hand top corner of fig. 4.16) and the occurrence of a crack so close to the hole clearly suggest that holes were present in the body of the ceramic. Such sharp-edged holes thus play an important role in the generation and propagation of cracks, mainly because they can act as stress raisers.

In the region near the sharp-edged pores and in many other areas, surface markings and cleavage are also observed. The surface markings change orientation, and the tilt in these traces may be due to a sub-boundary, due to twinning or slip on another plane or inclination of the slip or twin plane to the surface. There are many reasons for cleavage occurring in some grains and not in others. The cleavage or slip system in different grains within a polycrystalline sample are loaded to different degrees as their orientation to loading axes are different. Thus, in some grains the load may reach the stress necessary for cleavage. In other grains, where orientation for cleavage is unfavourable, the fracture stress for grain boundaries is reached earlier and fracture is intercrystalline. Some grains may be in a state of high stress due to the processing of the material and the material will cleave.



Black holes are pores
 FIG.4.15. ALUMINA- CLEAVAGE FRACTURE

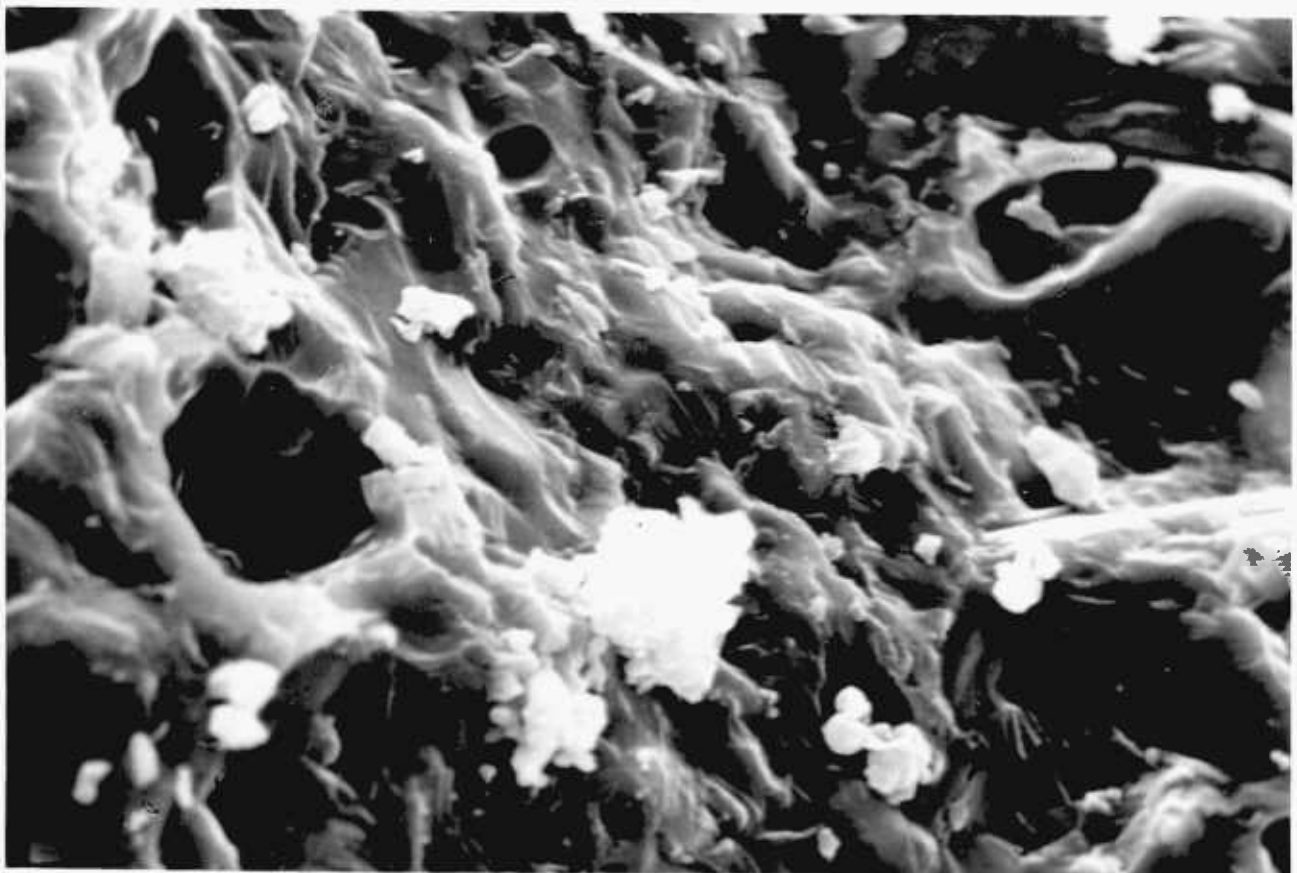


FIG.4.16. ALUMINA- INITIATION OF FRACTURE STARTS FROM PORES
 (SEE RIGHT HAND TOP CORNER)

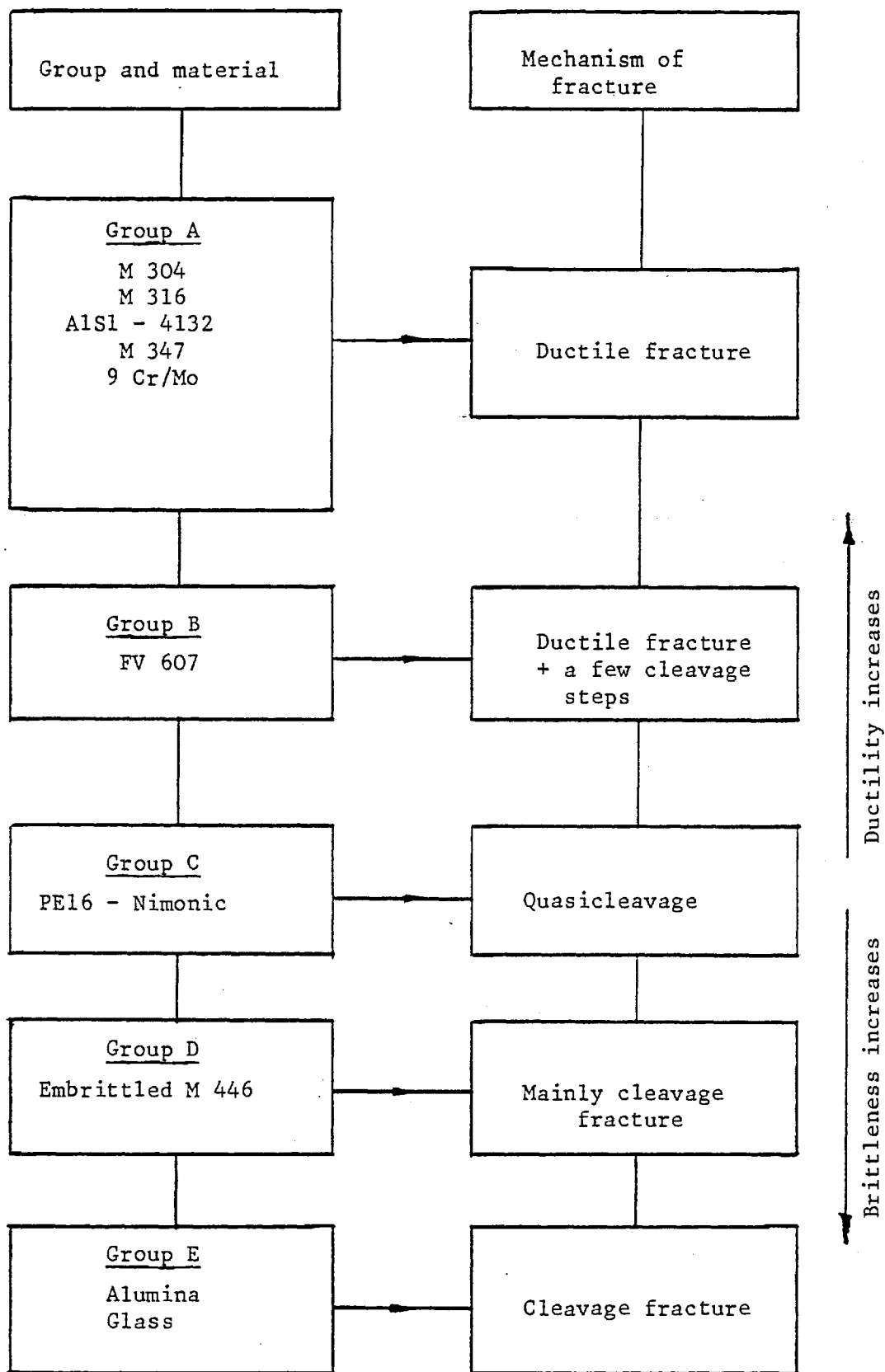


FIG. 4.17 SCHEMATIC DIAGRAM OF THE MATERIALS AND THE MECHANISMS OF FRACTURE IN CROPPING

Higher stress may also be caused by stress raisers (such as porosity). These non-uniform internal stresses can also be a cause of the variety of cleavage types observed in terms of the size, shape, and appearance of steps. The impurity may be dissolved in the grain itself, or may be present as fine precipitates. The presence and location of these particles can cause cleavage steps of many shapes and sizes - some long, others short; some wide, others narrow. The predominant cause of cleavage appears to be a geometrical orientation of cleavage planes relative to the loading axis, and contributions are also made by stress concentration due to porosity or processing and by impurities within the grain.

4.4 CONCLUSIONS

Although the central interest of fractography is the nature of the topography of a fracture, an interpretation of the fracture features is also important for an increased understanding of various aspects of the fracture process. The study of fractography enables assessment of the degree of deformation occurring during separation and the reason for material weakness in the path of the particular fracture.

Microscopic examination of fracture in stainless steels has shown that the mechanism of fracture in cropping is mainly of ductile features. Three distinctly different, but related modes of void coalescence have been observed. "Normal rupture", where equiaxed dimples are formed, and "shear rupture", where elongated dimples point in opposing directions on the mating surfaces, are widely recognised. The third coalescence mode is less widely recognised and is characterised by elongated dimples that point towards the fracture origin on both fracture surfaces which is in contrast to those surfaces formed by shear rupture. In fact,

identification of these three different modes has supported most of the comments made regarding explanation of the cropping cycle (cutting zone, shearing zone, tearing zone etc.) in Chapter 2. Most of the stainless steel specimens contain equiaxed dimples in local areas and normal to the applied load and elongated dimples resulting from combined shear and normal stresses in the fracture area. A significant portion of each of the fracture surfaces in stainless steels has been covered by shear dimples. These dimples may have been caused by the shear tear-out of large second-phase particles or the extensive deformation around voids which are caused by local deposits of nonmetallic material.

Quasicleavage fracture has been identified in nimonic-PE16 material. In fact, this particular alloy is a highly ductile material according to its chemical composition. However, it has been cold-drawn and heat treated during the process of manufacture of the tubes. Perhaps that might have reduced its ductility at room temperature and the material may well be crack sensitive and this could be the reason for it having less deformation than stainless steels. The fracture mechanism in embrittled stainless steel M446 has been identified as a mixed version of intergranular and transgranular cleavage. Fracture in brittle materials like alumina and glass, occurs from defects like mechanically produced cracks, pores and inclusions.

Based on the comments made so far, a schematic diagram of materials and mechanisms of fracture may be made, as shown in fig. 4.17. Thus, the mechanism of the shearing process is not an action in a single plane. It is a summation of different processes, namely bending, stretching of the grains and fibres, and tearing. The shearing process will be discussed in detail in Chapter 6.

CHAPTER 5THEORETICAL WORK5.1 INTRODUCTION

Cropping under pre-load is discussed theoretically based on yield criteria of metals. The reasons for higher cropping loads at low temperatures were explained using the theoretical background relevant to the behaviour of metals at different temperatures.

By adopting material properties obtained from tension tests, cropping loads were predicted for all the thin-walled tubes using the von Mises criterion of yielding. Also, the deflection of the blade at maximum cropping load was estimated using simple theory.

For many metal working operations, no exact solutions for the load to cause unconstrained plastic deformation are available, and accordingly means have been sought whereby loads can be estimated approximately. An upper-bound solution for the cropping of thin-walled tubes described in this chapter has been developed to predict the load-deflection behaviour up to the point of first shearing. For a given deflection, the plastic work done was calculated by assuming a deformation pattern of plastic hinges. Having calculated the plastic work, the load was estimated by numerical differentiation with respect to the deflection.

5.2 THEORETICAL EXPLANATIONS FOR CROPPING UNDER PRE-LOAD

Illustrated in fig. 5.1 is a thin-walled tube subjected to shearing and tensile loads.

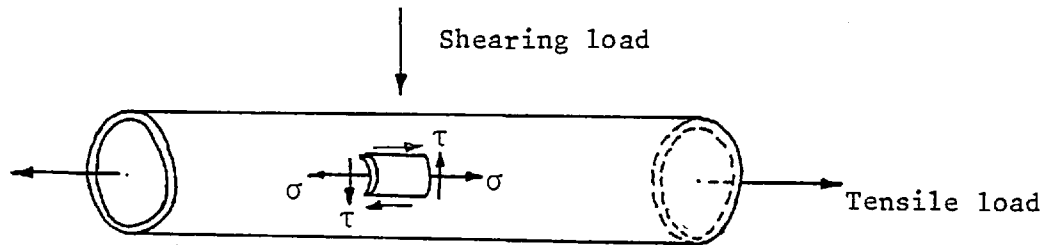
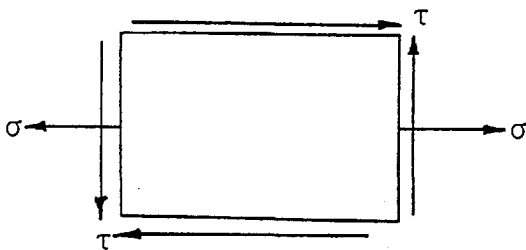


FIG. 5.1

Imagine an element cut from the tube wall and let σ be the applied tensile stress, and τ the shear stress.



Stresses on element of tube wall

FIG. 5.2

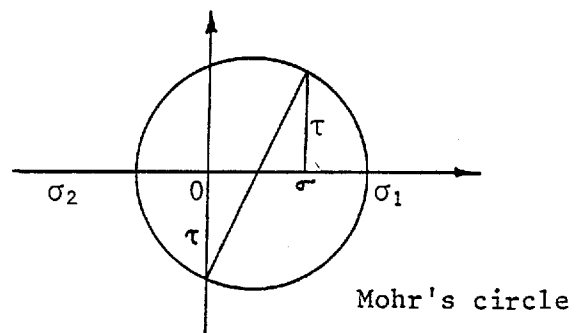


FIG. 5.3

The principal stresses at a point in the tube wall are

$$\sigma_1 = \frac{1}{2}\sigma + \left(\frac{1}{4}\sigma^2 + \tau^2\right)^{1/2}$$

$$\sigma_2 = \frac{1}{2}\sigma - \left(\frac{1}{4}\sigma^2 + \tau^2\right)^{1/2}$$

(5.1)

$$\sigma_3 = 0$$

The yield criterion of von Mises may be expressed by the relationship

$$2Y^2 = (\sigma_1 - \sigma_2)^2 + (\sigma_2 - \sigma_3)^2 + (\sigma_3 - \sigma_1)^2 = 2(\sigma^2 + 3\tau^2)$$

whilst that of Tresca may be expressed as (5.2)

$$Y^2 = (\sigma_1 - \sigma_2)^2 = \sigma^2 + 4\tau^2 .$$

where 'Y' is the uniaxial yield stress of the material in tension.

Summarizing, therefore:

(i) Tresca's criterion gives

$$Y^2 = \sigma^2 + 4\tau^2 \quad (5.3)$$

(ii) Mises' criterion gives

$$Y^2 = \sigma^2 + 3\tau^2 \quad (5.4)$$

From equations (5.3) and (5.4) it can be observed that the original stresses are squared and it emphasizes the fact that the yield condition is independent of their sign. Hence the shearing load decreases with increasing pre-load whether it be tensile or compressive *on the basis of simple model.*

5.3 THEORETICAL EXPLANATIONS FOR CROPPING AT LOW TEMPERATURES

As explained earlier in the context of strain-hardening, an increased stress is required in order to facilitate further progress of the dislocations in metals. The presence of impurities means that a greater stress is required to move dislocations right through the crystal and produce deformation. At high temperatures, thermal activation energy associated with thermal vibrations of the crystal lattice, helps the

applied stress to move dislocations past the obstacles due to inclusions in the metal. Since, at low temperature the thermal activation energy is less, a greater stress is necessary. Hence the external stress required to produce a given deformation at high temperatures is less than that required at low temperatures. For this reason, most metals become stronger and harder as the temperature is reduced.

The strain-hardening rate of most f.c.c. metals increases when the temperature is lowered [41]. A higher strain hardening rate means that a smaller strain is needed to increase the stress required.

5.4 PREDICTION OF CROPPING LOAD BASED ON SHEAR YIELD STRESS

As explained earlier in Chapter 3, most metals and alloys do not show pronounced yielding. In such cases, it is standard practice to define a 'proof stress'. Three different approaches were used in the present work to evaluate the mean yield stress from the true stress-strain curve obtained from a tension test.

(i) The 0.5% proof stress can be taken as the mean yield strength of the material as shown in fig. 5.4.

From the von Mises criterion of yielding, the shear yield stress k can be calculated as

$$k = Y/\sqrt{3} \quad (5.5)$$

The cropping load, P , can be calculated as

$$P = kA_0 \quad (5.6)$$

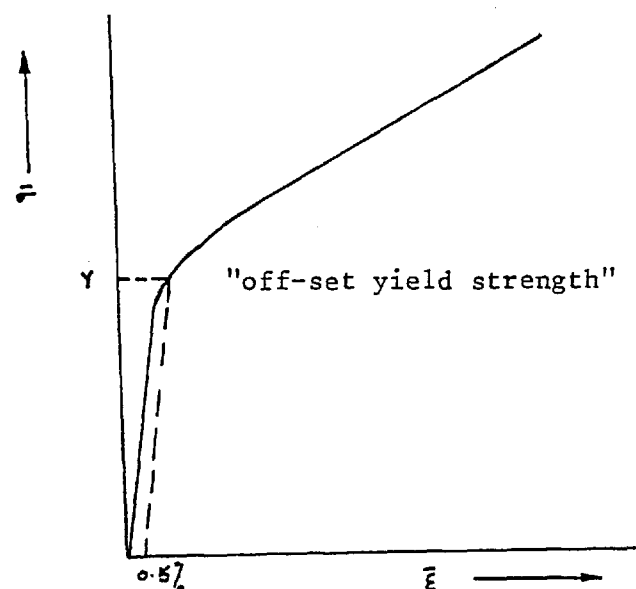


FIG. 5.4

(ii) As shown in fig. 5.5, Y can be estimated by approximating the true stress-strain curve by two linear expressions.

$$\sigma = E\epsilon \quad \text{from } 0 - Y \quad (5.7)$$

$$\sigma = \sigma_0 + B\epsilon \quad \text{from } Y \text{ onwards}$$

where E = Elastic modulus and

B = plastic modulus.

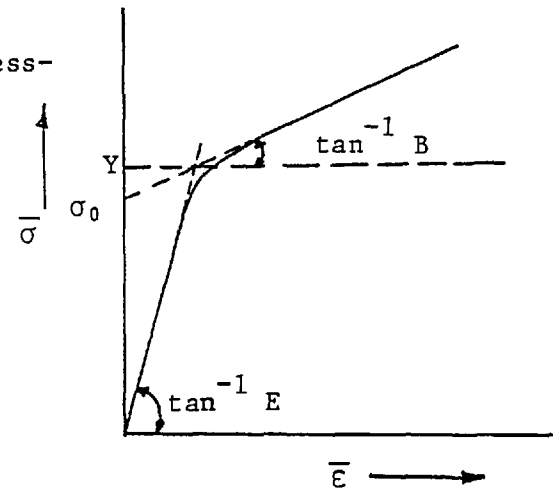


FIG. 5.5

Then, the intersection of the two linear expressions (5.7) determines Y .

Then, k can be calculated from eqn (5.5) and P can be calculated from eqn (5.6).

(iii) An empirical formula can be assumed to exist between the shear yield strength k and the fracture stress σ_f , thus:

$$\sigma_f \propto k$$

$$\text{i.e. } \sigma_f = mk$$

where $m = 3$ for good agreement with the cropping results.

$$\text{Thus, } \sigma_f = 3k \quad (5.8)$$

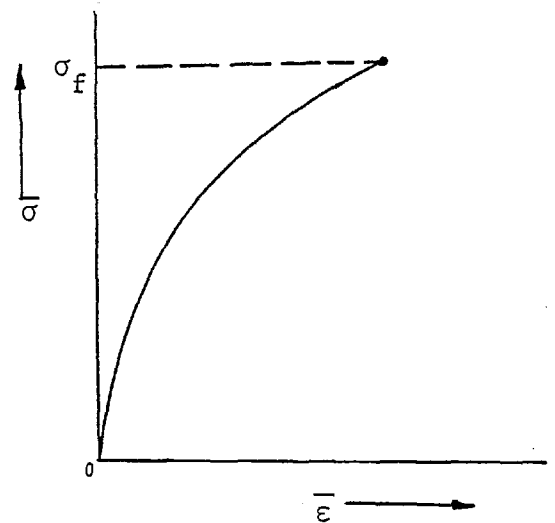


FIG. 5.6

5.5 PREDICTION OF DEFLECTION AT MAXIMUM CROPPING LOAD

In the simple tension test, the true strain $\bar{\epsilon}$ is

$$\bar{\epsilon} = \ln(1 + e) \quad (5.9)$$

It will be assumed that, at maximum cropping load the effective strain will be

$$\bar{\epsilon}_c = \bar{\epsilon}_{UTS} \quad (5.10)$$

where $\bar{\epsilon}_c$ = Effective strain or reduced strain at the maximum cropping load and $\bar{\epsilon}_{UTS}$ is the effective strain at maximum load in the tensile test.

It is well known that

$$\begin{aligned} \bar{\epsilon} &= \frac{\sqrt{2}}{3} \sqrt{(\epsilon_1 - \epsilon_2)^2 + (\epsilon_2 - \epsilon_3)^2 + (\epsilon_3 - \epsilon_1)^2} \quad (5.11) \\ &= \sqrt{2/3 (\epsilon_1^2 + \epsilon_2^2 + \epsilon_3^2)} \quad (\text{since } \epsilon_1 + \epsilon_2 + \epsilon_3 = 0) \end{aligned}$$

Equation (5.11) can therefore be written for the present tubular thin-walled specimens as

$$\bar{\epsilon} = \sqrt{2/3 (\epsilon_\theta^2 + \epsilon_x^2 + \epsilon_t^2)} \quad (5.12)$$

Neglecting ϵ_t ,

$$\bar{\epsilon} = \sqrt{2/3 (\epsilon_\theta^2 + \epsilon_x^2)} \quad (5.13)$$

Assuming volume constancy, $\epsilon_\theta = -\epsilon_x$, so that

$$\bar{\epsilon} = 2/\sqrt{3} \epsilon_\theta \quad \text{or} \quad 2/\sqrt{3} \epsilon_x \quad (5.14)$$

If it is assumed that the material is strained over some distance, x , it is known from the literature on the behaviour of thin-walled tubes [42], that ' x ' depends on the tube size. An empirical relation can be established, namely

$$x = n \sqrt{R_1 T} \quad (5.15)$$

where ' n ' is a constant which can be chosen as being equal to 4.7 to give good agreement with the present experimental results.

Thus

$$x = 4.7 \sqrt{R_1 T} \quad (5.16)$$

also the engineering strain in x direction is

$$e_x = \rho \cdot T/2 \quad (5.17)$$

where ρ is the change of curvature

$$\rho = \frac{\alpha_1}{x} \quad (5.18)$$

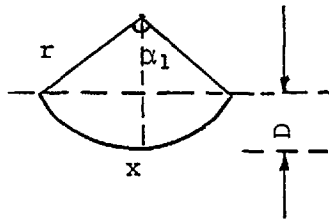


FIG. 5.7

$$x = r\alpha_1 \quad (5.19)$$

$$r - r \cos \frac{\alpha_1}{2} = D \quad (5.20)$$

From (5.19) and (5.20)

$$\frac{(1 - \cos \frac{\alpha_1}{2})}{\alpha_1} = \frac{D}{x} \quad (5.21)$$

From equation (5.18),

$$\frac{1 - \cos \frac{\alpha_1}{2}}{D} = \frac{\alpha_1}{x} = \rho \quad (5.22)$$

Hence

$$\bar{\epsilon} = \frac{2}{\sqrt{3}} \ln(1 + e_x) = \frac{2}{\sqrt{3}} \ln \left[1 + \frac{(1 - \cos \frac{\alpha_1}{2})}{D} \cdot T/2 \right] \quad (5.23)$$

For any given deflection D , α_1 can be calculated from eqn (5.21) Hence $\bar{\epsilon}_c$ can be obtained from eqn (5.23), by assuming that when $\bar{\epsilon}_c$ is equal to $\bar{\epsilon}_{UTS}$, that that particular deflection can be taken as the deflection at maximum cropping load. The results are shown in Table 5.2.

5.6 UPPER BOUND SOLUTION FOR TUBE CROPPING

(i) Free end of the tube

A non-dimensional equation for decay length has been established based on the evidence from the incremental tests, illustrated in Fig. 5.8.

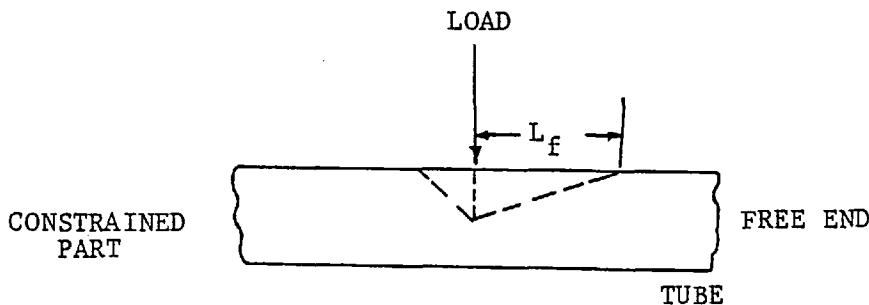


FIG. 5.8

It was observed from the incremental cropping experiments, *and also from ref.87* that the decay L_f can be approximated by the expression

$$L_f = D_m \sqrt{R_i/T}$$

Where D_m is the mean diameter of the tube and $R_i/T = \text{Tube constant}$.
 In non-dimensional form,

$$\frac{L_f}{D_m} = \sqrt{\frac{R_i}{T}} \quad (5.24)$$

The decay length depends on the size and material of the tube.
 In the present analysis, the material factor is negligible because all the tubes are stainless steels, albeit of different composition. Hence decay length depends mainly on the size of the tube.

The geometry and notation used for the plastic hinge deformation pattern observed is illustrated in fig. 5.9.

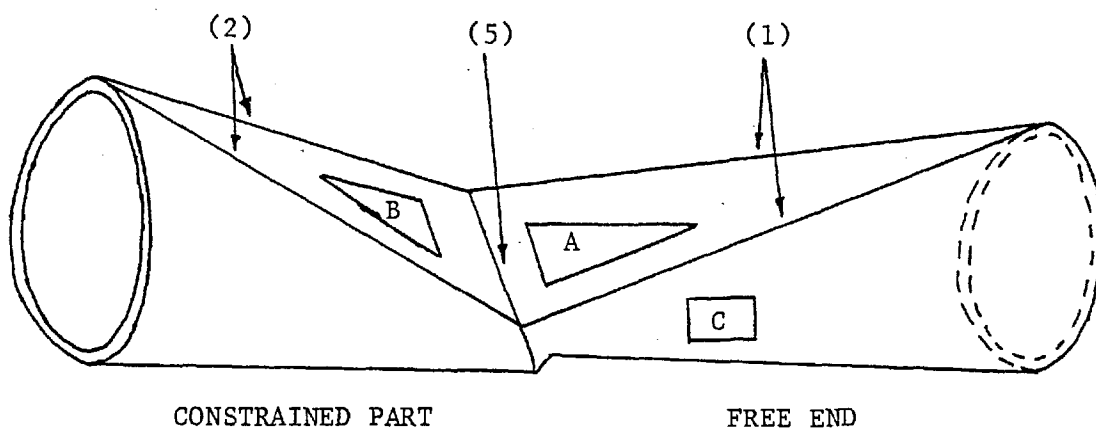

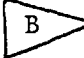
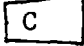


FIG. 5.9

- (1) Two "longitudinal" hinges on the top surface of the free end of the tube.
- (2) Two "longitudinal" hinges on the top surface of the constrained part of the tube
- (5) One "transverse" hinge across the tube
-  Indicates a surface which has become substantially flat due to the deformation
-  Deformed surface of the constrained part
-  Indicates a curved surface which has suffered a change of curvature from that of the original tube

$$A = \frac{D_o + D_i}{4} \quad (5.25)$$

$$T = \frac{D_o - D_i}{2} \quad (5.26)$$

$$M_p = \frac{YT^2}{4} \quad (5.27)$$

Model for free end of the tube

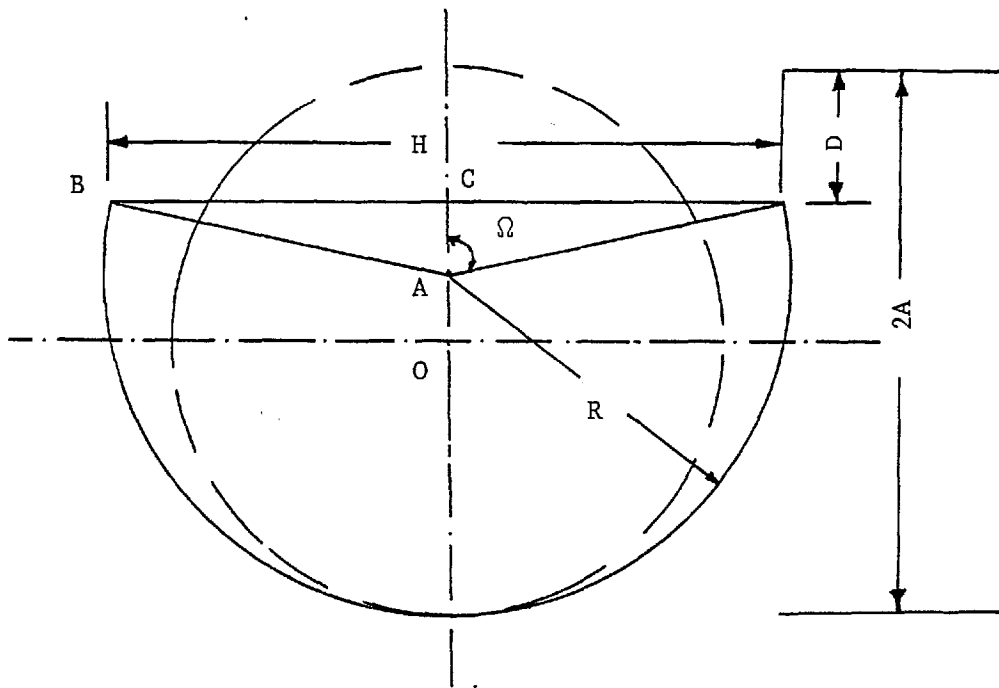


FIG. 5.10

The basic equations are

$$\frac{H}{2} + R(\pi - \Omega) = A\pi \quad \text{from inextensibility} \quad (5.28)$$

$$\tan \Omega = \frac{H}{2(2A - D - R)} \quad (5.29)$$

$$\sin \Omega = \frac{H}{2R} \quad \text{from triangle ABC} \quad (5.30)$$

From the above equations, it is possible to obtain

$$\frac{H}{2A} = \frac{\pi \sin \Omega}{\pi - \Omega + \sin \Omega} \quad (5.31)$$

$$\frac{D}{A} = 2 - \frac{\pi(1 + \cos \Omega)}{\pi - \Omega + \sin \Omega} \quad (5.32)$$

$$\frac{R}{A} = \frac{\pi}{\pi - \Omega + \sin \Omega} \quad (5.33)$$

From eqn (5.32), Ω can be calculated. For this purpose equation (5.32) can be written in the more convenient form:

$$\left(\frac{D}{A} - 2\right)(\sin \Omega - \Omega) + \pi \cos \Omega + \pi\left(\frac{D}{A} - 1\right) = 0 \quad (5.32a)$$

The instantaneous radius of the deformed tube is R which is, from equation (5.33)

$$R = \frac{A\pi}{\pi - \Omega + \sin \Omega} \quad (5.33a)$$

The length of the flat across the tube, H , can be calculated from eqn (5.28), as follows:

$$H = 2[A\pi - R(\pi - \Omega)] \quad (5.28a)$$

Equation for effective length of hinge

In practice, the plastic work varies exponentially with deflection. To obtain an appropriate curve of variation of work with respect to deflection, possible considerations are 1) length of the hinge varies exponentially with deflection and the rotation of the hinge varies linearly along the length of the hinge or 2) length of the hinge varies linearly with deflection and the rotation of the hinge varies exponentially

along the length of the hinge.

Considering the first assumption

The decay length, L , varies exponentially with deflection, i.e.

$$\begin{aligned} L &= f(D) \\ L &= ae^{-bD} + c \end{aligned} \quad (5.34)$$

where a , b , c are constants.

Boundary conditions

$$D = 0, \quad L = 0 \quad \text{and} \quad D = D_{\max}, \quad L = L_f$$

From the first condition

$$\begin{aligned} D = 0, \quad L = 0 \\ \therefore a = -c \\ L = a(e^{-bD} - 1) \end{aligned} \quad (5.35)$$

From the second condition

$$a = \frac{L_f}{(e^{-bD_{\max}} - 1)} \quad (5.36)$$

$$\therefore L = \frac{L_f}{(e^{-bD_{\max}} - 1)} (e^{-bD} - 1) \quad (5.37)$$

The constant 'b' can be chosen to fit the experimental results. It depends on the diameter of the tube and, for good agreement can be taken to be

$$b = 6/D_m \quad (5.38)$$

Plastic work calculations

From eqn (5.37), the decay length L can be calculated for a given deflection and the lengths S_1 and L_1 illustrated in Figs 5.11 and 5.12 can be calculated from the following equations:

$$S_1 = \sqrt{L_f^2 + D^2} \quad (5.39)$$

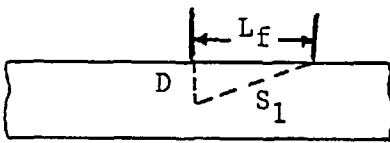


FIG. 5.11

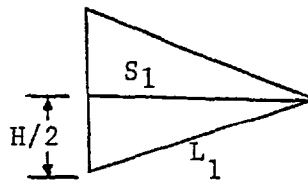


FIG. 5.12

$$L_1 = \sqrt{S_1^2 + (H/2)^2} \quad (5.40)$$

Work done in the longitudinal hinges (W_1)

From the model, the rotation Ω at the hinge for a given deflection is Ω , with respect to the deformed model. In fact, the actual angle of rotation of the hinge would be higher than Ω if it were taken with respect to the original tube.

The actual angle of rotation at the point of loading

$$= (\Omega + \Omega_1)$$

where Ω_1 is the change in the angle due to change in the radius from A to R which can be calculated separately as shown below.

To obtain Ω_1

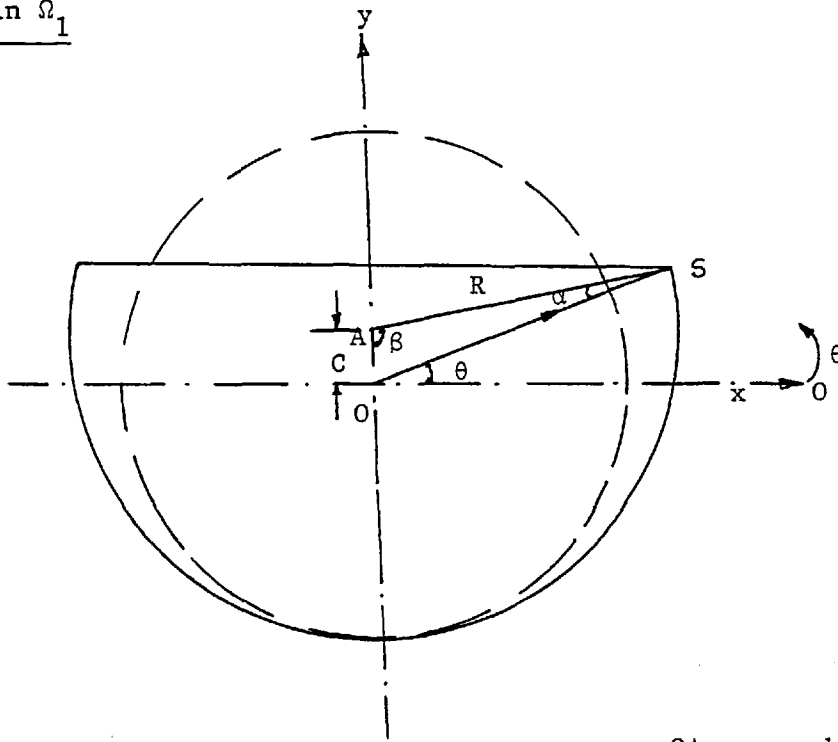


FIG. 5.13

$OA = c =$ distance between
two centres

$$\angle OAS = \beta$$

$$\angle AOS = 90^\circ - \theta$$

$$\angle ASO = \alpha$$

$$y_A = \sqrt{A^2 - x_A^2} \quad (5.41)$$

$$y_R = \sqrt{R^2 - x_R^2} + c \quad (5.42)$$

$$\frac{dy_A}{dx} = -\frac{x_A}{\sqrt{A^2 - x_A^2}} \quad (5.43)$$

$$\frac{dy_R}{dx} = -\frac{x_R}{\sqrt{R^2 - x_R^2}} \quad (5.44)$$

$$\Omega_1 = \left| \frac{dy_A}{dx} - \frac{dy_R}{dx} \right| \quad (5.45)$$

$$= \left| -\frac{x_A}{\sqrt{A^2 - x_A^2}} \right| - \left| -\frac{x_R}{\sqrt{R^2 - x_R^2}} \right|$$

$$x_A = A \cos \theta \quad (5.46)$$

$$x_r = \bar{r} \cos \theta \quad \text{where } \bar{r} = OS \quad (5.47)$$

From triangle OAS

$$\beta = 180^\circ - \alpha - (90^\circ - \theta)$$

$$\beta = 90^\circ + \theta - \alpha \quad (5.48)$$

$$\frac{OS}{\sin \beta} = \frac{C}{\sin \alpha} \quad (5.49)$$

$$\bar{r} = OS = \frac{\sin \beta}{\sin \alpha} \cdot C$$

$$\bar{r} = \frac{\sin(90^\circ + \theta - \alpha)}{\sin \alpha} \cdot C \quad (5.50)$$

From triangle OAS

$$\frac{R}{\sin(90^\circ - \theta)} = \frac{C}{\sin \alpha} \quad (5.51)$$

$$\therefore \sin \alpha = C/R \cos \theta$$

$$\alpha = \sin^{-1} [C/R \cos \theta]$$

From triangle ACS

$$\cos \Omega = \frac{AC}{AS}$$

$$AC = R \cos \Omega \quad (5.52)$$

$$OA = OC - AC$$

$$\therefore C = A - D - R \cos \Omega \quad (5.53)$$

From triangle OAS

$$\tan \theta = \frac{OC}{CS} \quad (5.54)$$

$$= \frac{A - D}{H/2}$$

$$\theta = \tan^{-1} \left[\frac{2(A - D)}{H} \right]$$

$$\bar{r} = \frac{R \sin[90^\circ + \theta - \sin^{-1}\{C/R \cos \theta\}]}{\cos \theta} \quad (5.55)$$

\bar{r} can be calculated from eqn (5.55).

Hence Ω_1 can be calculated and the various components of the plastic work are then as follows:

W_1 = plastic moment \times length of the hinge \times average angle of rotation

$$= M_p \cdot L_1 (\Omega + \Omega_1) \quad (5.56)$$

W_5 = work done in the transverse hinge

$$= M_p \cdot H \cdot \tan^{-1}(D/L_f) \quad (5.57)$$

W_A = work done in flattening the top surface of the tube

$$= M_p \cdot S_1 \cdot (\Omega + \Omega_1) \quad (5.58)$$

W_c = work done in changing the curvature from $1/A$ to $1/R$

= plastic moment \times area \times change in the curvature

$$= M_p \cdot L_f (2\pi A - H/2) \cdot (1/A - 1/R) \quad (5.59)$$

WD_1 = work done due to stretching the flat area

$$\text{strain in the flat area} = (S_1/L_f - 1)$$

$$\text{area of the flat} = HS_1/2$$

$$WD_1 = Y \cdot T \cdot (HS_1/2) (S_1/L_f - 1) \quad (5.60)$$

(ii) Constrained part of the tube

A non-dimensional equation for the decay length in the constrained part of the tube, L_c has been established based on the evidence obtained from incremental tests, illustrated in fig. 5.14.

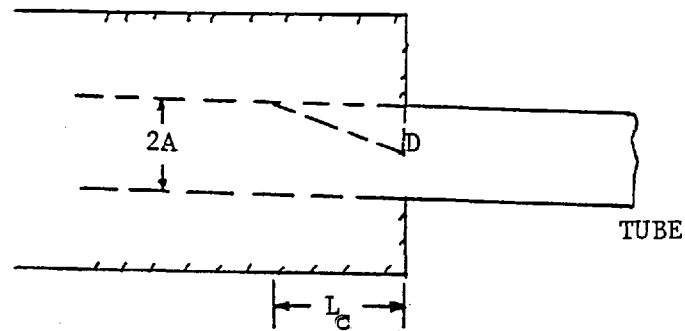


FIG. 5.14

$$L_c = A \ln (R_i/T)$$

In non-dimensional form

$$\frac{L_c}{A} = \ln (R_i/T) \quad (5.61)$$

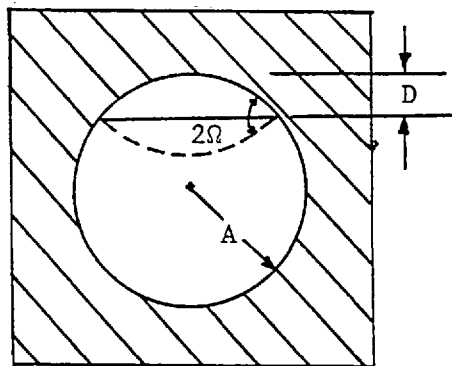


FIG. 5.15

For a given deflection, D , the angle of rotation of the hinge is Ω for the free end of the tube. For the same deflection, D , the angle of rotation of the hinge in the constrained part of the tube should be 2Ω because the tube is held in a work holder. It has no other choice except deforming into the hollow portion of the tube. From figure 5.9, there are two longitudinal hinges and one curved part of the tube in the work holder.

$$L_c = L_{\max} \quad \text{when} \quad D = D_{\max}$$

This can be obtained from eqn (5.37).

From Figs 5.16 and 5.17

$$S_2 = \sqrt{L_c^2 + D^2} \quad (5.62)$$

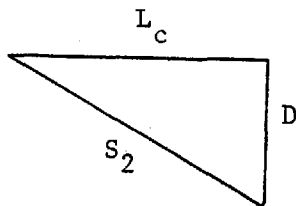


FIG. 5.16

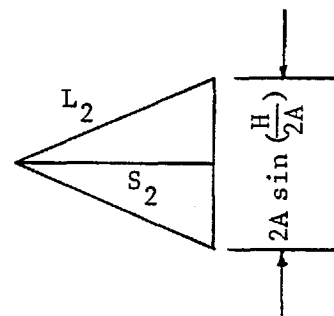


FIG. 5.17

$$\text{The length of the flat} = 2A \sin(H/2A) \quad (5.63)$$

and

$$L_2 = \sqrt{S_2^2 + \{A \sin(H/2A)\}^2} \quad (5.64)$$

If the work done in the longitudinal hinges = W_2 , then

$$\begin{aligned} W_2 &= 2 \cdot M_p \cdot L_2 \cdot \left(\frac{2\Omega}{2}\right) \\ &= 2M_p \cdot L_2 \cdot \Omega \end{aligned} \quad (5.65)$$

$$\begin{aligned}
 W_B &= \text{work done in deforming } \triangleleft \quad (\text{see fig. 5.9}) \\
 &= 2 \cdot M_p \cdot S_2 \cdot \Omega \quad (5.66)
 \end{aligned}$$

(iii) Energy dissipated by the mismatching

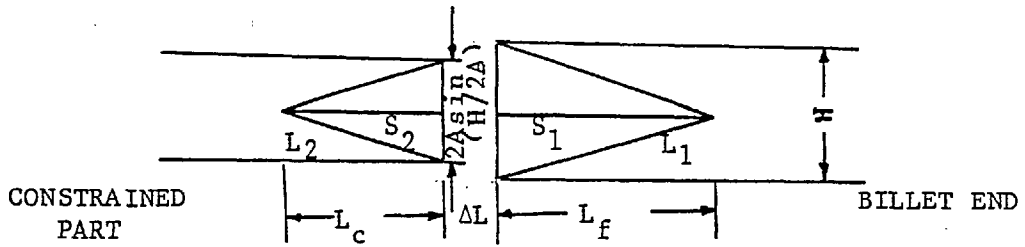


FIG. 5.18

In practice, the constrained and free parts of the tube are connected together up to the point of actual first shearing. Hence the energy dissipated by the "mismatching" of the two different geometries can be calculated by superimposing a transverse hinge across the tube and stretching the constrained part of the tube over a small length ΔL at the point of loading. A small percentage of the decay length of the billet end can be taken as ΔL . It was found from experiments that ΔL was approximately 12.5% of L_f , i.e.

$$\Delta L = 0.125 L_f \quad (5.67)$$

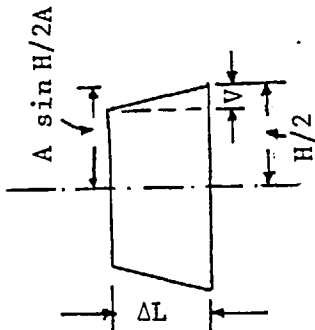


FIG. 5.19

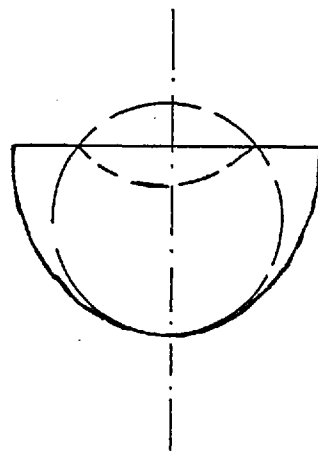


FIG. 5.20

From Fig. 5.19,

$$V = H/2 - A \sin(H/2A) \quad (5.68)$$

The average angle of rotation of the transverse hinge across the tube is equal to $\psi_1/2$, where

$$\psi_1 = \tan^{-1}(V/\Delta L) \quad (5.69)$$

The average angle of rotation of the transverse hinge on the top of the tube at the point of loading is equal to $\psi_2/2$, where

$$\psi_2 = \tan^{-1}(D/\Delta L) \quad (5.70)$$

If W_3 = energy dissipated by mismatching of the flat (free end) and curved part of the tube in the work holder, then

$$W_3 = M_p \cdot H \cdot \psi_2/2 \quad (5.71)$$

W_4 = work done in the curved hinge across the tube, then

$$W_4 = M_p \cdot (2\pi A - H) \cdot \psi_1/2 \quad (5.72)$$

(iv) Work done in stretching

This can be divided into two parts - one part is due to stretching the flat from $[2A \sin(H/2A)]$ to H over a length ΔL and the second part is stretching the curved part of the tube over a length ΔL .

$$\begin{aligned} \text{Now } W_{D_2} &= \text{yield stress} \times \text{volume} \times \text{average strain} \\ &= Y \cdot (H \cdot \Delta L \cdot T) [V/2A \sin(H/2A)] \end{aligned} \quad (5.73)$$

If W_{D_3} = stretching curved part over a length ΔL , then

$$\begin{aligned} W_{D_3} &= Y \cdot [T \cdot \Delta L \cdot (2\pi A - H)] \cdot \frac{1}{2} \left(\frac{R - A}{A} \right) \\ &= Y \left(\frac{R - A}{2A} \right) [T \cdot \Delta L \cdot (2\pi A - H)] \end{aligned} \quad (5.74)$$

Thus, if W_D = Total work done due to stretching, then

$$W_D = W_{D_1} + W_{D_2} + W_{D_3} \quad (5.75)$$

If W = Total work done, then

$$W = W_1 + W_2 + W_3 + W_4 + W_5 + W_A + W_B + W_C + W_D \quad (5.76)$$

The load can be calculated by numerical differentiation of total work with respect to deflection as given by equation (5.77).

$$\text{Load} = P = \frac{dW}{dD} \quad (5.77)$$

Theoretical and experimental results are compared in Table 5.3 and the load-deflection curves are shown in figs. 5.21 to 5.34.

5.7 COMPARISON OF EXPERIMENTAL AND THEORETICAL RESULTS

From the theoretical predictions, the cropping load should decrease with increasing pre-load whether it be tensile or compressive. The cropping results under tensile pre-load agree with the theory. However, the cropping load was found to increase under compressive axial load. In this case, the original expectation that the externally applied compressive load would result in a certain distribution of stress and cumulative strain was therefore not met. The compressive axial load applied on the billet side created a bending effect on the billet. Hence the experiments produced negative results. Reduced loads are anticipated if the compressive pre-load arrangement were to be modified.

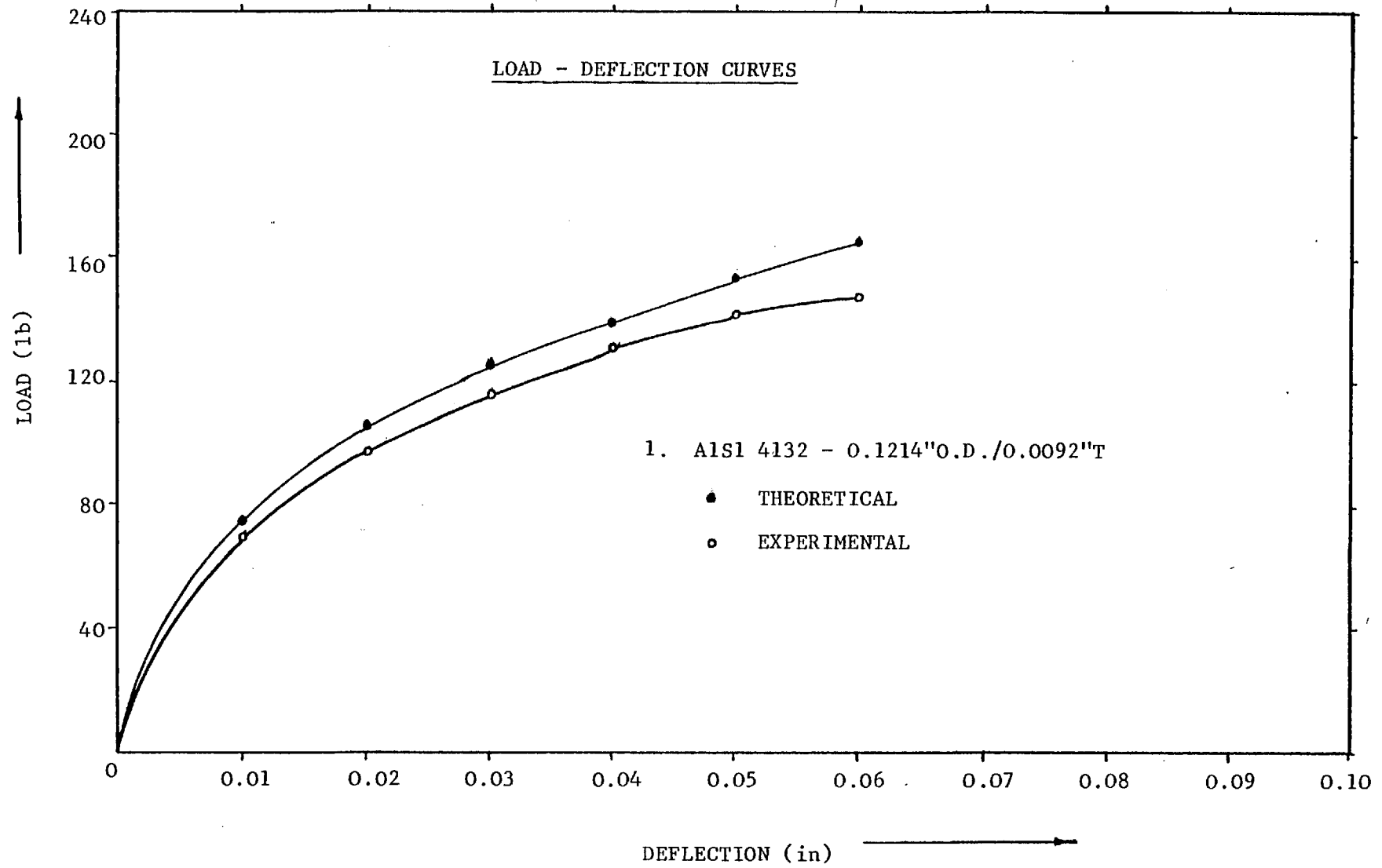


FIG. 5.21

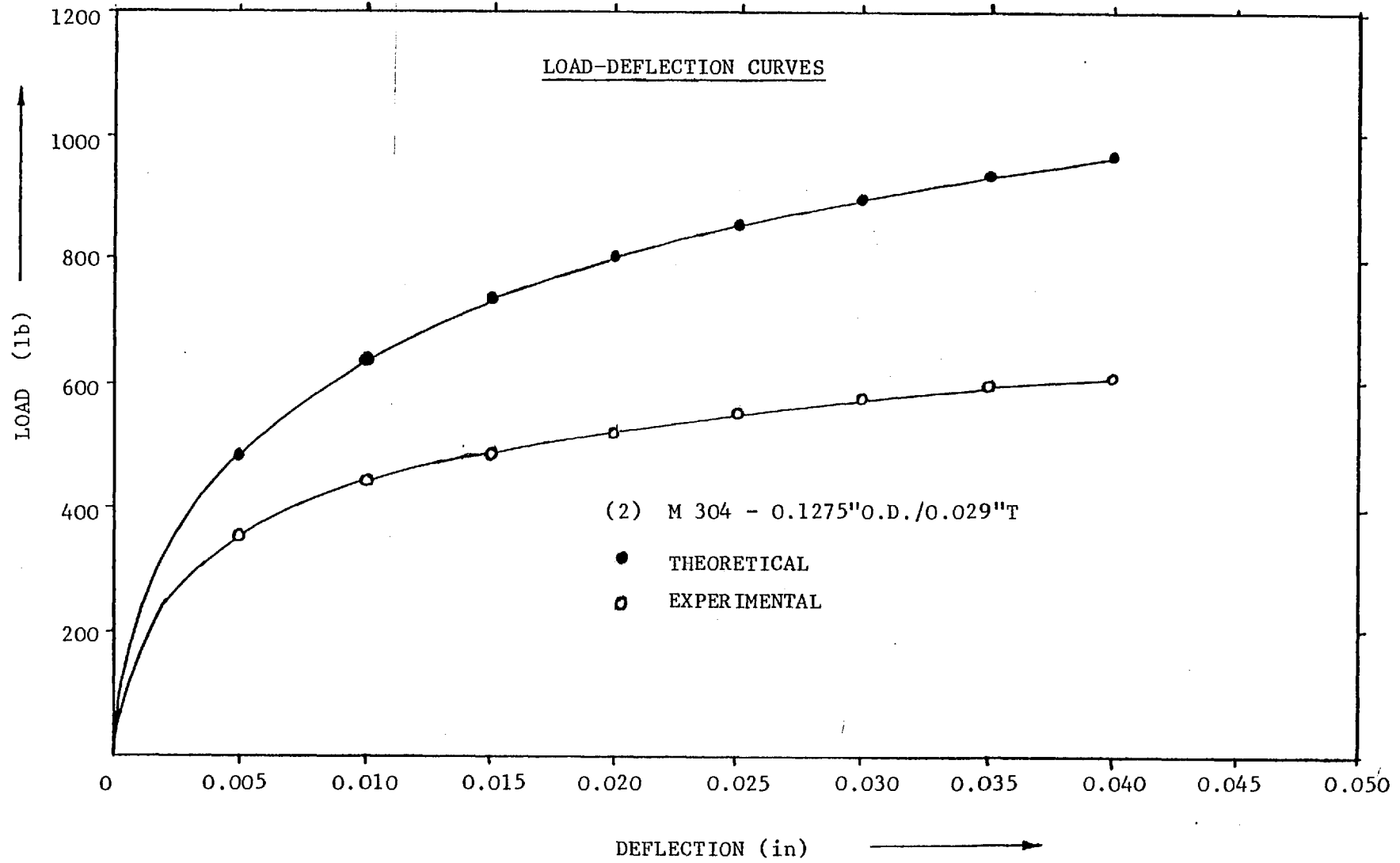


FIG. 5.22

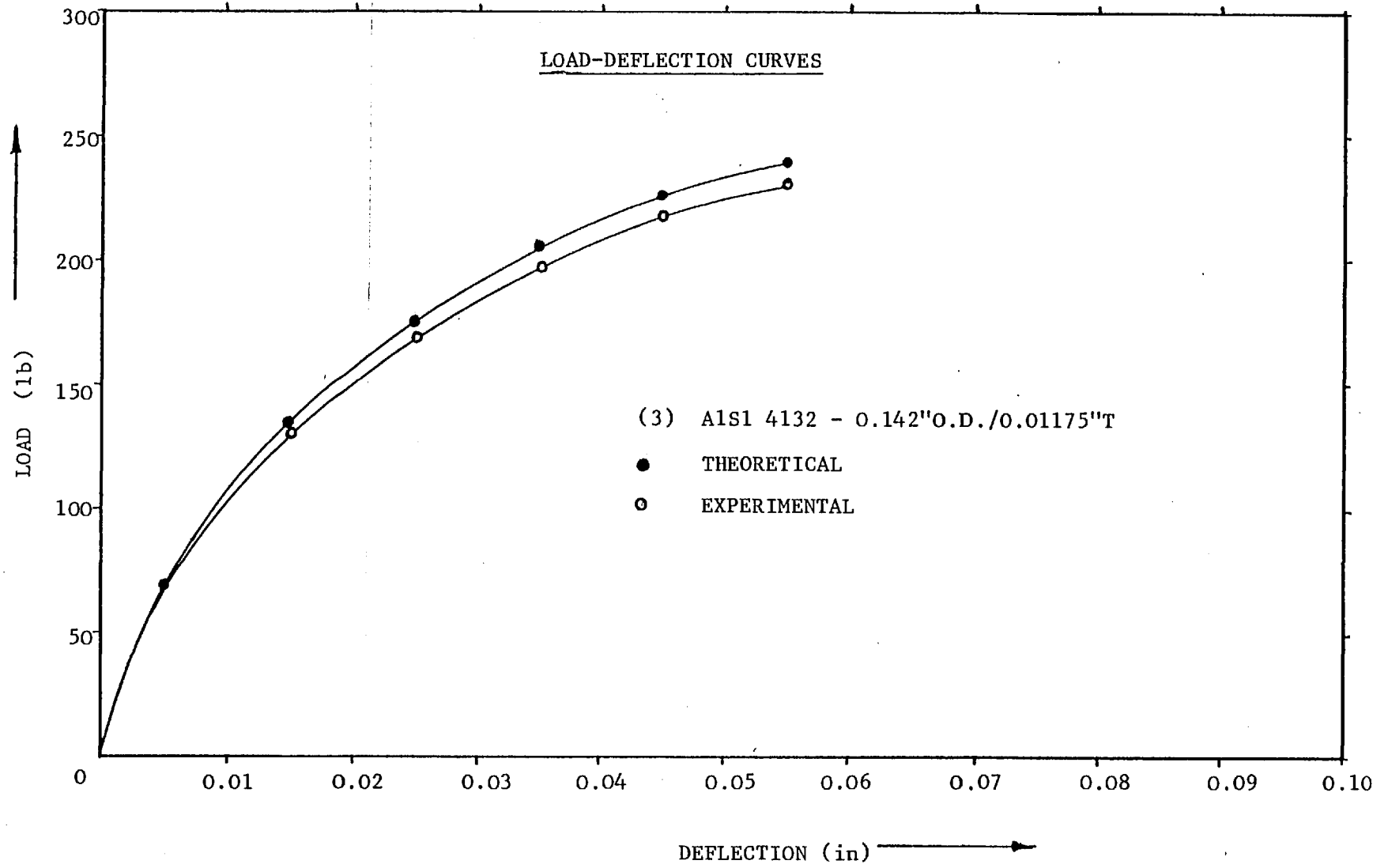


FIG. 5.23

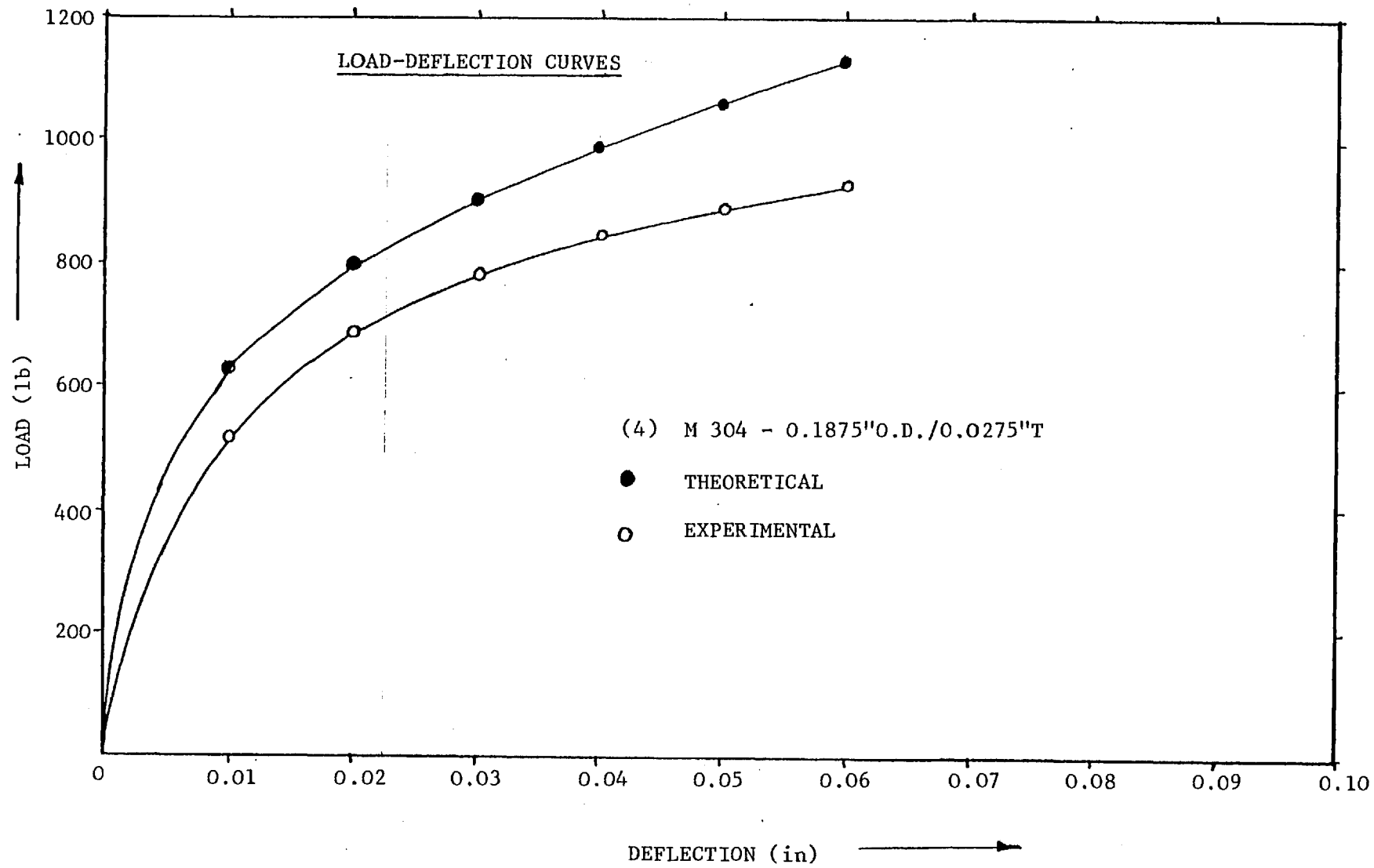


FIG. 5.24

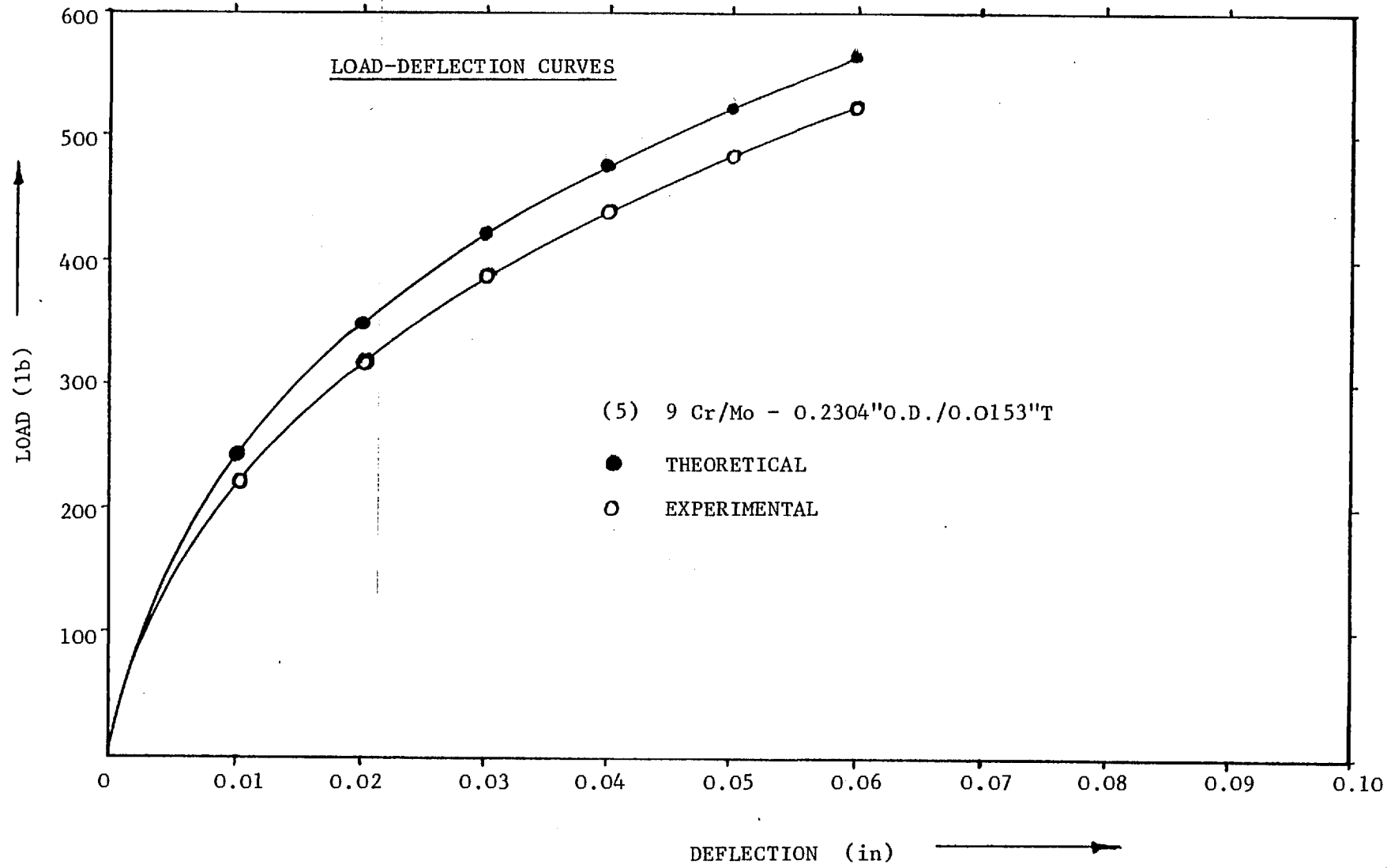


FIG. 5.25

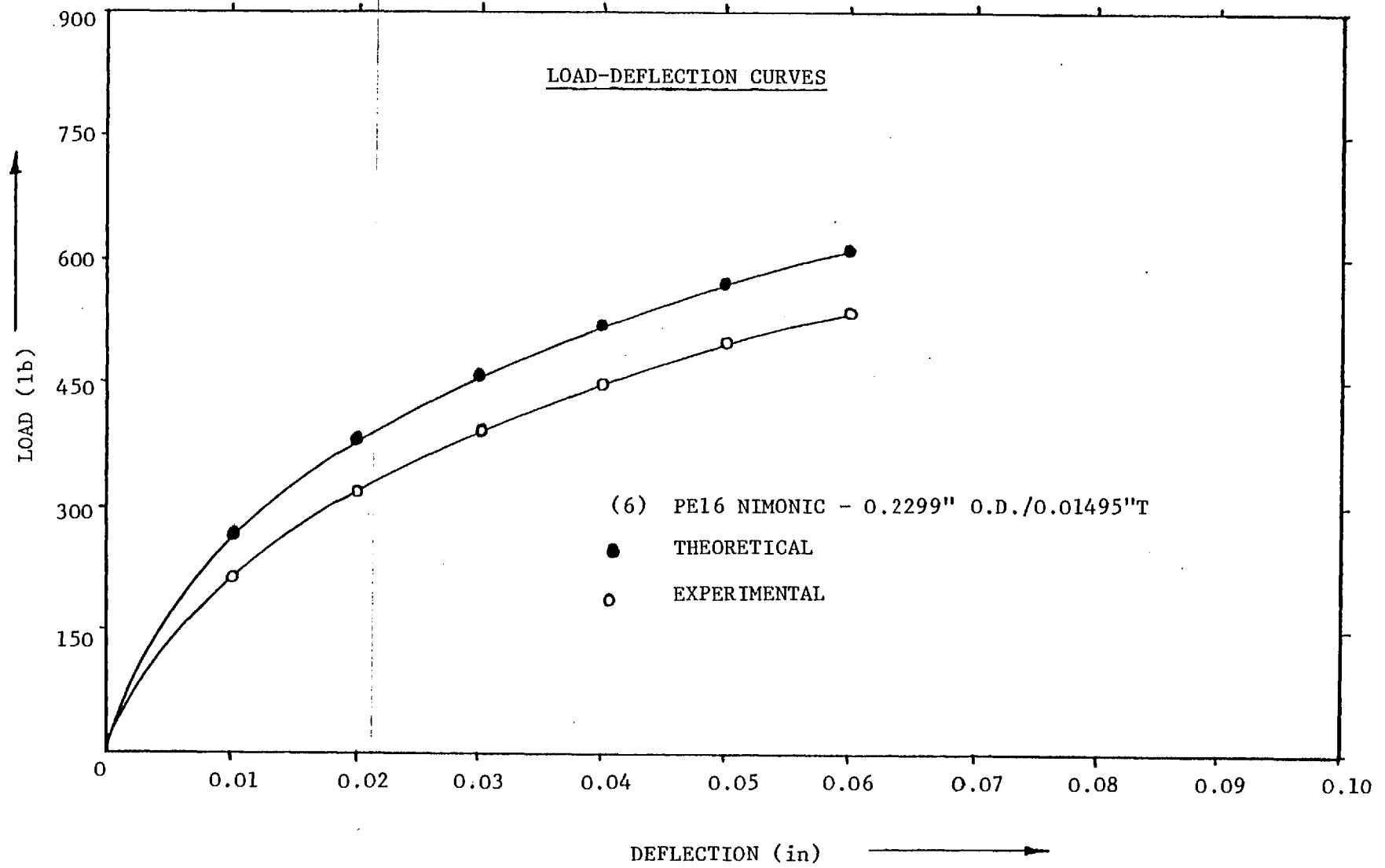


FIG. 5.26

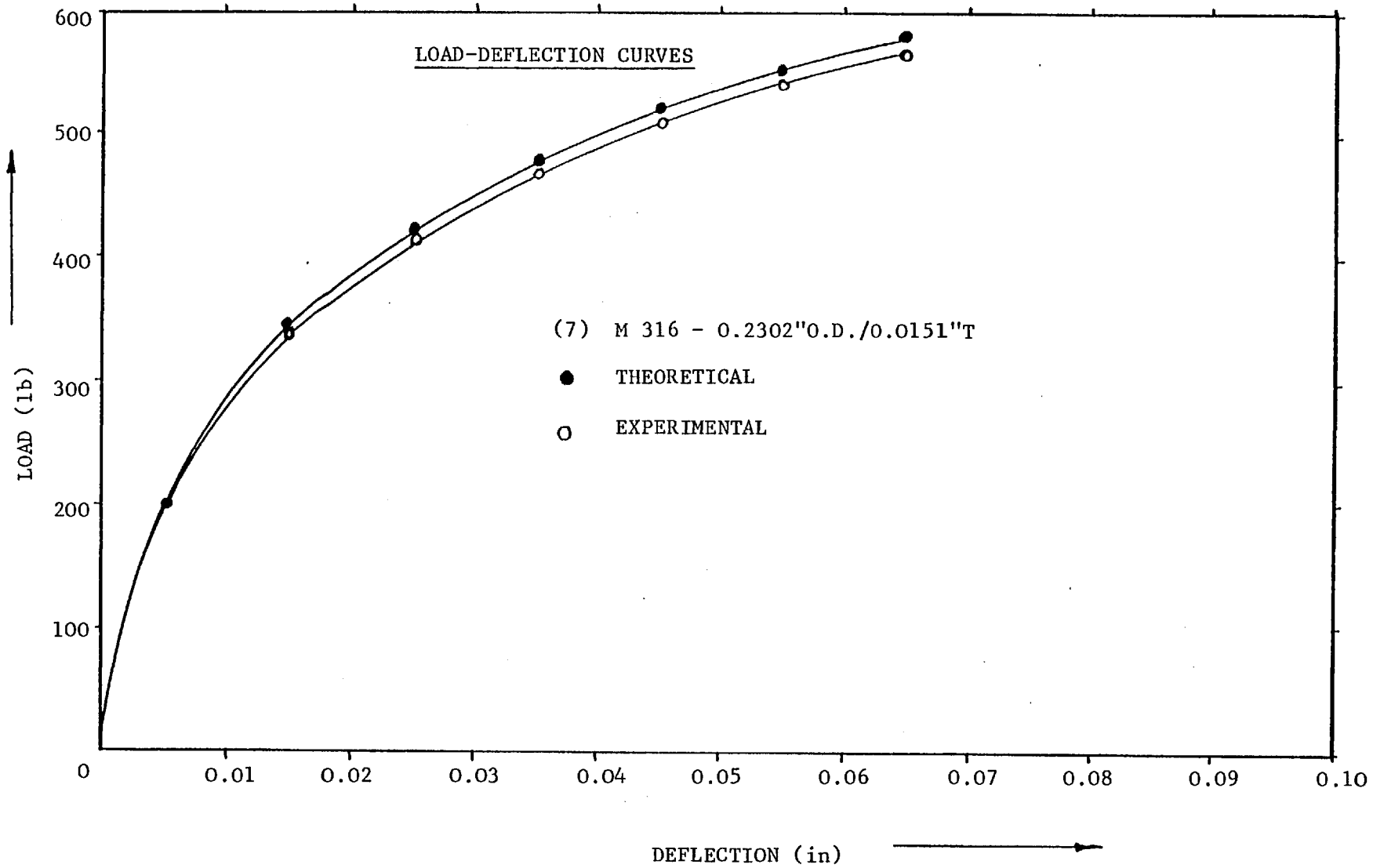


FIG. 5.27

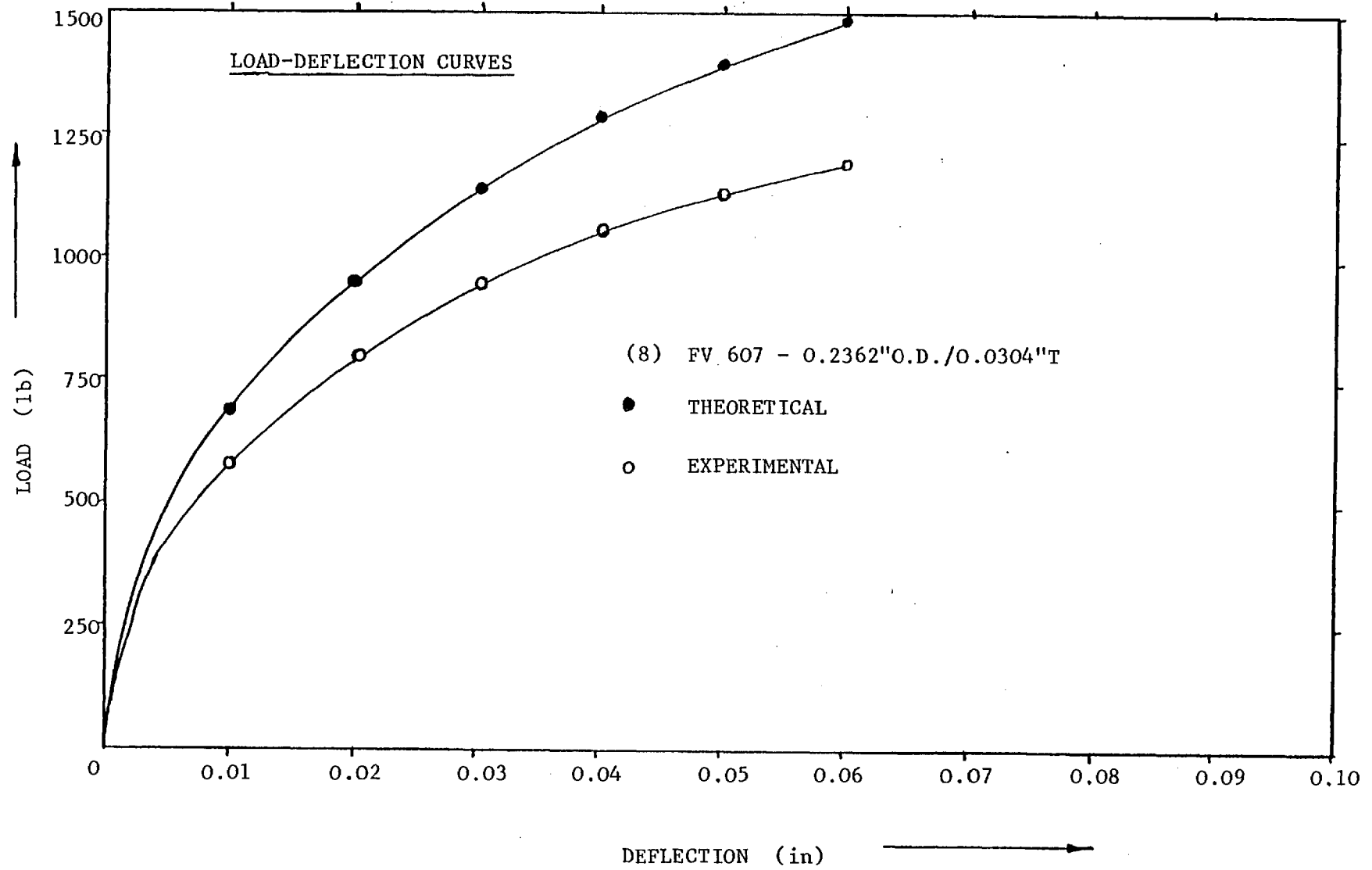


FIG. 5.28

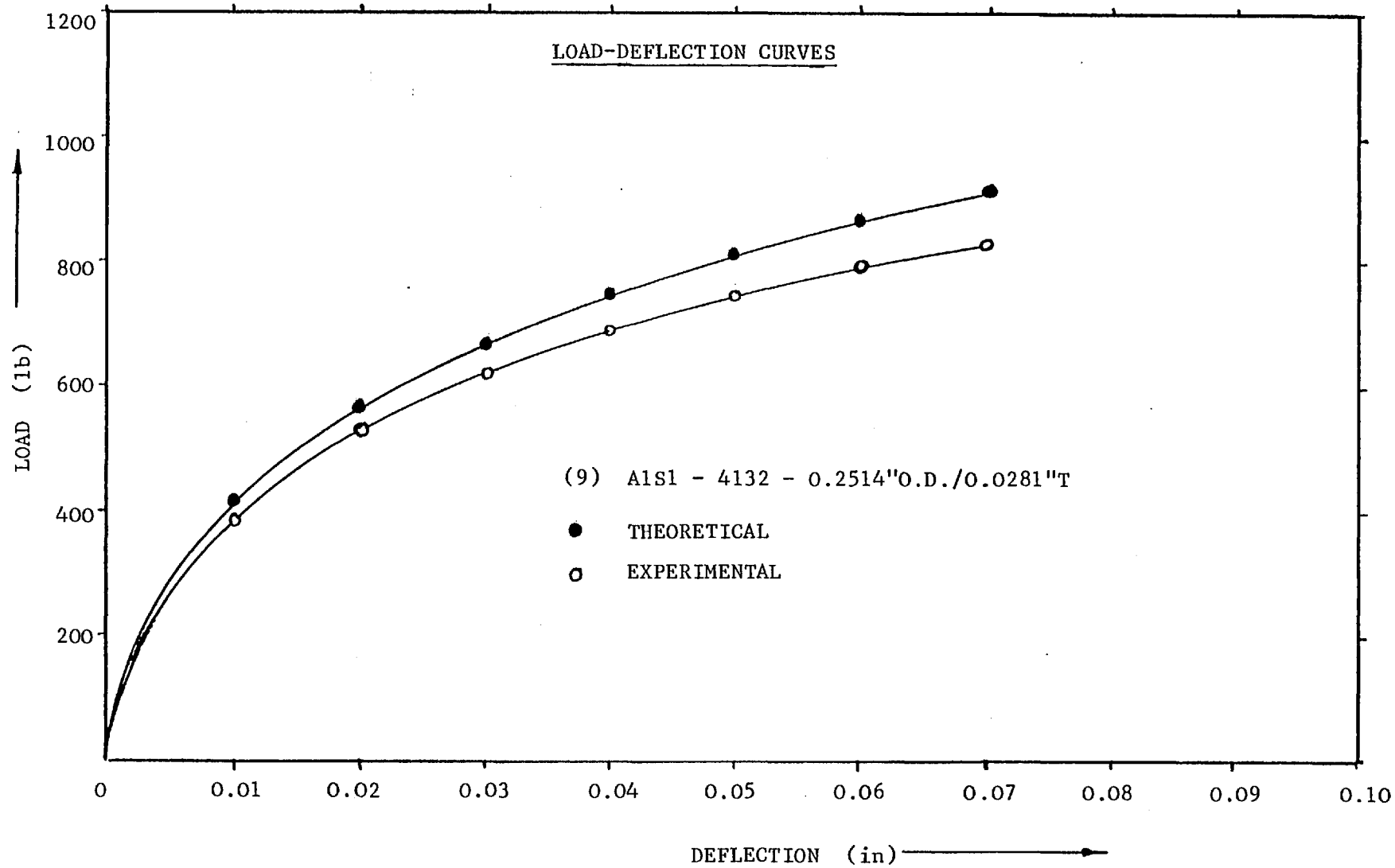


FIG. 5.29

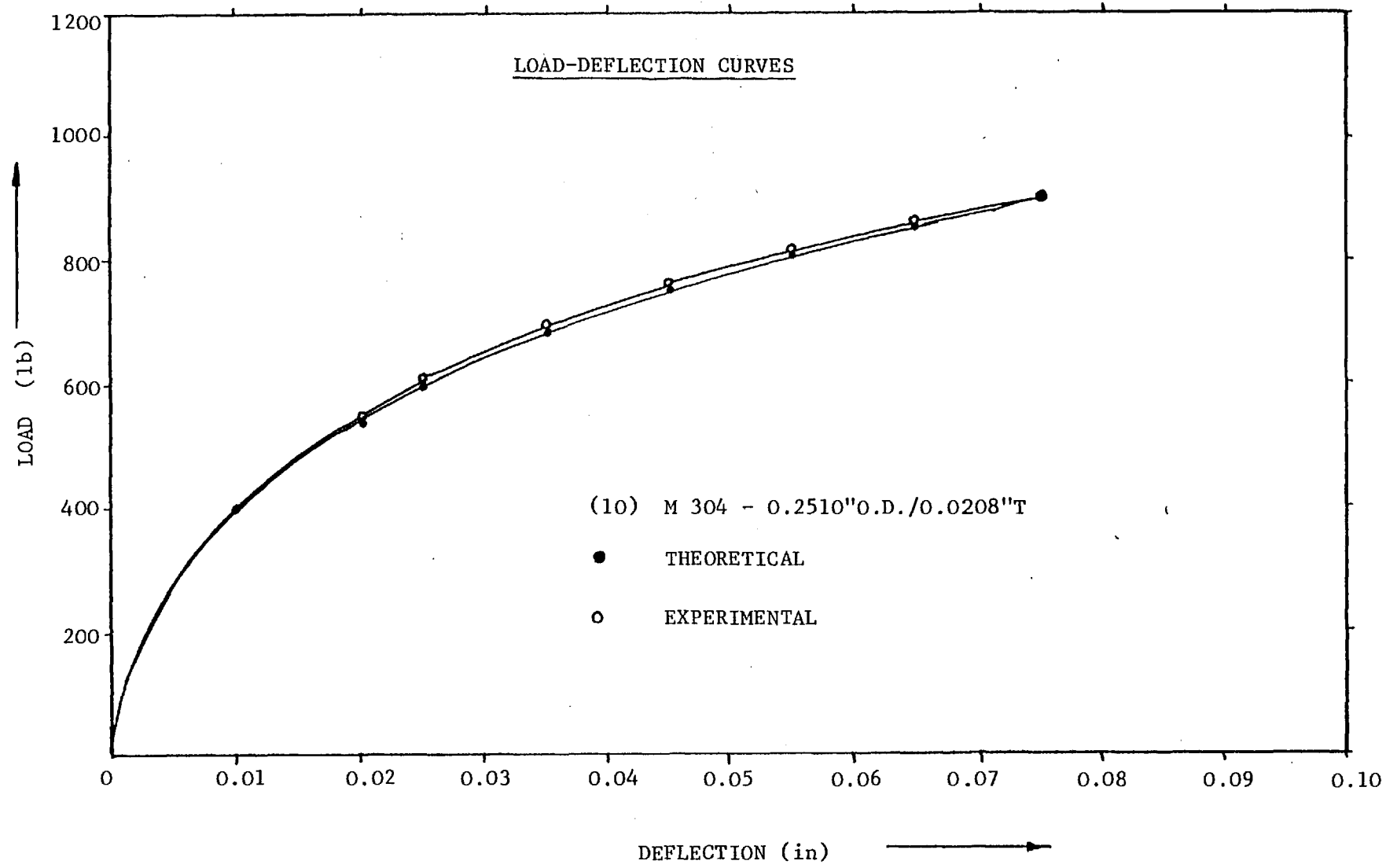


FIG. 5.30

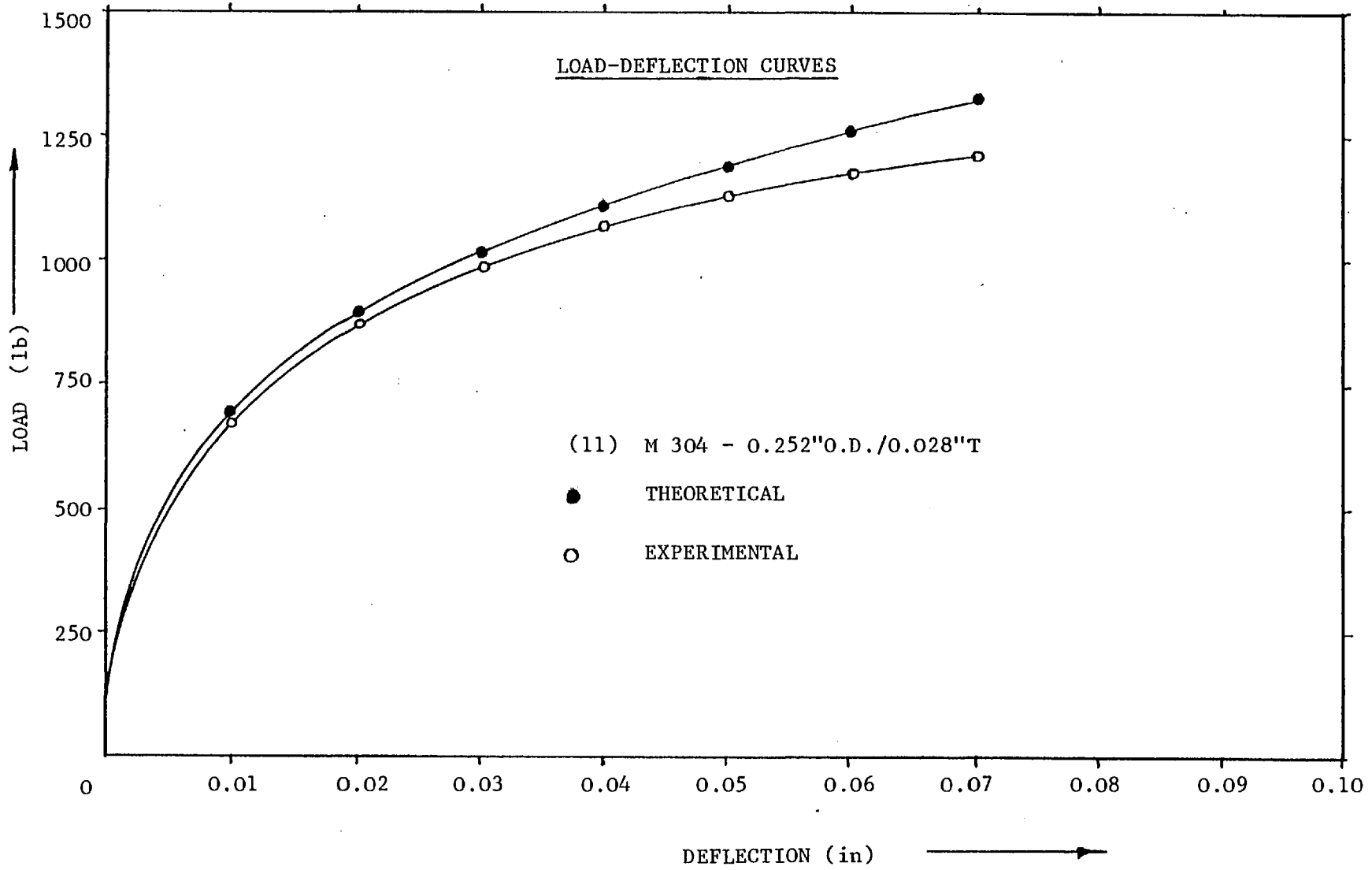


FIG. 5.31

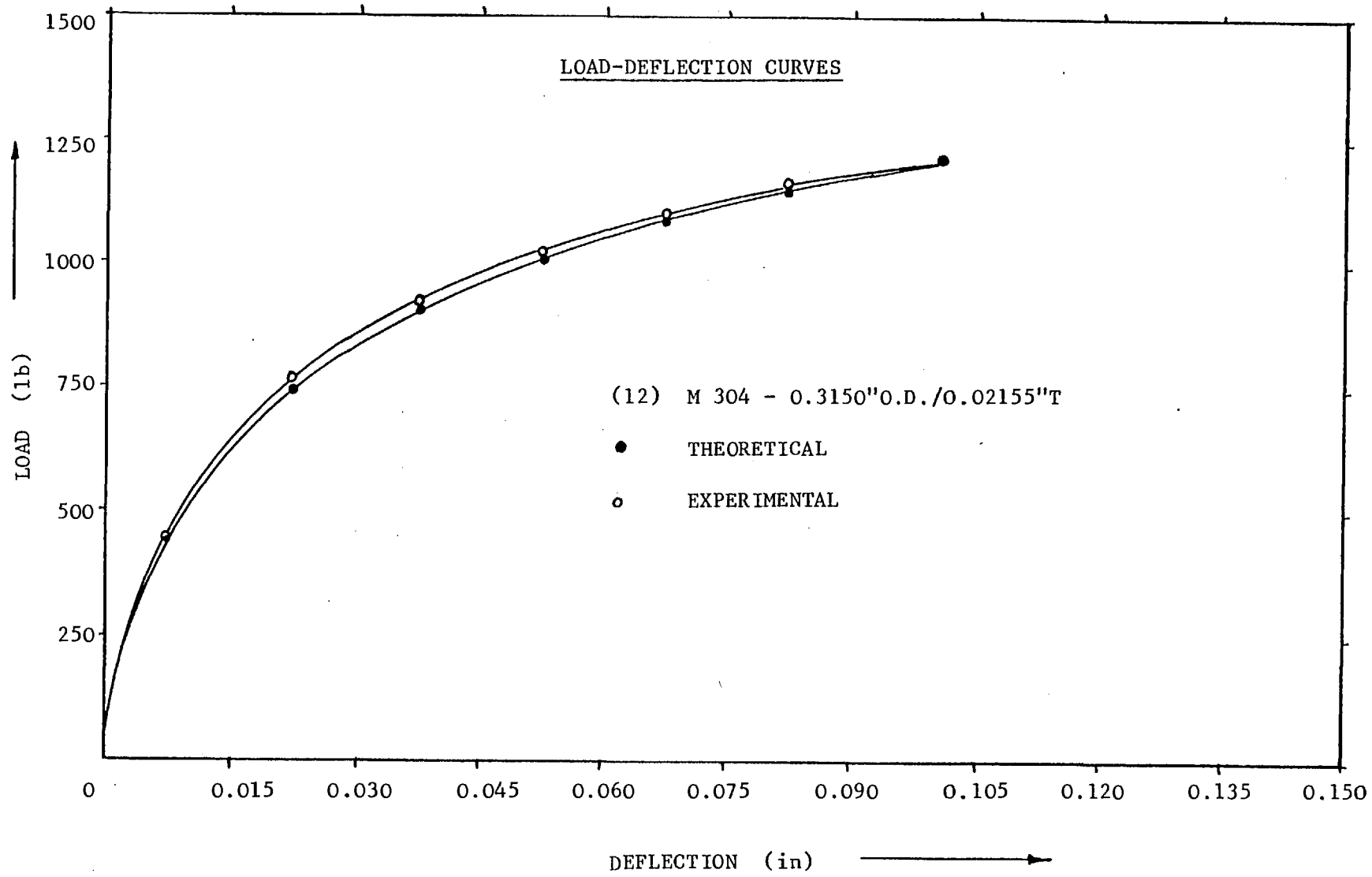


FIG. 5.32

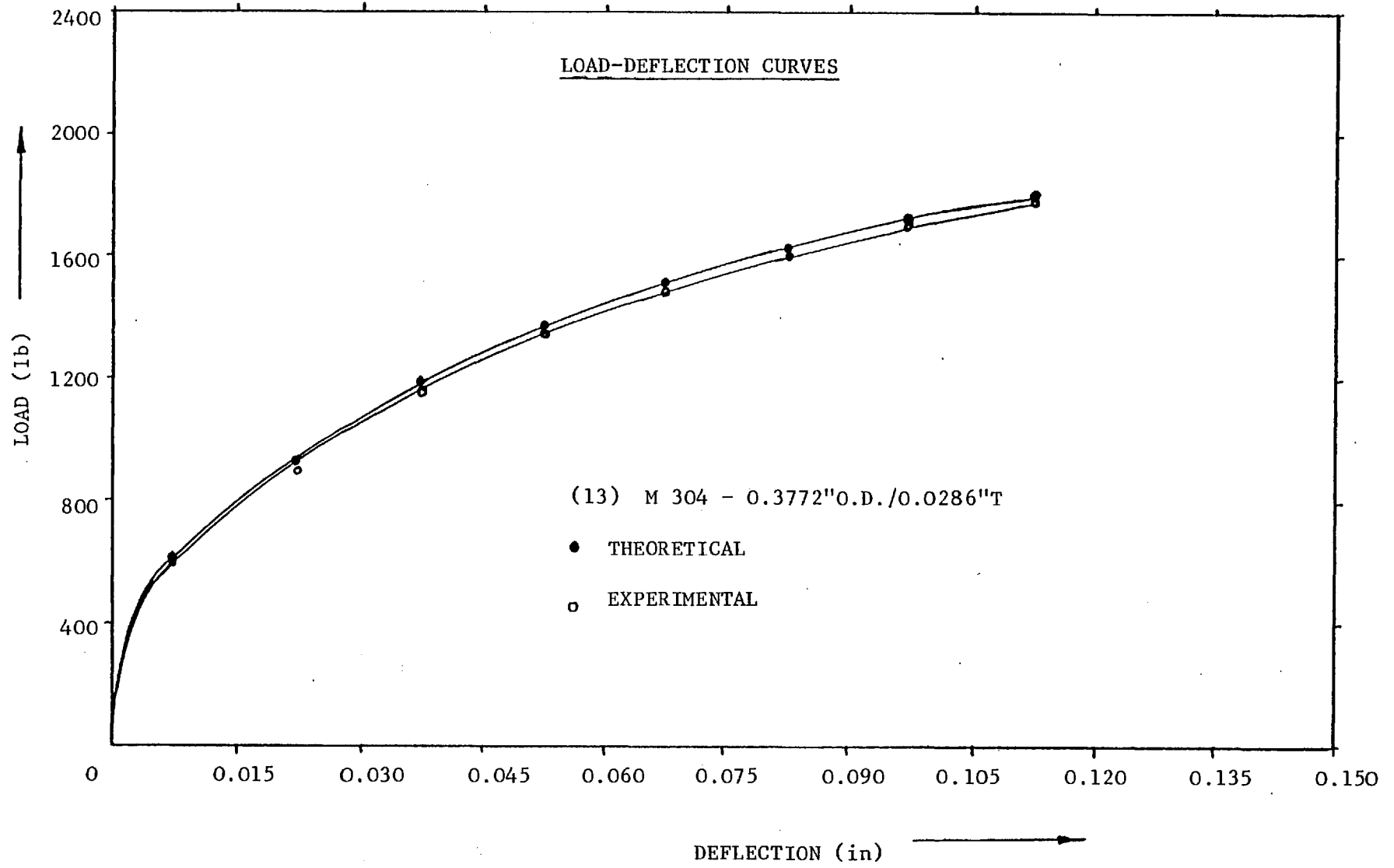


FIG. 5.33

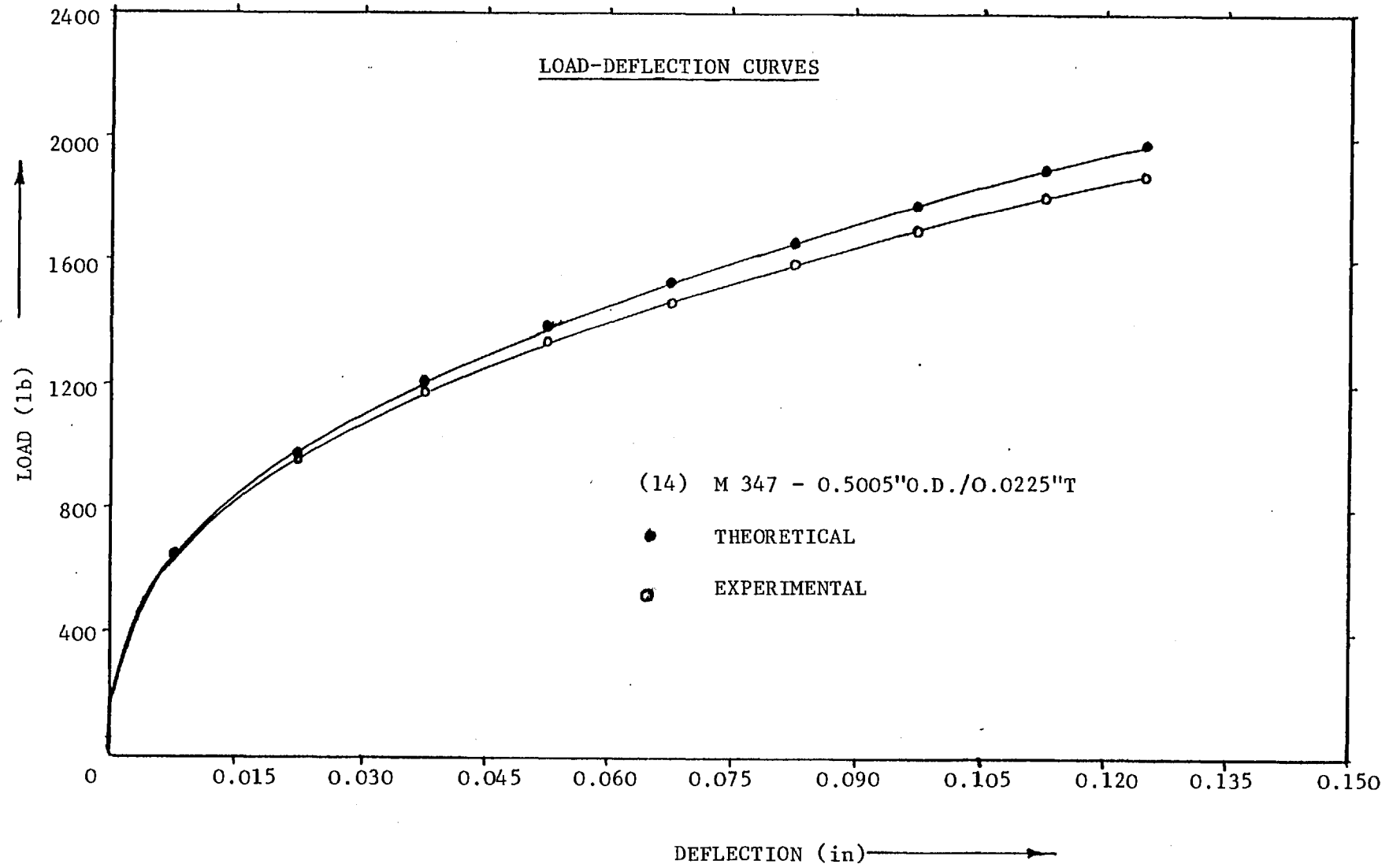


FIG. 5.34

TABLE 5.1

Sl. No.	Original cross-sectional areas in ²	Yield strength lb/in ²			Exp. P _{max} lb.	Theory P _{max} = Y/√3 .A			% Difference = $\frac{\text{Exp}-\text{Theory}}{\text{Exp}} \times 100$		
		0.5% Y (1)	Y _{approx} (2)	Y _{empirical} = σ _F /√3 (3)		(1)	(2)	(3)	(1)	(2)	(3)
1	0.00324288	75,500	86,500	82,720	148	140	162	155	5.4	-9.5	-4.7
2	0.0089740	104,000	117,500	123,403	610	539	609	639	11.6	1.6	-4.7
3	0.004808	76,000	86,000	85,508	230	211	239	237	8.2	-3.9	-3.0
4	0.013995	110,500	117,500	119,539	930	893	949	966	3.9	-2.0	-3.8
5	0.010339	93,000	104,000	90,189	522	555	620	538	-6.3	-18.7	-3.0
6	0.010095	102,500	116,000	101,348	535	597	676	590	-11.6	-26.3	-10.2
7	0.010204	98,000	108,500	102,524	567	577	639	604	-1.7	-12.6	-6.5
8	0.019655	108,000	119,500	106,401	1196	1225	1356	1207	-2.4	-13.3	-0.01
9	0.0197126	70,500	76,000	77,666	825	802	865	884	2.7	-4.8	-7.1
10	0.015042	97,500	106,000	110,117	907	847	921	956	6.6	-1.5	-5.4
11	0.019704	102,000	111,000	116,310	1208	1160	1263	1323	3.9	-4.5	-9.5
12	0.019866	101,000	112,500	108,538	1216	1158	1290	1245	4.7	-6.0	-2.3
13	0.031321	98,000	105,000	109,564	1780	1772	1898	1981	0.0	-6.6	-11.3
14	0.033788	100,000	120,000	109,671	1874	1950	2340	2139	-4.0	-24.8	-14.1

TABLE 5.2

Sl. No.	Material of size (in)	$\bar{\epsilon} = \bar{\epsilon}_c$ ($= \bar{\epsilon}_{UTS}$)	δ Exp. in	δ Theory in	$\frac{\text{Exp}-\text{Theory}}{\text{Exp}} \times 100\%$
1	0.1214/0.0092 A151-4132	0.210	0.060	0.038	36
2	0.1275/0.029 M304-MILT	0.320	0.040	0.046	-15
3	0.142/0.01175 A151-4132	0.166	0.055	0.041	25
4	0.1875/0.0275 M304-MILT	0.270	0.060	0.067	-11
5	0.2304/0.0153 9Cr/Mo-COMM	0.092	0.060	0.044	26
6	0.2299/0.01495 PE16-NIMONIC	0.090	0.055	0.041	25
7	0.2302/0.0151 M316-SS	0.203	0.065	0.065	-
8	0.2362/0.0304 FV607-COMM	0.120	0.060	0.051	15
9	0.2514/0.0281 A151-4132	0.234	0.070	0.082	-17
10	0.2510/0.0208 M304-MILT	0.312	0.075	0.066	12
11	0.3150/0.02155 M304-MILT	0.283	0.070	0.086	-23
12	0.3150/0.02155 M304-MILT	0.293	0.100	0.080	20
13	0.3772/0.0286 M304-MILT	0.331	0.1125	0.095	15
14	0.5005/0.0225 M347-T-58	0.216	0.125	0.110	12

TABLE 5.3

Sl. No.	Material of size (in)	T/D _m	Exp. deflection at max. load (in.)	Exp. Max. load lb.	Theory Max. load lb.			% diff. = $\frac{\text{Exp}-\text{Theory}}{\text{Exp}} \times 100$		
					Based on 0.2% Y (1)	Based on Y _{app} (2)	Based on Y _{emp} (3)	(1)	(2)	(3)
1	0.1214/0.0092 A151-4132	0.082	0.06	148	146	165	157	1	-11	-6
2	0.1275/0.029 304-MILT	0.294	0.04	610	859	970	998	-40	-59	-63
3	0.142/0.01175 A151-4132	0.090	0.055	230	212	240	238	8	-4	-3
4	0.1875/0.0275 304-MILT	0.172	0.06	930	1060	1130	1150	-14	-21	-24
5	0.2304/0.0153 9 Cr/Mo-COMM	0.071	0.06	522	505	565	490	3	-8	6
6	0.2299/0.01495 PE16/NIMONIC	0.069	0.06	535	541	612	535	-1	-14	0
7	0.2302/0.0151 M316	0.069	0.065	567	527	583	551	7	-3	3
8	0.2362/0.0304 FV607-COMM	0.148	0.06	1196	1350	1490	1330	-13	-24	-11
9	0.2514/0.0281 A151-4132	0.126	0.07	825	847	913	934	-3	-10	-13
10	0.2510/0.0208 304-MILT	0.090	0.075	907	822	894	929	9	0	-2
11	0.252/0.028 304-MILT	0.125	0.07	1208	1220	1330	1390	-1	-10	-15
12	0.3150/0.02155 304-MILT	0.073	0.100	1216	1080	1210	1160	11	0	4
13	0.3772/0.0286 304-MILT	0.082	0.1125	1780	1680	1800	1880	6	-1	-6
14	0.5005/0.0225 M347-T-58	0.047	0.125	1874	1660	1990	1820	11	-6	3

TABLE 5.4

Sl. No.	Area of c/s (in ²)		Max. cropping load separately (lb)		Max. cropping load together (lb)		% Error $\frac{\text{Exp}-\text{Emp}}{\text{Exp}} \times 100$
	Tube (i)	Glass rod (inside tube) (ii)	Tube $P_1=(KA)_i$	Glass rod $P_2=(KA)_{ii}$	Empirical ($P_{\max} = P_1+P_2$)	Experim- mental (P_{\max})	
1	0.003243	0.00833	155	57	212	350	39
2	0.008974	0.00352	639	24	663	820	19
3	0.004808	0.01093	237	75	312	414	24
4	0.013995	0.01327	966	91	1057	1160	9
5	0.010339	0.03080	538	211	749	828	9
6	0.010010	0.03080	590	211	801	860	7
7	0.010204	0.03080	604	211	815	890	8
8	0.019655	0.02296	1207	157	1364	1592	14
9	0.019713	0.02835	884	194	1078	1095	2
10	0.015042	0.03398	956	233	1189	1208	2
11	0.019704	0.02895	1323	198	1521	1510	-1
12	0.019866	0.05599	1245	384	1629	1570	-3
13	0.031321	0.07892	1981	541	2522	2278	-10
14	0.033788	0.16188	2139	1110	3249	2590	-25

In considering the mechanical properties of metals at different temperatures, the yield and ultimate strengths increase with decreasing temperature. It was observed from the experiments that the cropping load increased at low temperature (-196°C) for stainless steels. However, there is neither change in the shape of the load-deflection graph nor improvement in the quality of billets. The M300 series stainless steels are, of course, one of the most interesting classes of ferrous steels because of their unique combination of great ductility with immunity from atmospheric corrosion.

Reasonable agreement was established between tension and cropping results. Assuming the flow stress to be equal to the 0.5% proof stress predicted lower cropping loads. However, the yield strength derived from the fracture stress predicted more realistic values in the sense that the theoretical and experimental results agreed to within 10%. The approximate yield strength estimated cropping loads within 10% for majority of the tubes. There is a higher percentage of error (up to 26%) for the relatively brittle material nimonic-PE16. Deflection at maximum load based on simple strain theory was calculated for all the tubes as shown in Table 5.2. The error is as high as 36% which is a very crude estimate. Considering the simplicity and nature of the analysis, the results may be considered to be reasonable and they give a rough idea of the magnitude of the deflection at maximum cropping load.

The degree of correlation between any theory and the physical situation it attempts to describe depends on how closely the theoretical model can be made to fit the real situation. In the present analysis, the model proposed by Thomas et al. [43] has been adopted and the load-deflection graph predicted up to maximum load. Results are compared as shown in Table 5.3.

It may be observed from the theoretical estimates that the cropping loads are higher for higher T/D_m ratios (see Table 5.3). The solution was obtained for thin-walled tubes subjected to shearing loads under the assumption of the tubes being made of rigid, perfectly plastic material. The yield condition for combined bending and shear is well known, of the form

$$\left(\frac{M}{M_0}\right)^2 + \left(\frac{Q}{Q_0}\right)^2 = 1 \quad (5.78)$$

where $|M| \leq M_0$ (M_0 is the limiting moment without shear) and $|Q| \leq Q_0$ (Q_0 is the limiting shear without moment).

For thin tubes, the shear effect can be neglected

$$\left(\frac{M}{M_0}\right)^2 + \left(\frac{Q}{Q_0}\right)^2 = 1$$

$$M = M_0 \quad (5.79)$$

Thus the present theory is concerned only with bending moments, shear deformations and the influence of shear on the yield stress are neglected. Therefore, the theory becomes increasingly inaccurate as the mean diameter becomes smaller relative to a fixed wall thickness. The error is about 60% for the thickest of these fourteen tubes. Agreement between theory and experiment is within 10% for tubes having T/D_m ratio less than 0.1.

De Runtz and P.G. Hodge [44] suggested that the effect of shear must be considered for tubes having T/D_m ratios higher than 0.1. About 5 tubes fall outside this range in the present work. Hence the upper bound theory predicts a more conservative value for the limit load, particularly for tubes having T/D_m ratios higher than 0.1. Hence it would appear reasonable to use simple beam theory for $T/D_m \leq 0.1$ and

combined shear and bending theory for $T/D_m > 0.1$.

In view of the approximate nature of the analysis, it is ~~surprising~~ that there is some agreement with experiment and the numerical magnitude is of the right order for most of the tubes. According to the present theory, the load-deflection curve continuously increases unless the deflection at maximum load or the maximum load itself is known. For this purpose, the above two approaches discussed separately to predict the maximum cropping load and the deflection at maximum load can be used to estimate the point of termination of the load-deflection graph.

The maximum cropping load for filled tube may be estimated by calculating cropping loads separately on the basis of shear yield strengths of tube and filling as shown in Table 5.4.

CHAPTER 6

GENERAL DISCUSSION

6.1 INTRODUCTION

The experimental work, the correlation of cropping results with material property data, fractography, and theoretical work described in earlier chapters gave an account of the behaviour of thin-walled steel tubes, subjected to shearing load. A standard tensile test was used to correlate the results obtained from the cropping tests. An upper bound solution was developed for thin-walled tube cropping to predict the maximum cropping load. Where there is a disagreement between theory and experiment, fractography can help to explain the reasons for the disagreement. The central idea of the present discussion is mainly to bring the different approaches together to draw some important conclusions. In this chapter some fundamental facts about the billet materials used and the tube cropping process itself, as observed and analysed during the course of research work, are discussed.

6.2 THE BEHAVIOUR OF MATERIALS WHEN SUBJECTED TO SHEARING LOAD

The materials used for these cropping tests were cold-worked stainless steels of different compositions and a nimonic alloy. As explained elsewhere in the thesis, these complex materials are of increasing interest to designers of nuclear reactors, particularly in the case of the Advanced Gas-Cooled Reactor and Sodium-Cooled Reactor systems. Based on research and development, chiefly by the UKAEA, these alloys have been found to be important as fuel sub-assembly and core structural materials for the sodium-cooled Fast Breeder Reactor [45]. The main reasons for the success of these alloys, particularly M316

and PE16, are their resistance to corrosion by liquid sodium and their outstanding resistance to swelling by void formation in the fast neutron environment.

It is well known that if a piece of metal is bent back and forth several times, the yield stress is increased after each bending and unbending. Though at the end the piece may be brought back to its original shape, yet it would have undergone considerable strain hardening at the location of former bends and such a metal is said to be 'cold-worked'. Cold-working can be defined as plastic deformation of a metal at a temperature and rate of straining such that the rate of work-hardening exceeds rate of annealing due to recrystallization. Normally, it is used to increase the strength and hardness of metals and alloys. The austenitic stainless steels strain-harden rapidly when worked at ambient temperatures, so that cold-working is used to increase their hardness and strength where high structural strength is needed. In fact, cold-working is the only practical method for strengthening the M300 series of austenitic stainless steels, as they cannot be strengthened by heat treatment.

It has been proposed that if distortions are stopped from being propagated either because of their movement being impeded by other dislocations, grain boundaries or impurities, then regions of high strain will be created within the crystals. Obviously, increased stress will be required in order to facilitate further progress of the dislocations. This leads to the phenomenon of strain-hardening. It is evident from the present tensile tests that there was marked strain-hardening for all the cold-worked stainless steels. However, the degree of strain-hardening depends on the composition of the stainless steel, impurities, size, the amount of cold-work received and other features. For example, strain hardening was observed to be higher for nimonic-PE16 than for the stainless steels.

As shown by the true stress-strain diagrams, each additional increase of plastic deformation requires an additional increment of stress. Although 0.5% proof stress is taken as a material property to correlate the results obtained from cropping, it is difficult to establish a standard yield strength that can be applied to all these materials. As explained in Chapter 5, alternative methods have also been proposed to establish a mean yield strength from the true stress-strain curves. With these methods, a reasonable correlation between the tension and cropping tests was obtained. However, the tension and cropping tests did not seem to agree very well for the high tensile strength material, nimonic-PE16. The reasons for this disagreement may be explained by interpretation of the fractographic studies.

Nimonic-PE16 is a wrought nickel-chromium-iron-base alloy strengthened by additions of molybdenum, titanium and aluminium. It has been developed for service mainly in the temperature range 500-750 °C, and combines the high strength of the age hardening nickel-base alloy with excellent fabrication characteristics. Quasi-cleavage *fracture* has been identified in nimonic-PE16 tube when it is subjected to shearing load. Cold-working must have seriously impaired its ductility and this could be the reason for its billets having less cross-sectional distortion. The material may well be crack-sensitive in the transverse direction and this may explain the disagreement between tension and cropping results.

Microscopic examination of fracture in stainless steels has shown that the mechanism of fracture in cropping possesses mainly ductile features. However, materials like M347, FV607 show a few cleavage steps. It is well known that the cold-working type M347 stainless steel converts some of the austenite to ferrite [46]. Perhaps this could be the reason for traces of cleavage steps and for the better quality of billets as

compared with austenitic steels. As far as the cropping loads are concerned there is good correlation between tension and cropping tests for stainless steels.

The high chromium type M446 stainless steel had been purposely embrittled to observe its behaviour under shearing load. It is observed that the cropping load is higher than the tensile load for M446 embrittled steel which is exactly opposite to the trend reported for cold-worked steels. For brittle materials, it is known that a much larger compressive stress is required to produce the same deformation behaviour as that which would be produced by an applied tensile stress [47]. In shearing, the billet is compressed by the shearing blade before it actually shears through the metal. As a result of that the fracture occurs at and spreads from defects like mechanically produced cracks, pores, and inclusions. The fracture mechanism in embrittled M446 steel has been identified as a mixed version of intergranular and transgranular cleavage. In tension tests, the pores in embrittled steel specimens seem to act as stress raisers and they promote crack initiation and propagation at lower loads. That is why these brittle materials have no real strength in tension. Hence it cannot be included in the materials list as its behaviour is entirely different from cold-worked steels and should be treated separately for theoretical analysis.

Clad swelling or void swelling is a phenomenon important only in materials irradiated in a fast reactor [48]. It is the formation of voids which causes swelling. One of the main reasons for using a cold-worked material as a cladding is to reduce the swelling rate [49]. Fuel swelling is caused by bubbles of fission gas trapped in the fuel. Fuel swelling or clad swelling is outside the limits of the present work in which the tubes were only filled with alumina or glass to simulate Commercial Fast Reactor fuel. From the fractographic analysis, it is

clear that the initiation and propagation of fracture in alumina starts from pores, since they act as stress raisers. As it is not possible to study the behaviour of irradiated cladding material under shearing load in normal environmental conditions, cropping tests were carried out on embrittled stainless steel to simulate irradiated material. Therefore, experimental investigation of embrittled stainless steel and ceramic filling material was considered to be quite useful in simulating the clad swelling of irradiated cladding material and fuel swelling in fast reactor fuel in real situations.

From the experiments, it was found that the quality of the billet depends mainly on the material. It has been explained that preparation of a good billet by cropping involves the initiation of a crack at the earliest possible opportunity during indentation by the cropping tool. In this way distortion is kept to a minimum. The theoretical ideal would be suitable cracking with no indentation at all. In practice, the brittleness which gives the early initiation of crack in metals also leads to uncontrolled cracking, and in an extreme case such as that of embrittled M446 stainless steel the material shatters in a random manner. There is thus an optimum ductility in materials for cropping, and deviations either side of this value result in deterioration of quality due either to increased plastic flow such as found with M316 stainless steel, and hence greater distortion, or to uncontrolled cracking in materials such as embrittled M446 steel. In cropping stainless steel tube materials, the process has been found to be ineffective. This is primarily due to insufficient propagation of fracture around the circumference of the tube.

In general, all metals exhibit sensitivity to speed of working [50]. It is known that the tensile strength as well as the yield strength increases with increasing strain-rate. This means that certain metals

which suffer considerable distortion as a result of their ductility at low speeds tend to exhibit less distortion, particularly Nimonic-PE16, when cropped at high speeds. However, the velocity of blade has very little influence on stainless steels. It was evident from the present cropping experiments that materials like embrittled M446 steel exhibit uncontrolled cracking when cropped at low speeds and this unfavourable behaviour exists to an even greater extent at high speeds. The quality of the billets was improved for filled tubes at higher velocities of the cropping blade.

6.3 THE TUBE CROPPING PROCESS

The mechanism of 'pure shear', independent of the tool, does not occur in metal processing. However, the final effect of shearing on the material is the same in all cases, namely, the separating of two adjacent sections of the material by means of a reciprocal translation. In tension, compression, bending, and torsion tests the stress-strain diagram is an accepted means of understanding the elastic and plastic deformation encountered. For shearing, no standard mechanical test is found in the literature and the reason for this might be the unknown effect of the various tools used in such tests.

In the simple shearing process, the force can be divided into two, namely 1) that forcing the tool into the material, and 2) that which presses against and deforms the material. In the uppermost layers the fibres remain straight and parallel to the axis of the tube, particularly up to the cut itself. If the cutting edge (the lowest point of the shearing tool) could actually separate the material, the fibres of the tube would be severed straight and no bending would occur.

The material which is pushed downwards, however, is still connected with the material of the tube and thus pulls it downwards as far as the plastic deformation is propagated to the billet side - thus producing bent fibres. As the specific pressure in the vertical direction reaches its maximum value, overcoming the transverse stress in this direction, the whole billet is pushed down as a separate entity and the process of 'pure shear' begins along the theoretical shear plane, in which the stretched grains are torn in the vertical direction. Therefore, what is commonly called 'shearing' is not an action in a single plane, but as has been explained, is in fact a bending and stretching of the grains and fibres for a certain depth on both sides of the final separating plane. It is the summation of different processes, one following the other and resulting in a rupture of grains in tension. In fact, the mechanism of shearing has been explained earlier through the interpretation of fractographs and the different processes - stretching, tearing, and shearing have all been identified in cropped billets. Hence it is not easy to correlate results obtained from a complex mechanism such as cropping with a stress-strain curve obtained from a standard tensile test unless the 'passive' forces such as those due to bending and friction are known.

Recently, some work has been done in this area by W. Johnson et al [51] under the heading "Large deformations of thin-walled circular tubes under transverse loading". These workers were, apparently, interested in the behaviour of simply supported circular tubes under the action of the transverse loading of a large wedge-shaped indenter up to the point of maximum load and the aspects of the load carrying capacity of thin-walled tubes subjected to transverse loading by opposed indenters when the deformation is finite and extensive. The object of their investigation is to facilitate the assessment of the energy absorbing capability of tube in an impact situation which is exactly opposite to the present work.

It is interesting to note that the deformed tubes are very similar to those obtained from cropping up to the maximum load. Initially localized deformation is observed under the blade. As loading progresses, the distortion spreads forming a deformed pattern. Under further loading, the section depth again reduces and the points of the deformed pattern spread towards the end of the tube. Distinct 'hinge lines' are observed during the cropping cycle and as loading progresses, the hinge lines extend.

The main characteristic features of thin-walled tube cropping are 1) a flat on the top surface of the tube and 2) a sudden load drop during the cycle. The length of flat depends on the size and material of the tube. Flattening is inevitable but can be minimized by cropping under pre-load conditions. The sudden load drop during the cycle is bound to occur for hollow metallic tubes as explained below.

At maximum cropping load, the contact between the material and the tool is only at the edges. After some penetration of the tool, the crack initiates at both edges simultaneously and propagates towards the centre and separation of the material occurs on the top surface of the tube. It is evident from the different techniques used - the incremental tests, paint technique and cine films, that the initiation of the crack starts immediately after the maximum load. This sudden load drop immediately after the maximum cropping load, is due to the sudden change in the pressure from a maximum, developed between the material and the tool (solid medium), to the atmospheric pressure (air medium) because the tube is empty. Had the tube been filled with some material, the sudden drop in the load during the cycle would not have occurred. However, a small drop in the load can be seen on the load variation with time trace for filled tubes as it is extremely difficult to fit the glass rod inside the tube without any air gap due to the non-uniformity of

the tube. Due to this gap, however small it may be, the load drops off suddenly during the cycle because there is a sudden change in the pressure from solid medium to air medium.

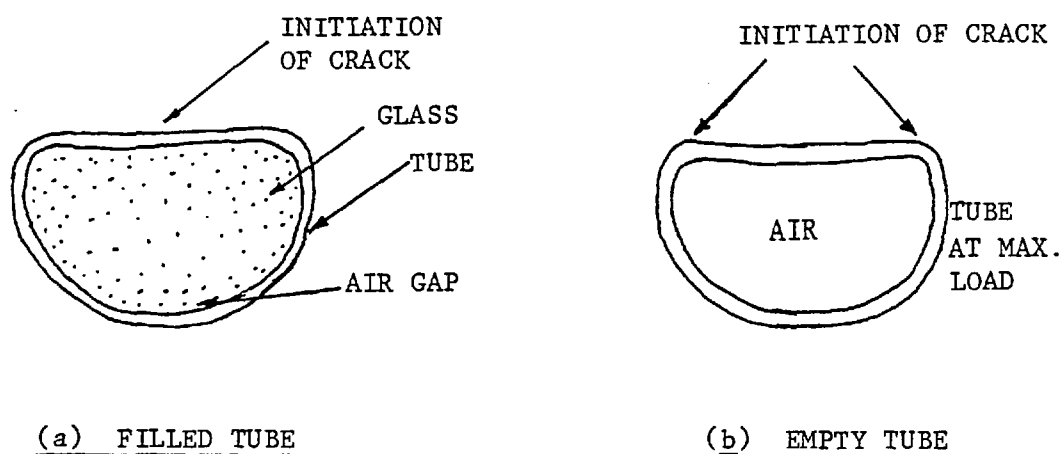


FIG. 6.1

It is noticeable from the experiments that the sudden load drop decreases with decreasing clearance between tube and filling and vanishes for a tube tightly filled with glass rod and a tube filled with mild steel. For glass tube, the load increases to its maximum and then drops quickly to zero. For any metallic tube, however brittle it may be, there will be some deformation and hence the sudden load drop during the cycle occurs.

One of the main drawbacks in cropping metallic tubes is that they act as energy absorbers rather than energy transmitters. This is the main reason for the extensive cross-sectional distortion of the cropped billets. For a solid rod, there is a continuity of particles within the cross-section and the particles close to the tool are pushed down by the tool itself and these particles push those next to them and so on. The situation is different for a tube in the sense that the top surface of tube flattens into two different triangular shapes (the bigger on the billet side) by absorbing the energy. Of course, the rest of the tube

acts as a rigid support and helps in forming the plastic hinges on the top surface of the tube, at least up to the maximum cropping load. However, the mechanism is similar to bar cropping to a greater extent when the tubes are cropped with tight fillings within them.

As described in Chapter 5, it is possible to predict the load-deflection graph up to the point of first shearing. The maximum cropping load is predicted from a standard tension test and the deflection of the tool at maximum load is predicted from simple strain theory. It is important to note that the length of the plastic hinge depends mainly on the tube parameter, the R_1/T ratio. By using empirical formulae for decay lengths, the deformed region can be calculated for any given thin-walled stainless steel tube. It is not possible to develop a theoretical solution for filled tubes, as it is a complicated situation involving two entirely different materials. However, the empirical equation based on shear yield stresses of the two materials seems to be adequate to estimate the maximum cropping load for filled tubes.

CHAPTER 7

GENERAL CONCLUSIONS

7.1 INTRODUCTION

The present thesis has attempted to contribute mainly towards a better understanding of four aspects of tube cropping. Firstly, the tube cropping process was examined in detail by using different techniques. Secondly, the influence of various cropping parameters on the cropping load and the quality of billets was studied at great length. Thirdly, the mechanism of fracture in cropping was described through the medium of fractographic studies. Finally, an upper-bound solution for tube cropping was developed based on a plastic hinge approach which enabled prediction of the cropping load for any given size and material of the thin-walled metallic tubes. The relevant conclusions are described below.

7.2 TUBE CROPPING PROCESS

- (i) The tube cropping process is different from the bar cropping process in that the load suddenly drops off to some extent, immediately after reaching its maximum.
- (ii) The cropping blade flattens the top surface of the tube and the length of the flat at maximum cropping load depends on the size of the tube and is found to be approximately the mean diameter of the tube.
- (iii) The cross-sectional distortion of the constrained end of the bar is less than that of the billet end.
- (iv) Empirical formulae for 'decay lengths' on both sides of the tube have been established and these help in predicting the extent of the

deformed region. Decay length mainly depends on the inside radius to thickness ratio of the tube.

- (v) As there is no standard form of stress-strain diagram available in the literature for shearing, these cropping tests have been correlated with standard tests such as tension, torsion, etc. However, it was virtually impossible to conduct torsion tests on the small thin-walled tubes used in this work because they fail by buckling rather than shearing.

7.3 EFFECT OF THE PROCESS PARAMETERS

- (i) The choice of blade clearance depends on the billet material, blade geometry, and conditions of bar constraint. For the cropping of thin-walled tubes, the clearance between blade and work holder has to be maintained at a minimum.
- (ii) Overall bending of the billet impairs its quality due to the non-uniform stress field which is thereby introduced across the cross-section of the tube. It has been minimized by providing a support under the billet. This can also be done by constraining the whole billet within the cropping blade.
- (iii) Cropping blade and work holder must be made of a strong, hard material such as high strength tool steel. This is vital because the quality of the cropped billet can be expected to deteriorate with increasing blade wear. Periodic checks are necessary to ensure that the tool has not worn excessively as this would affect the clearance between tool and work holder.

- (iv) The design of cropping tool is aimed at controlling the nature and direction of the crack such that the cropped billet produced has acceptable ends. As different sharp-edged blades were observed not to influence either the cropping load or the cross-sectional distortion of billet, a flat blade was used and is recommended.
- (v) One of the parameters that affects the quality of billet is its size. The quality of billet improves with decreasing mean diameter to thickness ratio but it was found not to be influenced by varying the billet length, particularly up to one inch length which was fortunate as it was intended to crop one inch length billets only in the present work.
- (vi) Though it is extremely difficult to fill the tube without any air gap it is clear that a tight fit between tube and filling will certainly improve the quality of billets.
- (vii) The behaviour of either glass or alumina within the tube was found to be identical except for higher loads for tubes filled with alumina.
- (viii) Cropping at low temperature (-196°C) showed that stainless steel materials do not exhibit the phenomenon of low temperature brittleness.
- (ix) The velocity of the blade has very little influence on cropping load or cross-sectional distortion of billet for empty tubes. However, filled tubes exhibit a sensitivity to speed of working. In fact, the quality of billets improves for filled tubes at higher velocities of the blade.

- (x) Work-hardening appears to be the most important parameter in cropping. For example, the cross-sectional distortion of billets is less for nimonic-PE16 material whose strain-hardening rate is higher than that of stainless steels and this difference in quality of billets decreases when they are filled with glass or alumina. There is no cross-sectional distortion of billets for embrittled steel filled with glass or alumina. However, the material shatters in a random manner due to its high brittleness. An optimum ductility has to be established as between cold-worked nimonic-PE16 and embrittled stainless steel for better quality billets.
- (xi) Cropping under pre-load is an asset, in that it helps in minimizing distortion of billets. Better quality billets were produced under tensile or compressive axial pre-load. The points described in (ix), (x) and (xi) are considered to be the most important cropping parameters as far as the quality of billet is concerned.

7.4 MECHANISM OF FRACTURE

- (i) Fractographic studies reveal that shearing is not an action in a single plane. It is in fact a summation of different processes such as bending, stretching and tearing of the grains and fibres for a certain depth on both sides of the final separating plane.
- (ii) Microscopic examination of fracture in stainless steels shows that the mechanism of fracture in cropping possesses mainly ductile features. Tearing and shear patterns of dimples have been identified which suggest domination of the opening and shear modes of fracture. Quasi-cleavage fracture has been identified in nimonic-PE16 material which explains the reasons for the better quality billets. It was found that fracture in brittle materials such as alumina and glass

occurs from defects like mechanically produced cracks, pores and occlusions.

7.5 THEORETICAL ASPECTS

- (i) Reasonable correlation has been obtained between tension and cropping tests. However, the yield stress derived from the fracture stress seems to be more realistic than the 0.5% proof stress.
- (ii) From the upper-bound solution it is possible to estimate the cropping load and the shape of the load-deflection graph up to the point of actual first shearing, for any given thin-walled tube.

CHAPTER 8

SUGGESTIONS FOR FURTHER WORK

8.1 DEVELOPMENT OF THE CROPPING RIG

- (i) The modified cropping rig with a support under the billet as described in Chapter 2 has shown some improvement in the quality of billets. The rig may be further modified by considering closed-type tooling. The billet to be cropped can itself also be enclosed within the cropping blade which is made of two halves for the purpose. A more sophisticated design could be achieved for production purposes through the incorporation of provision for ejection of the billet, a faster hydraulic clamping system or a mechanical system synchronized with the press ram stroke, etc. Such sophistication may not be appropriate for cropping irradiated fuel, of course.
- (ii) From the experience of the experimental work presented in this thesis, a further study and improvement in the design and development of tube cropping under axial load may prove to be rewarding.
- (iii) The experimental test rig could be modified to accommodate more than one tube, i.e., a small tube bundle which could simulate the actual spent fuel element. Again, tubes both empty and filled will have to be studied.

8.2 INVESTIGATION OF THE FRACTURE MECHANISM

- (i) In the present work, the mechanism of fracture has been studied on a microscopic scale. As fracture is obviously the major mode of separation in cropping, the study should be extended to macroscopic scale also, to obtain a thorough understanding of the process and its parameters.

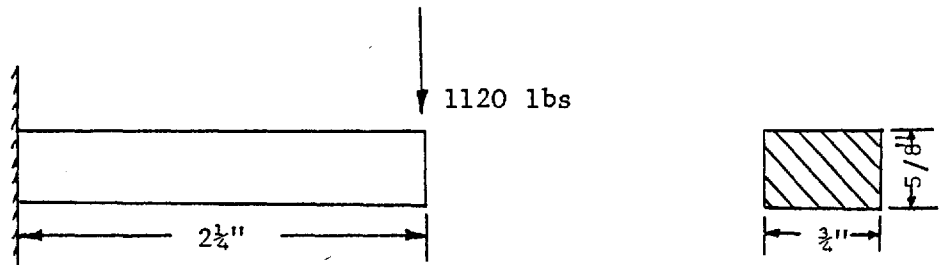
- (ii) Microscopic analysis of fracture propagation should be extended to different areas of the fractured surface of the billet to establish a criterion for controlling the route of the crack growth.

8.3 DEVELOPMENT OF THE THEORETICAL ANALYSIS

- (i) The present theoretical model can be improved by considering a minimization technique to avoid having to establish experimentally empirical formulae for decay length. Both bending and shearing should be considered in the theoretical analysis, particularly for tubes whose thickness to mean diameter ratio is greater than 0.1.
- (ii) A new kinematic model of plastic flow can be set up based on the experimental observations using visio-plasticity approach, high speed cinematography, etc.
- (iii) A finite element program could possibly be developed to solve the problem for the stress field and the associated distortions under progressively increasing loads. The problem is exceedingly complex, however, due to the large distortions of the thin-walled tubes which are involved and the difficulty of predicting the initiation and propagation of fracture. For these reasons it may not be profitable to employ finite element techniques which would necessarily be very expensive both in their development and their execution.

APPENDIX - IDESIGN OF LOAD CELL - 1

The load cell comprises a simply supported beam of rectangular cross-section, made from En 24 steel. The dimensions of the beam are 5" x 3/4" x 5/8" and is loaded by knife edges which are attached to the beam at shown in fig. 2.3. Being symmetrical, the simply supported beam may be regarded as being made up of two cantilevers, loaded as shown below.



Maximum bending moment	$M = 2,520 \text{ lb. in}$
Second moment of area of cross-section	$I = 0.01525 \text{ in}^4$
Section modulus	$Z = 0.0488 \text{ in}^3$
Stress	$\sigma = \frac{M}{Z}$ $\approx 2.3 \text{ tons/in}^2$

Since the yield strength of En 24 is about 50 T/in², the factor of safety is approximately 2.17.

	$E = 13,650 \text{ T/in}^2$
Maximum strain	$\epsilon = 0.168\%$
Deflection	$D = \frac{wl^3}{3EI}$ for a cantilever
where $w =$ load and	$l =$ length
	$D = 0.0091''$.

DESIGN OF LOAD CELL - 2

The conventional load cell comprises a hollow cylinder, made of En 24 steel. The dimensions of the hollow cylinder are 1"φ x 2" high x 3/32" thick. It was designed to carry up to 5 tons load.


```

AL1=SQRT (S1*S1+H/2.*H/2.)
AL2=SQRT (S2*S2+A*A*SIN (H/DM)*SIN (H-DM))
THETS=ATAN (2.*(A-D(I))/H)
CALL CALC (THETS,DANG1)
OMEG1=DANG1
C
CALCULATE WORK
V=H/2.-A*SIN (H/DM)
F=0.125*DL1
SI1=ATAN (V/F)
SI2=ATAN (D(I)/F)
W1=AMP*AL1*(OMEG+OMEG1)
W2=2.*AMP*AL2*OMEG
W3=AMP*H*(SI2/2.)
W4=AMP*(2.0*PI*A-H)*(SI1/2.)
W5=AMP*H*ATAN (D(I)/DL1)
W6=AMP*S1*(OMEG+OMEG1)
W7=2.*AMP*S2*OMEG
W8=AMP*DL1*(1./A-1./R)*(PI*DM-H/2.)
STR=Y*T*F*H*V/(2.*A*SIN (H/(2.*A)))
WD=Y*T*(H*(S1/2.*(S1/DL1-1.))+F*(2.*PI*A-H)*((R-A)/(2.*A)))+STR
W=W1+W2+W3+W4+W5+W6+W7+W8
RETURN
END
SUBROUTINE LOAD
DIMENSION RESX(100),RESY(100),D(100),P(100)
COMMON C,C1,C2,C3,CC,OMEG
COMMON A,R,H,Y,T,AMP,PI
COMMON DMAX,DM,AI,I,D,P,W
WOLD=W
D(I)=D(I)+0.00001
CALL WORK
P(I)=(W-WOLD)/0.00001
RETURN
END
SUBROUTINE ITERAT
DIMENSION RESX(100),RESY(100),D(100),P(100)
COMMON C,C1,C2,C3,CC,OMEG
COMMON A,R,H,Y,T,AMP,PI
COMMON DMAX,DM,AI,I,D,P,W
K=0
CU=1.E-6
1 OMEG=ABS (OMEG)
IF (OMEG.GT.PI/2.AND.K.LT.100) OMEG=ABS (OMEG-PI/2.)
F=(C1*SIN (OMEG)+C2*COB (OMEG)-C1*OMEG+C3)/SIN (OMEG)
K=K+1
G=C1*COB (OMEG)-C2*SIN (OMEG)-C1
GN=(G-F*COB (OMEG))/SIN (OMEG)
OMEGN=OMEG-F/GN
RCO=ABS (1.-ABS (OMEG/OMEGN))
OMEG=OMEGN
IF (RCO.LT.CC) RETURN
IF (K.GT.1000) WRITE (6,2)
IF (K.GT.1000) STOP
GO TO 1
2
FORMAT (*NO CONVERGENCE POSSIBLE*)

```

```
END
SUBROUTINE CALC (THET,DANG)
DIMENSION RESX(100),RESY(100),D(100),P(100)
COMMON C,C1,C2,C3,CC,OMEG
COMMON A,R,H,Y,T,AMP,PI
COMMON DMAX,DM,AI,I,D,P,W
C=A-D(I)-R*COS(OMEG)
RBAR=R*SIN(PI/2.+THET-ASIN(C/R*SIN(PI/2.-THET)))
1/(SIN(PI/2.-THET))
XA=A*COS(THET)
XR=RBAR*COS(THET)
DYA=-XA/(SQRT(A*A-XA*XA))
DYR=-XR/(SQRT(R*R-XR*XR))
DANG=ABS(ABS(ATAN(DYA))-ABS(ATAN(DYR)))
RETURN
END
```

REFERENCES

1. SCHEY, J.A.
"Introduction to Manufacturing processes", McGraw-Hill Book Company, U.S.A., 1977.
2. ALEXANDER, J.M. and BREWER, R.C.
"Manufacturing Properties of Materials", Van Nostrand Reinhold Company, London, 1963.
3. ALEXANDER, J.M.
"New forming processes for reducing wasteful cutting", Metals Technology, pp.393-411, Sept. 1976.
4. HOWARD, F. and DENNISON, H.A.J.
"Development and application of cold extrusion techniques", Sheet Metal Industries, pp.183-190, March 1966.
5. ANON.
"Cold-flow shearing", Metalworking Production, pp.59-60, Oct. 1965.
6. ORGAN, A.J.
"Economic Aspects of Metal Billet Production", 9th Int. M.T.D.R. Conference, Birmingham, 1968.
7. AHMED, M.H.M.
"A Study of the Multiple Cropping Process", Ph.D. Thesis, University of Birmingham, 1978.
8. EMERSON, C.
"How to cut off metals, part I, Single point cutting off", Metalworking production, pp.1823-1827, Nov. 1956.
9. EMERSON, C.
"Shearing and friction sawing", Metalworking production, pp.1871-1876 Nov. 1956.
10. EMERSON, C.
"Sawing and Grinding", Metalworking production, pp.1913-1917, Nov. 1956.

11. WIDMONT, J.C.
"The cheapest cold forming slug", Metalworking Production, p.139,
Dec. 1961.
12. GREEN, R.E.
"Russian machines for working metal by rolling", Machinery and
Production Engineering, V.109, pp.60-66, July 1966.
13. ASM
"Metals Handbook", Vol. 5, Forming, American Society of Metals, 1974.
14. DAVIES, R. and AUSTIN, E.R.
"Developments in high speed metal forming", The Machinery Publishing
Co. Ltd., London, 1970.
15. WATKINS, M.T.
"Bar Cropping - A Survey", NEL Report No. 550, Nov. 1973.
16. ORGAN, A.J. and MELLOR, P.B.
"Mechanics of High-speed Bar Cropping", Proc. Instn. Mech. Engrs,
Vol. 180, Pt. 3I, pp.151-162, 1965-66.
17. ORGAN, A.J. and MELLOR, P.B.
"Some Factors Effecting the Quality of Cropped Billets",
Int. J. Mach. Tool Des. Res., Vol. 7, pp.369-389, 1967.
18. NAKAGAWA, T. and SHIMORI, K.
"Production of Crank Shafts by Clamp Shearing", 14th Int. M.T.D.R.
Conf., Birmingham, 1974.
19. AHMED, M.H.M. and DAS, M.K.
"A Study of Stresses in the Double Cropping Process", Proc. of
18th Int. M.T.D.R. Conf., London, 1977.
20. DAS, M.K. and TOBIAS, S.A.
"Recent Advances in High Speed Cropping", 5th Int. Cold Forging
Congress, Brighton, 1975.

21. DAS, M.K. and TOBIAS, S.A.
"The Petro-Force HERF Cropping System", SME, No. MF72-143,
Michigan, U.S.A., 1972.
22. ZAPF, F.W.
"Production of slugs from cold extrusion bars or wire", 4th Int.
Meeting Cold Forging, Dusseldorf, pp.301-324, 1970.
23. HERBST, U.
"The cropping of billets for cold extrusion", Dr Ing Diss., Technische
Hochschule, Hanover, 1967.
24. VINGOE, R.C. and ORGAN, A.J.
"Blade wear in bar cropping", Proc. 8th Int. M.T.D.R. Conf.,
Manchester, Pt. 2., pp.1075-1106, 1967.
25. ORGAN, A.J.
"Bar cropping in high energy-rate forming machines", Ph.D. thesis,
Birmingham University, 1968.
26. ORGAN, A.J. and MELLOR, P.B.
"The preparation of metal billets by bar cropping", Iron & Steel,
London, 39 (11) pp.481-487, (12) pp.534-537, 1966.
27. SCHRODER, G. and KAMMERER, M.
"Influence of temperature on the quality and the forces in the
cropping of steels with low carbon contents (in German)", Industrie
Anzeiger, 94(2), pp.32-33, 1972.
28. PATTERSON, W.C.
"Nuclear Power", Penguin Books Ltd., London, 1976.
29. MURRAY, R.I.
"Nuclear Energy", Pergamon Press Inc., New York, 1975.
30. HARVEY, D.C.
"Fatigue of fluid-supported thick-walled cylinders", Ph.D. thesis,
University of London, 1971.

31. STANWORTH, J.E.
"Physical properties of glass", Oxford at the Clarendon Press,
1950.
32. POPPER, P.
"Special Ceramics", Heywood & Company Ltd., London, 1960.
33. KIENZLE, O. and ZABEL, H.
"Separation of metal billets by cropping", British Iron and Steel
Industry Translation Service No. 4596, 1966.
34. ORGAN, A.J.
"Description of the quality of cropped billets", Communication to the
Bar Cropping Sub-Group of the BCFG, 1970.
35. ROBERT F. REED-Hill
"Physical Metallurgy Principles", D. Van Nostrand Company, New York,
1973.
36. BRIDGMAN, P.W.
"Studies in large plastic flow and fracture", McGraw-Hill Book
Company, 1950.
37. COX, T.B. and LOW, J.R. (Jr).
"Investigations of the plastic fracture of high-strength steels",
NASA Technical Report, Research Grant NGR 39-087-003, 1972.
38. BEACHEM, C.D.
"An electron fractographic study of the influence of plastic
strain conditions upon ductile rupture process in metals",
Trans. ASM, Vol.56, pp.318-326, 1963.
39. ASM
"Metals Handbook", Vol. 9, Fractography and Atlas of Fractographs,
American Society of Metals, 1974.
40. BRADT, R.C. and TRESSLER, R.E.
"Deformation of Ceramic Materials", Plenum Press, New York, 1975.
41. WIGLEY, D.A.
"Mechanical Properties of Metals at Low Temperatures",

- Plenum Press, London, 1971.
42. EASON, G. and SHIELD, R.T.
 "The influence of free ends on the load carrying capacities of cylindrical shells", J. of the Mechanics and Physics of Solids, Vol. 4, pp.17-27, 1955.
43. THOMAS, S.G.
 "Transverse Loading of Simply Supported Thin-walled Tubes", M.Sc. Dissertation, UMIST, Manchester, 1974.
44. DE RUNTZ, J.A. (Jr) and HODGE, P.G. (Jr).
 "Crushing of a Tube Between Rigid Plates", Journal of Applied Mechanics, pp. 391-395, Sept. 1963.
45. BETTERIDGE, W. and HESLOP, J.
 "Nimonic alloys", Edward Arnold Publishers Ltd., 1974.
46. CLAUSS, F.J.
 "Engineer's Guide to High-Temperature Materials", Addison-Wesley Publishing Company, U.S.A., 1969.
47. KINGERY, W.D. et al.
 "Introduction to Ceramics", John Wiley & Sons, 1976.
48. GROSBERG, A.J.
 "Studies of the Behaviour of Fast Reactor Fuel Elements Using a Computer Model", Ph.D. Thesis, 1979.
49. FULRATH, R.M. and PASK, J.A. (Editors).
 "Ceramic Microstructures", John Wiley & Sons, 1966.
50. IME
 The Institution of Mechanical Engineers Proc. of the Conference on "The Properties of Materials at High Rates of Strain", London, April 1957.
51. JOHNSON, W. et al.
 "Large Deformations of Thin-walled Circular Tubes Under Transverse Loading - I, II, III, Int. J. of Mechanical Science, Vol. 18,

pp. 325-333, 387-397, 501-509 respectively, 1976.

52. ALEXANDER, J.M.

"An approximate analysis of the collapse of thin cylindrical shells under axial loading", J. Mech. Appl. Math., 13, pp.10-15, 1960.

53. AL-QURESHI, H.A. and DAS, M.K.

"Thin-walled Tube Cropping Using Elastomer", Int. J. Mach. Tool Des. Res., Vol. 16, pp.77-85, 1976.

54. ANON

"High Tool Velocity Cropping: Production of billets for backward extrusion", P.E.R.A., Report No. 170, Sept. 1967.

55. ANON

"Terminology for features of cropped billets", British Cold Forging Group-Sub Committee on Bar Cropping, 1969.

56. AMSTEAD, B.H. et al.

"Manufacturing Processes", John Wiley & Sons, New York, 1969.

57. BAKHTAR, F. and AUSTIN, E.R.

"Relative economics of conventional and high strain-rate forming, Int. J. of M.T.D.R., Vol. 5, p.139, 1965.

58. BACKOFEN, W.A.

"Deformation processing", Addison-Wesley Publishing Company, U.S.A., 1972.

59. LOW, J.R. (Jr.)

"Effects of microstructure on fracture toughness of high strength alloys", Engineering Fracture Mechanics, Vol. 1, pp.47-53, 1968.

60. CRANE, E.V.

"What happens in shearing metals?", Machinery, 30, p.225, 1927.

61. CHANG, T.M. and SWIFT, H.W.

"Shearing of metal bars", J. Inst. Metals, 78, pp.119-146, 1950.

62. ROSENTHAL, D. and ASIMOW, R.M.
"Introduction to Properties of Materials", Van Nostrand Reinhold Company, New York, 1971.
62. EVERETT, J.
"Fully automated feeding equipment for the high speed, precision cropping of bar stock", Int. Cold Forging Congress, Oct. 1-3, pp.446-456, Brighton, 1975.
63. ELLINGTON, J.P.
"On obtaining the shear stress-strain relationship from a hollow specimen in torsion", J.R. Aero. Society, 60, Dec. 1956.
64. FORD, H. with ALEXANDER, J.M.
"Advanced Mechanics of Materials", Ellis Horwood Ltd., England, 1977.
65. FENNER, A.J.
"Mechanical Testing of Materials", George Newnes Ltd., London, 1965.
66. FORREST, J.S. (Edited by)
"The Breeder Reactor", Scottish Academic Press, Edinburgh, 1977.
67. GARKAVY, J.N.
"Distribution of stresses in material during punching and cutting with parallel shears", Engineering Review, Institute of Mechanics, Vol. III, Pt. 1, p.51, Moscow, 1946.
68. GLOVER, A.P. et al.
"The measurement in the fracture toughness studies", Engineering fracture mechanics, Vol. 2, pp.165-167, 1970.
69. GRONOSTAJSKI, J. and DZIDOWSKI, S.
"Effect of low temperature on the quality of the billets from carbon and alloy steel", Rep. No. 250, ITBM, Technical University of Wrocław, 1974.
70. HILL, R.
"Mathematical Theory of Plasticity", Clarendon Press, Oxford, 1971.

71. HOJO, H.
"Theoretical analysis of shearing mechanism", Journal of the Japan Soc. Precision Engrs., 30,p.785, 1964.
72. HOLLOWAY, D.G.
"Physical Properties of Glass", Wykeham Publications, London, 1973.
73. JOHNSON, W. et al.
"The compression of crossed layers of thin tubes", Int. J. Mechanical Science, Vol. 19, pp.423-437, 1977.
74. JOHNSON, W. and MELLOR, P.B.
"Plasticity for Mechanical Engineers", Van Nostrand Company Ltd., London, 1962.
75. KNOTT, J.F.
"Fundamentals of Fracture Mechanics", The Butterworth Group, 1973.
76. LATTEY, J.I. et al.
"Precision Metal Cropping Under Axial Load", 11th Int. M.T.D.R. Conf., Birmingham, Sept. 1970.
77. LAWSON, R. et al.
"Cropping billets for cold extrusion", A Review, Int. Cold-Forging Congress, pp.403-442, Brighton, Oct. 1975.
78. LITHERLAND, T.P.
"The Properties of Metallic Materials at Low Temperatures", Chapman & Hall, Ltd., London, 1950.
79. MCINTYRE, D.
"Fractographic Analysis of Fatigue Failures", ASME Trans., Vol. 97, pp.194-205, 1975.
80. KURREIN, M.
"Plasticity of Metals", Griffin, London, 1964.
81. MURRAY, R.L.
"Nuclear Energy", Pergamon Press, New York, 1975.

82. NADAI, A.
"Theory of Flow and Fracture of Solids", Vol. 1 & 2, McGraw-Hill
Book Company Ltd., 1950.
83. NAKAGAWA, T. and MAEDA, T.
"Billet Production by Clamp Shearing Method", 4th Int. Cold Forging
Meeting, pp.351-376, Dusseldorf, 1970.
84. O'NEILL, H.
"Hardness Measurement of Metals and Alloys", Chapman and Hall Ltd.,
1967.
85. REDDY, T.Y.
"Impact energy absorption using laterally compressed metal tubes",
Ph.D. Thesis, University of Cambridge, 1978.
86. REID, S.R. and REDDY, T.Y.
"Effect of strain-hardening on the lateral compression of tubes
between rigid plates", Int. J. Solids Structures, 14, pp.213-225, 1978.
87. REID, S.R.
"Influence of geometrical parameters on the mode of collapse of a
'pinched' rigid-plastic cylindrical shell", Int. J. Solids Structures,
Vol. 14, pp.1027-1043, 1978.
88. SCOTT, R.B.
"Cryogenic Engineering", Van Nostrand Company, 1959.
89. TETELMAN, A.S. and McEVILY, A.J. (Jr.)
"Fracture of Structural Materials", John Wiley & Sons, 1967.
90. TUCKER, W.C.
"Billet separation by the shear fracture method", Steel Processing,
40(11), pp.695-698, 731, 1954.
91. TIMOSHENKO, S.P. and GOODIER, J.N.
"Theory of Elasticity", McGraw-Hill Book Company Ltd., 1970.

92. VAS, I.
"Cropping under axial compression", preprints 4th Int. Meeting,
Cold Forging Group, Dusseldorf, 1970.
93. VOGEL, W.
"Structure and Crystallization of Glasses", Pergamon Press, Oxford, 1971.
94. WATSON, A.R.
"Finite deformation of thin-walled circular cylinders under transverse
loading", M.Sc. Dissertation, UMIST, Manchester, 1975.
95. WONG, V.G.
"Some aspects of bar cropping", Ph.D. Thesis, Birmingham University,
1973.
96. WONG, V.G. and DAS, M.K.
"Analysis of stresses in bar cropping", 15th Int. M.T.D.R. Conf.,
Birmingham, 1974.
97. RAO, R.S.
"Elucidation of the Mechanism of Tube Cropping", M.Sc. Dissertation,
University of London, 1977.
98. ALEXANDER, J.M. and RAO, R.S.
"The Cropping of Thin-Walled Steel Tubes", preparation of slugs
and billets for forging - BCFG Seminar, University of Birmingham,
April, 1979.